Studies of Coordination-Induced Bond Weakening in Divalent Samarium Complexes

Studies of Coordination-Induced Bond Weakening in Divalent Samarium Complexes

by

Nick G Boekell

A Dissertation

Presented to the Graduate and Research Committee

of Lehigh University

in Candidacy for the Degree of

Doctor of Philosophy

in

Department of Chemistry

Lehigh University

May 23, 2022

Approved and recommended for acceptance as a dissertation in partial fulfillment of the requirements for the degree of Doctor of Philosophy

Nick G. Boekell
Studies of Coordination-Induced Bond Weakening in Divalent Samarium Complexes

_____
Defense Date

_____
Approved Date

_____
Dissertation Director:

Committee Members:

_____
Committee Chair: Dr. Robert A. Flowers II

_____
Committee Member: Dr. Elizabeth Young

_____
Committee Member: Dr. Mark Chen

_____
Committee Member: Dr. Daniel Griffith

ACKNOWLEDGMENTS

First and foremost, I would like to give my thanks to my advisor Professor Robert Flowers, without whose expertise, guidance, and support none of the work herein would have been possible. While your infectious curiosity has made me a better scientist and researcher, it is your multidisciplinary approach to life and learning that I have found most inspiring and hope to carry forward in my future endeavors.

I would also like to extend my gratitude to the other past and current members of the Flowers lab who have been my colleagues and friends along the way. I owe thanks in particular to Dr. Tesia Chciuk for her very convincing sales pitch for the Flowers lab. As well, Dr. Caroline Bartulovich has been a great friend and an often needed sanity check during our time working together. I must also thank Nancy Oloyede, who has also been a source of great wisdom and friendship. Furthermore, I would like to thank all of the undergraduate researchers who I have been able to work with over the years; Nicole Capogna, Nicole Karpowicz, Meriam Deeb, and Gina Angelo. William Anderson Jr. has also been a great help to me in laying the groundwork for the computational studies in our work.

Of course I would never have made it this far without the support of my family, especially my sisters Hanne and Kimber. My friends and instructors at Lehigh Valley Taekwondo have also been instrumental during my time at Lehigh by being a second home outside the lab. Finally, I cannot express enough gratitude to my friends Greg, Jess, Kate, Alison, Melissa, Brigand, Phil, Connor, Molly, Chuck, Andrew, and Scott for all of their support and for all of the good times that we continue to share.

TABLE OF CONTENTS

LIST OF FIGURES

LIST OF TABLES

LIST OF SCHEMES

LIST OF ABBREVIATIONS

Proton-coupled electron transfer	PCET
N-Methylethanolamine	NMEA
Hexamethylphosphoramide	HMPA
Hexamethyldisilylazane	HMDS
Tetrabutylammonium bromide	TBABr
Tetrabutylammonium chloride	TBACl
Hydrogen atom transfer	HAT
Concerted proton electron transfer	CPET
Electron-transfer proton-transfer	ET PT
Proton-transfer electron-transfer	PT ET
Bond dissociation energy	BDE
Bond dissociation free energy	BDFE
Oxygen evolving complex	OEC
Density functional theory	DFT
2,2,6,6-tetramethylpiperidine 1-oxyl	TEMPO
Tetrahydrofuran	THF
Electron paramagnetic resonance	EPR
Electron transfer	ET
Methanol	MeOH
Nuclear magnetic resonance	NMR
Gas chromatograph mass spectrometry	GCMS
Ethyl acetate	EtOAc

Electrospray ionization mass spectrometry	ESI-MS
Equivalents	equiv.
Enthalpy of activation	$\Delta H^{\ddagger}$
Entropy of activation	$\Delta S^{\ddagger}$
Free energy of activation	$\Delta G^{\ddagger}$
Kinetic isotope effect	KIE
Tert-butyl alcohol	*t*-BuOH
Ethanol	EtOH
Triethylamine	Et_3N
Ultraviolet-visible	UV-Vis
Born-Oppenheimer molecular dynamics	BOMD
Extended X-ray Absorption Fine Structure	EXAFS
Lowest unoccupied molecular orbital	LUMO
Highest occupied molecular orbital	HOMO
Ethylene glycol	EG
Diethylene glycol	DEG
Ethanolamine	EA
Ethylenediamine	EDA
N,*N*-Dimethylethanolamine	DMEA

ABSTRACT

Divalent samarium reagents are widely used in organic synthesis as powerful single electron reductants. One of the most useful properties of Sm(II) is the tunability of the selectivity and reducing power of Sm(II) reagents via interactions with a wide range of chemical additives. Among these additives, water and other small protic ligands have been shown to form complexes with Sm(II) that can mediate proton-coupled electron transfer (PCET) reductions. Recent work has shown that the PCET reactivity of several Sm(II)-proton donor reagents is enabled by a reduction in the X-H bond strength of the proton donor ligand upon coordination to Sm(II). This phenomenon has been observed in a number of other low-valent metal complexes bearing protic ligands and is known as coordination-induced bond weakening.

This dissertation describes synthetic, mechanistic, and computational investigations of coordination-induced bond weakening in a variety of Sm(II)-proton donor reagents. Advances in the substrate scope and mechanistic understanding of the SmI_2-water reagent are described. Synthetic and mechanistic investigations of the novel reductants, SmI_2-ammonia and $SmBr_2$-NMEA, are also discussed. Finally, the degree of ligand X-H bond weakening upon coordination to SmI_2 and other low-valent metal complexes is analyzed in order to investigate the hypothesis that coordination-induced bond weakening is driven by backdonation from a low-valent metal into a ligand σ*-antibonding orbital. The results of these studies have potential applications in future utilization of divalent samarium reductants to achieve the reductions of challenging substrates and in the rational development of novel coordination-induced bond weakening systems.

Chapter 1: Introduction to Samarium(II) Chemistry and Coordination-Induced Bond Weakening

1.1 Background on Samarium(II) Reductants

Since the seminal report by Kagan and coworkers on the facile preparation of samarium diiodide, samarium(II) reagents have become staple single electron reductants in organic synthesis.[1–6] A key feature of samarium(II) is the tunability of its reactivity using a diverse set of additives.[7–15] Lewis basic ligands including hexamethylphosphoramide (HMPA) and hexamethyldisilylazane (HMDS) constitute one class of additives for SmI_2. Another class of additives is halide salts such as tetrabutylammonium bromide (TBABr) and tetrabutylammonium chloride (TBACl). Both Lewis basic ligands and halide salt additives have been shown in previous work by Flowers and coworkers to increase the redox potential of SmI_2 (Figure 1.1).[13,16–18] The third major class of SmI_2-additives is proton donors, which are discussed at length throughout this dissertation.

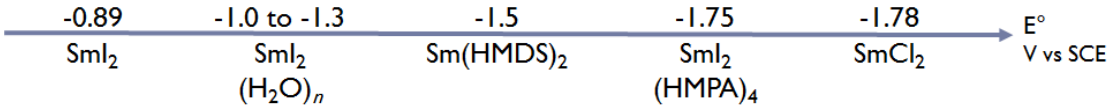

Figure 1.1. A selection of samarium(II) reductants organized by electrochemically determined redox potential[16]

Among proton donor additives for SmI_2, water is commonly used due to the ease of preparation and remarkable reducing power of the SmI_2-water reagent.[19–21] Notably, SmI_2-water has been found to facilitate the rapid reduction of substrates with redox potentials substantially more negative than the electrochemically determined redox potential of SmI_2-water itself.[16] A study on the comparative rates of SmI_2-water mediated reduction of anthracene and 1-iodododecane revealed both a greater rate of

reduction of anthracene and a greater dependence on [water] in the reduction of anthracene compared to 1-iododododecane by SmI_2. Since 1-iododododecane is known to be reduced by SmI_2 via a rate limiting dissociative electron transfer, these results demonstrated the ability of the SmI_2-water reagent to facilitate proton-coupled electron transfer (PCET) reductions of substrates.[22–24]

1.2 Background on PCET

Proton-coupled electron transfer reductions are a broad class of redox reactions in which the proton and electron move from the reductant and proton donor to one or more substrates in a single kinetic step.[25] The most well-known and thoroughly studied type of PCET reaction is hydrogen atom transfer (HAT), wherein the transferring proton and electron are quantum mechanically coupled. In contrast, concerted proton electron transfer (CPET) refers to PCET pathways in which the proton and electron are not quantum mechanically coupled but still move in the same kinetic step.

A key common feature of PCET reactions is a lack of the high energy charge-separated intermediates inherent to sequential electron-transfer proton-transfer (ET PT) and proton-transfer electron-transfer (PT ET) reactions (Scheme 1.1). This results in a lower thermodynamic barrier for PCET compared to stepwise processes. PCET pathways are therefore commonplace in biological processes, including DNA synthesis and nitrogen gas reduction by the iron-molybdenum cofactor in nitrogenases.[26,27] PCET reagents are also the subject of substantial interest and several reviews for their ability to facilitate conventionally challenging synthetic reductions under mild conditions.[25,28–30]

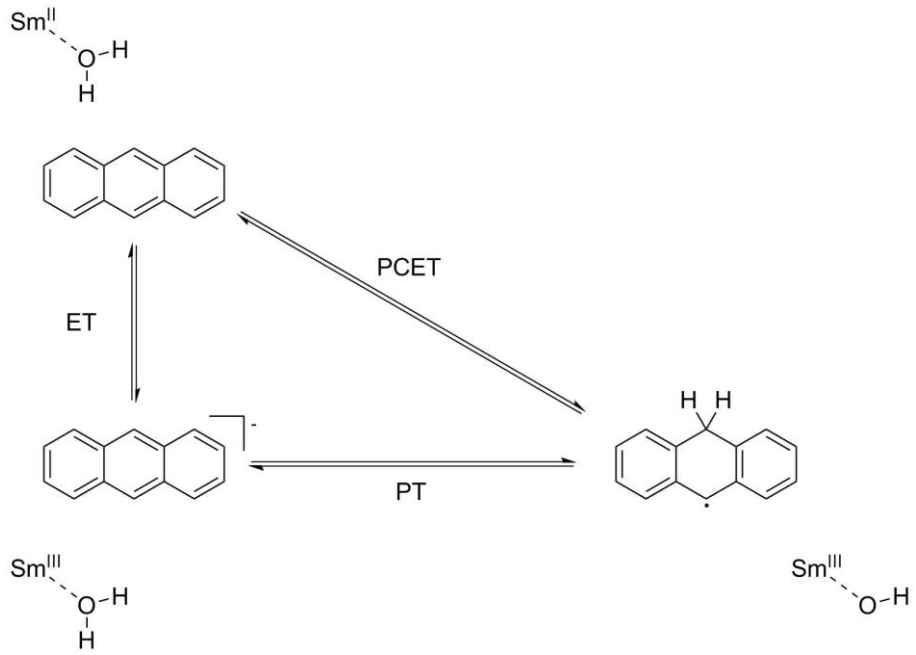

Scheme 1.1. ET-PT and PCET pathways for the Sm(II)-water mediated reduction of anthracene[22]

Since PCET pathways involve the movement of both an electron and a proton, redox potentials are an insufficient metric by which to measure the reducing power of PCET reductants. A more useful metric is the bond dissociation energy (BDE) or bond dissociation free energy (BDFE) of the cleaved X-H bond of the PCET reductant. However, for some CPET reagents, the BDFE of the cleaved X-H bond does not accurately reflect the reducing power of the overall PCET reagent. The reducing power of these reagents is therefore commonly discussed as the "effective BDFE" of the cleaved X-H bond. This effective BDFE value is defined by the Bordwell equation (Equation 1.1), which relates the redox potential of the electron donor in V (E^0), pK_a of the proton donor, and standard reduction potential of a solvated hydrogen atom (C_G) to the effective BDFE of the PCET reagent in kcal/mol.[31]

$$\mathrm{BDFE} = 1.37\mathrm{p}K_{\mathrm{ip}} + 23.06\mathrm{E}^0 + \mathrm{C}_\mathrm{G} \quad (1.1)$$

1.3 Background on Coordination-Induced Bond Weakening Systems

Recently, PCET systems wherein protic ligands are coordinated to low-valent metals have received increased attention.[32–34] The phenomenon of concerted homolytic ligand X-H bond cleavage and favorable metal oxidation in these complexes has been named coordination-induced bond weakening and has been shown to promote the formation of weak X-H bonds in reduced substrates. Notably, while coordination-induced bond weakening has been predominantly observed in low-valent metals, ligand X-H bond weakening upon coordination to electron rich main group elements has also been observed.[35,36]

1.3.1 Coordination-Induced Bond Weakening in Nature

Although the study of coordination-induced bond weakening has only recently emerged in the literature, the phenomenon has already been identified in several biological systems. The most notable of these is the oxygen evolving complex (OEC) of photosystem II, which is an integral cofactor for biophotosynthesis.[37] Within the OEC, a photoactivated Mn_4Ca cluster promotes coordination-induced O-H bond weakening of 32.5 and 15.5 kcal/mol in the first and second O-H bonds, respectively, of two water molecules coordinated to low-valent manganese binding sites.[37] This bond weakening enables formal hydrogen atom abstraction from water by proximal tyrosine residues and subsequent incorporation into nicotinamide adenine dinucleotide phosphate (NADPH) and adenosine triphosphate (ATP). The proposed mechanism for water oxidation by the OEC is shown in Scheme 1.2.

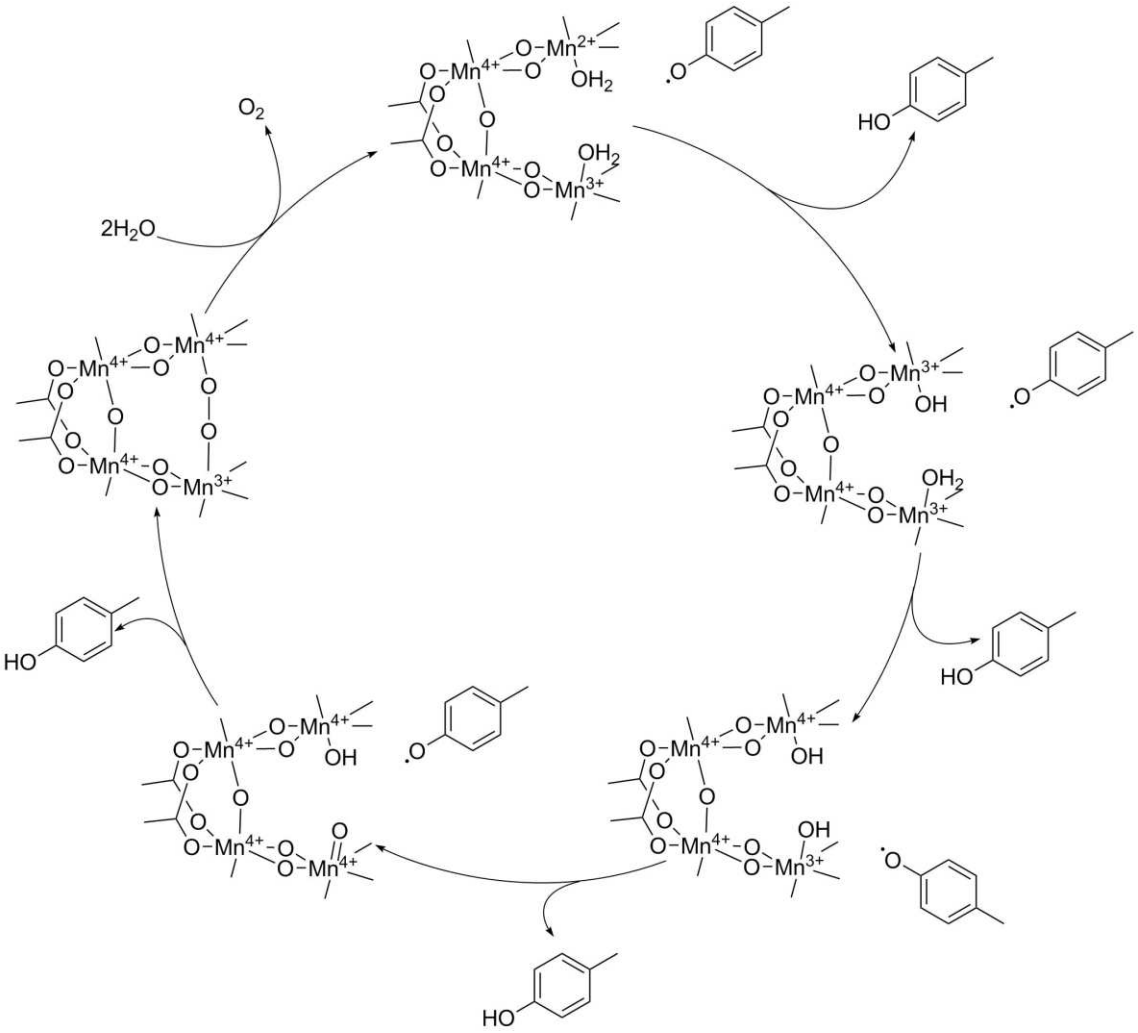

Scheme 1.2. Proposed catalytic cycle for the dehydrogenation of water and subsequent oxygen gas evolution by the OEC of photosystem II[37]

Another example of coordination-induced bond weakening in nature has been observed in the dehydrogenation and peroxidation of linoleic acid by soybean lipoxygenase-1.[38] In this process, shown in Scheme 1.3, an iron(II)-aqua species is generated within soybean lipoxygenase-1 and subsequently undergoes formal hydrogen atom transfer to a previously generated organoperoxy radical. Although direct thermochemical measurements are not reported in the literature, the O-H BDFE of water is estimated to be about 35 kcal/mol higher than the product peroxide O-H bond, necessitating significant homolytic bond weakening in the iron(II)-aqua complex.[39,40]

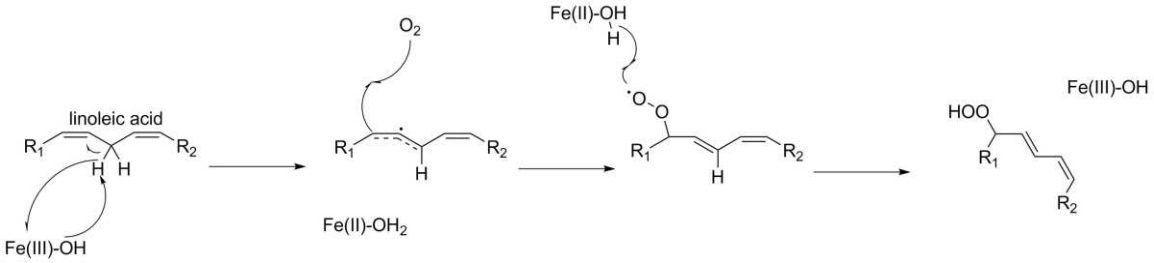

Scheme 1.3. Proposed pathway for linoleic acid dehydrogenation and peroxidation facilitated by the iron(III)-hydroxide core of soybean lipoxygenase-1[38]

1.3.2 Coordination-Induced Bond Weakening in Complexes of Main Group Metalloids and Transition Metals with Small Molecule Ligands

One outstanding challenge in modern chemistry is the development of water splitting methods for artificial photosynthesis. However, the high O-H BDFE of water (106.6 kcal/mol) presents a substantial barrier to these efforts.[41] Another similar challenge in modern chemistry is the development of methods for the transportation and storage of hydrogen fuel. Ammonia has been proposed as a hydrogen fuel storage medium given the existing global infrastructure and well established protocols for its transportation and storage.[42–45] Much as with water splitting, ammonia dehydrogenation is complicated by an N-H BDFE of 95.5 kcal/mol.[41] Given the ability of coordination-induced bond weakening systems to facilitate homolytic cleavage in otherwise strong X-H bonds, it is a promising strategy for the dehydrogenation of both ammonia and water.[32,46]

1.3.2.1 Coordination-Induced Bond Weakening in Complexes of Main Group Metalloids with Small Molecule Ligands

The first report of coordination-induced bond weakening in synthesis comes from Wood and coworkers in the course of their studies of the trialkylborane-water mediated catalytic deoxygenation of xanthates (Scheme 1.4).[35] After an isotopic labeling study

confirmed hydrogen atom abstraction from water, it was posited that water coordination to a trialkylborane induces homolytic activation of the water O-H bond. Using density functional theory (DFT) modeling this activation was quantified to an approximately 43 kcal/mol decrease in the O-H BDE of water upon coordination to trimethylborane.

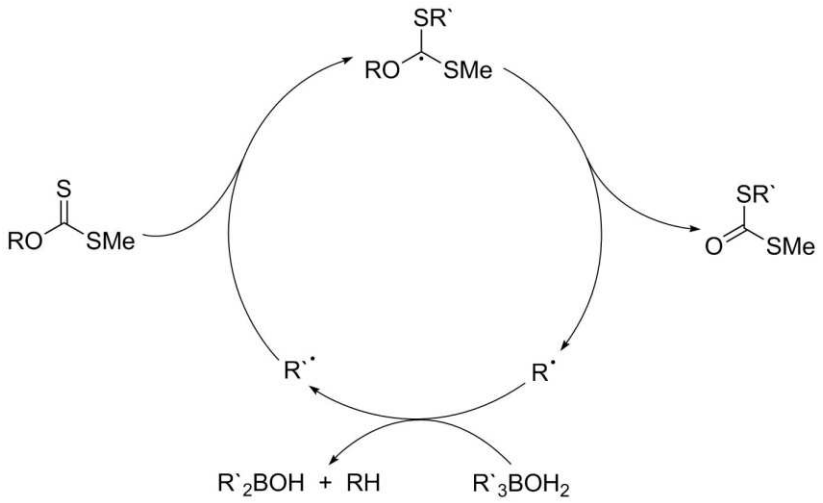

Scheme 1.4. Proposed catalytic cycle for the trialkylborane-water mediated reduction of xanthates[35]

Fu and coworkers described another instance of main group element-coordination-induced bond weakening in their report on amine N-H bond weakening by a germanium(III) corrole complex, [(TPFC)Ge(TEMPO)] (TPFC = tris(pentafluorophenyl)corrole, TEMPO = 2,2,6,6-tetramethylpiperidine 1-oxyl).[36] The addition of any of several amines, including ammonia, to [(TPFC)Ge(TEMPO)] was found to result in the formation of a dehydrogenated (TPFC)Ge-amido complex and TEMPOH (Scheme 1.5). A significant rate enhancement was observed for the reaction upon exposure to visible light, although the reaction was also found to proceed in the dark, indicating the presence of a photolytic pathway for the cleavage of the Ge-O bond in the initial [(TPFC)Ge(TEMPO)] complex. Although the authors do not report the degree of N-H bond weakening of the amine H-atom donors upon coordination to

germanium, we have calculated a difference in X-H BDFE between ammonia and TEMPOH of almost 46 kcal/mol, indicating significant N-H bond weakening in the germanium-amine complex.[41]

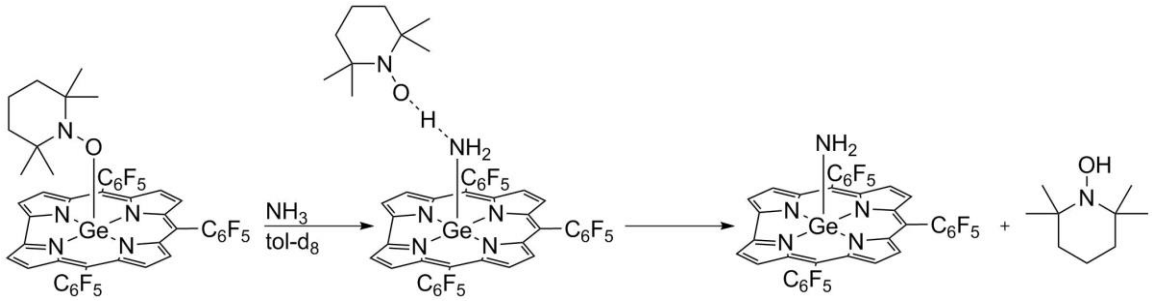

Scheme 1.5. Proposed mechanism for (TPFC)Ge-mediated hydrogen atom transfer from ammonia to TEMPO[36]

1.3.2.2 Coordination-Induced Bond Weakening in Complexes of Group IV Metals with Small Molecule Ligands

Low-valent titanium complexes are popular platforms for the study of transition metal bond weakening reductions.[34,47–49] Low-valent titanocene in particular is well represented in the coordination-induced bond weakening literature. Cuerva and coworkers were the first to demonstrate the efficacy of titanocene(III) chloride as a bond weakening platform in their report on the titanocene(III)-chloride-water mediated reduction of epoxides (Scheme 1.6).[49] Computational modeling revealed an O-H BDE of 49.4 kcal/mol for water upon coordination to titanocene(III)-chloride concomitant with a bond weakening of 58.6 kcal/mol.

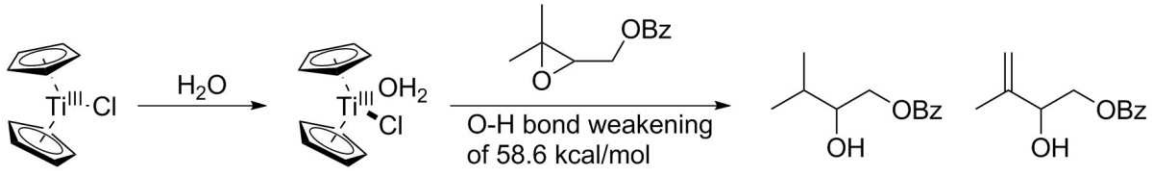

Scheme 1.6. Proposed reaction scheme for the reduction of an epoxide by Cp_2TiCl-water[49]

A subsequent investigation of the Cp_2TiCl-water system by van Gastel and coworkers revealed the necessity of chloride ligand dissociation from titanium preceding formal hydrogen atom transfer by a titanocene reagent coordinated to either one or two water ligands (Figure 1.2).[50] Using this corrected structure, we have calculated a BDFE of 47.4 kcal/mol for $Cp_2Ti(H_2O)_2$ and 51.7 kcal/mol for $Cp_2Ti(H_2O)$.[41]

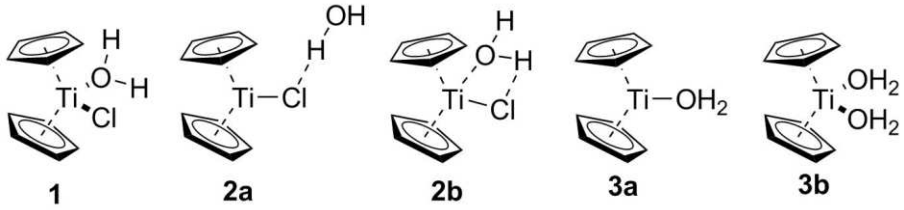

Figure 1.2. Proposed titanocene(III) aqua complexes. **1** not observed, **2a** and **2b** not observed in THF. **3a** and **3b** confirmed as active reductant structures[50]

Chirik and coworkers studied a series of four-coordinate titanocene derivatives, $(\eta^5\text{-}C_5Me_4SiMe_3)_2Ti^{III}(Cl)L$ (L = amine).[31] The researchers were able to isolate and interconvert at least three corners of the Bordwell thermodynamic square for the ammonia-containing complex $(\eta^5\text{-}C_5Me_4SiMe_3)_2Ti(Cl)NH_3$, shown in Scheme 1.7, allowing for the experimental determination of an N-H BDFE range of 52-65 kcal/mol for the complex. This was in good agreement with the calculated N-H BDFE value of 61 kcal/mol. A further report by the Chirik group described the related complex $(\eta^5\text{-}C_5Me_4SiMe_3)_2Ti^{III}(NH_3)$.[51] By observing the range of H-atom donors and acceptors capable of reducing $(\eta^5\text{-}C_5Me_4SiMe_3)_2Ti^{IV}(NH_2)$ and oxidizing $(\eta^5\text{-}C_5Me_4SiMe_3)_2Ti^{III}(NH_3)$, respectively, an N-H BDFE range of 35-48 kcal/mol was determined for $(\eta^5\text{-}C_5Me_4SiMe_3)_2Ti^{III}(NH_3)$, again in good agreement with the calculated N-H BDFE value of 42 kcal/mol.

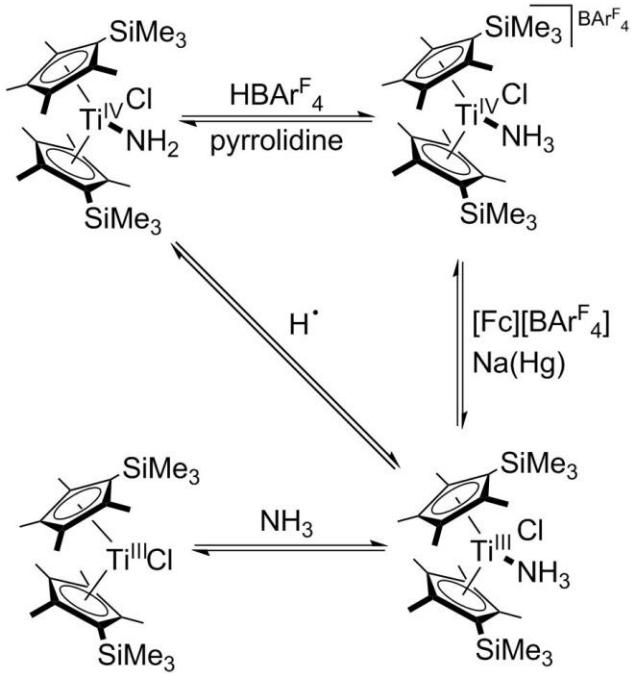

Scheme 1.7. Thermochemical cycle for the interconversion of $(\eta^5\text{-}C_5Me_4SiMe_3)_2Ti(Cl)NH_3$ with $(\eta^5\text{-}C_5Me_4SiMe_3)_2Ti(Cl)NH_2$[31]

The Chirik group extended their investigations to include a number of other small molecule amine $(\eta^5\text{-}C_5Me_4SiMe_3)_2Ti^{III}$ complexes.[51] Of particular interest among these complexes are those shown in Figure 1.3 containing unsubstituted hydrazine, iminyl, and hydrazide ligands. Notably, each of these ligands is a potential intermediate in the reduction of nitrogen gas to ammonia. Calculated N-H BDFE values were reported for each complex although the instability of $(\eta^5\text{-}C_5Me_4SiMe_3)_2Ti^{III}(N_2H_4)$ and $(\eta^5\text{-}C_5Me_4SiMe_3)_2Ti^{III}(N_2H_3)$ precluded experimental validation of the calculations.

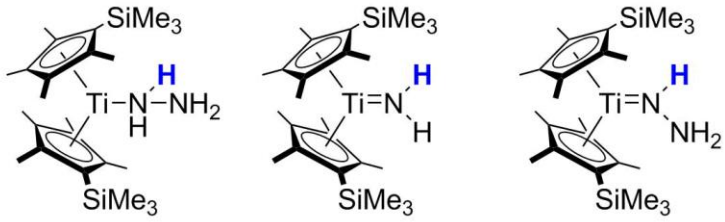

BDFE (calc)	42	79	67
BDFE (exp)	-	>77	-

Figure 1.3. $(\eta^5\text{-}C_5Me_4SiMe_3)_2Ti^{III}(N_2H_4)$, $(\eta^5\text{-}C_5Me_4SiMe_3)_2Ti^{III}(NH_2)$, and $(\eta^5\text{-}C_5Me_4SiMe_3)_2Ti^{III}(N_2H_3)$ with associated N-H BDFE values[51]

While the majority of Group IV bond weakening systems have utilized low-valent titanium, Cuerva and coworkers also computationally analyzed the O-H BDEs of $Cp_2ZrCl(OH_2)$ and $Cp_2HfCl(OH_2)$, determining values of 25.5 and 13.7 kcal/mol, respectively.[52] Similarly, Chirik and coworkers synthesized the zirconium(III) complex $(\eta^5\text{-}C_5Me_4SiMe_3)_2Zr(Cl)NH_3$ and experimentally determined an N-H BDFE range of 35 to 48 kcal/mol, in good agreement with the computationally determined 41 kcal/mol N-H BDFE.[51]

1.3.2.3 Coordination-Induced Bond Weakening in Complexes of Group VI Metals with Small Molecule Ligands

In addition to their work on coordination-induced bond weakening in Group IV systems, Chirik and coworkers also studied the molybdenum(I)-terpyridine complex $(^{Ph}Tpy)(PPh_2Me)_2Mo(NH_3)^+$ (^{Ph}Tpy = 4`-Ph-2,2`,6`,2``-terpyridine), shown in Scheme 1.8.[34] In the initial report on this complex, the Bordwell relation was used to determine an empirical N-H BDFE of 45.8 kcal/mol for $(^{Ph}Tpy)(PPh_2Me)_2Mo(NH_3)^+$. This value was supported by the calculation of an N-H BDFE value of 45.1 kcal/mol. The experimental determination of X-H BDFEs for the related complexes $(^{Ph}Tpy)(PPh_2Me)_2Mo(OH_2)^+$ and $(^{Ph}Tpy)(PPh_2Me)_2Mo(\kappa^2\text{-}N_2H_4)^+$ was precluded by their rapid decomposition to form hydrogen gas in solution. Computational modeling revealed an O-H BDFE of 33.7 kcal/mol for $(^{Ph}Tpy)(PPh_2Me)_2Mo(OH_2)^+$ and an N-H BDFE of 34.6 kcal/mol for $(^{Ph}Tpy)(PPh_2Me)_2Mo(\kappa^2\text{-}N_2H_4)^+$.

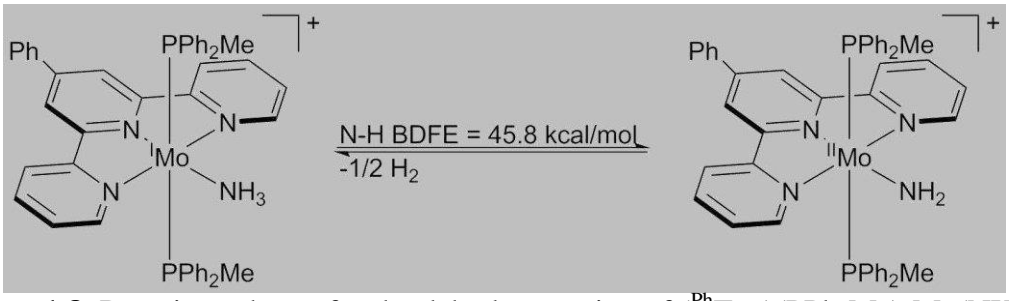

Scheme 1.8. Reaction scheme for the dehydrogenation of $(^{Ph}Tpy)(PPh_2Me)_2Mo(NH_3)^+$ to form $(^{Ph}Tpy)(PPh_2Me)_2Mo(NH_2)^{+}$[34]

Chirik and coworkers further sought to examine the effects of varying metal oxidation state on the redox potential, N-H bond acidity, and N-H BDFE of $(^{Ph}Tpy)(PPh_2Me)_2Mo(NH_3)$ complexes.[34] To this end, the Mo(0), Mo(I), and Mo(II) complexes; $(^{Ph}Tpy)(PPh_2Me)_2Mo(NH_3)^0$, $(^{Ph}Tpy)(PPh_2Me)_2Mo(NH_3)^+$, and $(^{Ph}Tpy)(PPh_2Me)_2Mo(NH_3)^{2+}$ were synthesized and electrochemically characterized. The electrochemical redox potentials were then applied to the Bordwell equation alongside the computationally determined N-H BDFEs of 34.5, 45.1, and 55.9 kcal/mol for the $Mo^{0/I/II}$ species respectively to yield the relevant N-H pK_as of 20.1, 3.6, and 2.2. The researchers found the uniformity in ΔBDFE between each redox couple remarkable, particularly given the relatively large change in N-H pK_a between the $Mo^{0/I}$ couple compared to the $Mo^{I/II}$ couple. This suggests that the predominant driving force for H-atom loss varies with changes in the oxidation state of the metal center. Specifically in the case of $(^{Ph}Tpy)(PPh_2Me)_2Mo(NH_3)^0$, the redox potential of molybdenum is noted as the predominant driving force for dehydrogenation.

Continuing their investigations of low-valent molybdenum, the Chirik group sought to examine the mechanism of hydrogen gas evolution from $(^{Ph}Tpy)(PPh_2Me)_2Mo(NH_3)^+$.[53] This endeavor was complicated by the lability of the N-H bonds in both the $(^{Ph}Tpy)(PPh_2Me)_2Mo(NH_3)^+$ reagent and $(^{Ph}Tpy)(PPh_2Me)_2Mo(NH_2)^+$

product, which enabled reagent-product deuterium scrambling and precluded deuterium labeling studies. Chirik and coworkers therefore prepared the Mo^{I}-pyrrolidine complex $(^{Ph}Tpy)(PPh_2Me)_2Mo(C_4H_9N)^+$, shown in Scheme 1.9.

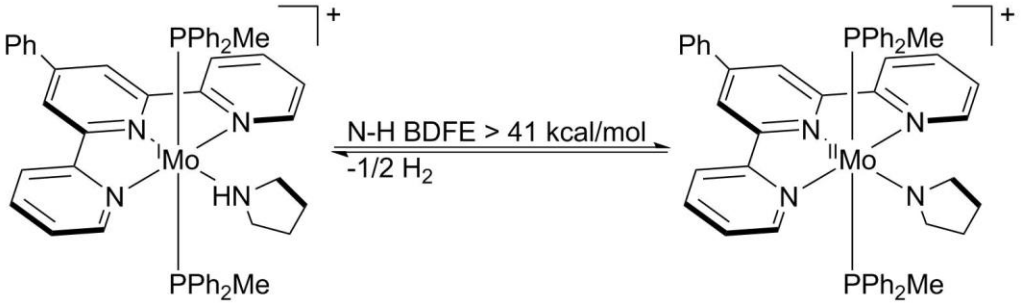

Scheme 1.9. Reaction scheme for the dehydrogenation of $(^{Ph}Tpy)(PPh_2Me)_2Mo(C_4H_9N)^+$ to form $(^{Ph}Tpy)(PPh_2Me)_2Mo(C_4H_8N)^+$[53]

Deuterium labeling studies undertaken via N-deuteration of pyrrolidine revealed a unimolecular hydrogen gas evolution pathway as well as low deuterium incorporation in the hydrogen gas product. The researchers identified the balance of the deuterium label on the α-carbons of the oxidized complex pyrrolidide ligand. This deuterium scrambling was confirmed to be concomitant with phosphine ligand dissociation followed by Mo^{III}-hydride formation by the observation of both ligand deuteration and hydrogen gas evolution inhibition in the presence of excess PPh_2Me. Applying this model to the $(^{Ph}Tpy)(PPh_2Me)_2Mo(NH_3)^+$ system, Chirik and coworkers proposed the unimolecular hydrogen gas evolution pathway shown in Scheme 1.10.

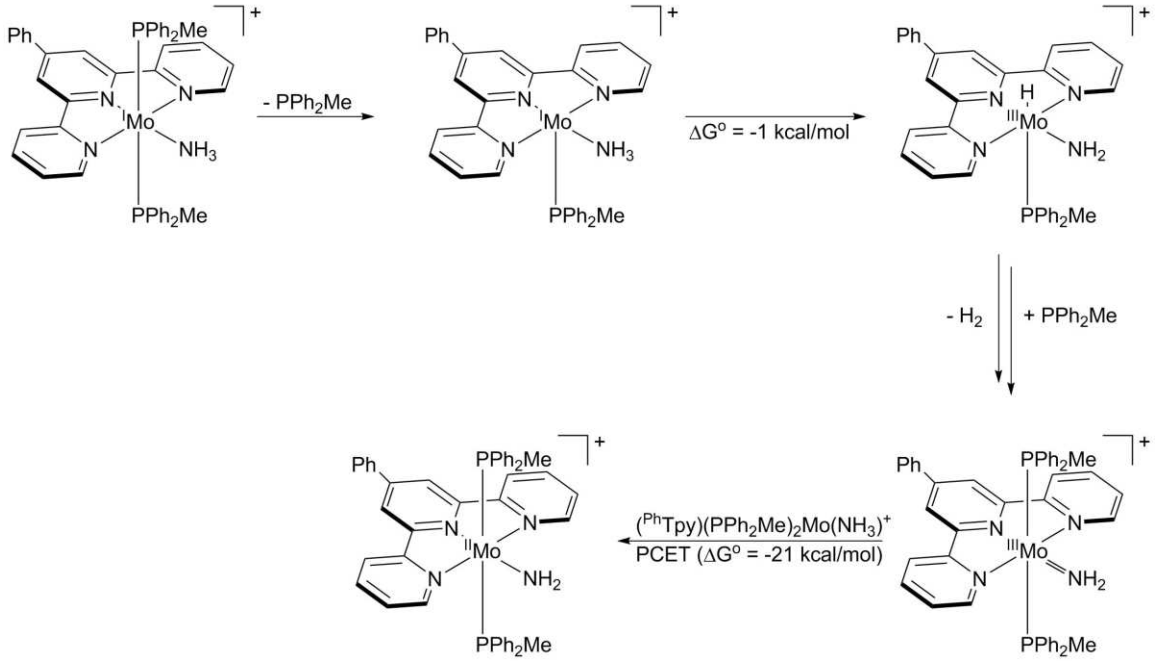

Scheme 1.10. Proposed pathway for H_2 gas evolution from $(^{Ph}Tpy)(PPh_2Me)_2Mo(NH_3)^{+}$[53]

1.3.2.4 Coordination-Induced Bond Weakening in Group VIII Complexes with Small Molecule Ligands

Iron complexes are commonly employed for a wide range of chemical processes due to the high abundance and low cost of elemental iron.[54] Since iron is also known to facilitate coordination-induced bond weakening in natural systems, low-valent iron is of considerable interest for the development of synthetic bond weakening systems.[38] Kovacs and coworkers reported one such iron(II) coordination-induced bond weakening system, $[Fe^{II}(O^{Me2}N_4(tren))(H_2O)]^{+}$ (tren = tris(2-aminoethyl)amine), shown in Scheme 1.11.[55]

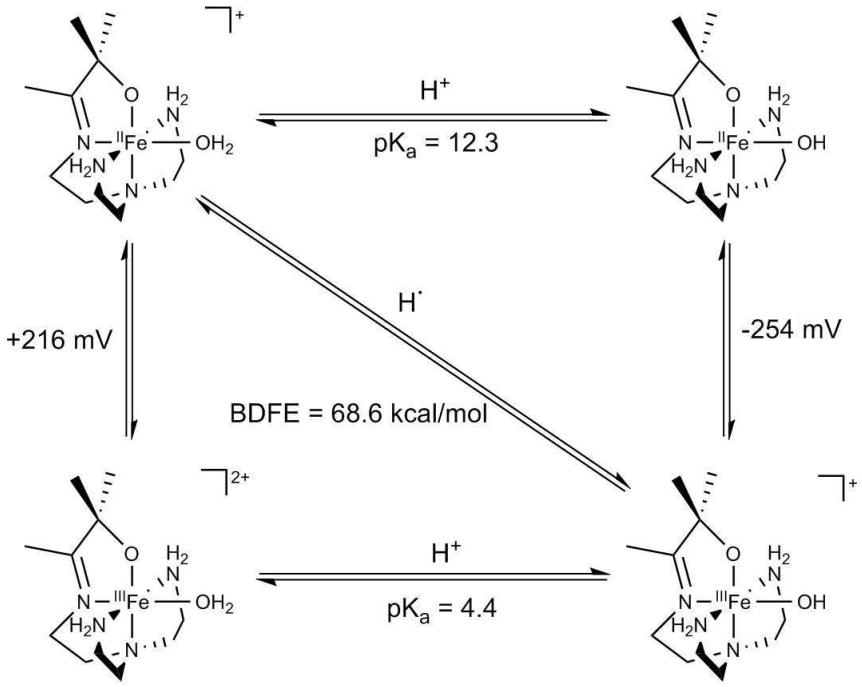

Scheme 1.11. Thermochemical cycle for the interconversion of $[Fe^{II}(O^{Me2}N_4(tren))(H_2O)]^+$ with $[Fe^{III}(O^{Me2}N_4(tren))(OH)]^{+55}$

Notably, each of the four compounds at the corners of the Bordwell thermochemical cycle shown in Scheme 1.11 was isolated and characterized. This enabled the measurement of the relevant redox potentials and O-H bond acidities to determine an O-H BDFE of 68.6 kcal/mol for $[Fe^{III}(O^{Me2}N_4(tren))(OH)]^+$. Comparison with the iron(II) aqua complex $[Fe(OH_2)_6]^{2+}$ revealed an additional 10.9 kcal/mol of bond weakening for $[Fe^{III}(O^{Me2}N_4(tren))(OH)]^+$. This difference in O-H BDFE was attributed to the greater electron donating character of the $O^{Me2}N_4(tren)$ ligand, highlighting the importance of ligand identity in coordination-induced bond weakening systems.

1.3.2.5 Coordination-Induced Bond Weakening in Complexes of Group XI Metals with Small Molecule Ligands

Due to the highly reducing nature of coordination-induced bond weakening systems, they often need to be prepared and used under inert conditions. The catalytic copper(I) (bpy)Cu^I(NMI) (bpy = 2,2`-bipyridine, NMI = N-methylimidazole) TEMPO

system reported by Stahl and coworkers is unique in this context, as it operates under air.[56] The (bpy)Cu^{I}(NMI) system is also unique among bond weakening systems in the literature for its incorporation of various primary alcohols as proton sources, facilitating their conversion to aldehydes.

Using IR kinetic studies, Stahl and coworkers determined a first order dependence on O_2 and a second order dependence on (bpy)Cu^{I}(NMI) at low catalyst concentrations, falling to unity at higher [(bpy)Cu^{I}(NMI)]. A zeroth order rate dependence was determined for both TEMPO and the alcohol proton source in the case of a benzyl alcohol while in the case of an aliphatic alcohol, both the alcohol substrate and TEMPO were found to have first order rate contributions. These results were combined to propose the catalytic cycle shown in Scheme 1.12, wherein molecular oxygen serves as a bridging ligand for two (bpy)Cu^{I}(NMI) complexes, facilitating reduction of the Cu dimer complex by TEMPOH, which enables subsequent oxygen abstraction from (bpy)Cu^{II}(NMI)-peroxide by water to form the (bpy)Cu^{I}(NMI)-hydroxyl species. This complex then deprotonates the alcohol substrate, providing a (bpy)Cu^{I}(NMI)-alkoxide, which undergoes hydrogen atom abstraction by TEMPO, regenerating (bpy)Cu^{I}(NMI) and yielding the aldehyde product.

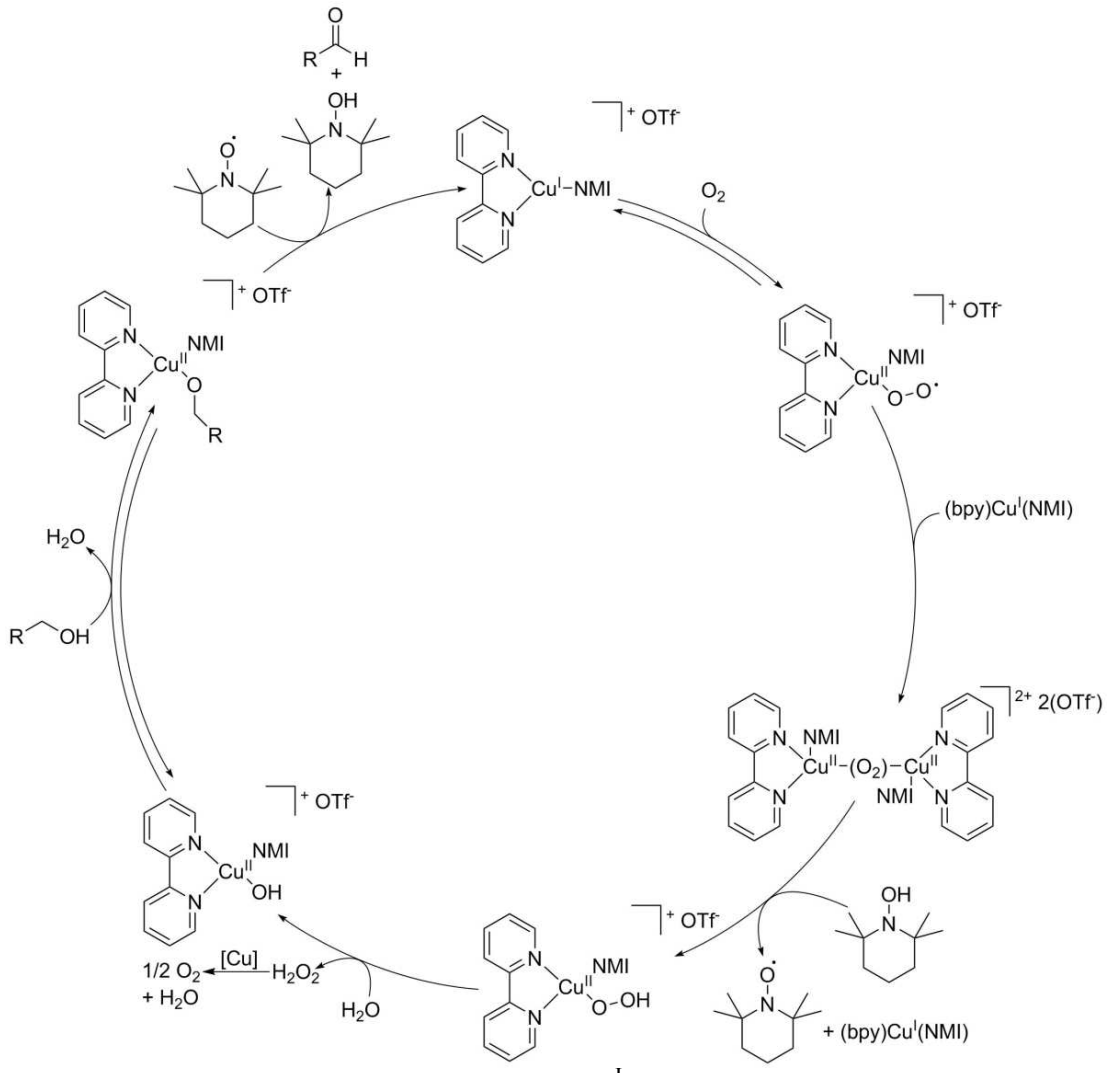

Scheme 1.12. Proposed catalytic cycle for the Cu^{I}-TEMPO mediated aerobic oxidation of primary alcohols[56]

1.3.3 Coordination-Induced Bond Weakening in Complexes of Transition Metals with Large Ligands

Small molecules like water and ammonia have received a great deal of attention as coordination-induced bond weakening ligands due to their desirability as chemical feedstocks. However large ligand proton donors have also been shown to form potent reductants in conjunction with low-valent metals. Remarkably, many of these complexes have demonstrated the potential to be tuned against hydrogen gas evolution and towards a variety of productive substrate reductions.[57,58]

1.3.3.1 Coordination-Induced Bond Weakening in Complexes of Group IV Metals with Large Ligands

Continuing the use of low-valent titanocenes as bond weakening platforms, Knowles and coworkers described the 5-exo-trig reductive cyclization of a range of N-aryl amides mediated by a catalytic Cp^*_2TiCl TEMPO system (Scheme 1.13).[34] Upon coordination of the amide oxygen to the titanium(III) metal center, significant N-H bond weakening of at least 36 kcal/mol in the amide species facilitates formal hydrogen atom transfer to TEMPO. The formed TEMPOH subsequently reduces the substrate olefin, promoting ring closure and product formation.

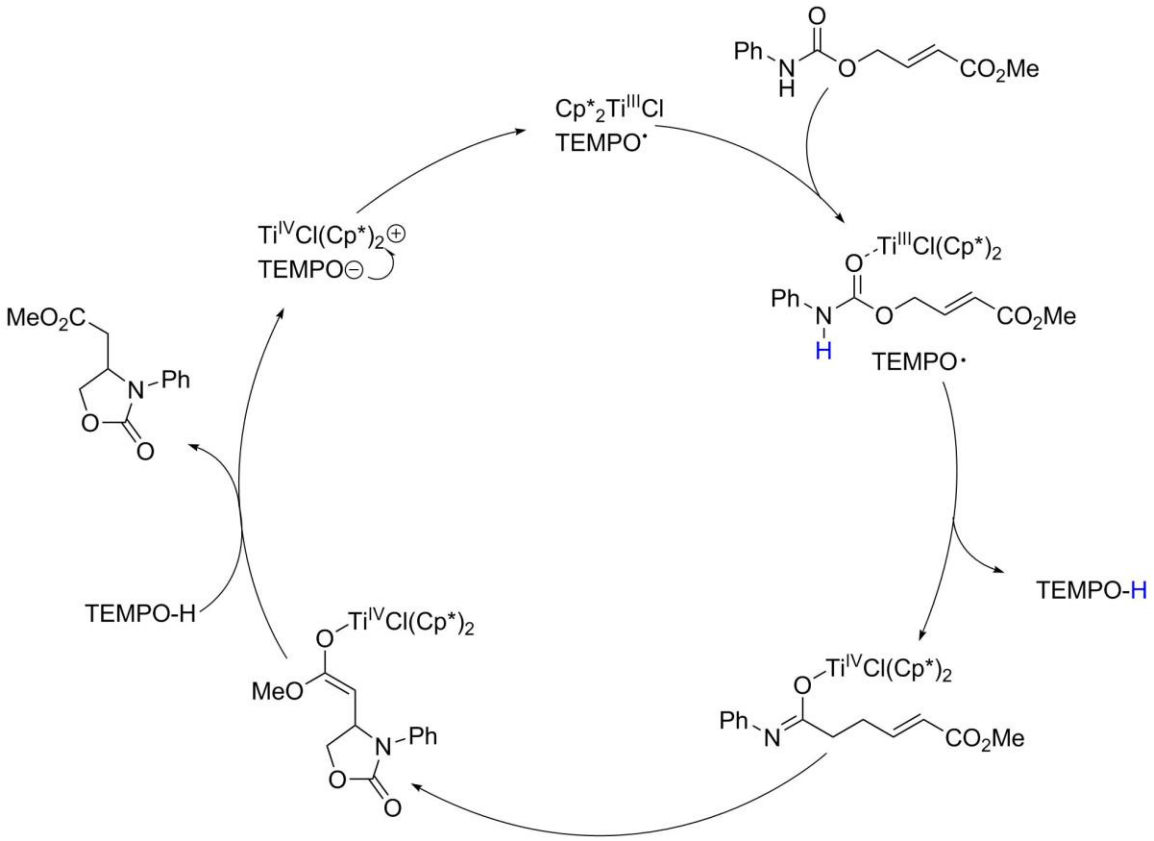

Scheme 1.13. Proposed catalytic cycle for Cp^*_2TiCl mediated 5-exo-trig radical cyclization of an N-aryl amide[34]

A report by Gansäuer and coworkers describes another titanocene-amide N-H bond weakening system.[47] Notably, the amide moiety in this work was appended to one

of the titanocene cyclopentadienyl ligands as shown in Scheme 1.14. Computational modeling of the cyclic form of the catalyst revealed a titanium(III) coordination-induced amide N-H ΔBDE of approximately 39 kcal/mol. This was found to be sufficient for the catalyst to promote the reductive ring opening of a wide range of functionalized epoxides.

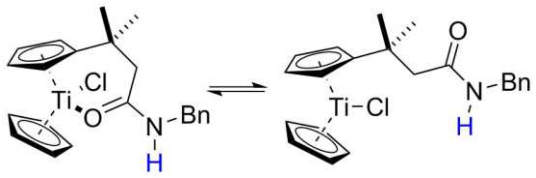

Scheme 1.14. Reaction scheme for the interconversion of the cyclic and acyclic active forms of the amide-pendant titanocene catalyst developed by Gansäuer and coworkers[47]

Remarkably, chiral modification of the titanocene catalyst as shown in Figure 1.4 promoted a diastereoselective epoxide ring opening with an enantiomeric ratio of 86:14. Further modifying the speciation of the N-benzyl group yielded only a slight increase in the diastereoselectivity of the catalyst, as did changing the solvent from THF to toluene. However, both Wilkinson's catalyst [$Rh(PPh_3)_3Cl$] and Crabtree's catalyst [$Ir(cod)PyPCy_3$]PF_6 were readily hydrogenated by the titanocene catalyst shown in Scheme 1.14 without the need for hydrogen gas and at temperatures as low as 10°C.[47,59,60] Subsequent epoxide ring opening by the activated Wilkinson's catalyst or Crabtree's catalyst was found to have an enantiomeric ratio as high as 95.5:4.5.

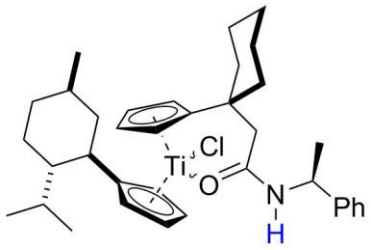

Figure 1.4. Functionalized titanocene catalyst developed by Gansäuer and coworkers for the enantioselective reductive ring opening of epoxides[47]

1.3.3.2 Coordination-Induced Bond Weakening in Complexes of Group VIII Metals with Large Ligands

In addition to being earth abundant, iron is also prevalent in biological systems, including the large class of iron-porphyrin heme complexes.[61] Mayer and coworkers reported a study of one such iron(II)-tetraphenylporphyrin (Scheme 1.15) with a pair of 4-methyl-imidazole ligands serving as histidine analogs.[62] The N-H BDFE of these imidazole ligands was found to be approximately 70 kcal/mol by observing the equilibrium constants of reversible HAT transfer between the iron(II)-porphyrin complex and the hydrogen atom acceptors TEMPO and 1-4 benzoquinone.

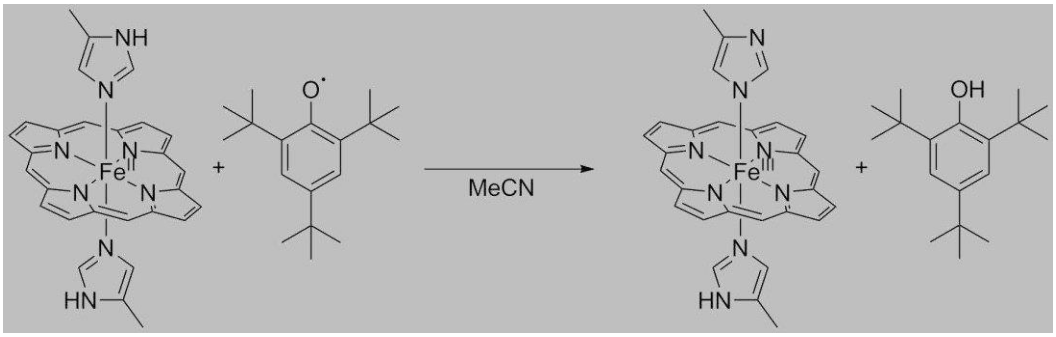

Scheme 1.15. Reaction scheme for hydrogen atom transfer from a 4-methyl-imidazole ligand on an iron(II)-porphyrin to a 2,4,6-tri-tert-butyl-phenoxy radical[62]

Following their report on η^5-ligand noninnocence in a ring-protonated Cp^*_2Co C-H bond weakening system *vide infra*, the Peters group reported an iron(II) half sandwich hydride complex $Fe(\eta^3{:}\eta^2\text{-Ind})(depe)H$ (Ind = indenide ($C_9H_7^-$), depe = 1,2-bis(diethylphosphino)ethane), shown in Scheme 1.16.[63] Oxidation of this complex by $[Fc]BAr^F_4$ ([Fc] = ferrocinium) yielded the iron(III) complex $[Fe(\eta^3{:}\eta^2\text{-Ind})(depe)H]BAr^F_4$. Electron paramagnetic resonance (EPR) spectroscopic observation of the formation of $[Fe(\eta^3{:}\eta^2\text{-Ind})(depe)H]BAr^F_4$ in solution revealed interconversion with an iron(I) complex, which was characterized by the researchers as $[Fe(\eta^6\text{-IndH})(depe)]BAr^F_4$ (Scheme 1.16). Computational analysis revealed an Fe-H and C-H

BDFE of approximately 50 kcal/mol for both the iron(III) and iron(I) complexes. The determination of this value was supported by spontaneous H_2 gas evolution from both complexes at room temperature in acetonitrile.

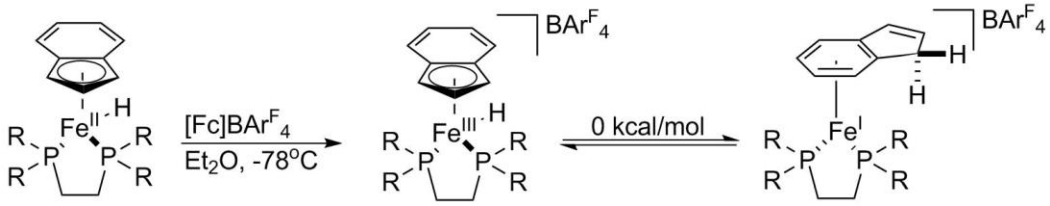

Scheme 1.16. Reaction scheme for the synthesis of [Fe(η^3:η^2-Ind)(depe)H]BAr$^F_4$ and resultant interconversion with the isoenergetic conformational isomer [Fe(η^6-IndH)(depe)]BAr$^F_4$[63]

Seeking to utilize this structural isomer interconversion for productive reductions, Peters and coworkers also studied the η^5-iron(III) half sandwich hydride complex, [Fe^{III}(η^5-Cp*)(dppe)H]$^+$ (dppe = 1,2-bis(diphenylphosphino)ethane).[58] This complex was previously reported to readily bind CO, forming an adduct that Peters and coworkers characterized as the ring-protonated species [Fe^I(*endo*- η^4-Cp*H)(dppe)(CO)]$^+$ (Scheme 1.17, top).[58] Dehydrogenation of [Fe^I(*endo*- η^4-Cp*H)(dppe)(CO)]$^+$ yielded [Cp*Fe^{II}(dppe)(CO)]$^+$. Subsequent protonation and oxidation of this iron(II) complex furnished [Fe^I(*exo*- η^4-Cp*H)(dppe)(CO)]$^+$ (Scheme 1.17, bottom). Using solvent-dependent relations for hydricity, redox potential, and homolytic bond strength, the researchers determined C-H BDFEs of 36 and 33.5 kcal/mol for the iron(I)-*endo* and -*exo* complexes, respectively.[64,65] These values were supported by the computational determination of similar values of 29 and 25 kcal/mol, respectively.

The Fe-H bond of [Fe^{III}(η^5-Cp*)(dppe)H]$^+$ was also analyzed experimentally and found to be less than 50 kcal/mol (DFT value 56 kcal/mol). Despite this weak bond, the hydride complex was found to be kinetically stable against hydrogen gas evolution at room temperature in ethereal solvents. Additionally, combination of [Fe^{III}(η^5-

Cp*)(dppe)H]$^+$ and azobenzene in solution produced no reaction. However, addition of CO to this solution initiated rapid formation of [Fe^I(*endo*- η^4-Cp*H)(dppe)(CO)]$^+$ and subsequent rapid PCET reduction of azobenzene to form 1,2-diphenylhydrazine (Scheme 1.17). Similar *in situ* preparation of [Fe^I(*exo*- η^4-Cp*H)(dppe)(CO)]$^+$ via the chemical oxidation of Fe(*exo*-η^4-Cp*H)(dppe)(CO) in the presence of azobenzene also resulted in rapid PCET substrate reduction. This use of molecular triggers to activate potent bond weakening systems *in situ* is a promising strategy for the development of reagents with exceptionally weak X-H bonds that can be prepared and stored under ambient conditions.

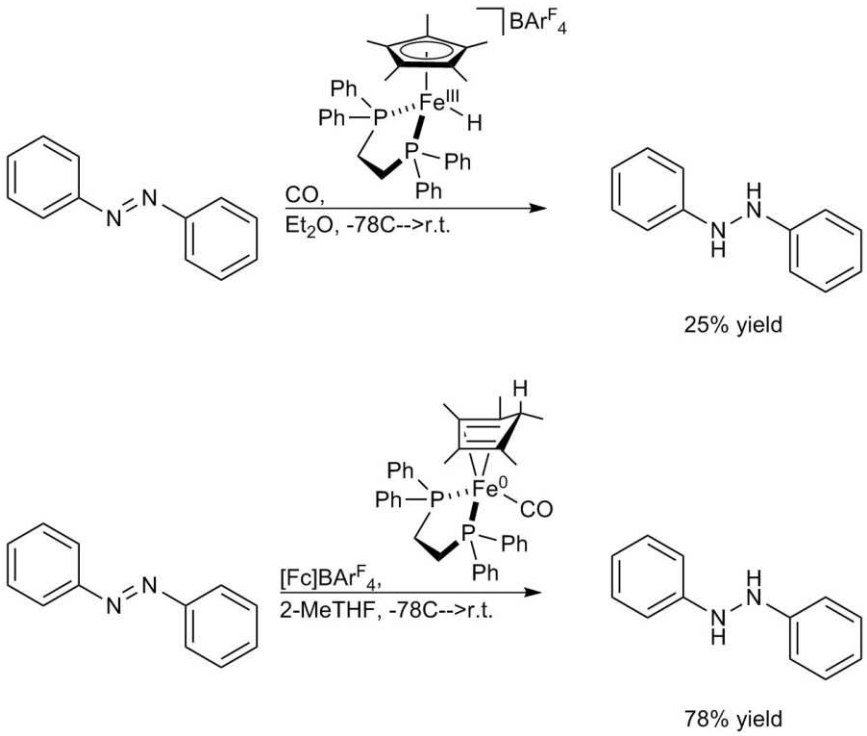

Scheme 1.17. Reaction schemes for the reduction of azobenzene by [Fe^I(*endo*-η^4-Cp*H)(dppe)(CO)]$^+$ (top) and [Fe^I(*exo*-η^4-Cp*H)(dppe)(CO)]$^+$ (bottom) with associated yields and DFT calculated C-H BDFEs[58]

The Mayer group also studied coordination-induced bond weakening in the heavier congeners of iron, ruthenium and osmium. The ruthenium(II) complex, Ru^{II}(acac)$_2$(py-imH) (acac = 2,4-pentanedionato, py-imH = 2-(2`-pyridyl)imidazole),

shown in Scheme 1.18, was synthesized and the oxidized and dehydrogenated derivatives were also isolated, enabling the experimental determination of an N-H BDFE of 62.0 kcal/mol for $Ru^{II}(acac)_2$(py-imH).[66] This BDFE value was supported by spontaneous irreversible formal hydrogen atom transfer from $Ru^{II}(acac)_2$(py-imH) to TEMPO. Remarkably, the k_H/k_D for this reaction was found to be approximately 23 at 25°C, which is consistent with a hydrogen atom tunneling pathway in the dehydrogenation of $Ru^{II}(acac)_2$(py-imH).[67]

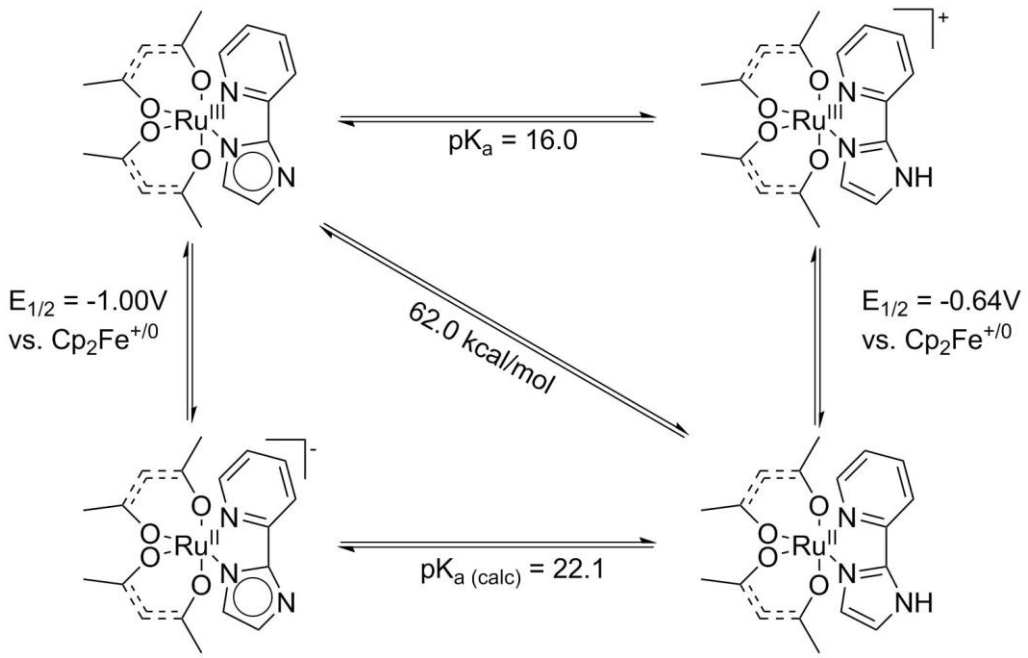

Scheme 1.18. Thermochemical cycle for the interconversion of $Ru^{II}(acac)_2$(py-imH) with $Ru^{III}(acac)_2$(py-im)[66]

Mayer and coworkers also examined hydrogen atom donation from the methyl-perfluorinated derivative $Ru^{II}(hfac)_2$(py-imH) (hfac = 1,1,1,5,5,5-hexafluoro-2,4-pentanedionato).[66] Isolation of the oxidized and dehydrogenated species enabled the determination of an N-H BDFE of 79.6 kcal/mol for the complex. The lesser degree of bond weakening in $Ru^{II}(hfac)_2$(py-imH) compared to $Ru^{II}(acac)_2$(py-imH) was attributed

to the relatively electron poor character of the fluorinated ligands, creating a less electron rich metal center and thus a weaker reductant.

Derivatives of $Ru^{II}(acac)_2$(py-imH) and $Ru^{II}(hfac)_2$(py-imH) with partially saturated imidazoline moieties, shown in Scheme 1.19, were also prepared by the Mayer group.[66] These complexes were found to react gradually with excess TEMPO to yield three and two equivalents of TEMPOH along with $Ru^{III}(acac)_2$(py-im) and $Ru^{II}(hfac)_2$(py-imH), respectively. This serial dehydrogenation was proposed to proceed through a Ru^{IV} intermediate since it was not observed for analogous iron complexes, which would need to pass through energetically inaccessibly Fe^{IV} states.[68–73]

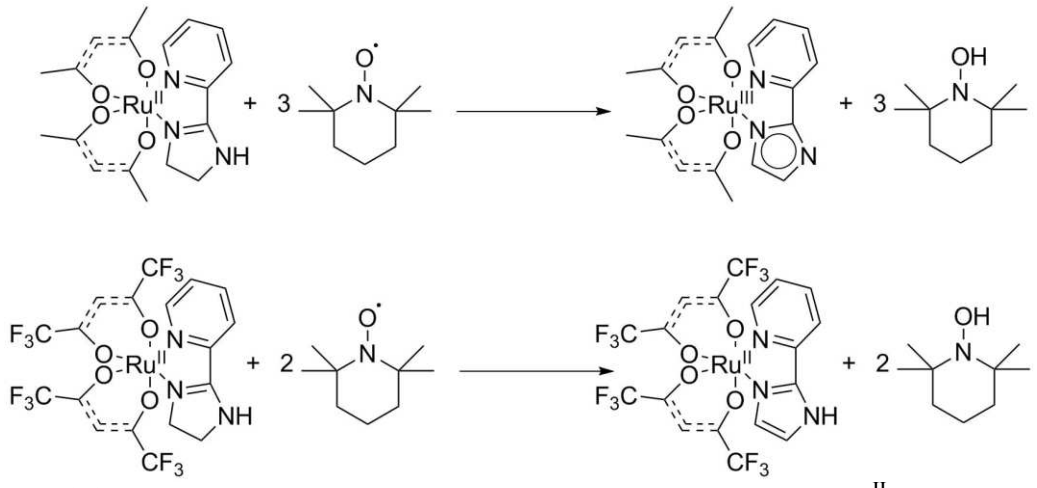

Scheme 1.19. Reaction scheme for the serial dehydrogenation of $Ru^{II}(acac)_2$(py-imH) and $Ru^{II}(hfac)_2$(py-imH) imidazoline derivatives by excess TEMPO[66]

In their investigation of $Os^{III/IV}$ complexes, Mayer and coworkers isolated and characterized the (Tp)Os-aniline and -anilido (Tp = hydrotris(1-pyrazolyl)borate) complexes constituting all four corners of the Bordwell thermochemical cycle shown in Scheme 1.20.[74] Irreversible formal hydrogen atom transfer from $(Tp)Os^{III}$-aniline to both TEMPO and di-tert-butyl nitroxide supported the determination of an N-H BDFE of 66 kcal/mol furnished by the Bordwell relation.[75]

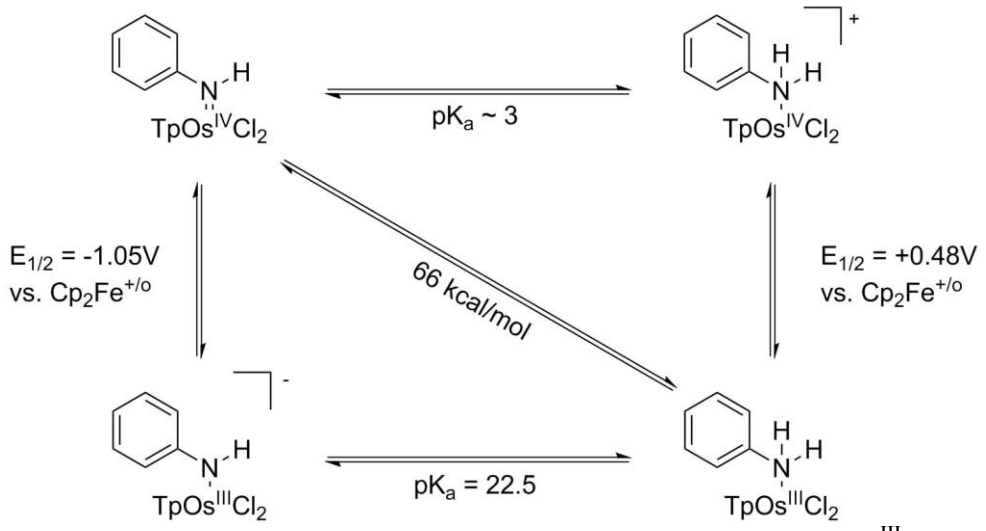

Scheme 1.20. Thermochemical cycle for the interconversion of (Tp)Os^{III}-aniline with (Tp)Os^{IV}-anilido[74]

1.3.3.3 Coordination-Induced Bond Weakening in Complexes of Group IX Metals with Large Ligands

The initial study of ring-protonated sandwich and half-sandwich complexes by Peters and coworkers began with the discovery of C-H bond formation in Cp*$_2$Co treated with HBAr$^F_4$, forming Cp*(η^4-C$_5$Me$_5$H)Co.[76] EPR spectroscopy confirmed the presence of both the *endo*- and *exo*- isomers of Cp*(η^4-C$_5$Me$_5$H)Co, shown in Figure 1.5. The observation of hydride transfer from Cp*(η^4-C$_5$Me$_5$H)Co$^+$ to [Pt(dmpe)$_2$]$^{2+}$ (dmpe = 1,2-dimethylphosphinoethane) revealed an upper limit of 29 kcal/mol for the C-H BDFE of Cp*(η^4-C$_5$Me$_5$H)Co$^+$, which was found to be in good agreement with the calculated value of 23 kcal/mol.

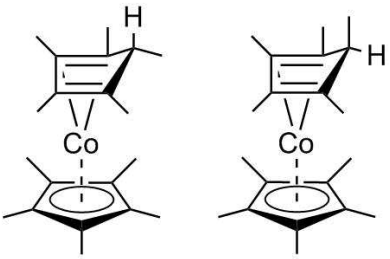

Figure 1.5. Cp*(*exo*-η^4-C$_5$Me$_5$H)Co (left) and Cp*(*endo*-η^4-C$_5$Me$_5$H)Co (right)[76]

Peters and coworkers also studied the low-valent cobalt complex $[(Cp)Co^{III}(Cp^{NH})]^+$ (Cp^N = 4-N,N-dimethylanilinecyclopentyldienyl), shown in Scheme 1.21, which contains a spatially separated proton donor and metal redox center.[77] Equilibrium pK_a experiments and electrochemical redox measurements revealed an N-H BDFE of approximately 39 kcal/mol, 40 kcal/mol weaker than the N-H BDFE of uncomplexed aniline. Applying this weak N-H bond to PCET catalysis, the researchers performed the $[(Cp)Co^{III}(Cp^{NH})]^+$-mediated reductive coupling of acetophenone using an electrochemical cell and excess acid to regenerate the pendant-amine cobaltocene catalyst.

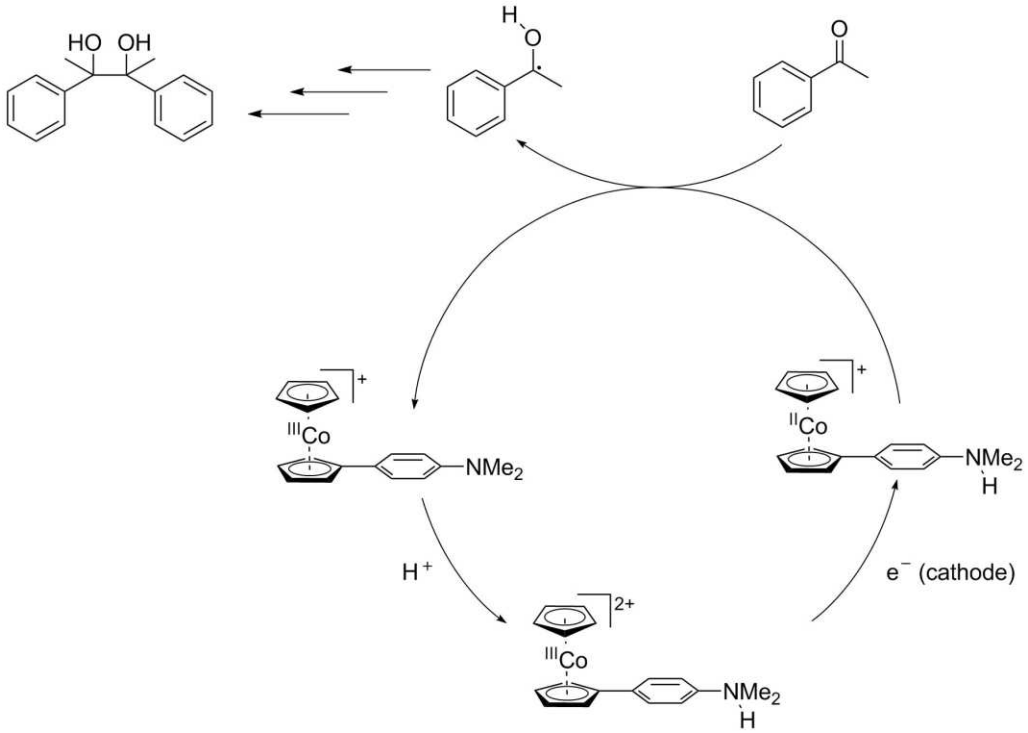

Scheme 1.21. Proposed catalytic cycle for the electrocatalytic reductive coupling of acetophenone by $[(Cp)Co^{III}(Cp^{NH})]^+$[77]

In subsequent work, Peters and coworkers expanded the reductive scope of electrocatalytic $[(Cp)Co^{III}(Cp^{NH})]^+$ to include C-C π bonds, using fumarates as model substrates.[57] Kinetic analysis of this reaction revealed a dynamic mechanism dependent

on the concentration of substrate, which is consistent with the catalytic cycle shown in Scheme 1.22 in which the rate limiting step is the initial PCET reduction of the fumarate at low substrate concentrations. At high substrate concentrations, Peters and coworkers proposed that protonation of the reduced fumarate substrate becomes rate limiting. Notably, regardless of substrate, hydrogen gas evolution from $[(Cp)Co^{III}(Cp^{NH})]^+$ was significantly decreased compared to $Cp(\eta^4\text{-}C_5H_6)Co^+$ despite the similar X-H BDFEs of the two complexes.[57] Peters and coworkers attributed this reduced rate of hydrogen gas evolution to the distance between the cobalt(II) redox center and the N-H proton donor. This spatial separation was proposed to mitigate H_2 gas evolution via either reduction of the N-H functional group or protonation of the cobalt(II), leaving bimolecular association as the only remaining pathway. Moreover, it was posited that such a bimolecular association was likely to be inhibited by the electrostatic repulsion between the formally cationic $[(Cp)Co^{III}(Cp^{NH})]^+$ catalysts.

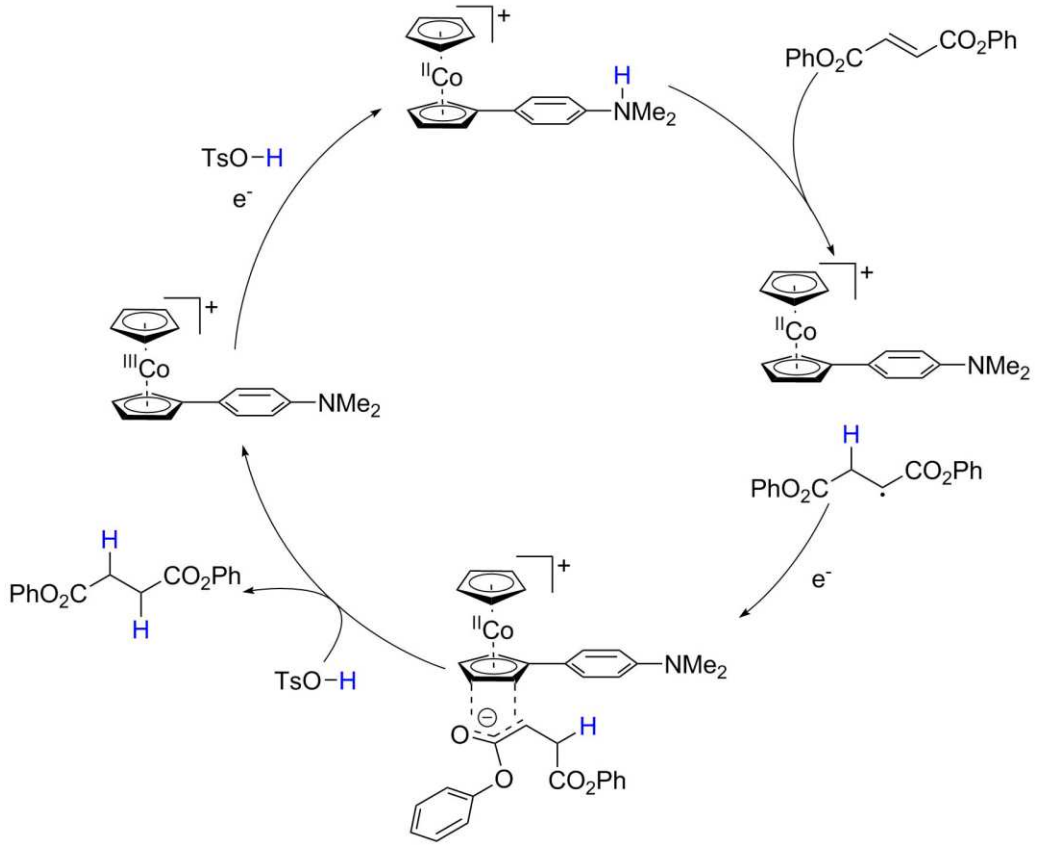

Scheme 1.22. Proposed catalytic cycle for the reduction of fumarates by $[(Cp)Co^{III}(Cp^{NH})]^{+}$[57]

1.3.3.4 Coordination-Induced Bond Weakening in Group X Metal Complexes with Large Ligands

In conjunction with their studies on the ring protonated cobalt(III) $Cp^*(\eta^4\text{-}C_5Me_5H)Co^+$, Peters and coworkers also investigated the related stable nickel(II) complex $Cp^*(\eta^4\text{-}C_5Me_5H)Ni^+$.[76] Upon electrochemical oxidation to $Cp^*(\eta^4\text{-}C_5Me_5H)Ni^{2+}$, the nickel(III) complex promotes a C-H bond weakening of nearly 20 kcal/mol to a C-H BDFE of 30 kcal/mol as determined by DFT. This weak C-H bond promotes rapid formal H-atom loss and concomitant formation of $Cp^*_2Ni^{2+}$ in solution.

1.3.3.5 Coordination-Induced Bond Weakening in Group XI Metal Complexes with Large Ligands

A report by Stack and coworkers describes an unusual instance of bond weakening in the three coordinate copper(II) complex, $[Cu^{II}(H33m)]^{2+}$, shown in Scheme 1.23.[78] It was observed that warming the complex from -20°C to 0°C in acetonitrile induced a disproportionation reaction to form a four coordinate dehydrogenated copper(III)-H33m complex and a copper(I)-acetonitrile complex along with a liberated H33m ligand (Scheme 1.23, top). Addition of TEMPO to $[Cu^{II}(H33m)]^{2+}$ before warming instead yielded only the dehydrogenated copper(III)-H33m complex and TEMPOH (Scheme 1.23, bottom), indicating the presence of a PCET pathway and significant C-H bond weakening in the dehydrogenation of $[Cu^{II}(H33m)]^{2+}$. Electron paramagnetic resonance spectroscopy and computational analysis of $[Cu^{II}(H33m)]^{2+}$ were found to be consistent with the formation of a 3-center-2-electron bond between the Cu^{II} and the C-H σ-bond of the nearby aryl moiety, which was noted as the first report of a σ-complex in a copper(II) species.

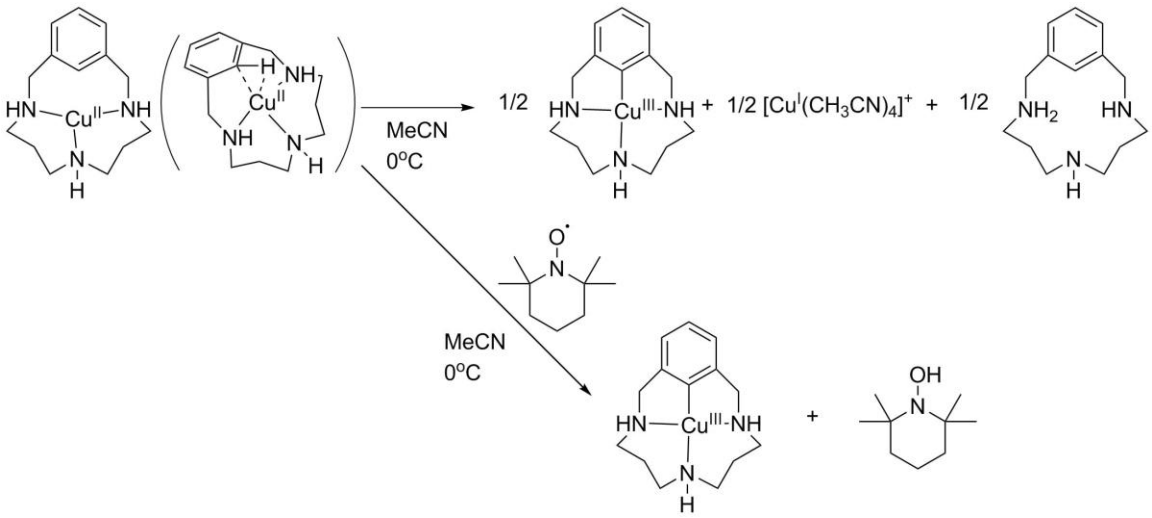

Scheme 1.23. Proposed reaction schemes for the disproportionation and TEMPO-mediated PCET oxidation of $[Cu^{II}(H33m)]^{2+}$[78]

1.3.4 Coordination-Induced Bond Weakening in Samarium(II) Complexes

A study by Flowers and coworkers revealed a significant difference in the mechanistic role of water in the SmI_2-water mediated reductions of anthracene and 1-iodododecane.[22] Since the reduction of alkyl halides by SmI_2-water is known to proceed through a rate limiting electron transfer (ET), an analogous pathway was ruled out for the reduction of anthracene.[22] Additionally, the recalcitrance of arenes to protonation precluded a PT-ET reduction mechanism. The reduction of arenes by SmI_2-water was therefore proposed to proceed through a PCET pathway.

Direct measurement of O-H BDFEs and coordination-induced bond weakening in SmI_2-water complexes is complicated by the uncertain composition of the SmI_2-water reagent in solution and the computational expense of modeling the energies of the samarium f-electrons. To establish an estimate for the degree of ligand X-H bond weakening upon coordination to SmI_2, the relevant X-H BDFEs for the uncomplexed proton donor and substrate were calculated, using the difference between the two values as an upper limit for the degree of bond weakening. Applying this methodology to a series of arenes that form increasingly weak C-H bonds upon reduction, a lower bound of 73.9 kcal/mol was established for the O-H bond weakening in water upon coordination to SmI_2 using *trans*-stilbene as the benchmark substrate.[79]

1.3.4.1 Samarium(II) Diiodide-Mediated Reductions of Carbonyls

Further investigations by Flowers and coworkers focused on the mechanism of reduction of carbonyls by SmI_2-water. These reductions are of particular interest given the remarkable capability of SmI_2-water systems to reduce even carbonyl substrates that commonly resist single electron reduction, such as lactones and derivatives of Meldrum's

acid.[80–87] Kinetic analysis of the SmI_2-water mediated reduction of heptanaldehyde, cyclohexanone, and 5-decanolide revealed uniformly low enthalpies of activation accompanied by high negative entropies of activation, consistent with an early transition state and a PCET reduction pathway.[88]

Rate order data was also collected for these reductions, revealing a first order dependence on SmI_2 and the carbonyl substrate. A second order rate dependence was determined for water at synthetically relevant concentrations. However, it was observed that with increasing concentration of water, the rate dependence on water fell gradually to zero or in some cases inverted. This unusual behavior suggests that at sufficiently high concentrations of water, dissociation of water from Sm(II) becomes a significant kinetic barrier to carbonyl-samarium(II) association and subsequent substrate reduction.[89]

Examining the reductions of an array of sterically encumbered and unencumbered ketones by SmI_2-water, Flowers and coworkers observed linear relations between the rates of substrate reduction and the O-H BDFEs of the bonds formed upon initial PCET reduction for both categories of substrates. These correlations are known as Evans-Polanyi relations and are shown in Figure 1.6. These linear relations are consistent with a CPET pathway for SmI_2-water-mediated ketone reductions.[88,90] However, the rate of reduction of methyl benzoate by SmI_2 was observed to be much more rapid than was predicted by the Evans-Polanyi relations for either class of ketones and aldehydes, indicating a mechanistic difference for ketone or aldehyde and ester reductions. Further investigation revealed a Hammett ρ value of 5.75 for methyl benzoate, indicating a buildup of significant anionic character on the substrate in the activated complex.[91] The reduction of methyl benzoate by SmI_2-water was therefore proposed to proceed through

either a sequential or asynchronous PCET pathway. In combination, the kinetic data for ketone and methyl benzoate reductions suggests that carbonyl reductions mediated by SmI_2-water occur through a range of concerted and sequential PCET pathways, dependent on the structural and electronic properties of the substrate.[90]

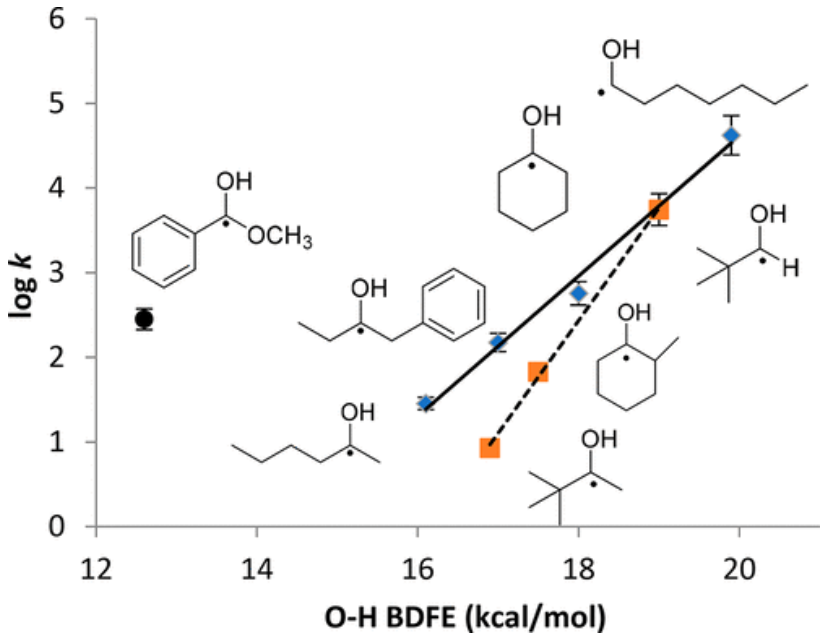

Figure 1.6. O-H BDFE vs *log k* Evans-Polanyi relation for hindered (orange squares) and unhindered carbonyls (blue diamonds)[90]

1.3.4.2 Samarium(II) Systems with Nitrogen-Containing Substrates

Although Sm(II) reagents are traditionally employed as reductants for oxygen-containing substrates such as carbonyls, recent work by Flowers and coworkers demonstrated the significant azaphilicity of SmI_2. This aspect of Sm(II) chemistry is utilized in much of the research described within this dissertation and will be discussed in greater depth in the relevant chapters. However there are several important literature reports on the interaction of SmI_2 reductants with N-containing species that will be discussed in this section.

One such study by the Flowers group investigated the use of amides as proton donors in conjunction with SmI_2.[92] Using 2-pyrrolidinone as a model amide ligand, pinacol couplings in benzylic and aliphatic aldehydes were achieved. Esters and lactones as well as nitrates were also reduced to alcohols and amines, respectively, using this system. Furthermore, the SmI_2-2-pyrrolidinone reagent was found to facilitate the 5-exo-trig reductive cyclization of the olefin-pendant ketone 2-but-3-enylcyclohexan-1-one as shown in Scheme 1.24.

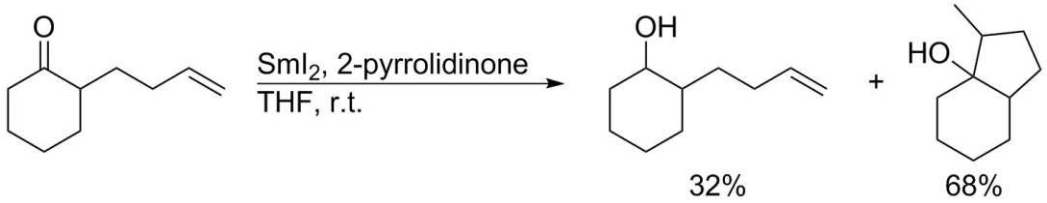

Scheme 1.24. Reaction scheme for the reduction and 5-exo-trig reductive cyclization of 2-but-3-enylcyclohexan-1-one by SmI_2-2-pyrrolidinone[92]

Replacing 2-pyrrolidinone with N-methyl-2-pyrrolidinone to form SmI_2-N-methyl-2-pyrrolidinone was found to fully inhibit reactivity in the samarium(II) species, consistent with PCET reduction by SmI_2-2-pyrrolidinone with the amide ligand as the proton source. Subsequently, observation of phenanthrene reduction by the SmI_2-2-pyrrolidinone system allowed the researchers to assign an N-H bond weakening of at least 70.8 kcal/mol to 2-pyrrolidinone upon coordination to SmI_2.

Mayer and coworkers demonstrated the utility of SmI_2 as a reductant for challenging nitrogen containing substrates in their report on the reduction of enamines by SmI_2-water.[20] Redox measurements and competition experiments ruled out ET-PT and PT-ET stepwise pathways, respectively, consistent with a PCET mechanism for the enamine reductions. Using available thermochemical data for enamines similar to those used in their study, Mayer and coworkers determined an upper bound for the O-H BDFE

of the SmI_2-water complex of 32 kcal/mol.[20] This value was further refined to 26 kcal/mol via the Bordwell relation using the known redox potential of aqueous Sm^{II} and taking the pK_a of $Sm^{III}(H_2O)_n$ to be equivalent to the literature value for $Eu^{III}(H_2O)_n$.[93–95] Notably, this is the weakest reported X-H bond for any reagent known to facilitate productive reductions under ambient temperature and pressure.

A seminal report by Nishibayashi and coworkers described the SmI_2-water-mediated reduction of nitrogen gas with a molybdenum-PNP/PCP (Scheme 1.25) (PNP = 2,6-bis(di-*tert*-butyphosphinomethyl)pyridine, PCP = 1,3-bis((di-*tert*-butylphosphino)methyl)benzimidazol-2-ylidine) catalyst.[21] Remarkably, this system returned a 92% yield of ammonia at room temperature under 1 atm of N_2 with only a 5% loss of hydrogen atom equivalents to H_2 gas evolution.

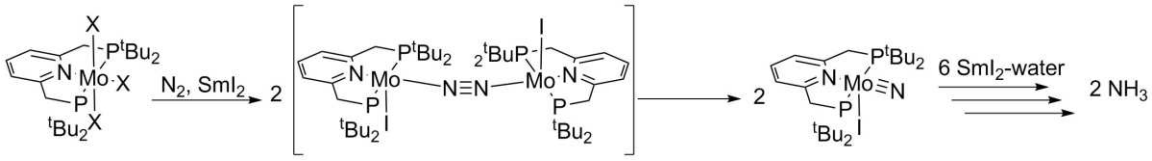

Scheme 1.25. Proposed reaction scheme for halide exchange between molybdenum-PNP and SmI_2 and subsequent molybdenum nitride formation and production of ammonia[21]

In the absence of water, combination of SmI_2 with molybdenum-PNP under a nitrogen atmosphere furnished the molybdenum nitride species shown in Scheme 1.25. Reintroduction of this molybdenum nitride to reaction conditions in place of the molybdenum-PNP catalyst resulted in ammonia formation, suggesting a key intermediate role for the nitride species. It was also observed that regardless of the halide species coordinated to the initial molybdenum catalyst, the molybdenum nitride was isolated bearing iodide ligands. This observation was attributed to halide exchange between the molybdenum catalyst and the SmI_2 terminal reductant, shown in Scheme 1.25, concomitantly forming the more powerful $SmBr_2$ or $SmCl_2$ reductants.

1.3.4.3 Samarium(II) Dibromide-and Dichloride-Mediated Reductions

Samarium(II) reagents are commonly prepared as SmI_2 but can be converted to $SmBr_2$ and $SmCl_2$ via halide exchange with bromide and chloride salts, respectively.[10,11] One of the effects of this halide substitution on SmI_2 is an increase in redox potential, with $SmCl_2$ being a stronger reductant than $SmBr_2$, which is in turn a stronger reductant than SmI_2. This trend is preserved in the presence of water, which has been attributed to the increasingly strong association of samarium(II) with bromide and chloride ligands providing additional electron density to Sm(II).[10,11] This hypothesis is supported by Born-Oppenheimer molecular dynamics simulations, which revealed that water solvation of Sm(II) leads to dissociation of both iodide ligands from SmI_2.[96] In contrast, only one bromide ligand was expelled from the inner sphere of $SmBr_2$ in the aqueous microsolvate model, and in the case of $SmCl_2$ both chloride ligands remain coordinated to Sm(II) under the same conditions.[10,11]

The effects of halide ligand speciation have also been observed experimentally in the increased O-H bond weakening in $SmBr_2$- and $SmCl_2$-water systems. The $SmBr_2$-water reagent has been shown to reduce arenes as challenging as phenanthrene (Scheme 1.26), demonstrating a bond weakening of at least 82.7 kcal/mol and an O-H BDFE of no more than 25.3 kcal/mol.[10] Likewise, $SmCl_2$-water has been shown to reduce 2-methoxynaphthalene, revealing a minimum bond weakening of between 82.9 and 88.5 kcal/mol for an O-H BDFE upper bound between 19.5 and 25.1 kcal/mol.[11]

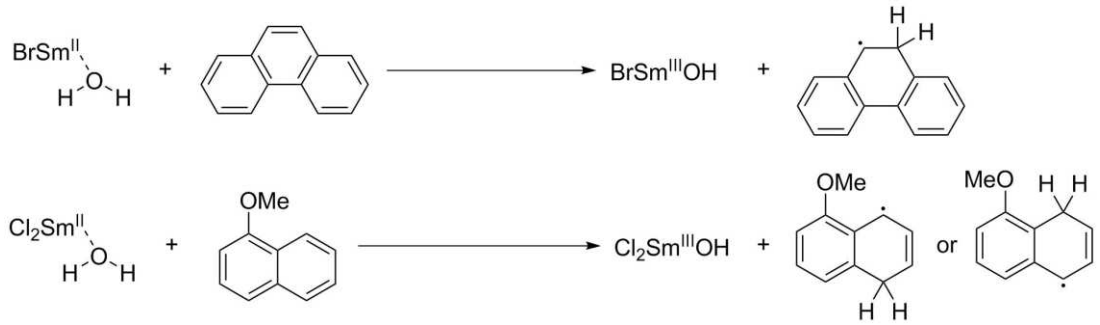

Scheme 1.26. Reaction schemes for the reduction of phenanthrene by $SmBr_2$-water and the reduction of 2-methoxynaphthalene by $SmCl_2$-water[10,11]

1.4 Project Goals

The remaining chapters of this dissertation describe recent research into coordination-induced bond weakening in Sm(II)-proton donor reducing systems using a diverse set of Sm(II), proton donor, and substrate species. Chapters 2 and 3 discuss research investigating the mechanisms of reduction of challenging N-containing substrates by SmI_2-water. Chapter 4 describes research investigating the hypothesis that the remarkable stability of the SmI_2-water system against hydrogen gas evolution is a consequence of the kinetic interactions of the SmI_2-water reagent in THF solution. Chapters 5 and 6 focus on the hypothesis that increasing proton donor affinity for Sm(II) yields a greater degree of coordination-induced bond weakening. Finally Chapter 7 discusses research investigating the hypothesis that coordination-induced bond weakening is driven by backdonation from a low-valent metal into the X-H σ*-antibonding orbital of a coordinated protic ligand.

1.5 References

(1) Girard, P.; Namy, J. L.; Kagan, B. Divalent Lanthanide Derivatives in Organic Synthesis. 1. Mild Preparation of SmI2 and YbI2 and Their Use as Reducing or Coupling Agents. *J. Am. Chem. Soc.* **1980**, *102* (8), 2693–2698.

(2) Chciuk, T. V.; Flowers, II, R. A. The Role of Solvents and Additives in Reactions of Samarium(II) Iodide and Related Reductants. In *Science of Synthesis*; Marek, I., Ed.; Georg Thieme Verlag KG: Stuttgart, 2016; pp 177–261.

(3) Edmonds, D. J.; Johnston, D.; Procter, D. J. Samarium(II)-Iodide-Mediated Cyclizations in Natural Product Synthesis. *Chem. Rev.* **2004**, *104* (7), 3371–3403.

(4) Molander, G. A.; Harris, C. R. Sequencing Reactions with Samarium(II) Iodide. *Chem. Rev.* **1996**, *96* (1), 307–338.

(5) Szostak, M.; Fazakerley, N. J.; Parmar, D.; Procter, D. J. Cross-Coupling Reactions Using Samarium(II) Iodide. *Chem. Rev.* **2014**, *114* (11), 5959–6039.

(6) Shi, S.; Szostak, M. Synthesis of Nitrogen Heterocycles Using Samarium(II) Iodide. *Molecules* **2017**, *22* (11), 1–22.

(7) Shotwell, J. B.; Sealy, J. M.; Flowers, R. A. Structure and Energetics of the Samarium Diiodide-HMPA Complex in Tetrahydrofuran. *J. Org. Chem.* **1999**, *64* (14), 5251–5255.

(8) Enemñrke, R. J.; Hertz, T.; Skrydstrup, T.; Daasbjerg, K. Evidence for Ionic Samarium(II) Species in THF/HMPA Solution and Investigation of Their Electron-Donating Properties. *Chem. Eur. J.* **2000**, *6* (20), 3747–3754.

(9) Chciuk, T. V.; Anderson, W. R.; Flowers, R. A. High-Affinity Proton Donors Promote Proton-Coupled Electron Transfer by Samarium Diiodide. *Angew. Chemie Int. Ed.* **2016**, *55* (20), 6033–6036.

(10) Ramírez-Solís, A.; Bartulovich, C. O.; César, C.; Iván, I.; León-Pimentel, L.; Saint-Martin, H.; Anderson, W. R.; Flowers II, R. A. Experimental and Theoretical Studies on the Aqueous Solvation and Reactivity of SmCl2 and Comparison with SmBr2 and SmI2. *Inorg. Chem.* **2019**, *18*, 13927−13932.

(11) Ramírez-Solís, A.; Bartulovich, C. O.; Chciuk, T. V.; Hernández-Cobos, J.; Saint-Martin, H.; Maron, L.; Anderson, W. R.; Li, A. M.; Flowers, R. A. Experimental and Theoretical Studies on the Implications of Halide-Dependent Aqueous Solvation of Sm(II). *J. Am. Chem. Soc.* **2018**, *140* (48), 16731–16739.

(12) Ramírez-Solís, A.; Bartulovich, C. O.; León-Pimentel, C. I.; Saint-Martin, H.; Boekell, N. G.; Flowers, R. A. Proton Donor Effects on the Reactivity of SmI2. Experimental and Theoretical Studies on Methanol Solvation vs. Aqueous Solvation. *Dalt. Trans.* **2020**, *49* (23), 7897–7902.

(13) Knettle, B. W.; Flowers, R. A. Influence of HMPA on Reducing Power and Reactivity of SmBr2. *Org. Lett.* **2001**, *3* (15), 2321–2324.

(14) Flowers, R. A. Mechanistic Studies on the Roles of Cosolvents and Additives in Samarium(II)-Based Reductions. *Synlett* **2008**, No. 10, 1427–1439.

(15) Miller, R. S.; Sealy, J. M.; Shabangi, M.; Kuhlman, M. L.; Fuchs, J. R.; Flowers, R. A. Reactions of SmI 2 with Alkyl Halides and Ketones: Inner-Sphere vs Outer-Sphere Electron Transfer in Reactions of Sm(II) Reductants. *J. Am. Chem. Soc.*

2000, *122* (32), 7718–7722.

(16) Szostak, M.; Spain, M.; Procter, D. J. Determination of the Effective Redox Potentials of SmI2, SmBr2, SmCl2, and Their Complexes with Water by Reduction of Aromatic Hydrocarbons. Reduction of Anthracene and Stilbene by Samarium(II) Iodide-Water Complex. *J. Org. Chem.* **2014**, *79* (6), 2522–2537.

(17) Shabangi, M.; Flowers, R. A. Electrochemical Investigation of the Reducing Power of SmI2 in THF and the Effect of HMPA Cosolvent. *Tetrahedron Lett.* **1997**, *38* (7), 1137–1140.

(18) Shabangi, M.; Sealy, J. M.; Fuchs, J. R.; Flowers, R. A. The Effect of Cosolvent on the Reducing Power of SmI2 in Tetrahydrofuran. *Tetrahedron Lett.* **1998**, *39* (25), 4429–4432.

(19) Duffy, L. A.; Matsubara, H.; Procter, D. J. A Ring Size-Selective Reduction of Lactones Using SmI2 and H2O. *J. Am. Chem. Soc.* **2008**, *130* (4), 1136–1137.

(20) Kolmar, S. S.; Mayer, J. M. SmI2(H2O)n Reduction of Electron Rich Enamines by Proton-Coupled Electron Transfer. *J. Am. Chem. Soc.* **2017**, *139* (31), 10687–10692.

(21) Ashida, Y.; Arashiba, K.; Nakajima, K.; Nishibayashi, Y. Molybdenum-Catalysed Ammonia Production with Samarium Diiodide and Alcohols or Water. *Nature* **2019**, *568* (7753), 536–540.

(22) Chciuk, T. V; Flowers, R. A. Proton-Coupled Electron Transfer in the Reduction of Arenes by SmI2-Water Complexes. *J. Am. Chem. Soc.* **2015**, *137*, 11526−11531.

(23) Prasad, E.; Flowers, R. A. Reduction of Ketones and Alkyl Iodides by Sml2 and Sm(II)-HMPA Complexes. Rate and Mechanistic Studies. *J. Am. Chem. Soc.* **2002**, *124* (24), 6895–6899.

(24) Andrieux, C. P.; Gallardo, I.; Savéant, J.-M.; In Encyclopedia of Electrochemistry of the Ele-ments, M. D.; Dekker, M.; J Am, K. B. Outer-Sphere Electron-Transfer Reduction of Alkyl Halides. A Source of Alkyl Radicals or of Carbanions? Reduction of Alkyl Radicals. *J. Am. Chem. Soc.* **2002**, *111* (5), 1620–1626.

(25) Huynh, M. H. V.; Meyer, T. J. Proton-Coupled Electron Transfer. *Chem. Rev.* **2007**, *107* (11), 5004–5064.

(26) Bjornsson, R.; Delgado-Jaime, M. U.; Lima, F. A.; Sippel, D.; Schlesier, J.; Weyhermüller, T.; Einsle, O.; Neese, F.; Debeer, S. Molybdenum L-Edge XAS Spectra of MoFe Nitrogenase. *J. Inorg. Gen. Chem.* **2015**, *641* (1), 65–71.

(27) Barry, B. A. Reaction Dynamics and Proton Coupled Electron Transfer: Studies of Tyrosine-Based Charge Transfer in Natural and Biomimetic Systems. *Biochim.*

Biophys. Acta - Bioenerg. **2015**, *1847* (1), 46–54.

(28) Weinberg, D. R.; Gagliardi, C. J.; Hull, J. F.; Murphy, C. F.; Kent, C. A.; Westlake, B. C.; Paul, A.; Ess, D. H.; McCafferty, D. G.; Meyer, T. J. Proton-Coupled Electron Transfer. *Chem. Rev.* **2012**, *112* (7), 4016–4093.

(29) Hammes-Schiffer, S. Theoretical Perspectives on Proton-Coupled Electron Transfer Reactions. *Acc. Chem. Res.* **2001**, *34* (4), 273–281.

(30) Warren, J. J.; Tronic, T. A.; Mayer, J. M. Thermochemistry of Proton-Coupled Electron Transfer Reagents and Its Implications. *Chem. Rev.* **2010**, *110* (12), 6961–7001.

(31) Pappas, I.; Chirik, P. J. Ammonia Synthesis by Hydrogenolysis of Titanium-Nitrogen Bonds Using Proton Coupled Electron Transfer. *J. Am. Chem. Soc.* **2015**, *137* (10), 3498–3501.

(32) Margulieux, G. W.; Máté, M.; Bezdek, M.; Turner, Z. R.; Chirik, P. J. Ammonia Activation, H2 Evolution and Nitride Formation from a Molybdenum Complex with a Chemically and Redox Noninnocent Ligand. *J. Am. Chem. Soc.* **2017**, *139*, 6110−6113.

(33) Tarantino, K. T.; Miller, D. C.; Callon, T. A.; Knowles, R. R. Bond-Weakening Catalysis: Conjugate Aminations Enabled by the Soft Homolysis of Strong N−H Bonds. *J. Am. Chem. Soc.* **2015**, *137*, 6440−6443.

(34) Bezdek, M. J.; Guo, S.; Chirik, P. J. Coordination-Induced Weakening of Ammonia, Water, and Hydrazine X–H Bonds in a Molybdenum Complex. *Science* **2016**, *354* (6313), 730–733.

(35) Spiegel, D. A.; Wiberg, K. B.; Schacherer, L. N.; Medeiros, M. R.; Wood, J. L. Deoxygenation of Alcohols Employing Water as the Hydrogen Atom Source. *J. Am. Chem. Soc.* **2005**, *127*, 12513–12515.

(36) Fang, H.; Ling, Z.; Lang, K.; Brothers, P. J.; De Bruin, B.; Fu, X. Germanium(III) Corrole Complex: Reactivity and Mechanistic Studies of Visible-Light Promoted N-H Bond Activations. *Chem. Sci.* **2014**, *5*, 916–921.

(37) Hoganson, C. W.; Babcock, G. T. A Metalloradical Mechanism for the Generation of Oxygen from Water in Photosynthesis. *Science* **1997**, *277* (5334), 1953–1956.

(38) Klinman, J. P. The Widespread Occurrence of Enzymatic Hydrogen Tunneling, and Its Unique Properties, Lead to a New Physical Model for the Origins of Enzyme Catalysis. *Procedia Chem.* **2011**, *3* (1), 291–305.

(39) Warren, J. J.; Tronic, T. A.; Mayer, J. M. The Thermochemistry of Proton-Coupled Electron Transfer Reagents and Its Implications. *Chem. Rev.* **2010**, *110* (12), 6961–7001.

(40) Ruscic, B.; Wagner, A. F.; Harding, L. B.; Asher, R. L.; Feller, D.; Dixon, D. A.; Peterson, K. A.; Song, Y.; Qian, X.; Ng, C. Y.; et al. On the Enthalpy of Formation of Hydroxyl Radical and Gas-Phase Bond Dissociation Energies of Water and Hydroxyl. *J. Phys. Chem. A* **2002**, *106* (11), 2727–2747.

(41) Gaussian 09, Revision D.01, M. J. Frisch, G. W. Trucks, H. B. Schlegel, G. E. Scuseria, M. A. Robb, J. R. Cheeseman, G. Scalmani, V. Barone, B. Mennucci, G. A. Petersson, H. Nakatsuji, M. Caricato, X. Li, H. P. Hratchian, A. F. Izmaylov, J. Bloino, G. Zheng, J. L. Sonnenberg, M. Hada, M. Ehara, K. Toyota, R. Fukuda, J. Hasegawa, M. Ishida, T. Nakajima, Y. Honda, O. Kitao, H. Nakai, T. Vreven, J. A. Montgomery, Jr., J. E. Peralta, F. Ogliaro, M. Bearpark, J. J. Heyd, E. Brothers, K. N. Kudin, V. N. Staroverov, T. Keith, R. Kobayashi, J. Normand, K. Raghavachari, A. Rendell, J. C. Burant, S. S. Iyengar, J. Tomasi, M. Cossi, N. Rega, J. M. Millam, M. Klene, J. E. Knox, J. B. Cross, V. Bakken, C. Adamo, J. Jaramillo, R. Gomperts, R. E. Stratmann, O. Yazyev, A. J. Austin, R. Cammi, C. Pomelli, J. W. Ochterski, R. L. Martin, K. Morokuma, V. G. Zakrzewski, G. A. Voth, P. Salvador, J. J. Dannenberg, S. Dapprich, A. D. Daniels, O. Farkas, J. B. Foresman, J. V. Ortiz, J. Cioslowski, and D. J. Fox, Gaussian, Inc., Wallingford CT, 2013

(42) Yun Zhao; Setzler, B. P.; Wang, J.; Nash, J.; Wang, T.; Xu, B.; Yan, Y. An Efficient Direct Ammonia Fuel Cell for Affordable Carbon-Neutral Transportation. *Joule* **2019**, *3*, 2472–2484.

(43) Valera-Medina, A.; Amer-Hatem, F.; Azad, A. K.; Dedoussi, I. C.; De Joannon, M.; Fernandes, R. X.; Glarborg, P.; Hashemi, H.; He, X.; Mashruk, S.; et al. Review on Ammonia as a Potential Fuel: From Synthesis to Economics. *Energy and Fuels* **2021**, *35* (9), 6964–7029.

(44) Dunn, P. L.; Cook, B. J.; Johnson, S. I.; Appel, A. M.; Bullock, R. M. Oxidation of Ammonia with Molecular Complexes. *J. Am. Chem. Soc.* **2020**, *142* (42), 17845–17858.

(45) *Storage and Handling of Anhydrous Ammonia.* | *Occupational Safety and Health Administration*; United States of America.

(46) Bartulovich, C. O.; Flowers, R. A. Coordination-Induced O-H Bond Weakening in Sm(II)-Water Complexes. *Dalt. Trans.* **2019**, *48* (43), 16142–16147.

(47) Zhang, Y.-Q.; Jakoby, V.; Stainer, K.; Schmer, A.; Klare, S.; Bauer, M.; Grimme, S.; Cuerva, J. M.; Gansäuer, A. Amide-Substituted Titanocenes in Hydrogen-Atom Transfer Catalysis. *Angew. Chemie Int. Ed.* **2016**, *55* (4), 1523–1526.

(48) Pappas, I.; Chirik, P. J. Ammonia Synthesis by Hydrogenolysis of Titanium−Nitrogen Bonds Using Proton Coupled Electron Transfer. *J. Am. Chem. Soc.* **2015**, *137*, 3498−3501.

(49) Cuerva, J. M.; Campaña, A. G.; Justicia, J.; Rosales, A.; Oller-López, J. L.;

Robles, R.; Cárdenas, D. J.; Buñuel, E.; Oltra, J. E. Water: The Ideal Hydrogen-Atom Source in Free-Radical Chemistry Mediated by TiIII and Other Single-Electron-Transfer Metals? *Angew. Chemie Int. Ed.* **2006**, *45* (33), 5522–5526.

(50) Gansäuer, A.; Behlendorf, M.; Cangönül, A.; Kube, C.; Cuerva, J. M.; Friedrich, J.; van Gastel, M. H2O Activation for Hydrogen-Atom Transfer: Correct Structures and Revised Mechanisms. *Angew. Chemie Int. Ed.* **2012**, *51* (13), 3266–3270.

(51) Pappas, I.; Chirik, P. J. Catalytic Proton Coupled Electron Transfer from Metal Hydrides to Titanocene Amides, Hydrazides and Imides: Determination of Thermodynamic Parameters Relevant to Nitrogen Fixation. *J. Am. Chem. Soc.* **2016**, *138*, 13379−13389.

(52) Paradas, M.; Campaña, A. G.; Jimé Nez, T.; Robles, R.; Oltra, J. E.; Buñ, E.; Justicia, J.; Cá, D. J.; Cuerva, J. M. Understanding the Exceptional Hydrogen-Atom Donor Characteristics of Water in TiIII-Mediated Free-Radical Chemistry. *J. Am. Chem. Soc.* **2010**, *132*, 12748–12756.

(53) Bezdek, M. J.; Pelczer, I.; Chirik, P. J. Coordination-Induced N–H Bond Weakening in a Molybdenum Pyrrolidine Complex: Isotopic Labeling Provides Insight into the Pathway for H2 Evolution. *Organometallics* **2020**, *39* (16), 3050–3059.

(54) Frey, P. A.; Reed, G. H. The Ubiquity of Iron. *ACS Chem. Biol.* **2012**, *7* (9), 1477–1481.

(55) Brines, L. M.; Coggins, M. K.; Chaau, P.; Poon, Y.; Toledo, S.; Kaminsky, W.; Kirk, M. L.; Kovacs, J. A. Water-Soluble Fe(II)−H2O Complex with a Weak O−H Bond Transfers a Hydrogen Atom via an Observable Monomeric Fe(III)−OH. *J. Am. Chem. Soc.* **2015**, *137*, 2253−2264.

(56) Hoover, J. M.; Ryland, B. L.; Stahl, S. S. Mechanism of Copper(I)/TEMPO-Catalyzed Aerobic Alcohol Oxidation. *J. Am. Chem. Soc.* **2013**, *135*, 2357–2367.

(57) Derosa, J.; Garrido-Barros, P.; Peters, J. C. Electrocatalytic Reduction of C–C π-Bonds via a Cobaltocene-Derived Concerted Proton–Electron Transfer Mediator: Fumarate Hydrogenation as a Model Study. *J. Am. Chem. Soc.* **2021**, *143* (25), 9303–9307.

(58) Schild, D. J.; Drover, M. W.; Oyala, P. H.; Peters, J. C. Generating Potent C–H PCET Donors: Ligand-Induced Fe-to-Ring Proton Migration from a Cp*FeIII–H Complex Demonstrates a Promising Strategy. *J. Am. Chem. Soc.* **2020**, *142* (44), 18963–18970.

(59) Crabtree, R. H.; Felkin, H.; Morris, G. E. Cationic Iridium Diolefin Complexes as Alkene Hydrogenation Catalysts and the Isolation of Some Related Hydrido Complexes. *J. Organomet. Chem.* **1977**, *141* (2), 205–215.

(60) Osborn, J. A.; Jardine, F. H.; Young, J. F.; Wilkinson, G. The Preparation and Properties of Tris(Triphenylphosphine) Halogenorhodium(I) and Some Reactions Thereof Including Catalytic Homogeneous Hydrogenation of Olefins and Acetylenes and Their Derivatives. *J. Chem. Soc. A Inorganic, Phys. Theor.* **1966**, *I* (6), 1711–1732.

(61) Poulos, T. L. Heme Enzyme Structure and Function. *Chem. Rev.* **2014**, *114* (7), 3919–3962.

(62) Warren, J. J.; Mayer, J. M. Hydrogen Atom Transfer Reactions of Iron-Porphyrin-Imidazole Complexes as Models for Histidine-Ligated Heme Reactivity. *J. Am. Chem. Soc.* **2008**, *130*, 2774–2776.

(63) Drover, M. W.; Schild, D. J.; Oyala, P. H.; Peters, J. C. Snapshots of a Migrating H-Atom: Characterization of a Reactive Iron(III) Indenide Hydride and Its Nearly Isoenergetic Ring-Protonated Iron(I) Isomer. *Angew. Chemie Int. Ed.* **2019**, *58* (43), 15504–15511.

(64) Wiedner, E. S.; Chambers, M. B.; Pitman, C. L.; Bullock, R. M.; Miller, A. J. M.; Appel, A. M. Thermodynamic Hydricity of Transition Metal Hydrides. *Chem. Rev.* **2016**, *116* (15), 8655–8692.

(65) Pearson, R. G. The Transition-Metal-Hydrogen Bond. *Chem. Rev.* **1985**, *85* (1), 41–49.

(66) Wu, A.; Masland, J.; Swartz, R. D.; Kaminsky, W.; Mayer, J. M. Synthesis and Characterization of Ruthenium Bis(β-Diketonato) Pyridine-Imidazole Complexes for Hydrogen Atom Transfer. *Inorg. Chem.* **2007**, *46* (26), 11190–11201.

(67) Wu, A.; Mayer, J. M. Hydrogen Atom Transfer Reactions of a Ruthenium Imidazole Complex: Hydrogen Tunneling and the Applicability of the Marcus Cross Relation. *J. Am. Chem. Soc.* **2008**, No. 130, 14745–14754.

(68) Roth, J. P.; Lovell, S.; Mayer, J. M. Intrinsic Barriers for Electron and Hydrogen Atom Transfer Reactions of Biomimetic Iron Complexes. *J. Am. Chem. Soc.* **2000**, *122* (23), 5486–5498.

(69) Roth, J. P.; Yoder, J. C.; Won, T. J.; Mayer, J. M. Application of the Marcus Cross Relation to Hydrogen Atom Transfer Reactions. *Science* **2001**, *294* (5551), 2524–2526.

(70) Roth, J. P.; Mayer, J. M. Hydrogen Transfer Reactivity of a Ferric Bi-Imidazoline Complex That Models the Activity of Lipoxygenase Enzymes. *Inorg. Chem.* **1999**, *38* (12), 2760–2761.

(71) Mader, E. A.; Larsen, A. S.; Mayer, J. M. Hydrogen Atom Transfer from Iron(II)-Tris[2,2′- Bi(Tetrahydropyrimidine)] to TEMPO: A Negative Enthalpy of Activation Predicted by the Marcus Equation. *J. Am. Chem. Soc.* **2004**, *126* (26),

8066–8067.

(72) Mader, E. A.; Davidson, E. R.; Mayer, J. M. Large Ground-State Entropy Changes for Hydrogen Atom Transfer Reactions of Iron Complexes. *J. Am. Chem. Soc.* **2007**, *129* (16), 5153–5166.

(73) Yoder, J. C.; Roth, J. P.; Gussenhoven, E. M.; Larsen, A. S.; Mayer, J. M. Electron and Hydrogen-Atom Self-Exchange Reactions of Iron and Cobalt Coordination Complexes. *J. Am. Chem. Soc.* **2003**, *125* (9), 2629–2640.

(74) Soper, J. D.; Mayer, J. M. Slow Hydrogen Atom Self-Exchange between Os(IV) Anilide and Os(III) Aniline Complexes: Relationships with Electron and Proton Transfer Self-Exchange. *J. Am. Chem. Soc.* **2003**, *125*, 12217–12229.

(75) Bordwell, F. G.; Liu, W. Z. Solvent Effects on Homolytic Bond Dissociation Energies of Hydroxylic Acids. *J. Am. Chem. Soc.* **1996**, *118* (44), 10819–10823.

(76) Chalkley, M. J.; Oyala, P. H.; Peters, J. C. Cp* Noninnocence Leads to a Remarkably Weak C−H Bond via Metallocene Protonation. *J. Am. Chem. Soc.* **2019**, *141*, 4721−4729.

(77) Chalkle, M. J.; Garrido-Barros, P.; Peter, J. C. A Molecular Mediator for Reductive Concerted Proton-Electron Transfers via Electrocatalysis. *Science* **2020**, *369* (6505), 850–854.

(78) Ribas, X.; Calle, C.; Poater, A.; Casitas, A.; Gó mez, L.; Xifra, R.; Parella, T.; Benet-Buchholz, J.; Schweiger, A.; Mitrikas, G.; et al. Facile C-H Bond Cleavage via a Proton-Coupled Electron Transfer Involving a C-H···Cu II Interaction. *J. Am. Chem. Soc.* **2010**, *132*, 12299–12306.

(79) Chciuk, T. V; Anderson, W. R.; Flowers, R. A. Reversibility of Ketone Reduction by SmI2-Water and Formation of Organosamarium Intermediates. *Organometallics* **2017**, *36*, 4579−4583.

(80) Guazzelli, G.; De Grazia, S.; Collins, K. D.; Matsubara, H.; Spain, M.; Procter, D. J. Selective Reductions of Cyclic 1,3-Diesters Using SmI2 and H2O. *J. Am. Chem. Soc.* **2009**, *131* (21), 7214–7215.

(81) Duffy, L. A.; Matsubara, H.; Procter, D. J. A Ring Size-Selective Reduction of Lactones Using SmI2 and H2O. *J. Am. Chem. Soc.* **2008**, *130* (4), 1136–1137.

(82) Szostak, M.; Sautier, B.; Spain, M.; Procter, D. J. Electron Transfer Reduction of Nitriles Using SmI2-Et 3N-H2O: Synthetic Utility and Mechanism. *Org. Lett.* **2014**, *16* (4), 1092–1095.

(83) Szostak, M.; Spain, M.; Choquette, K. A.; Flowers, R. A.; Procter, D. J. Substrate-Directable Electron Transfer Reactions. Dramatic Rate Enhancement in the Chemoselective Reduction of Cyclic Esters Using SmI2-H2O: Mechanism, Scope,

and Synthetic Utility. *J. Am. Chem. Soc.* **2013**, *135* (42), 15702–15705.

(84) Collins, K. D.; Oliveira, J. M.; Guazzelli, G.; Sautier, B.; De Grazia, S.; Matsubara, H.; Helliwell, M.; Procter, D. J. Selective Reductions of Cyclic 1,3-Diesters by Using SmI2 and H2O. *Chem. - A Eur. J.* **2010**, *16* (33), 10240–10249.

(85) Szostak, M.; Spain, M.; Procter, D. J. Ketyl-Type Radicals from Cyclic and Acyclic Esters Are Stabilized by SmI2(H2O)n: The Role of SmI2(H2O)n in Post-Electron Transfer Steps. *J. Am. Chem. Soc.* **2014**, *136* (23), 8459–8466.

(86) Just-Baringo, X.; Procter, D. J. Sm(II)-Mediated Electron Transfer to Carboxylic Acid Derivatives: Development of Complexity-Generating Cascades. *Acc. Chem. Res.* **2015**, *48* (5), 1263–1275.

(87) Kamochi, Y.; Kudo, T. The Novel Reduction of Pyridine Derivatives with Samarium Diiodide. *Heterocycles* **1993**, *36* (10), 2383.

(88) Chciuk, T. V.; Anderson, W. R.; Flowers, R. A. Proton-Coupled Electron Transfer in the Reduction of Carbonyls by Samarium Diiodide-Water Complexes. *J. Am. Chem. Soc.* **2016**, *138* (28), 8738–8741.

(89) Chciuk, T. V.; Anderson, W. R.; Flowers, R. A. Interplay between Substrate and Proton Donor Coordination in Reductions of Carbonyls by SmI2-Water Through Proton-Coupled Electron-Transfer. *J. Am. Chem. Soc.* **2018**, *140* (45), 15342–15352.

(90) Chciuk, T. V; Anderson, W. R.; Flowers, R. A. Interplay between Substrate and Proton Donor Coordination in Reductions of Carbonyls by SmI2-Water Through Proton-Coupled Electron-Transfer. *J. Am. Chem. Soc.* **2018**, *140*, 15342–15352.

(91) Usharani, D.; Lacy, D. C.; Borovik, A. S.; Shaik, S. Dichotomous Hydrogen Atom Transfer vs Proton-Coupled Electron Transfer during Activation of X-H Bonds (X = C, N, O) by Nonheme Iron-Oxo Complexes of Variable Basicity. *J. Am. Chem. Soc.* **2013**, *135* (45), 17090–17104.

(92) Chciuk, T. V; Li, A. M.; Vazquez-Lopez, A.; Anderson, W. R.; Flowers, R. A. Secondary Amides as Hydrogen Atom Transfer Promoters for Reactions of Samarium Diiodide. *Org. Lett.* **2016**, *19* (1), 290–293.

(93) Morss, L. R. Thermochemical Properties of Yttrium, Lanthanum, and the Lanthanide Elements and Ions. *Chem. Rev.* **1976**, *76* (6), 827–841.

(94) Bratsch, S. G. Standard Electrode Potentials and Temperature Coefficients in Water at 298.15 K. *J. Phys. Chem. Ref. Data* **2009**, *18* (1), 1.

(95) Mohapatra, P. K.; Khopkar, P. K. Hydrolysis of Actinides and Lanthanides: Hydrolysis of Some Trivalent Actinide and Lanthanide Ions Studied by Extraction with Thenoyltrifluoroacetone. *Polyhedron* **1989**, *8* (16), 2071–2076.

(96) Ramírez-Solís, A.; Amaro-Estrada, J. I.; Hernández-Cobos, J.; Maron, L.; México, M. Aqueous Solvation of SmI2 : A Born-Oppenheimer Molecular Dynamics Density Functional Theory Cluster Approach. *J. Phys. Chem. A* **2017**, *121*, 2293−2297.

Chapter 2. Studies of the Reduction of Pyridines and Quinolines by SmI_2-Water

2.1 Background and Significance

2.1.1 Introduction to Pyridines and Related Compounds

Pyridine and piperidine along with their derivatives are ubiquitous in medicinal chemistry, constituting approximately 12% of all commercially available small molecule pharmaceuticals as of 2014.[1] These include local anesthetics, opioids, antiretrovirals, and anti-cancer drugs.[1–3] Many of these drug molecules are highly complex with diverse functional groups as seen in Figure 2.1.

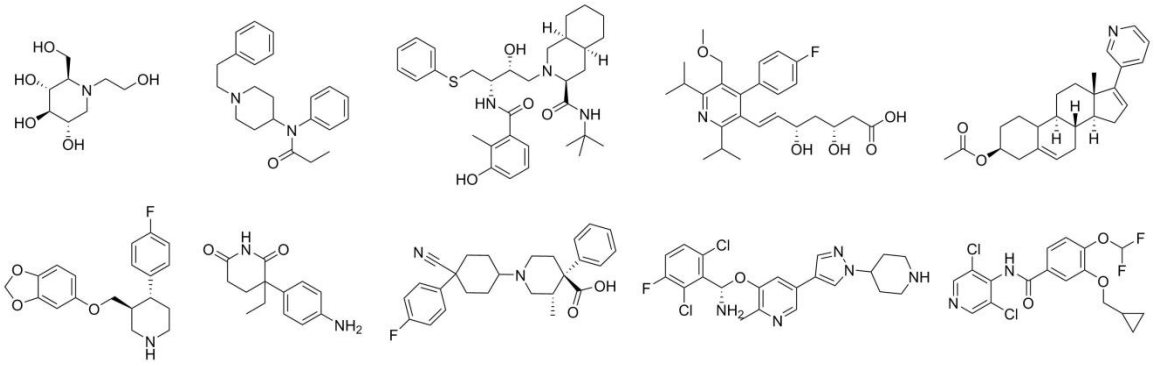

Figure 2.1. Examples of small molecule drugs containing pyridine and piperidine approved by the US FDA; Miglitol, Fentanyl, Nelfinavir, Cerivastatin, Abiraterone Acetate, Paroxetine, Aminogluthimide, Levocabastine, Crizotinib, Roflumilast (from left to right, top to bottom)[1]

This complexity makes the conversion of prefunctionalized pyridines to piperidines highly desirable for the creation of small molecule libraries for drug development. However, reduction of pyridine to piperidine is made challenging by the stability of pyridine, which is the most similar of the heteroaromatics to benzene and thus the most stable. Pyridine reductions are therefore carried out under conditions of catalytic hydrogenation, which necessitates high temperatures and high pressures of hydrogen gas over a transition metal catalyst.[4–6] These conditions preclude the prefunctionalization of pyridines and necessitate the synthetically expensive separate

construction of pyridine and piperidine small molecule pharmaceutical libraries. For this reason, a protocol for the reduction of pyridines to piperidines under mild conditions is potentially of great value.

2.1.2 Chemical Reductions of Pyridine and Related Compounds

Despite their lesser stability compared to pyridine, conjugated pyridine derivatives such as quinolines are also recalcitrant to chemical reduction. Reductions of quinoline often require elevated temperatures and transition metal catalysts.[7,8] In this context, a study published by Procter and coworkers presents an unusually mild method for the reductive dimerization of quinoline using SmI_2-methanol (Scheme 2.1).[9] Although the Procter group did not observe any monomeric reduced products in their SmI_2-methanol-mediated reduction of quinoline, the room temperature reduction of quinoline is nonetheless remarkable.

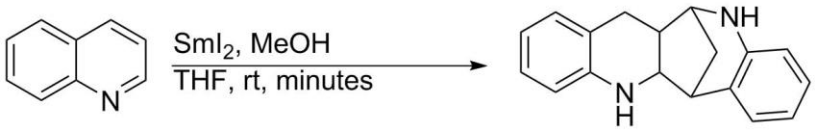

Scheme 2.1. Reaction scheme for the reductive coupling of quinoline by SmI_2-methanol[9]

While the reduction of a substrate as stable quinoline under mild conditions by SmI_2-methanol is remarkable it is nonetheless in line with a recently discovered trend of facile Sm(II)-proton donor-mediated reductions of challenging substrates utilizing the high azaphilicity of Sm(II).[10,11] Other examples of this can be found in the work of Mayer and coworkers in their SmI_2-water-mediated reduction of electron rich enamine substrates (Scheme 2.2) as well as in the seminal reduction of nitrogen gas by Nishibayashi and coworkers utilizing Sm(II)-water as the reductant (Scheme 2.3) among others.[12–14] Additionally, work by Kudo and coworkers indicates that the SmI_2-water reagent can mediate the complete reduction of pyridine to piperidine.[15,16] This chapter

describes work expanding upon the initial report of pyridine reduction by Kudo and coworkers, including analysis of the product distribution of the reaction of pyridine with SmI_2-water, expansion of the substrate scope, and an investigation of the mechanism behind the remarkable reduction.

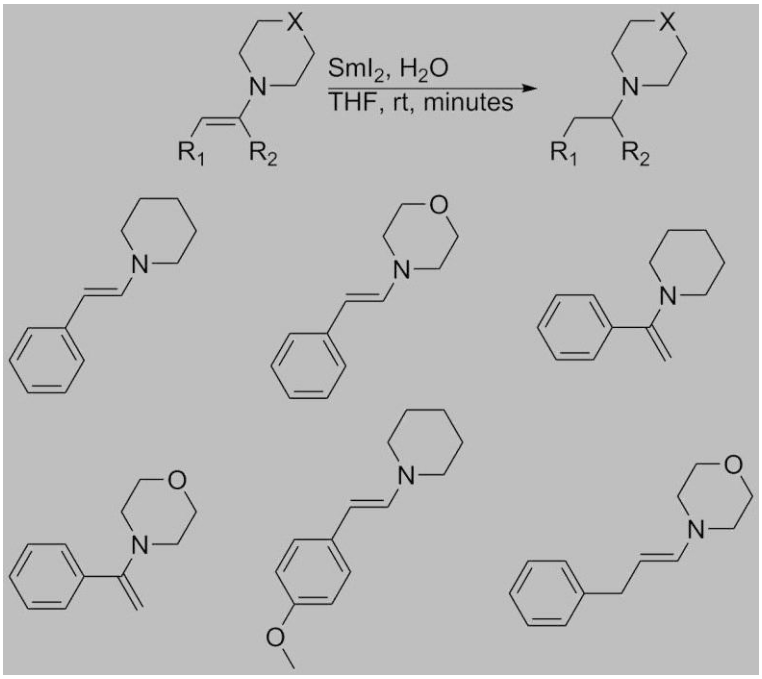

Scheme 2.2. Reaction scheme and substrate scope for the SmI_2-H_2O mediated reduction of enamines[12]

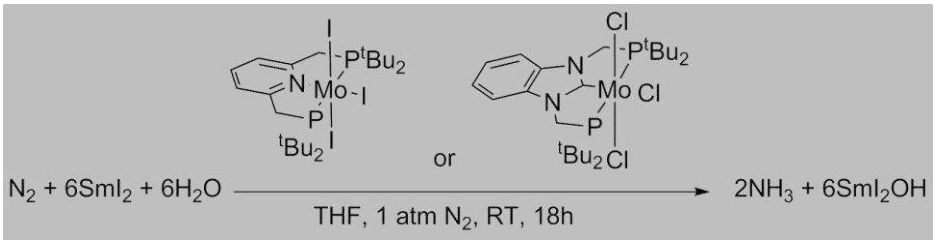

Scheme 2.3. Reaction scheme for the molybdenum PNP/PCP catalyzed reduction of N_2 to NH_3 by SmI_2-H_2O[13]

2.2 Experimental Details

2.2.1 Materials

Samarium powder was purchased from Acros Organics. Samarium diiodide was generated by the standard method of samarium metal combined with iodine in THF and

allowed to stir for at least 4 hours. Iodometric titrations were then performed to verify concentration of SmI_2 for use. Tetrahydrofuran was purified by a solvent purification system (Innovative Technology Inc.; MA). Pyridine, quinoline, and isoquinoline were purchased from Alfa Aesar and used without further purification. Liquid substrates as well as water and deuterium oxide were deoxygenated by bubbling with argon gas prior to use.

2.2.2 Instrumentation

^{1}H NMR and ^{13}C $\{^{1}H\}$ NMR spectra were recorded in $CDCl_3$ on a Bruker 400 MHz spectrometer at 400 and 125 MHz respectively. The ^{1}H NMR chemical shifts are given as δ values in ppm relative to TMS (0 ppm) as the internal reference. The $^{13}C\{1H\}$ NMR shifts are expressed with respect to the $CDCl_3$ (77.0 ppm). GCMS analyses were performed with a Shimadzu GCMS-QP2010 Ultra. GC analyses were performed using a Shimadzu Gas Chromatograph GC-2010 Plus with biphenyl as an internal standard. UV-Visible spectra experiments were performed with a computer-controlled SX.18 MV stopped-flow spectrophotometer (Applied Photophysics Ltd. Surrey, UK). Solutions were prepared under a dry argon atmosphere in flame dried glassware.

2.2.3 Methods

2.2.3.1 Procedure for Synthesis of Functionalized Quinolines

Iron powder (59 mmol, 3.3 g) was added to a solution of *o*-nitroarylcarbaldehyde (14.7 mmol) in ethanol (45 mL) in a round bottom flask. Subsequently, 0.1 M HCl (7.5 mL) was added to the reaction flask and the solution was stirred under reflux overnight. Once the reaction was complete, the respective carbonyl compound (14.7 mmol) was added to the flask followed by the gradual addition of powdered KOH (19 mmol, 1.00 g).

The reaction mixture was once again stirred overnight under reflux then allowed to cool to room temperature, diluted with CH_2Cl_2, and filtered over Celite. The filtrate was washed with water and the aqueous wash solution was back extracted with three portions of CH_2Cl_2. The organic phases were combined and dried over $MgSO_4$ then concentrated under reduced pressure. The desired quinoline product was then isolated by column chromatography over deactivated silica gel with an EtOAc/hexanes mobile phase.

2.2.3.2 Procedure for Reduction of Pyridines and Quinolines by SmI_2-Water

A flame dried vial equipped with a magnetic stir bar was charged with a solution of 0.1 M SmI_2 (10 mL, 1 mmol). To the vial was added substrate (0.14 mmol for pyridines, 0.2 mmol for quinolines). The solution was allowed to stir briefly before the addition of water (0.18 mL, 10 mmol). This solution was allowed to react until discoloration of the characteristic blue of SmI_2 to yellow was observed then quenched in air followed by 25% aqueous sodium-potassium tartrate. This solution was vacuum filtered and the filtrate was basified to pH 12 by addition of 2 M aqueous NaOH. Products were then extracted with three 7 mL portions of diethyl ether. The combined organic layers were dried over magnesium sulfate and concentrated under reduced pressure. Product analysis was carried out by GCMS, ^1H, ^{13}C, COSY, and HMQC NMR spectroscopy.

2.2.3.2.1 Procedure for GCMS Yields of Reductions of Pyridines and Quinolines by SmI_2-Water

A flame dried vial equipped with a magnetic stir bar was charged with a solution of 0.1 M SmI_2 (10 mL, 1 mmol). Substrate (0.14 mmol for pyridines, 0.2 mmol for quinolines) was then added to the vial. The solution was allowed to stir briefly before the

addition of water (0.18 mL, 10 mmol). This solution was allowed to react until discoloration of the characteristic blue of SmI_2 to yellow was observed then quenched in air followed by 25% aqueous sodium-potassium tartrate and biphenyl (0.2 mmol, 0.03 g). This solution was vacuum filtered and the filtrate was basified to pH 12 by addition of 2 M aqueous NaOH. The solution was then extracted with three 7 mL portions of diethyl ether. The combined organic layers were dried over magnesium sulfate and concentrated under reduced pressure. GCMS analysis was performed with a Shimadzu GCMS-QP2010 Ultra.

2.2.3.2.2 Procedure for Isolation of Products of Reductions of Pyridines and Quinolines by SmI_2-Water/Deuterium Oxide

Piperidine was extracted with diethyl ether and dried over magnesium sulfate. The resulting solution was concentrated by boiling away solvent at 35°C and characterized by ^{1}H NMR (400 MHz, $CDCl_3$) δ (ppm): 1.53 (m, 3H), 2.81 (m, 2H)

4-(*tert*-buty)piperidine-2,3,4,5,6-d_5 was extracted with diethyl ether and dried over magnesium sulfate. The resulting solution was concentrated under reduced pressure and characterized by ^{1}H (400 MHz, $CDCl_3$) δ (ppm): 0.85 (s, 9H), 1.16-1.22 (m, 2H), 2.55 (d, 1H), 3.14 (d, 1H);^{13}C NMR (100 MHz, $CDCl_3$) δ (ppm): 26.98, 28.87, 46.69

1,2,3,4-tetrahydroquinoline-2,3,4-d_3 was extracted with diethyl ether and dried over magnesium sulfate. The resulting solution was concentrated under reduced pressure and characterized by ^{1}H (400 MHz, $CDCl_3$) δ (ppm): 1.91-1.97 (m, 1H), 2.74-2.80 (m, 1H), 3.30 (d, 1H), 6.51 (d, 1H), 6.64 (td, 2H), 6.99-7.02 (m, 1H);^{13}C NMR (100 MHz, $CDCl_3$) δ (ppm): 21.61, 26.49, 41.56, 114.24, 117.00, 126.75, 129.56

1,2,3,4-tetrahydroisoquinoline-1,3,4-d_3 was extracted with diethyl ether and dried over magnesium sulfate. The resulting solution was concentrated under reduced pressure and characterized by ^{1}H (400 MHz, $CDCl_3$) δ (ppm): 2.80 (bs, 1H), 3.14 (bs, 1H), 4.02 (s, 1H), 7.00-7.20 (m, 5H);^{13}C NMR (100 MHz, $CDCl_3$) δ (ppm): 28.73, 43.48, 47.94, 125.76, 126.04, 126.22, 129.34, 135.99, 136.83

1,2,3,4,4a,9,9a,10-octahydroacridine-4a,9,9a-d_3 was extracted with diethyl ether and dried over magnesium sulfate. The resulting solution was concentrated under reduced pressure and characterized by ^{1}H (400 MHz, $CDCl_3$) δ (ppm): 1.32-1.78 (m, 8H), 2.72 (d, 1H), 6.49 (d, 1H), 6.61 (td,1H), 6.99 (t, 2H);^{13}C NMR (100 MHz, $CDCl_3$) δ (ppm): 20.79, 24.74, 27.21, 31.64, 32.14, 49.48, 113.26, 116.47, 119.26, 126.66, 129.78, 143.92

7-fluoro-1,2,3,4,4a,9,9a,10-octahydroacridine-4a,9,9a-d_3 was extracted with diethyl ether and dried over magnesium sulfate. The resulting solution was concentrated under reduced pressure and characterized by ^{1}H (400 MHz, $CDCl_3$) δ (ppm): 1.04 (t, 1H), 1.26-1.48 (m, 3H), 1.72-1.95 (m, 4H), 2.55 (d, 1H), 6.41-6.46 (m, 1H), 6.67-674 (m, 2H);^{13}C NMR (100 MHz, $CDCl_3$) δ (ppm): 24.63, 25.89, 31.79, 33.38, 34.13, 36.67, 55.53, 113.12, 114.41, 115.33, 154.30, 156.62

2-phenyl-1,2,3,4-tetrahydroquinoline-2,3,4-d_3 was extracted with diethyl ether and dried over magnesium sulfate. The resulting solution was concentrated under reduced pressure and characterized by ^{1}H (400 MHz, $CDCl_3$) δ (ppm): 2.10 (dd, 1H), 2.76-3.00 (m, 1H), 6.61 (d, 1H), 6.74 (td, 1H), 7.06-7.13 (m, 2H), 7.34-7.50 (m, 5H);^{13}C NMR (100 MHz, $CDCl_3$) δ (ppm): 26.95, 30.39, 55.80, 114.05, 117.19, 120.89, 126.62, 127.00, 127.53, 126.68, 129.38, 129.41, 144.82, 144.85

6-fluoro-2-phenyl-1,2,3,4-tetrahydroquinoline-2,3,4-d_3 was extracted with diethyl ether and dried over magnesium sulfate. The resulting solution was concentrated under reduced pressure and characterized by ^{1}H (400 MHz, $CDCl_3$) δ (ppm): 2.10 (dd, 1H), 2.74-3.01 (m, 1H), 6.54 (dd, 1H), 6.80-6.87 (m, 2H), 7.37-7.52 (m, 5H);^{13}C NMR (100 MHz, $CDCl_3$) δ (ppm): 26.08, 30.18, 55.85, 113.37, 113.70, 114.71, 115.46, 115.79, 126.66, 127.67, 128.67, 141.13, 114.64, 154.42, 156.76

5,6,6a,7,12,12a-hexahydrobenzo[c]acridine-6a,7,12a-d_3 was extracted with diethyl ether and dried over magnesium sulfate. The resulting solution was concentrated under reduced pressure and characterized by ^{1}H (400 MHz, $CDCl_3$) δ (ppm): 1.09-2.09 (m, 3H), 3.27 (dd, 1H), 6.27 (dd, 1H), 3.45 (td, 1H), 6.46 (t, 2H), 6.73 (t, 1H), 6.91-6.97 (m, 1H), 6.99-7.05 (m, 1H), 7.15 (d, 1H);^{13}C NMR (100 MHz, $CDCl_3$) δ (ppm): 24.65, 26.62, 29.55, 31.95, 42.13, 112.73, 113.79, 115.35, 116.84, 121.97, 123.58, 126.33, 127.26, 130.33, 130.76, 143.82, 144.89

5a,6,11,12,12a,13-hexahydro-5H-6,12-methanobenzo[6,7]azepino[4,3-b]quinoline was extracted with diethyl ether and dried over magnesium sulfate. The resulting solution was concentrated under reduced pressure and characterized by ^{1}H (400 MHz, $CDCl_3$) δ (ppm): 1.70 (d, 1H), 1.94-2.28 (m, 3H), 2.48-2.58 (m, 1H), 2.72-2.84 (m,2H), 3.41 (d, 1H), 3.63 (d, 1H), 6.40 (d, 1H), 6.55 (d, 2H), 6.67 (t, 1H), 6.84-7.01 (m, 4H)

5a,6,7,12,12a,13-hexahydro-5H-6,12-methanobenzo[6,7]azepino[3,4-b]quinoline was extracted with diethyl ether and dried over magnesium sulfate. The resulting solution was concentrated under reduced pressure and characterized by ^{1}H (400 MHz, $CDCl_3$) δ (ppm): 1.65 (d, 1H), 1.79-1.88 (m, 1H), 2.67 (t, 1H), 2.93 (d, 1H), 3.00 (dd,

1H), 3.16 (dd, 1H), 3.12 (d, 1H), 3.56 (d, 1H), 6.45-6.51 (m, 2H), 6.62 (td, 1H), 6.74 (td, 1H), 6.89-7.02 (m, 3H), 7.14-7.19 (m, 1H);^{13}C NMR (100 MHz, $CDCl_3$) δ (ppm): 30.35, 45.53, 49.14, 51.24, 51.62, 59.81, 115.32, 115.38, 118.00, 119.37, 126.39, 127.04, 127.57, 127.86, 129.95, 130.31, 142.52, 147.26

5,6,8,13,13a,14-hexahydro-6,14-methanobenzo[4,5][1,3]diazepino[1,7-b]isoquinoline was extracted with diethyl ether and dried over magnesium sulfate. The resulting solution was concentrated under reduced pressure and characterized by ^{1}H (400 MHz, $CDCl_3$) δ (ppm): 2.45 (d, 1H), 2.82-2.91 (m, 2H), 3.00 (t, 1H), 3.11 (dd, 1H), 3.29-3.36 (m, 1H), 4.19 (s, 1H), 4.44 (s, 1H), 4.50 (s, 1H), 7.03-7.26 (m, 8H); ^{13}C NMR (100 MHz, $CDCl_3$) δ (ppm): 24.86, 39.30, 46.35, 68.46, 70.44, 76.78, 125.40, 125.74, 126.32, 126.78, 127.52, 129.02, 129.85

2.2.3.2.3 Procedure for ESI-MS Analysis of Reductions of Pyridines and Quinolines by SmI_2-Water

A flame dried vial equipped with a magnetic stir bar was charged with a solution of 0.1 M SmI_2 (10 mL, 1 mmol). To the vial was added substrate (0.14 mmol for pyridines, 0.2 mmol for quinolines). The solution was allowed to stir briefly before the addition of water (0.18 mL, 10 mmol). This solution was allowed to react until discoloration of the characteristic blue of SmI_2 to yellow was observed then quenched in air and concentrated under reduced pressure. The solid residue was dried to a fine powder on a high-vacuum line. This powder was added to a solution of methanol and analyzed on an Applied Biosystems MDS Sciex ESI-MS equipped with a 3200 Q Trap.

2.2.3.3 Procedure for Stopped Flow Kinetics Studies

Kinetic experiments were performed with a computer-controlled SX.18 MV stopped- flow spectrophotometer (Applied Photophysics Ltd. Surrey, UK). Solutions were injected separately into the stopped-flow system using airtight, capped BD syringes prepared in a glove box under argon atmosphere. Between each experiment, the cell block was washed with dilute HNO_3 (1x), Deionized H_2O (1x), and THF (3x) before additional anhydrous deoxygenated THF washes (3x). The reaction rates were determined from the decay of SmI_2 at 560 nm. Kinetic measurements were carried out at 25°C unless otherwise specified.

2.3 Results and Discussion

2.3.1 Synthetic Investigations and Product Characterization of the Reduction of Pyridines and Quinolines by SmI_2-Water

Our investigation of the reduction of pyridines by SmI_2-water began while studying the effects of amine pK_a on the reactivity of SmI_2-water-amine systems with carbonyls. The use of pyridine as the amine in this system yielded a full recovery of the carbonyl starting material despite rapid discoloration of the characteristic blue of the SmI_2 solution, which indicates the oxidation of Sm(II) to Sm(III). Experiments with SmI_2-water-pyridine in the absence of a carbonyl substrate yielded the same rapid discoloration of SmI_2, which is consistent with the reduction of pyridine by SmI_2-water. This reactivity has been previously documented by Kudo and coworkers, who reported nearly quantitative conversion of pyridine to piperidine.[15,16] Although in our hands, the protocol described by Kudo and coworkers yielded no recovery of product or starting

material, treatment of the quenched reaction solution with potassium-sodium tartrate and extraction of the aqueous solution into diethyl ether enabled the isolation of piperidine.

A number of other pyridine and quinoline substrates, shown in Figure 2.2, were also prepared for reduction. Selective reduction of the N-aromatic functionality of each of these substrates was confirmed by GCMS and ^{1}H NMR with GCMS yields of between 15-30% for each substrate. Further analysis of the crude reaction products with electrospray ionization mass spectrometry (ESI-MS) revealed mass peaks consistent with a doubly bridged dimerized product for each substrate with the exception of **10**, shown in Figure 2.3. Dimer isolation was attempted for the reduction of pyridine but was unsuccessful, likely due to the high affinity of the putative products for Sm^{III}.

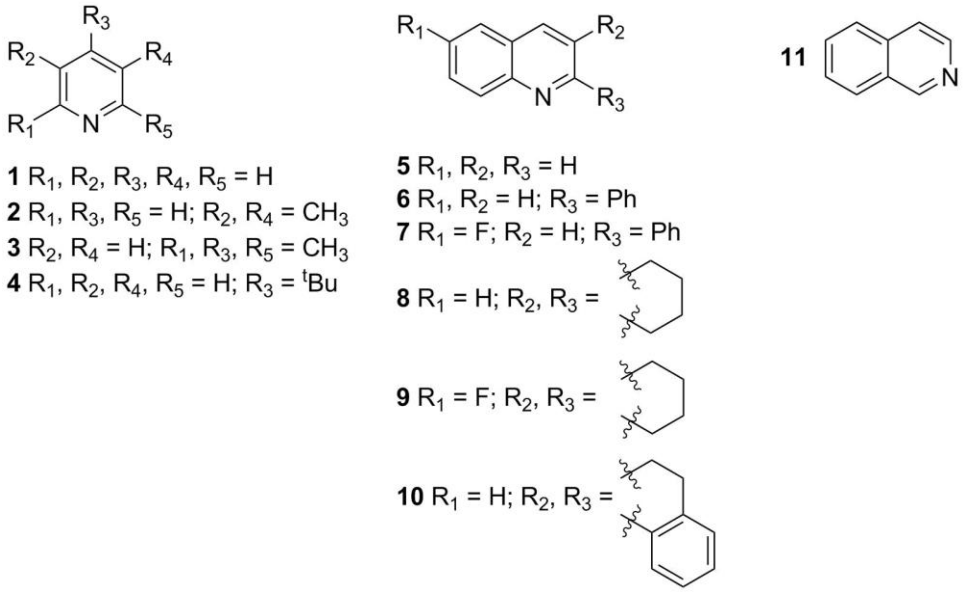

Figure 2.2. Substrate scope for the reduction of 6-membered N-heteroaromatics by SmI_2-water

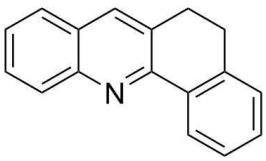

Figure 2.3. 5,6-dihydrobenzo[c]acridine (**10**)

The dimerized products of the reduction of quinoline were successfully isolated, yielding the products shown in Scheme 2.4. The presence of a similar pair of dimerized products was observed by GCMS analysis of the reduction of isoquinoline. The peaks were found to be analogous to those observed for the pair of dimerized products isolated from the reduction of quinoline, however only the product shown in Scheme 2.4 was isolated. This product is notable for its possession of a bridgehead nitrogen.

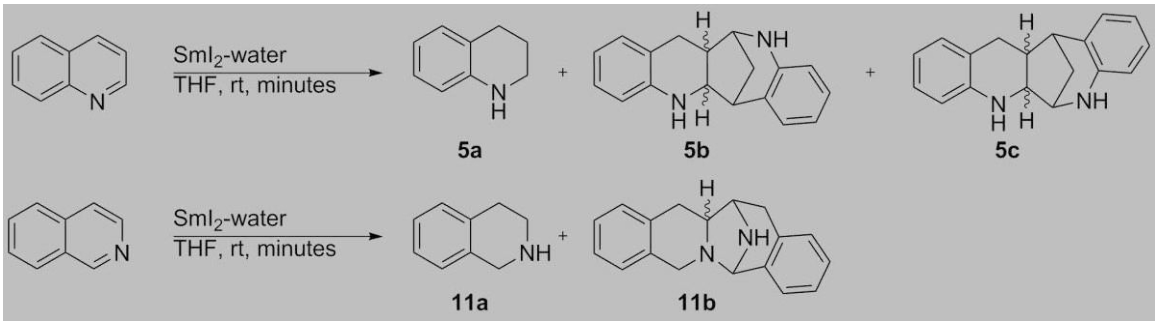

Scheme 2.4. Reaction scheme for the reduction and reductive dimerization of quinoline and isoquinoline by SmI_2-water

The lack of a dimerization pathway for **10** is notable given the ubiquity of dimerization among the other substrates studied. This unique behavior was attributed to the significant steric occlusion of the 2- and 3- position carbons in **10**, which are both bridgehead positions in the dimers of quinoline and isoquinoline. With this insight, it was proposed that the dimerization pathway in the reduction of pyridines and quinolines by SmI_2-water may be subject to steric control. This is important for pharmaceutical development, where both complex polyannulated alkaloids and the reduction of prefunctionalized pyridines to piperidines are highly desirable.

2.3.2 Kinetic Analysis of the Reductions of Pyridines and Quinolines by SmI_2-Water

2.3.2.1 Kinetic Rate Order Experiments

The mechanism of the reduction of pyridine was further investigated through rate studies using stopped flow kinetic analysis. Despite the stability of pyridine, its reduction

by SmI_2-water proceeded too rapidly for measurement under pseudo-first order conditions. Stopped flow kinetic analysis was therefore carried out under initial rates conditions, with [pyridine] and [water] within 25 equiv. of [SmI_2]. The rate order of each component was determined independently by observing the change in rate during the initial linear portion of the decay curve over a range of concentrations. The results of these experiments are shown in Table 2.1. The rate orders for SmI_2 and pyridine were found to be near unity. The rate order of water was also found to be near unity for relatively low [water] but fell rapidly to zeroth order at higher concentrations. This saturation behavior has been observed previously in the SmI_2-water-mediated reduction of carbonyl containing substrates. In those studies, it was hypothesized that coordination of substrate to Sm(II) was necessary for substrate reduction and that displacement of water by substrate in the first coordination sphere of Sm(II) presents a kinetic barrier to substrate reduction at high [water].[17] Since pyridine is also likely reduced through an inner sphere PCET, a similar kinetic water displacement barrier is also likely present in the SmI_2-water-mediated reduction of pyridine at high [water]. The saturation behavior of water in the SmI_2-water-mediated reduction of pyridine can be seen in the inset in Figure 2.4.

Table 2.1. Rate orders for the reductions of pyridine by SmI_2-water

entry	reaction component	rate order[a]
1	SmI_2	0.97 ± 0.04[b]
2	H_2O	1.1 ± 0.2[c]
3	Pyridine	0.78 ± 0.03[d]

[a]Errors reported as ± σ. [b]3-10mM SmI_2, 1mM substrate, 60mM H_2O in THF. [c]6mM SmI_2, 1mM substrate, 20-35mM H_2O in THF. [d]6mM SmI_2, 0.03125-3mM substrate, 60mM H_2O in THF.

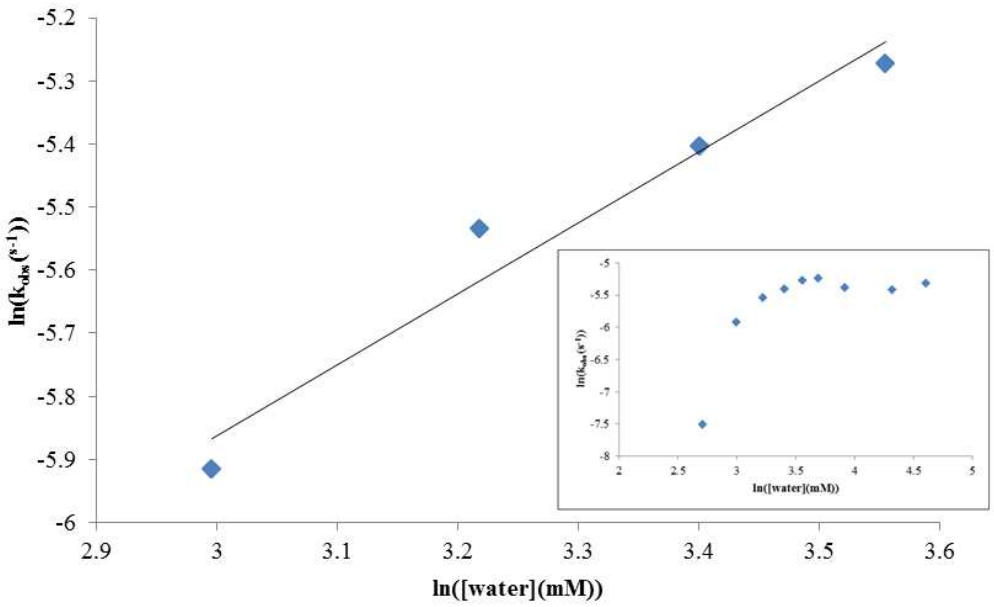

Figure 2.4. Plots of $\ln(k_{obs})$ vs [water] for the reduction of pyridine by SmI_2-water

2.3.2.2 Kinetic Activation Parameter Experiments

Additional rate studies were carried out for both pyridine and **10** over a 20°C temperature range with constant starting concentrations in order to acquire activation parameters for the reductions of both substrates. The results of these experiments are shown in Table 2.2. Both systems display a similarly intermediate degree of bond reorganization in their activated complexes. The free energies of activation differ slightly, however, with a greater free energy of activation for the reduction of **10** compared to pyridine. This difference is also reflected in the calculated rate constant for the reductions of the two substrates, $5 \times 10^4 \pm 2 \times 10^4$ $M^{-2}s^{-1}$ and $9 \times 10^2 \pm 4 \times 10^2$ $M^{-2}s^{-1}$ for the reductions of pyridine and **10** respectively. Given the nearly 10 kcal/mol greater N-H BDFE for the bond formed upon the initial reduction of **10** compared to pyridine, this trend is counterintuitive. Rationalization for this can be found in the respective entropies of activation for the two reductions, with the greater steric occlusion of nitrogen

in **10** giving rise to a greater entropic cost to reduction and outweighing the greater enthalpic cost to reduction for pyridine.

Table 2.2. Activation parameters for the reductions of pyridine and **10** by SmI_2-water

entry	activation parameter	pyridine[a]	**10**[a]
1	$\Delta H^{\ddagger}$ (kcal/mol)[b]	13 ± 1	10 ± 2
2	$\Delta S^{\ddagger}$ (cal/molK)[b]	-24 ± 4	-40 ± 6
3	$\Delta G^{\ddagger}$ (kcal/mol @ 25°C)[c]	20 ± 2	22 ± 2

[a]Conditions: 6mM SmI_2, 1mM substrate, 60mM H_2O in THF. Temperature varied between 15 and 35 °C. Errors reported as ± σ. [b]Obtained from $\ln\left(\frac{k_{obs}h}{kT}\right) = \frac{\Delta H^{\ddagger}}{RT} + \frac{\Delta S^{\ddagger}}{R}$ [c]Obtained from $\Delta G^{\ddagger} = \Delta H^{\ddagger} - T\Delta S^{\ddagger}$

2.3.2.3 Deuterium Kinetic Isotope Effect Experiments and Selective Deuteration Experiments

Deuterium kinetic isotope effect (KIE) data was also collected for the reduction of pyridine by SmI_2-water by comparing the rates of reduction in the presence of H_2O and D_2O over a range of concentrations. The results, shown in Figure 2.5, reveal a deuterium KIE of nearly 3, which is consistent with a CPET reduction.[18–21]

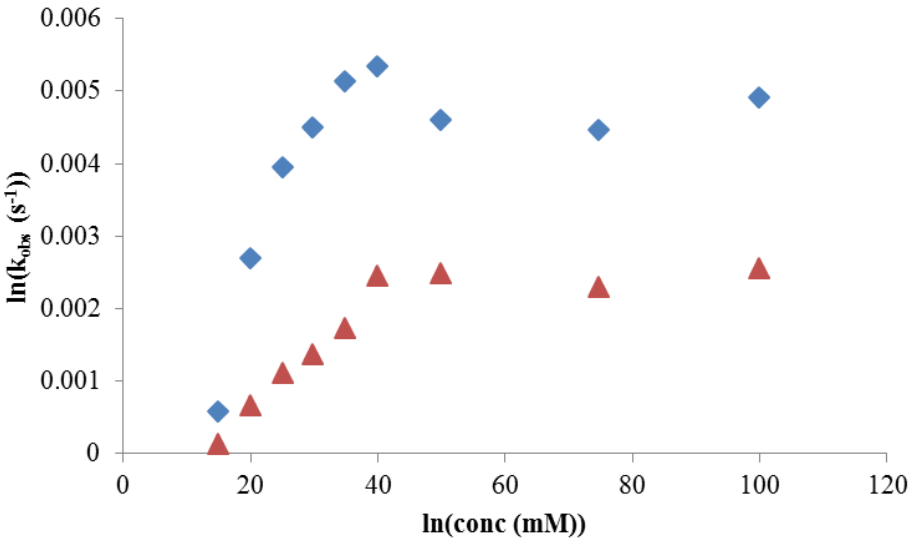

Figure 2.5. Plot of $\ln(k_{obs})$ vs [water] (blue diamonds) and [deuterium oxide] (red triangles) for the reduction of pyridine by SmI_2-water

In addition to measuring the difference in rate of reduction in the presence of water and deuterium oxide, the products of the reduction of several quinolines in the presence of deuterium oxide were isolated and characterized by GCMS, ^{1}H NMR, and ^{13}C NMR. The reaction scheme and substrate scope are shown in Scheme 2.5. Notably, the isolated products were protonated rather than deuterated at nitrogen. This is likely a consequence of the aqueous workup conditions and the lability of the N-D bond. The reductive deuteration of pyridine was also confirmed using ESI-MS, although the piperidine-d_2,d_3,d_4,d_5,d_6 product was not isolated.

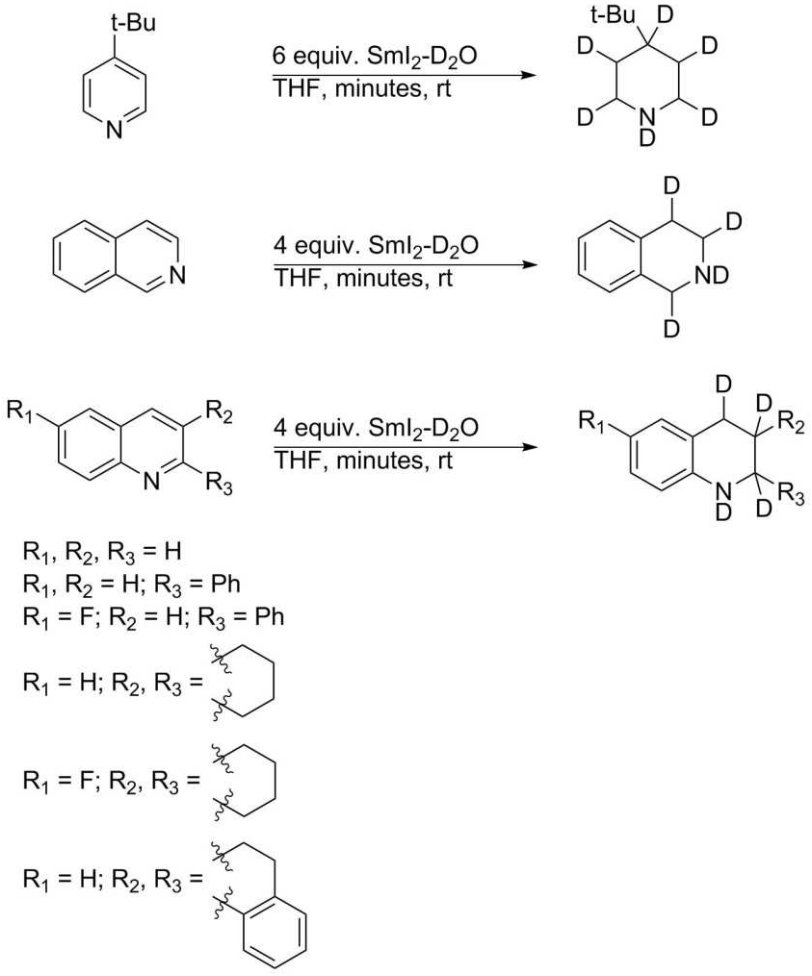

Scheme 2.5. Reaction scheme and isolated product scope for the selective reductive deuteration of quinolines by SmI_2-deuterium oxide

2.3.3 Mechanistic Insights into the Reductions of Pyridines and Quinolines by SmI_2-Water

Although the KIE and rate data were found to be consistent with a CPET reaction, it was considered that the SmI_2-water-mediated reduction of pyridines and quinolines could proceed through a PT-ET mechanism, shown in Scheme 2.6. This pathway is plausible due to the significant basicity of the nitrogen in pyridine, which could feasibly facilitate the deprotonation of water, forming a pyridinium intermediate. Subsequent electron transfer from SmI_2 and serial reductions by SmI_2-water could then provide the observed piperidine product. To test this hypothesis, pyridinium chloride was prepared by bubbling HCl gas through a solution of pyridine in diethyl ether. This pyridinium chloride was then added to an equimolar solution of SmI_2 in dry THF in the absence of a proton source. The solution of SmI_2 and pyridinium chloride was found to be stable over several days but decolored rapidly upon addition of water. The stability of SmI_2 in the presence of pyridinium chloride rules out a PT-ET mechanism. Likewise, the stability of SmI_2 in the presence of pyridine rules out an ET-PT mechanism. This leaves a PCET mechanism as the only remaining viable pathway for the reduction of pyridine by SmI_2-water.

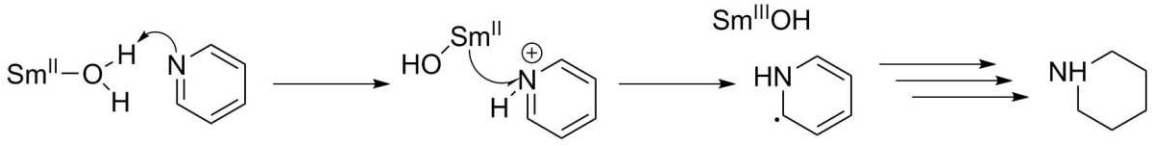

Scheme 2.6. Proposed PT-ET reaction mechanism for the reduction of pyridine by SmI_2-water

The mechanistic insights gained in the rate studies described above were combined to propose the reduction of pyridines and quinolines by SmI_2-water through an initial rate-limiting PCET. In one pathway, the initial reduction of pyridine or quinoline

is followed by substrate reduction by further SmI_2-water equivalents, yielding piperidine or 1,2,3,4-tetrahydroquinoline. The presence of reduced dimers of pyridines and quinolines suggests that another pathway is also operative in the reduction of pyridines and quinolines by SmI_2-water. In this mechanism, shown in Scheme 2.7, quinoline is reduced by an initial rate limiting PCET. The intermediate then initiates a radical addition on the 2- or 3-position of another substrate molecule, providing the cyclized products isolated from the reduction of quinoline *vide supra* (Scheme 2.4).

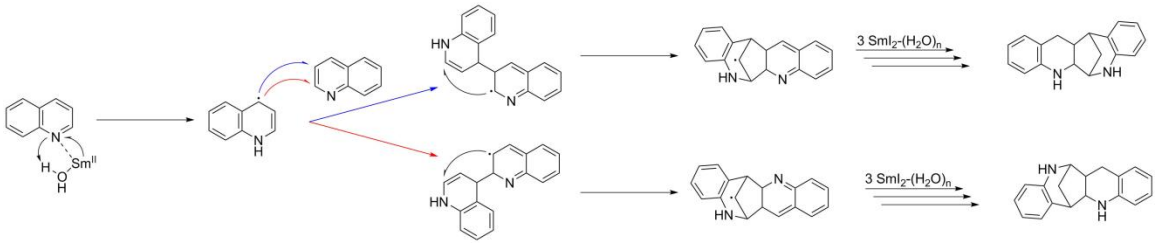

Scheme 2.7. Proposed reaction mechanism for the reduction and reductive dimerization of quinoline by SmI_2-water

Although the mechanism in Scheme 2.7 shows radical attack onto quinoline, only the 2- and 3-positions of the substrate are involved in the cyclization pathway. In light of this, it is likely that the partially reduced enamine intermediate is also susceptible to radical attack as shown in Scheme 2.8.

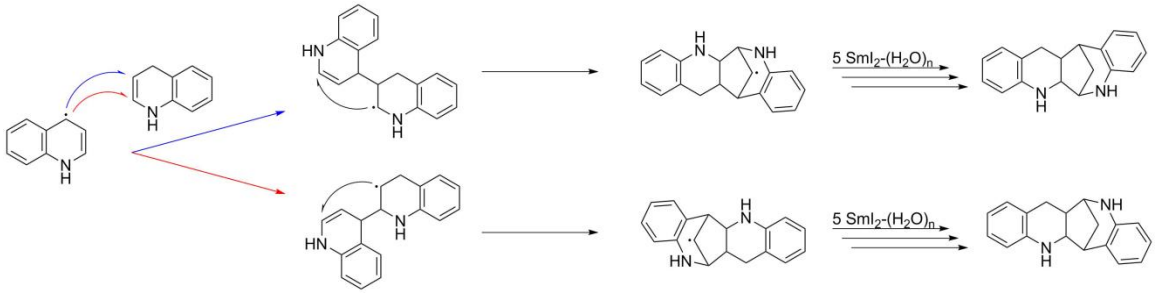

Scheme 2.8. Alternative pathways for the reductive dimerization of quinoline by SmI_2-water

2.4 Conclusions

The synthetic and mechanistic studies presented above demonstrate that the SmI_2-water reagent is capable of mediating the rapid selective reduction of a range of pyridines and quinolines. Both the selectively reduced piperidine and 1,2,3,4-tetrahydroquinoline products as well as complex polyannulated products can be achieved through this method with both carbon- and nitrogen-bridgeheads. Steric tuning of the pyridine or quinoline starting material can be utilized to reduce dimer formation and yield only the selectively reduced product. The ability of this system to provide access to a variety of desirable products makes it potentially valuable in a pharmaceutical context.

Moreover, the reduction of pyridines and quinolines by SmI_2-water enables the selective deuteration of products via substitution of water by deuterium oxide. Compared to C-H bonds, C-D bonds are more resistant to enzymatic degradation, which increases the metabolic half-life of deuterated drugs and thereby mitigates toxic metabolite formation.[22–24] Moreover, the metabolic differences between C-H and C-D bonds are primarily kinetic, allowing selectively deuterated drugs to maintain their target activity. While selective deuteration by SmI_2-D_2O is well documented in the literature, only a few alternative methods of selective deuteration exist and are subject to limited substrate scope or challenging reaction conditions.[25–27] The ability of SmI_2-water to affect the selective deuteration of piperidine products therefore significantly expands the scope of potential drug targets available for selective deuterium incorporation.

In addition to the medicinal and pharmaceutical implications of the reduction of pyridines by SmI_2-water, the reaction is also remarkable from a thermodynamic perspective. The N-H bond formed upon the PCET initial reduction of pyridine, shown

in Scheme 2.9, has a BDFE of 26.2 kcal/mol. This contrasts sharply with the 108.0 kcal/mol O-H bond of water. The coordination of pyridine to Sm(II) precludes the assignment of a degree of O-H bond weakening in water upon coordination to Sm(II) based on this reaction. Nonetheless, the SmI_2-water-mediated reduction of pyridine yields the formation of an exceptionally weak X-H bond under mild conditions. Even more remarkably, to our knowledge, the SmI_2-water reagent is the only system capable of facilitating the reduction of pyridine to piperidine under ambient conditions.[12]

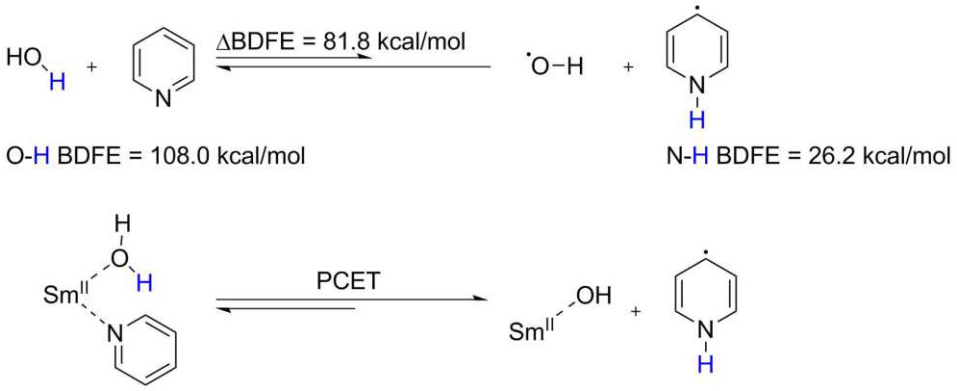

Scheme 2.9. Reaction scheme for the SmI_2-water-mediated reduction of pyridine and comparison of the O-H BDFE of water with the N-H BDFE of the bond formed upon initial PCET reduction of pyridine

Further investigations into the reductions of pyridines and quinolines by Sm(II)-water systems are underway. One promising strategy being investigated currently is the substitution of iodide ligands on Sm(II) with more bulky ligands such as hexamethyldisilazane to steer the reaction away from dimerization and towards selective reduction.

2.5 References

(1) Vitaku, E.; Smith, D. T.; Njardarson, J. T. Analysis of the Structural Diversity, Substitution Patterns, and Frequency of Nitrogen Heterocycles among U.S. FDA Approved Pharmaceuticals. *J. Med. Chem.* **2014**, *57* (24), 10257–10274.

(2) Shankaraiah, N.; Pilli, R. A.; Santos, L. S. Enantioselective Total Syntheses of Ropivacaine and Its Analogues. *Tetrahedron Lett.* **2008**, *49* (34), 5098–5100.

(3) Shaw, A. T.; Yeap, B. Y.; Solomon, B. J.; Riely, G. J.; Gainor, J.; Engelman, J. A.; Shapiro, G. I.; Costa, D. B.; Ou, S. H. I.; Butaney, M.; et al. Effect of Crizotinib on Overall Survival in Patients with Advanced Non-Small-Cell Lung Cancer Harbouring ALK Gene Rearrangement: A Retrospective Analysis. *Lancet Oncol.* **2011**, *12* (11), 1004–1012.

(4) Königs, C. D. F.; Klare, H. F. T.; Oestreich, M. Catalytic 1,4-Selective Hydrosilylation of Pyridines and Benzannulated Congeners. *Angew. Chemie - Int. Ed.* **2013**, *52* (38), 10076–10079.

(5) Murphy, R. A.; Chen, A. Y.; Nair, S. K.; Gallego, G. M.; Sach, N. W.; Smith, G. Diastereoselective Access to Substituted 4-Aminopiperidines via a Pyridine Reduction Approach. *Tetrahedron Lett.* **2016**, *57* (50), 5588–5591.

(6) Patnaik, P. Amines, Aliphatic. In *A Comprehensive Guide to the Hazardous Properties of Chemical Substances*; 2008; pp 235–250.

(7) Xu, L.; Lam, K. H.; Ji, J.; Wu, J.; Fan, Q. H.; Lo, W. H.; Chan, A. S. C. Air-Stable Ir-(P-Phos) Complex for Highly Enantioselective Hydrogenation of Quinolines and Their Immobilization in Poly(Ethylene Glycol) Dimethyl Ether (DMPEG). *Chem. Commun.* **2005**, No. 11, 1390–1392.

(8) Reetz, M. T.; Li, X. Asymmetric Hydrogenation of Quinolines Catalyzed by Iridium Complexes of BINOL-Derived Diphosphonites. *Chem. Commun.* **2006**, No. 20, 2159–2160.

(9) Yella, R.; Gottlieb, H. E.; Hoz, S. A [2 + 3] Reductive Cyclodimerization of Quinoline by SmI2. *J. Org. Chem.* **2015**, *80* (17), 8929–8932.

(10) Maity, S.; Flowers, R. A.; Hoz, S. Aza versus Oxophilicity of SmI2 : A Break of a Paradigm. *Chem. - A Eur. J.* **2017**, *23* (67), 17070–17077.

(11) Ramírez-Solís, A.; Bartulovich, C. O.; León-Pimentel, C. I.; Saint-Martin, H.; Boekell, N. G.; Flowers, R. A. Proton Donor Effects on the Reactivity of SmI2. Experimental and Theoretical Studies on Methanol Solvation vs. Aqueous Solvation. *Dalt. Trans.* **2020**, *49* (23), 7897–7902.

(12) Kolmar, S. S.; Mayer, J. M. SmI2(H2O)n Reduction of Electron Rich Enamines by Proton-Coupled Electron Transfer. *J. Am. Chem. Soc.* **2017**, *139* (31), 10687−10692.

(13) Ashida, Y.; Arashiba, K.; Nakajima, K.; Nishibayashi, Y. Molybdenum-Catalysed Ammonia Production with Samarium Diiodide and Alcohols or Water. *Nature* **2019**, *568* (7753), 536–540.

(14) Szostak, M.; Sautier, B.; Spain, M.; Procter, D. J. Electron Transfer Reduction of Nitriles Using SmI2-Et 3N-H2O: Synthetic Utility and Mechanism. *Org. Lett.* **2014**, *16* (4), 1092–1095.

(15) Kamochi, Y.; Kudo, T. Rapid Reduction of a Variety of Organic Functionalities Including a New Selective Reduction with Samarium Diiodide. *Yakugaku Zasshi* **2017**, *120* (3), 245–255.

(16) Kamochi, Y.; Kudo, T. The Novel Reduction of Pyridine Derivatives with Samarium Diiodide. *Heterocycles* **1993**, *36* (10), 2383–2396.

(17) Chciuk, T. V; Anderson, W. R.; Flowers, R. A. Interplay between Substrate and Proton Donor Coordination in Reductions of Carbonyls by SmI2-Water Through Proton-Coupled Electron-Transfer. *J. Am. Chem. Soc.* **2018**, *140*, 15342–15352.

(18) Hoover, J. M.; Ryland, B. L.; Stahl, S. S. Mechanism of Copper(I)/TEMPO-Catalyzed Aerobic Alcohol Oxidation. *J. Am. Chem. Soc.* **2013**, *135*, 2357–2367.

(19) Derosa, J.; Garrido-Barros, P.; Peters, J. C. Electrocatalytic Reduction of C–C π-Bonds via a Cobaltocene-Derived Concerted Proton–Electron Transfer Mediator: Fumarate Hydrogenation as a Model Study. *J. Am. Chem. Soc.* **2021**, *143* (25), 9303–9307.

(20) Cuerva, J. M.; Campaña, A. G.; Justicia, J.; Rosales, A.; Oller-López, J. L.; Robles, R.; Cárdenas, D. J.; Buñuel, E.; Oltra, J. E. Water: The Ideal Hydrogen-Atom Source in Free-Radical Chemistry Mediated by TiIII and Other Single-Electron-Transfer Metals? *Angew. Chemie Int. Ed.* **2006**, *45* (33), 5522–5526.

(21) William A. Pryor, K. G. K. Primary Kinetic Isotope Effects and the Nature of Hydrogen-Transfer Transition States. The Reaction of a Series of Free Radicals with Thiols. *J. Am. Chem. Soc.* **1971**, *93* (21), 5584–5586.

(22) Buckingham, A. D.; Fan-Chen, L. Differences in the Hydrogen and Deuterium Bonds. *Int. Rev. Phys. Chem.* **1981**, *1* (2), 253–269.

(23) Pirali, T.; Serafini, M.; Cargnin, S.; Genazzani, A. A. Applications of Deuterium in Medicinal Chemistry. *J. Med. Chem.* **2019**, *62* (11), 5276–5297.

(24) Schmidt, C. First Deuterated Drug Approved. *Nat. Biotechnol.* **2017**, *35* (6), 493–494.

(25) Koniarczyk, J. L.; Hesk, D.; Overgard, A.; Davies, I. W.; McNally, A. A General Strategy for Site-Selective Incorporation of Deuterium and Tritium into Pyridines, Diazines, and Pharmaceuticals. *J. Am. Chem. Soc.* **2018**, *140* (6), 1990–1993.

(26) Zhang, H. H.; Bonnesen, P. V.; Hong, K. Palladium-Catalyzed Br/D Exchange of Arenes: Selective Deuterium Incorporation with Versatile Functional Group Tolerance and High Efficiency. *Org. Chem. Front.* **2015**, *2* (9), 1071–1075.

(27) Khaskin, E.; Milstein, D. Simple and Efficient Catalytic Reaction for the Selective Deuteration of Alcohols. *ACS Catal.* **2013**, *3* (3), 448–452.

Chapter 3: Investigations of the Mechanism(s) of Reduction of Oximes by Divalent Samarium

3.1 Background and Significance

3.1.1 Reductions of Oxime and Oxime Ether Carbon-Nitrogen Double Bonds by SmI_2

While Sm(II) reductants are most commonly employed in the reductions of alkyl halides and carbonyls, reductions of other functional groups by Sm(II) reductants have been observed.[1] One example of this is the reduction of an oxime ether by SmI_2-HMPA in work by Nicolaou and coworkers on the total synthesis of Diazonamide A.[2] As shown in Scheme 3.1, the macrocyclic backbone of Diazonamide A was formed through a hetero-pinacol coupling between an aldehyde and an O-methyl oxime promoted by SmI_2-HMPA. In the proposed mechanism, SmI_2-HMPA facilitates the single electron reduction of the carbonyl as well as the C=N double bond of the O-methyl oxime. The proposal of this unusual reactivity was informed by the recovery of a side product containing both reduced functional groups with no cyclization. The proposed diradical intermediate then undergoes recombination and the remaining N-O bond is cleaved by excess SmI_2-HMPA. Aqueous workup in the presence of ammonium chloride furnished the fully reduced macrocyclic product shown in Scheme 3.1.[2]

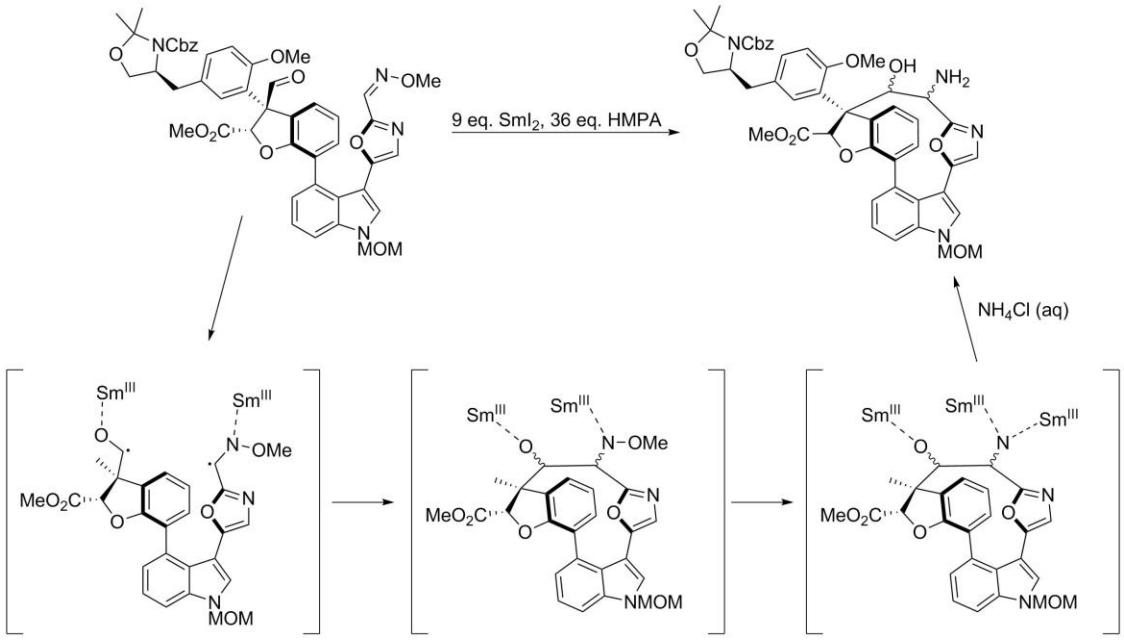

Scheme 3.1. Reaction scheme and proposed mechanism for the hetero-pinacol coupling of an aldehyde with an O-methyl oxime promoted by SmI_2-HMPA in the total synthesis of Diazonamide A[2]

Another example of a Sm(II)-mediated oxime reduction is presented in the report by Naito and coworkers on the total synthesis of (-)-martinellic acid.[3] In this work, SmI_2-*t*-BuOH was investigated as an alternative to tributyltin hydride in the reductive coupling of a benzyl oxime ether with an activated olefin, shown in Scheme 3.2. Although no mechanism was proposed for the reaction, the authors suggest that Sm(II) may undergo chelation by the oxime and proximal ester yielding the α-aza radical shown in Scheme 3.2. This intermediate then likely undergoes 6-*exo*-trig radical cyclization between the α-aza radical and activated olefin. Subsequent reductions by excess SmI_2-*t*-BuOH and radical cyclization between the ester carbonyl and nitrogen then yield the observed products.

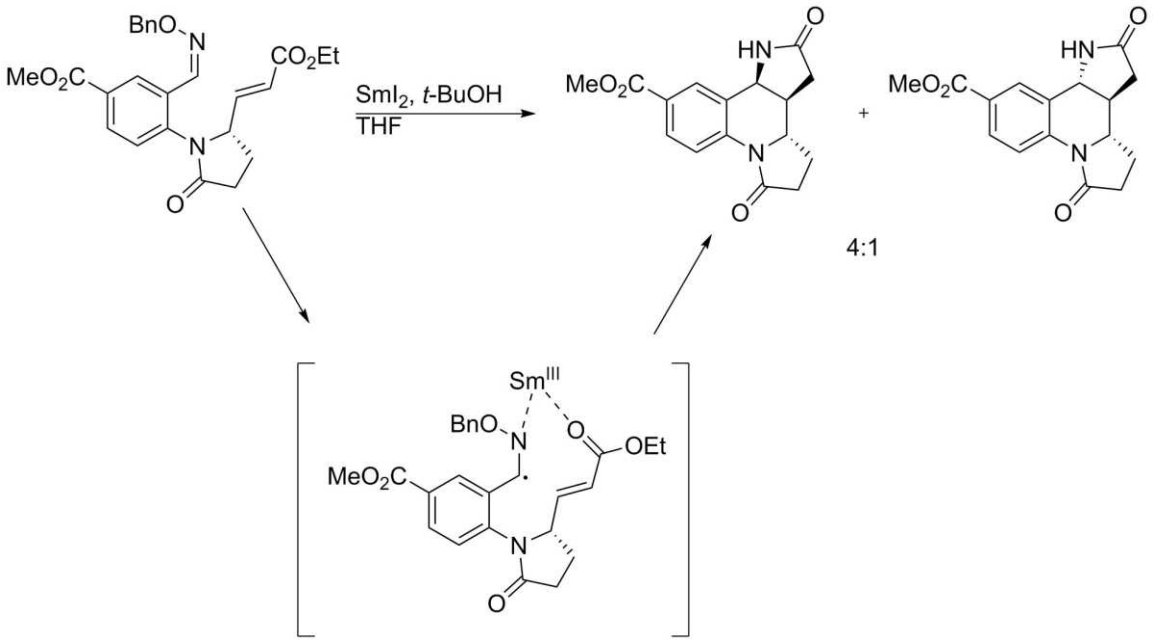

Scheme 3.2. Reaction scheme and proposed intermediate for the reductive cyclization of an activated olefin with a benzyl oxime ether promoted by SmI_2-*t*-BuOH in the total synthesis of (-)-martinellic acid[3]

An additional application of the reduction of oximes by Sm(II) reagents was demonstrated by An and coworkers in their investigation of the reductive deuteration of oximes by SmI_2-D_2O to form α-deuterated primary amines, shown in Scheme 3.3.[4] This reaction was found to tolerate a wide variety of substrate functionalization, including halide groups, which are commonly reduced by Sm(II) reagents. The tolerance of the reaction for these groups is likely a consequence of the affinity of Sm(II) for nitrogen leading to coordination of the Sm(II)-D_2O reagent to the oxime group. Although no mechanism is proposed by the authors, the reduction of the oxime to a primary amine necessitates the cleavage of the C=N double bond either in the initial reduction or after N-O bond cleavage.

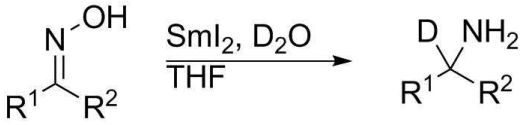

Scheme 3.3. Reaction scheme for the reductive deuteration of an oxime by SmI_2-D_2O[4]

3.1.2 Reductions of Oxime Ether Nitrogen-Oxygen Bonds by SmI_2

In light of the reports *vide supra* of oxime reduction through C=N double bond cleavage by Sm(II) reductants, work by Zhang and coworkers on the reductive cyclization of O-methyl oximes by SmI_2 to form five-membered cyclic imines is highly unusual. In the proposed mechanism, shown in Scheme 3.4, the N-O bond of the oxime ether is cleaved by SmI_2, followed by 5-*exo*-trig radical cyclization with the pendant olefin group. Subsequent reduction and proton abstraction in the aqueous workup yield the cyclic imine product.[5]

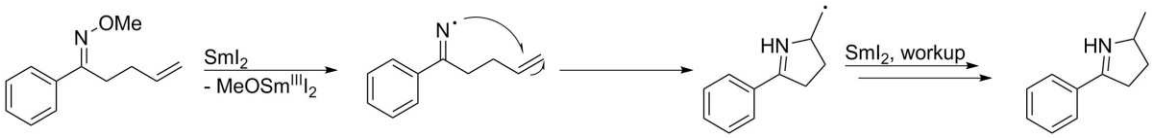

Scheme 3.4. Proposed mechanism for the reductive cyclization of an O-methyl oxime with an olefin by SmI_2[5]

3.2 Experimental Details

3.2.1 Materials

Samarium powder was purchased from Acros Organics. Samarium diiodide was generated by the standard method of samarium metal combined with iodine in THF and allowed to stir for at least 4 hours. Iodometric titrations were then performed to verify concentration of SmI_2 for use. Tetrahydrofuran was purified by a solvent purification system (Innovative Technology Inc.; MA).

3.2.2 Instrumentation

^1H NMR NMR spectra were recorded in $CDCl_3$ on a Bruker 400 MHz spectrometer at 400 MHz. The 1H NMR chemical shifts are given as δ values in ppm relative to TMS (0 ppm) as the internal reference. GCMS analyses were performed with a Shimadzu GCMS-QP2010 Ultra. GC analyses were performed using a Shimadzu Gas

Chromatograph GC-2010 Plus with biphenyl as an internal standard. UV-Visible spectra experiments were performed with a computer-controlled SX.18 MV stopped-flow spectrophotometer (Applied Photophysics Ltd. Surrey, UK). Solutions were prepared under a dry argon atmosphere in flame dried glassware.

3.2.3 Methods

3.2.3.1 Procedure for Synthesis of Oximes

Ketone (101 mmol, 10.5 mL cyclohexanone, 11.8 mL acetophenone, 15.2 mL 4-phenyl-2-butanone) was added to a round bottom flask equipped with a magnetic stir bar containing a solution of 37 mL EtOH in 76 mL water. Sodium acetate (251 mmol, 20.6 g) and hydroxylamine hydrochloride (165 mmol, 11.5 g) were then added to the flask, which was allowed to stir overnight. The reaction solution was then extracted 3x with EtOAc. The organic layers were washed with brine and dried over magnesium sulfate then concentrated under reduced pressure. The crude product was recrystallized in EtOH (4-phenyl-2-butanone oxime) or MeOH (acetophenone oxime, cyclohexanone oxime).

3.2.3.2 Procedure for Synthesis of O-Methyl Oximes

Ketone (101 mmol, 10.5 mL cyclohexanone, 11.8 mL acetophenone, 15.2 mL 4-phenyl-2-butanone) was added to a round bottom flask equipped with a magnetic stir bar containing MeOH (100 mL). Pyridine (150 mmol, 12.0 mL) and methoxyamine hydrochloride (150 mmol, 12.5 g) were then added to the flask, which was allowed to stir overnight. The reaction solution was then diluted with 50 mL extracted 3x with CH_2Cl_2. The organic layers were washed 2x with 1 M HCl and brine then dried over magnesium and concentrated under reduced pressure.

3.2.3.3 Procedure for Reduction of Oximes and O-Methyl Oximes by SmI_2 and SmI_2-Water

A flame dried vial equipped with a magnetic stir bar was charged with a solution of 0.1 M SmI_2 (10 mL, 1 mmol). For reactions with water, water (0.14 mL, 8 mmol) was added to the vial. Substrate (0.2 mmol for reactions with water, 0.33 mmol for reactions without water) was then added to the vial. The solution was allowed to react until discoloration of the characteristic blue of SmI_2 to yellow was observed then quenched in air followed by 2 M NaOH. This solution was extracted 3x into EtOAc. The combined organic layers were washed with a saturated aqueous solution of $Na_2S_2O_4$ and dried over magnesium sulfate then concentrated under reduced pressure.

3.2.3.3.1 Procedure for Isolation of Products of Reductions of Oximes and O-Methyl Oximes by SmI_2 and SmI_2-Water

1-phenylethan-1-amine was extracted with EtOAc and dried over magnesium sulfate. The resulting solution was concentrated under reduced pressure and characterized by ^{1}H NMR (400 MHz, $CDCl_3$) δ (ppm): 1.42 (d, 3H), 4.22 (q, 1H), 7.23-7.44 (m, 5H)

1-phenylethan-1-imine was extracted with EtOAc and dried over magnesium sulfate. The resulting solution was concentrated under reduced pressure and characterized by ^{1}H NMR (400 MHz, $CDCl_3$) δ (ppm): 1.97 (t, 3H), 7.22-7.54 (m, 5H)

cyclohexanamine was extracted with EtOAc and dried over magnesium sulfate. The resulting solution was concentrated under reduced pressure and characterized by ^{1}H NMR (400 MHz, $CDCl_3$) δ (ppm): 1.18 (tt, 1H), 1.30 (qt, 2H), 1.49 (qd, 2H), 1.63 (dt, 1H), 1.78 (dt, 2H), 2.03-2.11 (m, 2H), 3.22 (tt, 1H)

3.2.3.4 Procedure for Stopped Flow Kinetics Studies

Kinetic experiments were performed with a computer-controlled SX.18 MV stopped- flow spectrophotometer (Applied Photophysics Ltd. Surrey, UK). Solutions were injected separately into the stopped-flow system using airtight, capped BD syringes prepared in a glove box under argon atmosphere. Between each experiment, the cell block was washed with dilute HNO_3 (1x), Deionized H_2O (1x), and THF (3x) before additional anhydrous deoxygenated THF washes (3x). The reaction rates were determined from the decay of SmI_2 at 560 nm. Kinetic measurements for the reduction of anthracene were carried out at 25°C unless otherwise specified.

3.3 Results and Discussion

3.3.1 Synthetic Investigations and Product Characterization of the Reduction of Oximes and O-Methyl Oximes by SmI_2 and SmI_2 Water

Following up on the reports of oxime reductions by Sm(II) systems *vide supra*, we sought to reconcile the observations of initial N-O and C=N bond reduction. For this purpose, several oximes and O-methyl oximes, shown in Figure 3.1, were synthesized. The substrate scope for these studies was chosen to include both the activated acetophenone oxime and O-methyl oxime and unactivated cyclohexanone oxime and O-methyl oxime.

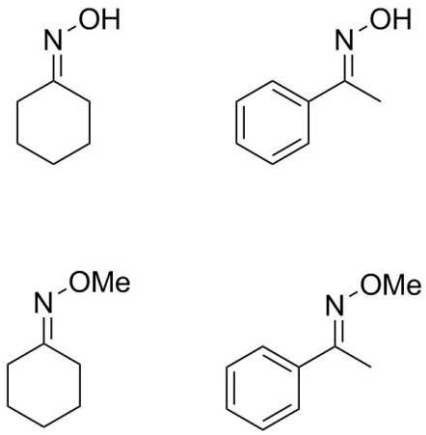

Figure 3.1. Cyclohexanone oxime (top left), cyclohexanone O-methyl oxime (bottom left), acetophenone oxime (top right), acetophenone O-methyl oxime (bottom right)

To gauge the reactivity of SmI_2-water with oximes, both cyclohexanone oxime and acetophenone oxime were introduced to solutions of SmI_2-water in THF. Both reactions yielded the fully reduced primary amine products as shown in Scheme 3.5 in quantitative yields. These results are consistent with the findings of An and coworkers demonstrating the cleavage of oxime C=N double bonds by SmI_2-water.[4]

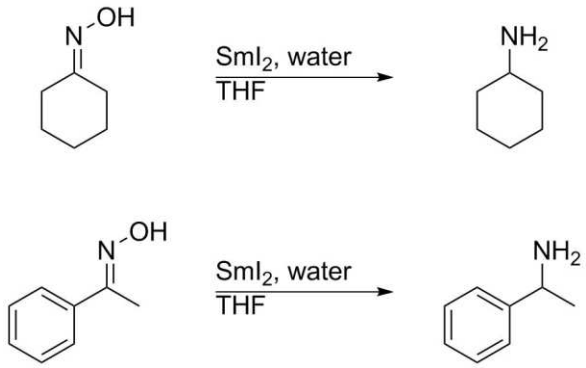

Scheme 3.5. Reaction schemes for the reductions of cyclohexanone oxime and acetophenone oxime by SmI_2-water

Interestingly, when acetophenone oxime is introduced to a solution of SmI_2 in THF in the absence of a proton donor, the imine product shown in Scheme 3.6 is recovered in quantitative yield. This reactivity is consistent with the N-O bond cleavage observed by Zhang and coworkers. Combined with the observation of oxime reduction to a primary amine by SmI_2-water, this result indicates an unusual tunable chemoselectivity

for the Sm(II)-mediated reduction of oximes in the presence or absence of water. Notably, when cyclohexanone oxime is introduced to a solution of SmI_2 in dry THF, no reaction is observed and only the oxime starting material is recovered.

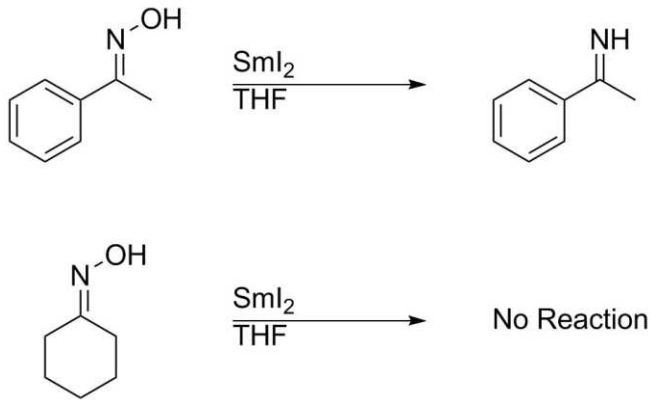

Scheme 3.6. Reaction schemes for the reduction of acetophenone oxime by SmI_2 and addition of cyclohexanone oxime to SmI_2

Subsequently, the reactivity of SmI_2 and SmI_2-water with O-methyl oximes was examined. Introduction of acetophenone O-methyl oxime to a solution of SmI_2-water afforded quantitative conversion to the primary amine product shown in Scheme 3.7. No reaction was observed upon introduction of cyclohexanone O-methyl oxime to a solution of SmI_2-water. Notably, hydrogenation of the C=N bonds of cyclohexanone oxime and cyclohexanone O-methyl oxime was calculated to be nearly isoenergetic. The recalcitrance of cyclohexanone O-methyl oxime to reduction by SmI_2-water was therefore attributed to the additional steric hindrance provided by the methoxy group.

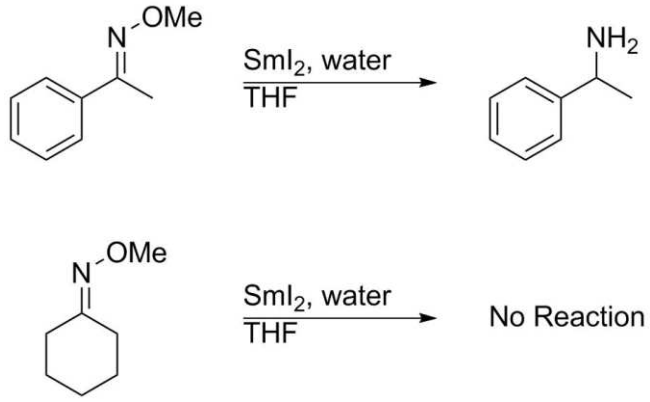

Scheme 3.7. Reaction schemes for the reduction of acetophenone O-methyl oxime by SmI_2-water and addition of cyclohexanone O-methyl oxime to SmI_2-water

The reactivity of O-methyl oximes in the absence of water was also investigated. Introduction of acetophenone O-methyl oxime to a dry solution of SmI_2 yielded quantitative conversion to the imine product shown in Scheme 3.8. However, no reaction was observed upon addition of cyclohexanone O-methyl oxime to a dry solution of SmI_2.

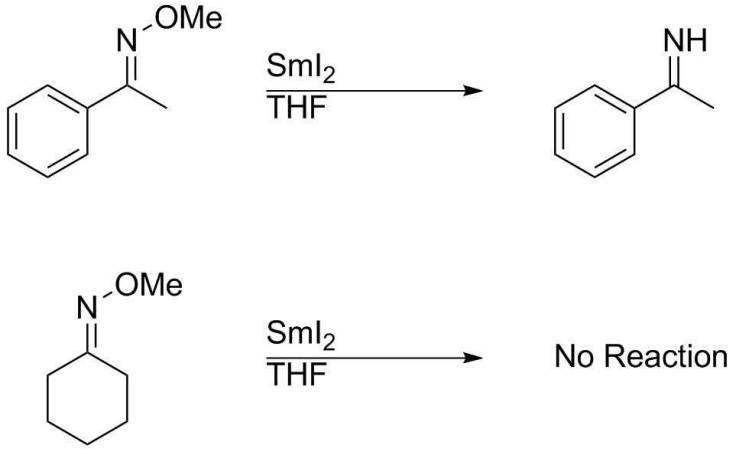

Scheme 3.8. Reaction schemes for the reduction of acetophenone O-methyl oxime by SmI_2 and addition of cyclohexanone O-methyl oxime to SmI_2

3.3.2 Kinetic Analysis of the Reduction of Oximes and O-Methyl Oximes by SmI_2 and SmI_2 Water

3.3.2.1 Kinetic Rate Order Experiments

The reductions of oximes and O-methyl oximes by SmI_2 and SmI_2-water were further investigated via rate studies using stopped flow spectrophotometric kinetic

analysis. These stopped flow rate studies were performed under pseudo-first order conditions, with substrate and water concentrations maintained in excess of ten equivalents with respect to [SmI_2]. The decay of the characteristic absorbance of SmI_2 at 560 nm was observed to track reaction progress. The value for k_{obs} for each reaction was determined as the exponent a single exponential function that was fit to the decay curve acquired for the reaction. All rate measurements were performed in triplicate with independently prepared samples. The rate order for SmI_2 in each reaction was determined using the fractional times method. The rate orders for the components of the reduction of cyclohexanone oxime by SmI_2-water are shown in Table 3.1.

Table 3.1. Rate orders for the reduction of cyclohexanone oxime by SmI_2-water

entry	reaction component	rate order[a]
1	SmI_2	0.94 ± 0.08[b]
2	Water	1.04 ± 0.03[c]
3	Cyclohexanone Oxime	0.9 ± 0.1[d]

[a]Errors reported as ± σ. [b]Fractional times method. [c]4 mM SmI_2, 40-80 mM cyclohexanone oxime, 400 mM water in THF. [d]4 mM SmI_2, 40 mM cyclohexanone oxime, 50-700 mM water in THF.

The rate orders for all components of the reduction of cyclohexanone oxime by SmI_2-water were found to be near unity. Given the approximately 33 kcal/mol greater stability of the N-O compared to the C=N bond of cyclohexanone oxime against hydrogenation (Scheme 3.9), C=N bond cleavage was proposed to be rate limiting in the reduction of cyclohexanone oxime by SmI_2-water. Additionally, the C=N bond of cyclohexanone oxime was calculated to be approximately 10 kcal/mol stronger than the C=N BDFE of acetophenone oxime (Scheme 10). Notably, while the rate of reduction of cyclohexanone oxime by SmI_2-water was found to be moderate, with an observed rate constant of 170 ± 60 $M^{-2}s^{-1}$, the reductions of both acetophenone oxime and acetophenone O-methyl oxime by SmI_2-water proceeded too rapidly to be measured by

the stopped flow instrument. Taken together, the rate orders of unity for SmI_2 and water in the reduction of cyclohexanone oxime and the significantly greater rate of reduction of acetophenone oxime compared to cyclohexanone oxime by SmI_2-water are fully consistent with the initial reduction of the C=N bond of oximes by SmI_2-water.

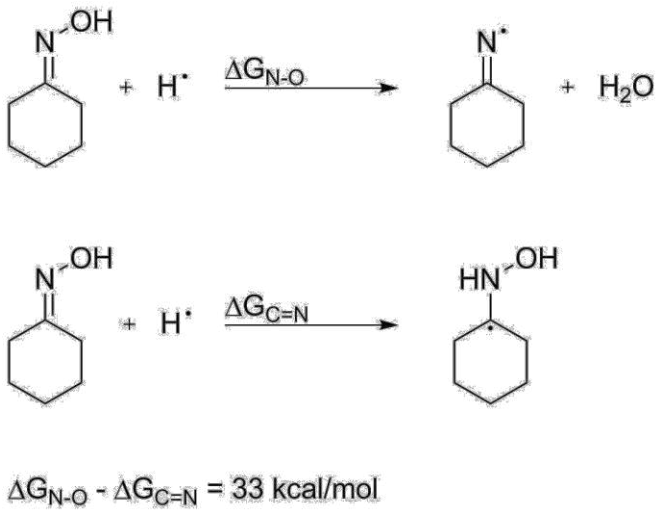

$\Delta G_{N-O} - \Delta G_{C=N} = 33$ kcal/mol

Scheme 3.9. Reaction schemes for the hydrogenation of the N-O and C=N bonds of cyclohexanone oxime

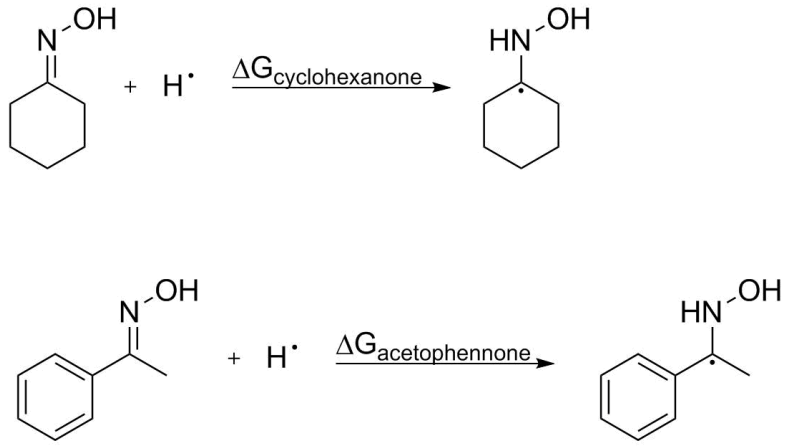

$\Delta G_{cyclohexanone} - \Delta G_{acetophenone} = 10$ kcal/mol

Scheme 3.10. Reactions schemes for the hydrogenations of the C=N bonds of cyclohexanone oxime and acetophenone oxime

Rate orders were also determined for the reduction of acetophenone O-methyl oxime by SmI_2 in the absence of a proton donor under pseudo-first order conditions. The

rate order for SmI_2 was determined using the fractional times method. The rate orders of acetophenone O-methyl oxime and SmI_2 are shown in Table 3.2.

Table 3.2. Rate orders for the reduction of acetophenone O-methyl oxime by SmI_2

entry	reaction component	rate order[a]
1	SmI_2	0.96 ± 0.08[b]
2	Acetophenone O-Methyl Oxime	0.95 ± 0.09[c]

[a]Errors reported as ± σ. [b]Fractional times method. [c]4 mM SmI_2, 40-80 mM acetophenone O-methyl oxime in THF.

The rate orders for both components in the reduction of acetophenone O-methyl oxime by SmI_2 were found to be near unity. These results are consistent with a rate limiting initial electron transfer from SmI_2 to the substrate. Notably, while the reduction of acetophenone O-methyl oxime by SmI_2 was found to proceed at a moderate rate with a rate constant of 128 ± 6 $M^{-1}s^{-1}$, the reduction of acetophenone oxime by SmI_2 proceeded too rapidly for measurement under pseudo-first order conditions. This rate difference highlights the importance of substrate sterics and coordination to Sm(II) in the reduction of oximes and oxime ethers by SmI_2.

3.3.2.2 Kinetic Activation Parameter Experiments

Rate data was also acquired for the reduction of cyclohexanone oxime using pseudo-first order methodology over a 20°C temperature range to acquire activation parameters for the reaction. The results of these rate experiments, shown in Table 3.3, reveal a low enthalpy of activation and relatively high entropy of activation in the reduction of cyclohexanone oxime by SmI_2-water. These findings are consistent with a late, relatively ordered transition state for the reaction.

Table 3.3. Activation parameters for the reduction of cyclohexanone oxime by SmI_2-water

entry	activation parameter	value[a]
1	$\Delta H^{\ddagger}$ (kcal/mol)[b]	12 ± 2
2	$\Delta S^{\ddagger}$ (cal/molK)[b]	-28 ± 6
3	$\Delta G^{\ddagger}$ (kcal/mol @ 25°C)[c]	20 ± 2

[a]Conditions: 4 mM SmI_2, 40 mM cyclohexanone oxime, 400 mM water in THF. Temperature varied between 15 and 35 °C. Errors reported as ± σ. [b]Obtained from $\ln\left(\frac{k_{obs}h}{kT}\right) = \frac{\Delta H^{\ddagger}}{RT} + \frac{\Delta S^{\ddagger}}{R}$ [c]Obtained from $\Delta G^{\ddagger} = \Delta H^{\ddagger} - T\Delta S^{\ddagger}$

3.3.2.3 Deuterium Kinetic Isotope Effect Experiments

The rate of reduction of cyclohexanone oxime by SmI_2-D_2O was also observed in order to obtain a deuterium kinetic isotope effect (KIE). The results of these rate measurements revealed a deuterium KIE of 1.2 ± 0.5 for the reduction of cyclohexanone oxime by SmI_2-water. Previous studies have determined similarly low deuterium KIE values for Sm(II)-mediated PCET reductions of substrates.[6,7] This finding was therefore considered to be consistent with the of reduction of oximes by SmI_2-water via PCET.

3.3.3 Mechanistic Insights into the Reductions of Oximes and O-Methyl Oximes by SmI_2 and SmI_2-Water

The results of the rate studies on the reductions of oximes and O-methyl oximes by SmI_2-water *vide supra* are consistent with an initial rate limiting PCET reduction of these substrates by SmI_2-water. These rate studies also revealed a significantly greater rate of reduction for conjugated compared to unconjugated oximes and oxime ethers. Computational modeling of these two classes of substrates revealed a negligible difference in N-O BDFE and an approximately 10 kcal/mol more stable C=N bond in unactivated substrates against hydrogenation. The difference in rate of reduction between conjugated and unconjugated oximes was therefore found to be consistent with initial

C=N bond cleavage by SmI_2-water. The stability of acetophenone imine in the presence of SmI_2-water supports this hypothesis by demonstrating the infeasibility of initial N-O bond cleavage in these reductions. The above results were combined to propose the mechanism shown in Scheme 3.11. In this mechanism, the substrate C=N bond is reduced by an initial PCET from Sm(II)-water, yielding a C-centered radical intermediate, which is subsequently reduced by three further equivalents of Sm(II)-water, furnishing the amine product. This mechanism is consistent with the reports by Naito and An and their respective coworkers of oxime and oxime ether C=N bond reduction by SmI_2 in the presence of a proton donor.[3,4]

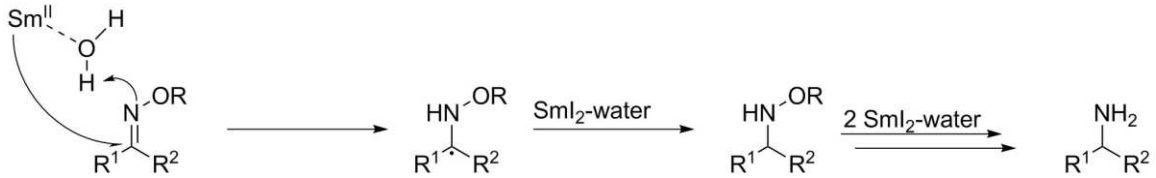

Scheme 3.11. Proposed mechanism for the reduction of an oxime by SmI_2-water

The mechanism of reduction for oximes and oxime ethers by SmI_2 in the absence of a proton donor was also investigated. The results of the rate studies *vide supra* are consistent with an initial rate limiting electron transfer. One plausible mechanism is shown in Scheme 3.12, in which SmI_2 mediates an initial dissociative electron transfer to cleave the substrate N-O bond. However, single electron reduction of cyclohexanone O-methyl oxime by SmI_2 is not observed despite the nearly isoenergetic formation of an iminyl radical anion from both cyclohexanone O-methyl oxime and acetophenone O-methyl oxime. Initial dissociative electron transfer to cleave the substrate N-O bond was therefore discounted as a potential mechanism.

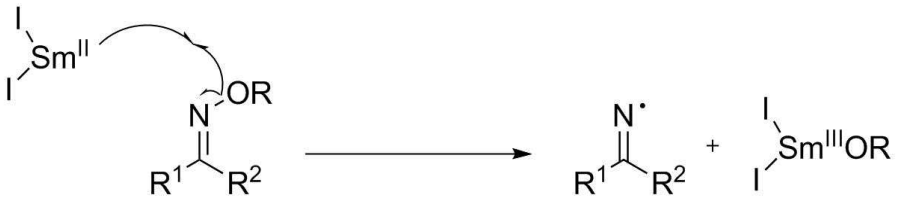

Scheme 3.12. Potential mechanism for the reduction of acetophenone O-methyl oxime by SmI_2 via dissociative electron transfer

Further computational modeling of the single electron reductions of oximes to form oxime radical anions was undertaken. The results of this modeling revealed that non-dissociative single electron reduction of acetophenone oxime is more than 21 kcal/mol more favorable than the analogous single electron reduction of cyclohexanone oxime (Scheme 3.13). This difference was attributed to the availability of resonance stabilization in acetophenone oxime that is not present in cyclohexanone oxime. Oxime and oxime ether reduction by SmI_2 was therefore proposed to proceed through initial non-dissociative electron transfer to the substrate as shown in Scheme 3.14, yielding a radical anion intermediate. Subsequent N-O bond cleavage to form a Sm^{III}-alkoxide or Sm^{III}-hydroxide yields the iminyl radical intermediate observed by Zhang and coworkers.[5] Further electron transfer from SmI_2 to the substrate and basic aqueous workup then furnishes the observed imine product. This mechanism is also consistent with the observation of oxime ether C=N bond reduction by SmI_2-HMPA by Nicolaou and coworkers.[2] Additionally, as suggested by Nicolaou and coworkers, although initial substrate reduction yields a formally anionic oxime radical, coordination of the oxidized Sm(III) complex likely affords additional stabilization to the radical anion intermediate.

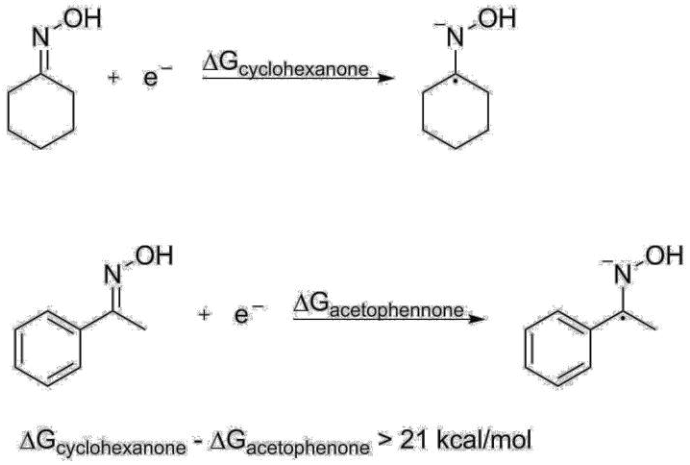

Scheme 3.13. Reaction schemes for the non-dissociative reductions of cyclohexanone oxime and acetophenone oxime

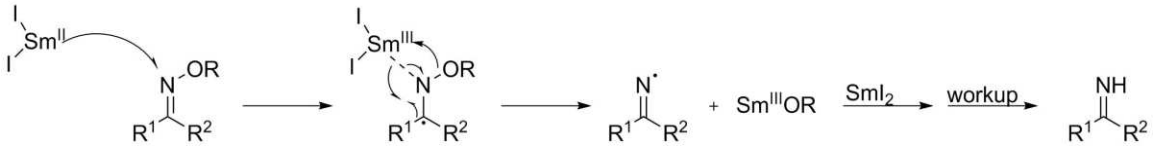

Scheme 3.14. Proposed mechanism for the reduction of oximes and oxime ethers by SmI_2

3.4 Conclusion

The synthetic studies presented in this chapter revealed the remarkable chemoselectivity of the Sm(II)-mediated reduction of oximes and oxime ethers. The use of dry SmI_2 afforded the quantitative reduction of acetophenone oxime and acetophenone O-methyl oxime to acetophenone imine as shown in Scheme 3.15. Addition of water to form a SmI_2-water system enabled the quantitative reduction of acetophenone oxime, acetophenone O-methyl oxime, and cyclohexanone oxime to the respective primary amine products as shown in Scheme 3.16.

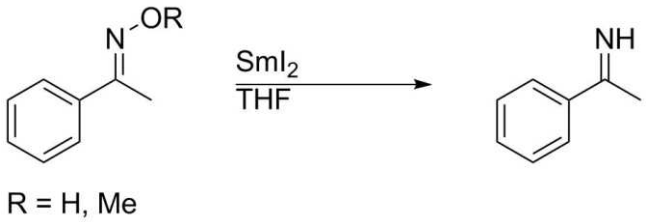

Scheme 3.15. Reaction scheme for the reductions of acetophenone oxime and acetophenone O-methyl oxime by SmI_2

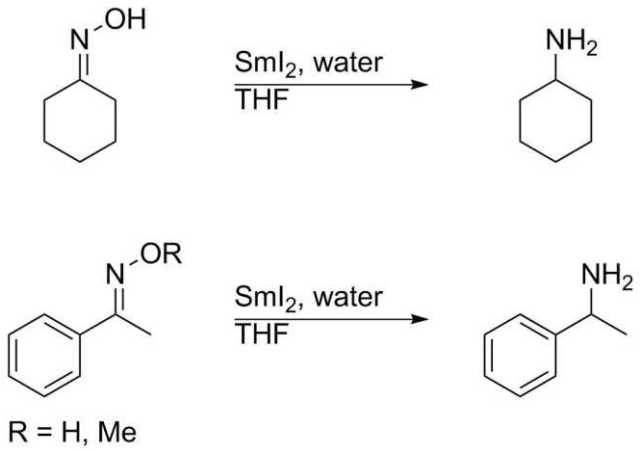

Scheme 3.16. Reaction schemes for the reductions of cyclohexanone oxime, acetophenone oxime, and acetophenone O-methyl oxime by SmI_2-water

Mechanistic investigations of the reductions of oximes and O-methyl oximes by SmI_2-water were also undertaken. Kinetics studies revealed rate orders of unity for each component of the reaction. This indicates that the initial substrate reduction by SmI_2-water is rate limiting. Notably, C=N bond hydrogenation was calculated to be significantly less endergonic for acetophenone oxime compared to cyclohexanone oxime. Given the greater rate of reduction of acetophenone oxime compared to cyclohexanone oxime by SmI_2-water, these results are consistent with initial C=N bond reduction in the reduction of oximes and oxime ethers by SmI_2-water. The proposed mechanism, in which initial PCET from SmI_2-water to the substrate yields a C-centered radical intermediate that is subsequently reduced by excess SmI_2-water is shown in Scheme 3.11 above. This mechanism is consistent with reports by An and Naito and their respective coworkers of oxime and oxime ether C=N bond cleavage by Sm(II)-proton donor systems.[3,4]

The mechanism of reduction for oximes and oxime ethers by dry SmI_2 was also investigated. Kinetics studies revealed rate orders of unity for both SmI_2 and substrate, which is consistent with an initial rate limiting electron transfer. Synthetic studies

revealed that while activated oximes and oxime ethers are amenable to reduction by SmI_2, unactivated oximes and oxime ethers are not reduced. Computational modeling revealed that the dissociative single electron N-O bond reductions of acetophenone oxime and cyclohexanone oxime are nearly isoenergetic. However, the non-dissociative single electron reduction of acetophenone oxime is approximately 21 kcal/mol more favorable than the non-dissociative single electron reduction of cyclohexanone oxime. These results are consistent with the proposed mechanism shown in Scheme 3.14. In that mechanism, the substrate undergoes a single electron reduction by SmI_2 to form an oxime radical anion intermediate. Subsequent abstraction of the O-R group by Sm(III) yields an iminyl radical intermediate, which is further reduced by excess SmI_2 and protonated by the aqueous workup conditions to provide the isolated imine product. This mechanism is consistent with observations made by Nicolaou and coworkers in their report on oxime reduction by SmI_2-HMPA and by Zhang and coworkers on the SmI_2-mediated 5-*exo*-trig radical cyclization of oxime ethers to form cyclic imines.[2,5]

3.5 References

(1) Nicolaou, K. C.; Ellery, S. P.; Chen, J. S. Samarium Diiodide Mediated Reactions in Total Synthesis. *Angew. Chemie Int. Ed.* **2009**, *48* (39), 7140–7165.

(2) Nicolaou, K. C.; Snyder, S. A.; Giuseppone, N.; Huang, X.; Bella, M.; Reddy, M. V.; Rao, P. B.; Koumbis, A. E.; Giannakakou, P.; O'Brate, A. Studies toward Diazonamide A: Development of a Hetero-Pinacol Macrocyclization Cascade for the Construction of the Bis-Macrocyclic Framework of the Originally Proposed Structure. *J. Am. Chem. Soc.* **2004**, *126* (32), 10174–10182.

(3) Shirai, A.; Miyata, O.; Tohnai, N.; Miyata, M.; Procter, D. J.; Sucunza, D.; Naito, T. Total Synthesis of (-)-Martinellic Acid via Radical Addition-Cyclization- Elimination Reaction. *J. Org. Chem.* **2008**, *73* (12), 4464–4475.

(4) Ning, L.; Li, H.; Lai, Z.; Szostak, M.; Chen, X.; Dong, Y.; Jin, S.; An, J. Synthesis of α-Deuterated Primary Amines via Reductive Deuteration of Oximes Using D2O as a Deuterium Source. *J. Org. Chem.* **2021**, *86* (3), 2907–2916.

(5) Huang, F.; Zhang, S. Iminyl Radicals by Reductive Cleavage of N-O Bond in Oxime Ether Promoted by SmI2: A Straightforward Synthesis of Five-Membered Cyclic Imines. *Org. Lett.* **2019**, *21* (18), 7430–7434.

(6) Ramírez-Solís, A.; Bartulovich, C. O.; Chciuk, T. V; Hernández-Cobos, J.; Saint-Martin, H.; Maron, L.; Anderson, W. R.; Li, A. M.; Flowers II, R. A. Experimental and Theoretical Studies on the Implications of Halide-Dependent Aqueous Solvation of Sm(II). *J. Am. Chem. Soc.* **2018**, *140*, 16731−16739.

(7) Chciuk, T. V.; Flowers, R. A. Proton-Coupled Electron Transfer in the Reduction of Arenes by SmI2-Water Complexes. *J. Am. Chem. Soc.* **2015**, *137* (35), 11526–11531.

Chapter 4. Investigation of the Unusual Stability of the SmI_2-Water Reagent

4.1 Background and Significance

4.1.1 Introduction to PCET from SmI_2-Water

Since the introduction of SmI_2 to the synthetic community by Kagan and coworkers, the reagent has been widely utilized in organic synthesis as a selective and powerful single electron reductant.[1,2] One of the unique features of SmI_2 is the tunability of the reducing power and selectivity of Sm(II) reagents through the use of a wide array of chemical additives. Among these additives, proton donors have been demonstrated to promote unusual reactivity. Several Sm(II)-proton donor reagents, most notably SmI_2-water, are capable of reducing substrates with redox potentials far more negative than the redox potential of the Sm(II) reductant.[3,4] This unusual behavior was investigated by Flowers and coworkers. In this work, the SmI_2-water-mediated reduction of anthracene was compared with the SmI_2-water-mediated reduction of 1-iodododecane, which is known to be reduced through a rate limiting dissociative electron transfer.[5,6] The results revealed a significantly greater rate dependence on [water] for the reduction of anthracene by SmI_2-water compared to the reduction of 1-iodododecane by SmI_2-water. Moreover, even at relatively low [water], the reduction of anthracene by SmI_2-water was found to proceed significantly faster than the reduction of 1-iodododecane. Taken together, these results rule out an initial electron transfer in the reduction of anthracene by SmI_2-water. Since arenes are recalcitrant to initial proton transfer, SmI_2-water was determined to mediate arene reduction via proton-coupled electron transfer (PCET).[3] Further work by Flowers and coworkers demonstrated that the reductions of other

challenging substrates, including coordinating substrates such as carbonyls, by SmI_2-water also proceed through PCET.[7–9]

4.1.2 Synthetic Applications of SmI_2-Water

Proton-coupled electron transfer mediated by SmI_2-water has been successfully utilized in the reductions of a wide array of substrates. Carbonyl-containing substrates are among the most commonly reduced by SmI_2-water in synthetic processes, due to the high affinity of Sm(II) for oxygen. In addition to aldehydes and ketones, SmI_2-water has also been shown to mediate the reduction of esters. Work by Procter and coworkers demonstrates the versatility of SmI_2-water-mediated carbonyl reductions in their work reducing challenging carbonyl substrates including cyclic esters and derivatives of Meldrum's acid as shown in Scheme 4.1.[10–13]

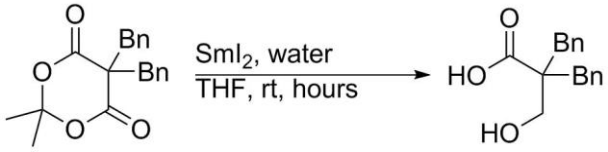

Scheme 4.1. Reaction scheme for the reduction of a derivative of Meldrum's acid by SmI_2-water[13]

Procter and coworkers further utilized the high affinity of SmI_2-water for carbonyls to achieve SmI_2-water-mediated reductive cyclization reactions in carbonyl substrates coupled to olefins.[10,14] In conjunction with the broad scope of lactone reductions by SmI_2-water, these reductive cyclizations are capable of delivering a number of complex value added products, as shown in Scheme 4.2.[10]

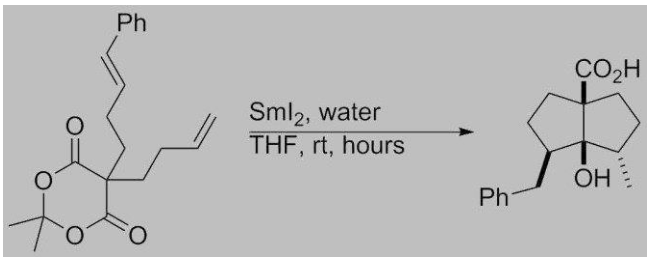

Scheme 4.2. Reaction scheme for the reductive cyclization of a derivative of Meldrum's acid by SmI_2-water[10]

In addition to the common use of SmI_2 as a single electron reductant for oxygen-containing systems such as carbonyls, Sm(II) reagents have also demonstrated a remarkable affinity for nitrogen.[15] This azaphilicity has been utilized to increase the reducing power of SmI_2-water reagents via addition of a aprotic amines to form a number of SmI_2-water-amine systems, which have been found to mediate a broad scope of challenging reductions. Much of this work has been spearheaded by Hilmersson and coworkers, including reductions of alkyl halides, conjugated olefins, and imines, shown in Scheme 4.3.[16–18] Moreover, Hilmersson and coworkers combined the reduction of aryl iodides and olefins by SmI_2-water-amine systems to achieve a number of 5/6-exo-trig and 5/6-exo-dig cyclizations to form a diverse set of functionalized heterocycles, shown in Scheme 4.4.[19] Furthermore, collaborative work between Hilmersson and Flowers demonstrated the ability for SmI_2-water-amine systems to achieve both reduction and reductive coupling in a variety of conjugated imines, shown in Scheme 4.5.[20]

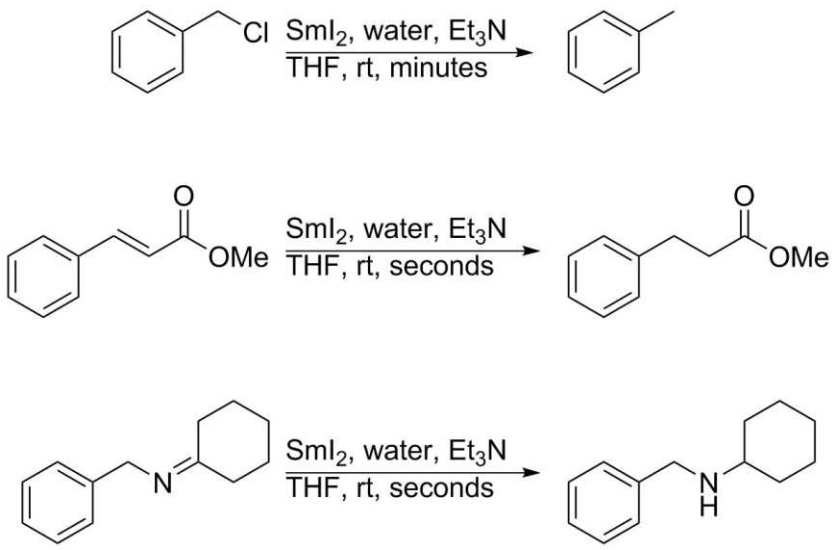

Scheme 4.3. Reaction schemes for the reductions of benzyl chloride, a conjugated olefin, and an imine by SmI_2-water-Et_3N[16–18]

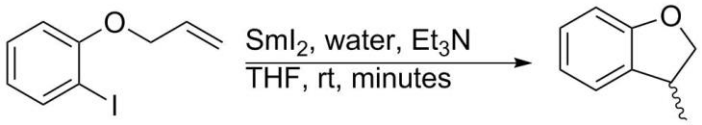

Scheme 4.4. Reaction scheme for the 5-exo-trig reductive cyclization of an aryl iodide with an olefin by SmI_2-water-Et_3N[19]

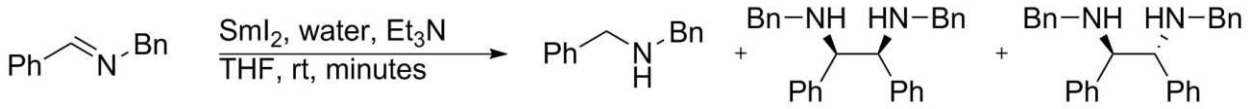

Scheme 4.5. Reaction scheme for the reduction and reductive coupling of a conjugated imine by SmI_2-water-Et_3N[20]

In addition to the cooperativity of SmI_2-water with aprotic amines to enable rapid reduction of diverse substrates, SmI_2-water has also been shown to facilitate the reduction of a number of challenging nitrogen-containing substrates. Previous chapters in this dissertation have described the SmI_2-water-mediated reductions of oxime and pyridine substrates, shown in Scheme 4.6-4.8. Work by Mayer and coworkers has also demonstrated the ability of SmI_2-water to achieve the reduction of a variety of electron rich enamines.[9] Furthermore, work by the Nishibayashi group achieved the remarkable reduction of nitrogen gas by SmI_2-water in conjunction with a molybdenum catalyst.[21]

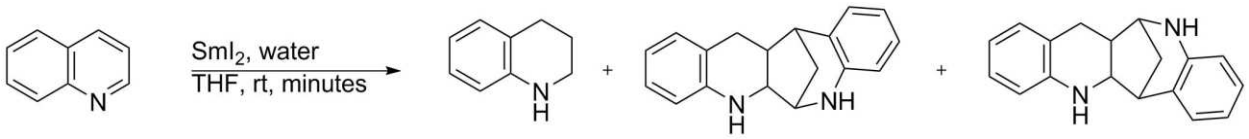

Scheme 4.6. Reaction scheme for the reduction and reductive dimerization of quinoline by SmI_2-water

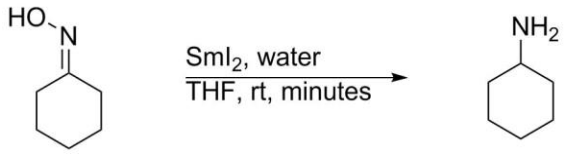

Scheme 4.7. Reaction scheme for the reduction of cyclohexanone oxime by SmI_2-water

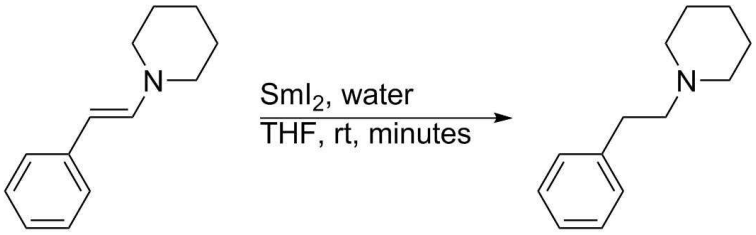

Scheme 4.8. Reaction scheme for the reduction of an enamine by SmI_2-water[9]

4.1.3 Determination of the Degree of Coordination-Induced Bond Weakening in Sm(II)-Proton Donor Reagents

Despite the unique reactivity of SmI_2-water and the utility of Sm(II) reagents in synthesis, solution phase characterization of many Sm(II) species remains elusive. Quantification of coordination-induced bond weakening in Sm(II) systems is therefore performed via comparison of the X-H BDFE of the uncomplexed proton donor ligand with the X-H BDFE of the bond formed upon initial reduction of the substrate. Flowers and coworkers used this strategy to determine an upper limit of approximately 34.2 kcal/mol for the O-H BDFE of water coordinated to SmI_2, as shown in Scheme 4.9.[3] Mayer and coworkers refined this upper limit to approximately 32 kcal/mol in their study of SmI_2-water-mediated enamine reductions.[22] Moreover, Mayer and coworkers used the literature values for the redox potential of aqueous Sm(II) and the pK_a of $Eu^{III}(H_2O)_n$ as an approximation of the pK_a of $Sm^{III}(H_2O)_n$ to propose an O-H BDFE of 26 kcal/mol for

water coordinated to SmI_2. Notably, this value was calculated for an aqueous solution of SmI_2-water and so is likely not reflective of the O-H BDFE of the SmI_2-water complex in the bulk THF solution in which the reagent is commonly prepared.

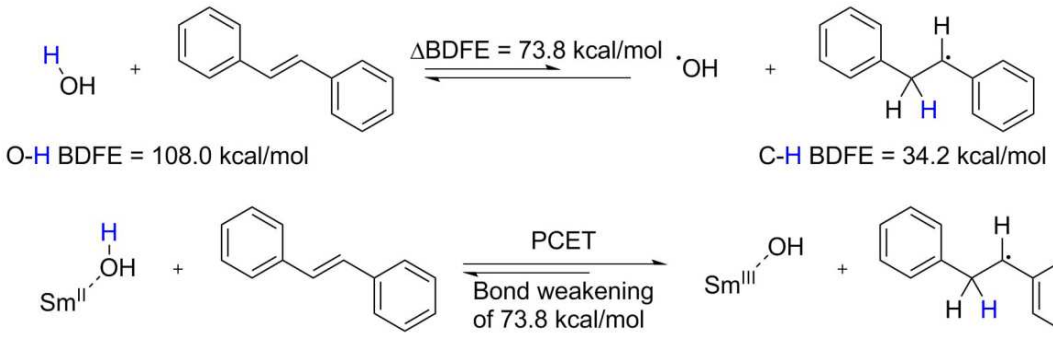

Scheme 4.9. Reaction scheme and bond strength comparison for the reduction of *trans*-stilbene by SmI_2-water

While the exceptionally weak O-H bond of water coordinated to Sm(II) enables the facile reduction of the diverse and challenging substrates *vide supra*, it is also far below the 48 kcal/mol thermodynamic threshold for spontaneous H_2 gas evolution.[23] This contrasts with reports of a number of other coordination-induced bond weakening reagents with similarly low X-H BDFE values, which undergo rapid H_2 gas evolution on timescales faster than substrate reduction, precluding their use in synthesis.[24–27] Remarkably, H_2 gas evolution from SmI_2-water is only observed on a timescale of hours to minutes, which is often much slower than substrate reduction. This raises an important question: given the thermodynamic favorability of hydrogen gas evolution from SmI_2-water, why is SmI_2-water stable on timescales sufficient to enable the nearly quantitative reductions of such challenging substrates?

4.2 Experimental

4.2.1 Materials

Samarium powder was purchased from Acros Organics. Samarium diiodide was generated by the standard method of samarium metal combined with iodine in THF and allowed to stir for at least 4 hours. Iodometric titrations were then performed to verify concentration of SmI2 for use. Tetrahydrofuran was purified by a solvent purification system (Innovative Technology Inc.; MA).

4.2.2 Instrumentation

^{1}H NMR spectra were recorded in $CDCl_3$ on a Bruker 400 MHz spectrometer at 400. The 1H NMR chemical shifts are given as δ values in ppm relative to TMS (0 ppm) as the internal reference. UV-Visible spectra experiments were performed with a computer-controlled SX.18 MV stopped-flow spectrophotometer (Applied Photophysics Ltd. Surrey, UK). Solutions were prepared under a dry argon atmosphere in flame dried glassware.

4.2.3 Methods

4.2.3.1 Procedure for Generation of Samarium Dibromide

A solution of 0.1 M SmI_2 was prepared by combination of samarium metal powder with iodine in a stirred solution of THF. The supernatant from this solution was then removed and subsequently charged with 4 equiv. of dry LiBr in a flame dried vial equipped with a stir bar. This solution was allowed to stir for 10 minutes after which the remaining solids were allowed to settle to the bottom of the vial and the supernatant solution of 0.1 M $SmBr_2$ was used without further purification.

4.2.3.2 Procedure for Stopped Flow Kinetics Studies

Kinetic experiments were performed with a computer-controlled SX.18 MV stopped- flow spectrophotometer (Applied Photophysics Ltd. Surrey, UK). Solutions were injected separately into the stopped-flow system using airtight, capped BD syringes prepared in a glove box under argon atmosphere. Between each experiment, the cell block was washed with dilute HNO_3 (1x), Deionized H_2O (1x), and THF (3x) before additional anhydrous deoxygenated THF washes (3x). The reaction rates were determined from the decay of SmI_2 at 560 nm. Kinetic measurements for the reduction of anthracene were carried out at 25°C unless otherwise specified.

4.2.3.3 Procedure for Headspace ^{1}H NMR Experiments

A solution of 0.1 M SmI_2 (10 mL, 1 mmol) was prepared under an Ar atmosphere in a sealed vial equipped with a septum cap. A solution of water, deuterium oxide, or water and deuterium oxide (0.45 mL, 25 mmol) was added to the vial by syringe. This solution was allowed to stir until the discoloration of the characteristic blue of the Sm(II) was observed. A syringe was then charged with 1 mL of headspace gas from the reaction vial. This headspace gas was then bubbled through $CDCl_3$ in an NMR tube, which was immediately sealed. A ^{1}H NMR spectrum was then promptly acquired for the sample.

4.3 Results and Discussion

4.3.1 Kinetic Analysis of the Evolution of H_2 Gas from Sm(II)-Water Systems

4.3.1.1 Kinetic Rate Order Experiments

To determine the basis for the unusual stability of the SmI_2-water reagent, several hypotheses regarding H_2 gas evolution pathways and potential barriers to H_2 gas evolution were examined. The addition of water to SmI_2 in THF has been shown to

induce the dissociation of both iodide ligands from the Sm(II) complex at sufficiently high [water].[28,29] The resulting Sm(II)-water complex thus bears a formal +2 charge. It was proposed that the coulombic repulsion between two dicationic Sm(II)-water complexes could provide a rate limiting kinetic barrier to self-association and subsequent H_2 gas evolution. To test this hypothesis, the evolution of H_2 gas from SmI_2-water and $SmBr_2$-water was investigated via rate studies utilizing stopped flow kinetic analysis. These rate studies were performed under initial rates conditions, with [water] never in excess of 167 equivalents with respect to [SmI_2] or [$SmBr_2$]. Reaction progress was observed via the decay of the characteristic absorptions of SmI_2 and $SmBr_2$ at 560 and 540 nm, respectively. The value of k_{obs} for each reaction was acquired as the slope of the initial linear portion of the decay curve. Each rate measurement was repeated thrice with independently prepared samples. The rate orders of SmI_2, $SmBr_2$, and water in the evolution of H_2 gas by SmI_2-water and $SmBr_2$-water are shown in Table 4.1 and Table 4.2, respectively.

Table 4.1. Rate orders for the evolution of H_2 gas by SmI_2-water

entry	reaction component	order[a]
1	SmI_2	1.09 ± 0.06[a]
2	H_2O	0.93 ± 0.09[b]

[a]Errors reported as ± σ. [b]2-21 mM SmI_2, 100 mM H_2O in THF. [c]3mM SmI_2, 25-500 mM H_2O in THF.

Table 4.2. Rate orders for the evolution of H_2 gas by $SmBr_2$-water

entry	reaction component	order[a]
1	$SmBr_2$	0.87 ± 0.02[a]
2	H_2O	1.05 ± 0.02[b]

[a]Errors reported as ± σ. [b]5-12 mM $SmBr_2$, 100mM H_2O in THF. [c]3 mM $SmBr_2$, 25-500 mM H_2O in THF.

The rate dependence on all components in the evolution of H_2 gas by both SmI_2-water and $SmBr_2$-water was found to be near unity. Notably, these results are

inconsistent with the hypothesized rate limiting coulombic barrier to self-association between Sm(II)-water reductants, which was predicted to induce a second order rate dependence on Sm(II) and at least a second order rate dependence on water.

4.3.1.2 Kinetic Activation Parameter Experiments

The mechanism of H_2 gas evolution by SmI_2-water and $SmBr_2$-water was further investigated by acquiring rate data for the evolution of H_2 gas by SmI_2-water and $SmBr_2$-water over a 20 °C temperature range to determine the activation parameters for the reactions. These rate measurements were made under initial rates conditions with initial concentrations of 3 mM SmI_2 and $SmBr_2$ and 50 mM water. All activation parameter data is shown in Table 4.3.

Table 4.3. Activation parameters for the evolution of H_2 gas by SmI_2-water and $SmBr_2$-water

entry	proton donor	SmI_2[a]	$SmBr_2$[b]
1	$\Delta H^{\ddagger}$ (kcal mol^{-1})[c]	20 ± 2	11.6 ± 0.5
2	$\Delta S^{\ddagger}$ (cal mol^{-1}K^{-1})[c]	-7 ± 6	-36 ± 2
3	$\Delta G^{\ddagger}$ (kcal mol^{-1})[d]	22 ± 3	22 ± 1

[a]Conditions: 3 mM SmI_2 and 50 mM water in THF. The activation parameters are the averages of three independent experiments from 15 to 35 °C. [b]Conditions: 3 mM $SmBr_2$ and 50 mM water in THF. The activation parameters are the averages of three independent experiments from 15 to 35 °C. [c]Obtained from $\ln(k_{obs}h/kT) - \Delta H^{\ddagger}/RT + \Delta S^{\ddagger}/R$ and errors are reported as ±σ. [d]Calculated from $\Delta G = \Delta H^{\ddagger} - T\Delta S^{\ddagger}$ and errors are reported as ±σ.

The results of the activation parameter experiments reveal a high enthalpic barrier and low entropic barrier to H_2 gas evolution from SmI_2-water, which is consistent with a relatively late, disordered transition state. This is further evidence against the coulombic barrier hypothesis, which would lead to an early, highly ordered transition state.

Notably, H_2 gas evolution from $SmBr_2$-water has a lower enthalpic and higher entropic barrier than H_2 gas evolution from SmI_2-water. While this result is partially consistent with a rate limiting coulombic barrier to self-association in the evolution of H_2

from $SmBr_2$-water, the rate orders of one for both $SmBr_2$ and water in this reaction make that unlikely. It has been demonstrated that addition of water to $SmBr_2$ in THF only induces the dissociation of a single bromide ligand from Sm(II) while the other remains coordinated.[30] It was therefore proposed that the differences in $\Delta H^{\ddagger}$ and $\Delta S^{\ddagger}$ for the evolution of H_2 gas from SmI_2-water and $SmBr_2$-water are driven by the greater redox potential and increased steric interference around Sm(II) induced by the presence of an additional bromide ligand.

4.3.2 Deuterium Labeling Headspace ^{1}H NMR Experiments

With a rate limiting self-association ruled out for the evolution of H_2 gas from Sm(II)-water, it was proposed that the Sm(II)-water reagent may be generating a free H atom, which could abstract an H atom from the homolytically labile α-C-H bond of the bulk THF solvent to form H_2 gas as shown in Scheme 4.10. To test this hypothesis, a series of deuterium labeling experiments were carried out. In these experiments, a solution of SmI_2 was prepared in a sealed vial equipped with a septum cap. Water was then added to the solution via syringe and the reaction was allowed to proceed until discoloration of the characteristic blue of SmI_2 was observed. Headspace gas from the reaction vial was then withdrawn and bubbled into $CDCl_3$ and observed by ^{1}H NMR. As shown in Figure 4.1, this spectrum was found to contain a singlet peak corresponding to H_2 gas. This experiment was repeated with a 50:50 mole amount solution of water and deuterium oxide, which was similarly added to a sealed solution of SmI_2. The headspace ^{1}H NMR spectrum for this reaction was found to contain both a singlet peak corresponding to H_2 gas and a 1:1:1 triplet corresponding to HD gas as shown in Figure 4.2. Finally, when only deuterium oxide was added to a sealed solution of SmI_2, no

peaks corresponding to H_2 or HD gas were observed in the headspace ^{1}H NMR spectrum, indicating that all of the evolved gas was D_2 gas, which is silent in ^{1}H NMR spectra. These results are consistent with both H atom equivalents in the H_2 gas evolved from SmI_2-water originating from the water added to the system. Hydrogen atom abstraction from THF was therefore ruled out as a pathway for H_2 gas evolution from SmI_2-water.

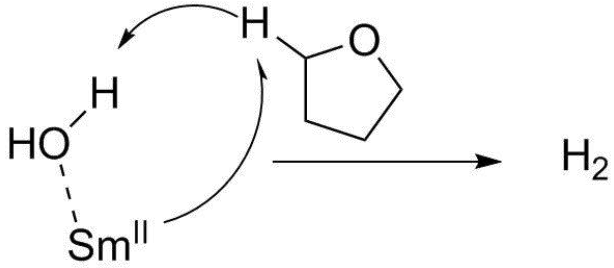

Scheme 4.10. Proposed mechanism of H-atom abstraction from THF by SmI_2-water

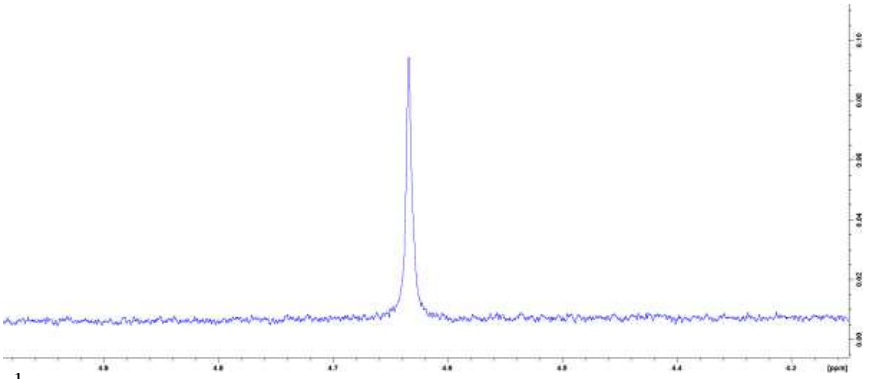

Figure 4.1. ^{1}H NMR spectrum of the headspace of the reaction of SmI_2 with water

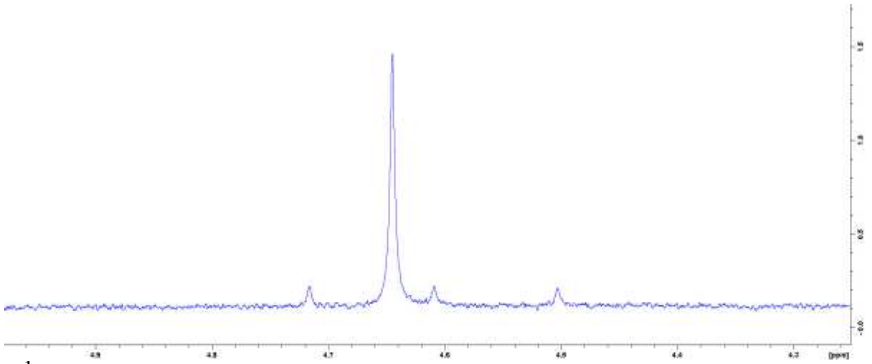

Figure 4.2. ^{1}H NMR spectrum of the headspace of the reaction of SmI_2 with a 50:50 mole amount solution of water and deuterium oxide

4.3.3 Density Functional Theory Modeling

Computational investigations of H_2 evolution from SmI_2-water were also undertaken via collaboration with Vlaisavljevich and coworkers at the University of South Dakota. These studies were performed using density functional theory (DFT) using the Turbomole V7.3 program package.[31] Preliminary calculations were performed to assess the relative energies of a range of $Sm^{II}(THF)_n(H_2O)_m$ complexes in THF. The seven-coordinate $Sm^{II}(THF)_2(H_2O)_5$ complex was found to be the most stable of those modeled.

Further calculations were performed to model the free energy of H atom loss from a series of seven-coordinate $Sm^{II}(THF)_n(H_2O)_m$ complexes (n + m = 7). These calculations revealed that H atom loss is nearly isoenergetic with the group of seven-coordinate $Sm^{II}(THF)_n(H_2O)_m$ complexes modeled, with the free energies for H atom loss ranging from 19-26 kcal/mol. These values are in good agreement with the measured $\Delta G^{\ddagger}$ of approximately 22 kcal/mol (Table 4.3). These results were considered together with the lack of rate limiting self-association or solvent H atom abstraction mechanisms. The findings were determined to be consistent with the activation of the O-H bond of Sm(II)-water complex necessary to cleave the O-H bond of the water being reduced as the primary barrier to H_2 gas evolution from SmI_2-water.

4.4 Conclusions

In the studies discussed above, several hypotheses regarding the basis of the unusual stability of the SmI_2-water reagent were tested. Stopped flow rate studies revealed rate orders of unity for SmI_2 and water in the evolution of H_2 gas from SmI_2-water. Additionally, the determination of activation parameters for this reaction revealed

a late, relatively disordered transition state. These results indicate that self-association between two Sm(II)-water complexes is not rate limiting in the evolution of H_2 gas.

Additionally, deuterium labeling experiments were conducted on the headspace gasses of reactions of SmI_2 with water and deuterium oxide. The results of these experiments revealed that both H atom equivalents in the H_2 gas evolved by SmI_2-water originate from the water introduced to the reaction.

Finally, DFT modeling of H atom loss from a family of seven-coordinate $Sm(II)(THF)_n(H_2O)_m$ complexes was performed by Vlaisavljevich and coworkers. The combined results of this modeling were taken together with the experimental studies *vide supra*. This allowed for the determination of the O-H bond activation necessary to cleave the strong O-H bond of the molecule of water being reduced as the predominant barrier to H_2 gas evolution from SmI_2-water.

4.5 References

(1) Girard, P.; Namy, J. L.; Kagan, B. Divalent Lanthanide Derivatives in Organic Synthesis. 1. Mild Preparation of SmI2 and YbI2 and Their Use as Reducing or Coupling Agents. *J. Am. Chem. Soc.* **1980**, *102* (8), 2693–2698.

(2) Nicolaou, K. C.; Ellery, S. P.; Chen, J. S. Samarium Diiodide Mediated Reactions in Total Synthesis. *Angew. Chemie Int. Ed.* **2009**, *48* (39), 7140–7165.

(3) Chciuk, T. V.; Flowers, R. A. Proton-Coupled Electron Transfer in the Reduction of Arenes by SmI2-Water Complexes. *J. Am. Chem. Soc.* **2015**, *137* (35), 11526–11531.

(4) Ramírez-Solís, A.; Bartulovich, C. O.; León-Pimentel, C. I.; Saint-Martin, H.; Boekell, N. G.; Flowers, R. A. Proton Donor Effects on the Reactivity of SmI2. Experimental and Theoretical Studies on Methanol Solvation vs. Aqueous Solvation. *Dalt. Trans.* **2020**, *49* (23), 7897–7902.

(5) Prasad, E.; Flowers, R. A. Reduction of Ketones and Alkyl Iodides by Sml2 and Sm(Ii)-HMPA Complexes. Rate and Mechanistic Studies. *J. Am. Chem. Soc.* **2002**, *124* (24), 6895–6899.

(6) Andrieux, C. P.; Gallardo, I.; Savéant, J.-M.; In Encyclopedia of Electrochemistry

of the Ele-ments, M. D.; Dekker, M.; J Am, K. B. Outer-Sphere Electron-Transfer Reduction of Alkyl Halides. A Source of Alkyl Radicals or of Carbanions? Reduction of Alkyl Radicals. *J. Am. Chem. Soc.* **2002**, *111* (5), 1620–1626.

(7) Chciuk, T. V.; Anderson, W. R.; Flowers, R. A. Proton-Coupled Electron Transfer in the Reduction of Carbonyls by Samarium Diiodide-Water Complexes. *J. Am. Chem. Soc.* **2016**, *138* (28), 8738–8741.

(8) Chciuk, T. V; Anderson, W. R.; Flowers, R. A. Interplay between Substrate and Proton Donor Coordination in Reductions of Carbonyls by SmI2-Water Through Proton-Coupled Electron-Transfer. *J. Am. Chem. Soc.* **2018**, *140*, 15342–15352.

(9) Kolmar, S. S.; Mayer, J. M. SmI2(H2O)n Reduction of Electron Rich Enamines by Proton-Coupled Electron Transfer. *J. Am. Chem. Soc.* **2017**, *139* (31), 10687−10692.

(10) Sautier, B.; Lyons, S. E.; Webb, M. R.; Procter, D. J. Radical Cyclization Cascades of Unsaturated Meldrum's Acid Derivatives. *Org. Lett.* **2012**, *14* (1), 146–149.

(11) Hutton, T. K.; Muir, K. W.; Procter, D. J. Switching between Novel Samarium(II)-Mediated Cyclizations by a Simple Change in Alcohol Cosolvent. *Org. Lett.* **2003**, *5* (25), 4811–4814.

(12) Collins, K. D.; Oliveira, J. M.; Guazzelli, G.; Sautier, B.; De Grazia, S.; Matsubara, H.; Helliwell, M.; Procter, D. J. Selective Reductions of Cyclic 1,3-Diesters by Using SmI2 and H2O. *Chem. – A Eur. J.* **2010**, *16* (33), 10240–10249.

(13) Guazzelli, G.; De Grazia, S.; Collins, K. D.; Matsubara, H.; Spain, M.; Procter, D. J. Selective Reductions of Cyclic 1,3-Diesters Using SmI2 and H2O. *J. Am. Chem. Soc.* **2009**, *131* (21), 7214–7215.

(14) Plesniak, M. P.; Garduño-Castro, M. H.; Lenz, P.; Just-Baringo, X.; Procter, D. J. Samarium(II) Folding Cascades Involving Hydrogen Atom Transfer for the Synthesis of Complex Polycycles. *Nat. Commun. 2018 91* **2018**, *9* (1), 1–9.

(15) Maity, S.; Flowers, R. A.; Hoz, S. Aza versus Oxophilicity of SmI2 : A Break of a Paradigm. *Chem. - A Eur. J.* **2017**, *23* (67), 17070–17077.

(16) Dahlén, A.; Hilmersson, G. Samarium(II) Iodide Mediated Reductions - Influence of Various Additives. *Eur. J. Inorg. Chem.* **2004**, No. 17, 3393–3403.

(17) Dahlén, A.; Hilmersson, G. Instantaneous SmI2/H2O/Amine-Mediated Reductions in THF. *Chem. - A Eur. J.* **2003**, *9* (5), 1123–1128.

(18) Dahlén, A.; Hilmersson, G.; Knettle, B. W.; Flowers, R. A. Rapid SmI2-Mediated Reductions of Alkyl Halides and Electrochemical Properties of

SmI2/H2O/Amine. *J. Org. Chem.* **2003**, *68* (12), 4870–4875.

(19) Dahlén, A.; Petersson, A.; Hilmersson, G. Diastereoselective Intramolecular SmI 2 – H2O – Amine Mediated Couplings. *Org. Biomol. Chem.* **2003**, *1* (14), 2423–2426.

(20) Kim, M.; Knettle, B. W.; Dahlén, A.; Hilmersson, G.; Flowers, R. A. Reduction and Reductive Coupling of Imines by Sm(II)-Based Reagents. *Tetrahedron* **2003**, *59* (52), 10397–10402.

(21) Ashida, Y.; Arashiba, K.; Nakajima, K.; Nishibayashi, Y. Molybdenum-Catalysed Ammonia Production with Samarium Diiodide and Alcohols or Water. *Nature* **2019**, *568* (7753), 536–540.

(22) Kolmar, S. S.; Mayer, J. M. SmI2(H2O)n Reduction of Electron Rich Enamines by Proton-Coupled Electron Transfer. *J. Am. Chem. Soc.* **2017**, *139* (31), 10687–10692.

(23) Warren, J. J.; Tronic, T. A.; Mayer, J. M. The Thermochemistry of Proton-Coupled Electron Transfer Reagents and Its Implications. *Chem. Rev.* **2010**, *110* (12), 6961–7001.

(24) Drover, M. W.; Schild, D. J.; Oyala, P. H.; Peters, J. C. Snapshots of a Migrating H-Atom: Characterization of a Reactive Iron(III) Indenide Hydride and Its Nearly Isoenergetic Ring-Protonated Iron(I) Isomer. *Angew. Chemie Int. Ed.* **2019**, *58* (43), 15504–15511.

(25) Chalkley, M. J.; Oyala, P. H.; Peters, J. C. Cp* Noninnocence Leads to a Remarkably Weak C−H Bond via Metallocene Protonation. *J. Am. Chem. Soc.* **2019**, *141*, 4721−4729.

(26) Schild, D. J.; Drover, M. W.; Oyala, P. H.; Peters, J. C. Generating Potent C–H PCET Donors: Ligand-Induced Fe-to-Ring Proton Migration from a Cp*FeIII–H Complex Demonstrates a Promising Strategy. *J. Am. Chem. Soc.* **2020**, *142* (44), 18963–18970.

(27) Bezdek, M. J.; Guo, S.; Chirik, P. J. Coordination-Induced Weakening of Ammonia, Water, and Hydrazine X–H Bonds in a Molybdenum Complex. *Science* **2016**, *354* (6313), 730–733.

(28) Ramírez-Solís, A.; Amaro-Estrada, J. I.; Hernández-Cobos, J.; Maron, L.; México, M. Aqueous Solvation of SmI2 : A Born-Oppenheimer Molecular Dynamics Density Functional Theory Cluster Approach. *J. Phys. Chem. A* **2017**, *121*, 2293−2297.

(29) Sadasivam, D. V.; Teprovich, J. A.; Procter, D. J.; Flowers, R. A. Dynamic Ligand Exchange in Reactions of Samarium Diiodide. *Org. Lett.* **2010**, *12* (18), 4140–4143.

(30) Ramírez-Solís, A.; Bartulovich, C. O.; Chciuk, T. V.; Hernández-Cobos, J.; Saint-Martin, H.; Maron, L.; Anderson, W. R.; Li, A. M.; Flowers, R. A. Experimental and Theoretical Studies on the Implications of Halide-Dependent Aqueous Solvation of Sm(II). *J. Am. Chem. Soc.* **2018**, *140* (48), 16731–16739.

(31) Balasubramani, S. G.; Chen, G. P.; Coriani, S.; Diedenhofen, M.; Frank, M. S.; Franzke, Y. J.; Furche, F.; Grotjahn, R.; Harding, M. E.; Hättig, C.; et al. TURBOMOLE: Modular Program Suite for Ab Initio Quantum-Chemical and Condensed-Matter Simulations. *J. Chem. Phys.* **2020**, *152* (18), 184107.

Chapter 5. Theoretical and Mechanistic Studies on the SmI_2-Ammonia Bond Weakening System

5.1 Background and Significance

5.1.1 Metal-Ligand Affinity and Coordination-Induced Bond Weakening in Sm(II)-Water and Sm(II)-Alcohol Complexes

Following the discovery of PCET in the reductions of arenes by SmI_2 by Flowers and coworkers, the PCET reactivity of Sm(II) was further demonstrated to include SmI_2 reagents with strongly-coordinating alcohol additives like ethylene glycol, diethylene glycol, and sufficiently high concentrations of methanol.[1,2] The generality of Sm(II) coordination-induced bond weakening in high-affinity alcohol ligands is supported by the thermochemical cycle shown in Scheme 5.1, which demonstrates the dependence of coordination-induced bond weakening upon the affinity of an alcohol ligand for Sm(II).[1]

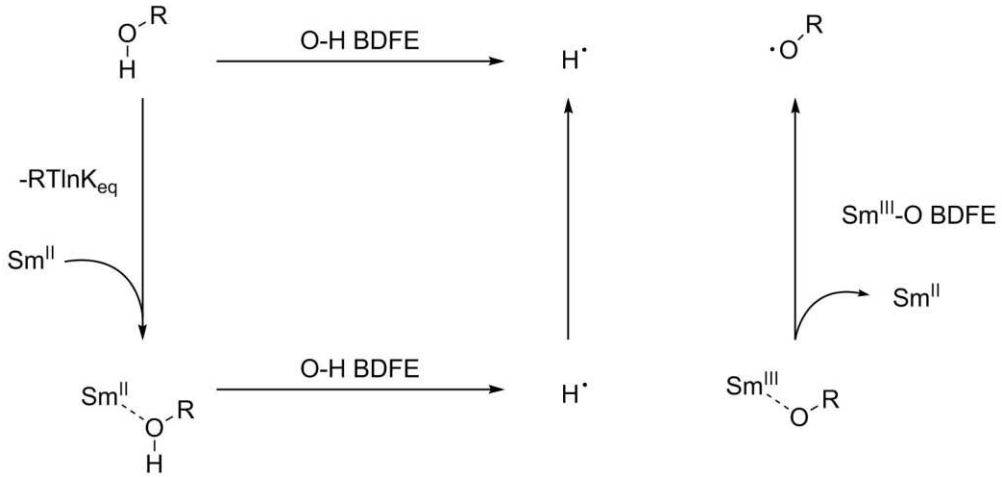

Scheme 5.1. Thermochemical cycle for hydrogen atom loss from an alcohol and the Sm(II)-alcohol complex[1]

5.1.2 Coordination-Induced N-H Bond Weakening in Sm(II) Systems

Weakening of N-H bonds upon ligand coordination to Sm(II) has also been observed in systems such as the SmI_2-2-pyrrolidinone system shown in Scheme 5.2.[3]

Coordination of 2-pyrrolidinone to Sm(II) was found to promote a weakening of at least 70.8 kcal/mol in the amide N-H bond via comparison with the C-H bond formed upon the initial PCET reduction of phenanthrene.

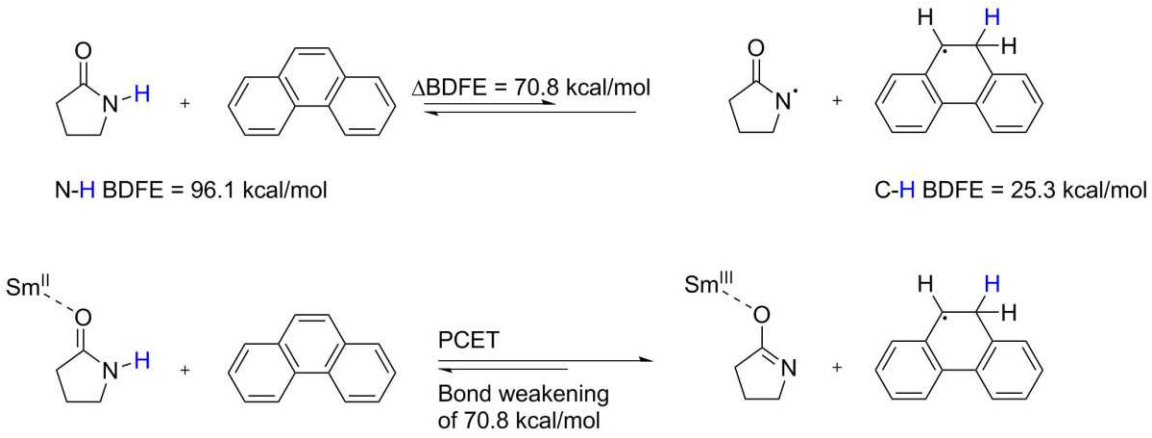

Scheme 5.2. Reaction scheme and bond strength comparison for the reduction of phenanthrene by SmI_2-2-pyrrolidinone[3]

Subsequently, the affinity of a range of oxygen- and nitrogen-containing ligands for Sm(II) were observed by UV-Vis absorption spectroscopy.[4,5] These measurements revealed significantly greater UV-Vis spectral shifts in the absorption spectra for SmI_2 upon addition of nitrogen-containing ligands compared to their oxygen-containing counterparts. This difference in behavior for nitrogen- and oxygen-containing ligands is consistent with a greater affinity of Sm(II) for nitrogen than for oxygen. An example of this paradigm can be seen in the comparison of the UV-Vis spectra of SmI_2 in the presence of increasing concentrations of ammonia and water in Figure 5.1.

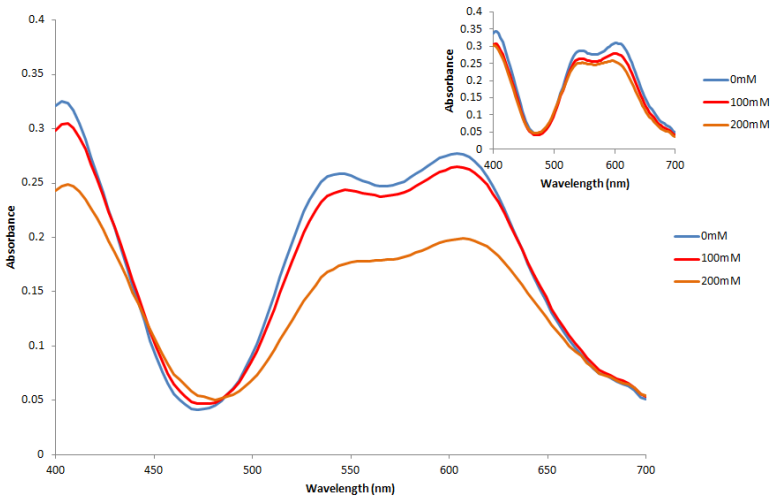

Figure 5.1. 4 mM SmI_2 in THF containing 0, 100, and 200 mM ammonia. Inset: 4 mM SmI_2 in THF containing 0, 100, 200 mM water[5]

5.1.3 Introduction to Ammonia as a Hydrogen Fuel Source

Taken together with the demonstrated Sm(II) coordination-induced N-H bond weakening of an amide, the significant azaphilicity of Sm(II) suggests it should be possible to utilize amines as proton donors for Sm(II)-mediated PCET reductions of substrates. Ammonia is of particular interest in this context. Ammonia is a key component of industrial fertilizers, for which purpose more than 160 million tonnes of ammonia was projected to be produced globally in 2022.[6] Concomitant with this production, global infrastructure already exists for the transportation, storage, and safe handling of ammonia.[7,8] Moreover, unlike many small protic feedstock molecules, ammonia lacks carbon and its homolysis therefore does not contribute to greenhouse emissions. For these reasons, ammonia is a promising candidate for large scale carbon-free hydrogen fuel systems.[7,9–11]

5.2 Experimental Details

5.2.1 Materials

Samarium powder was purchased from Acros Organics. Samarium diiodide was generated by the standard method of samarium metal combined with iodine in THF and allowed to stir for at least 4 hours. Iodometric titrations were then performed to verify concentration of SmI_2 for use. Tetrahydrofuran was purified by a solvent purification system (Innovative Technology Inc.; MA). Acenaphthalene, anthracene, and *trans*-stilbene were purchased from Alfa Aesar and used without further purification. Ammonia was purchased as a 0.4 M solution in dry THF from Sigma-Aldritch and was used without further purification. Water was deoxygenated by bubbling with argon gas prior to use.

5.2.2 Instrumentation

^{1}H NMR and ^{13}C $\{^{1}H\}$ NMR spectra were recorded in $CDCl_3$ on a Bruker 400 MHz spectrometer at 400 and 125 MHz respectively. The ^{1}H NMR chemical shifts are given as δ values in ppm relative to TMS (0 ppm) as the internal reference. The $^{13}C\{1H\}$ NMR shifts are expressed with respect to the $CDCl_3$ (77.0 ppm). GCMS analyses were performed with a Shimadzu GCMS-QP2010 Ultra. GC analyses were performed using a Shimadzu Gas Chromatograph GC-2010 Plus with biphenyl as an internal standard. UV-Visible spectra experiments were performed with a computer-controlled SX.18 MV stopped-flow spectrophotometer (Applied Photophysics Ltd. Surrey, UK). Solutions were prepared under a dry argon atmosphere in flame dried glassware.

5.2.3 Methods

5.2.3.1 Procedure for Reductions of Arenes by SmI_2-Ammonia or SmI_2-Water

Inside an Ar glove box, a flame dried vial equipped with a magnetic stir bar was charged with 0.1 M SmI_2 in THF (2 mL, 0.2 mmol). Substrate was then added to the SmI_2 solution (10.3 mg acenaphthalene, 0.067 mmol) (11.9 mg anthracene, 0.067 mmol) (12.0 mg *trans*-stilbene, 0.067 mmol) (11.9 mg phenanthrene, 0.067 mmol) and the solution was allowed to stir for several minutes. The vial was then charged with proton donor dissolved in dry, anaerobic THF (12.5 mL 0.4 M ammonia, 5 mmol) (5 mL 1.0 M water, 5 mmol). This solution was allowed to react overnight. Once the reaction was complete, vials were removed from the glove box and quenched under atmosphere over the course of several minutes and an aqueous solution of 0.2 M HCl was added to the vial. The quenched solution was extracted into diethyl ether (3x). The organic layers were combined then washed with deionized water, then with saturated aqueous sodium thiosulfate, then with brine. The remaining organic solution was dried over magnesium sulfate then filtered and concentrated under reduced pressure. All products were analyzed by GCMS and ^{1}H and ^{13}C NMR.

5.2.3.1.1 Procedure for GCMS Yields of Reductions of Arenes by SmI_2-Ammonia or SmI_2-Water

The reaction solution was removed from the glove box and quenched under atmosphere over the course of several minutes. Biphenyl (10.3 mg, 0.067 mmol) was added to the reaction vial as an internal standard along with 0.2 M HCl. The quenched solution was extracted into diethyl ether (3x). The organic layers were combined then washed with deionized water, then with saturated aqueous sodium thiosulfate, then with

brine. The remaining organic solution was dried over magnesium sulfate then filtered and analyzed by GCMS.

5.2.3.1.2 Procedure for Isolation of Products of Reductions of Arenes by SmI_2-Ammonia or SmI_2-Water

1,2-dihydroacenaphthalene was extracted with diethyl ether. The combined organic layers were washed with water, saturated aqueous sodium thiosulfate, and brine. The resulting solution was dried over magnesium sulfate then concentrated under reduced pressure and characterized by ^{1}H (400 MHz, $CDCl_3$) δ (ppm): 3.33 (s, 4H), 7.20 (d, 2H), 7.36 (t, 2H), 7.51 (d, 2H); ^{13}C NMR (100 MHz, $CDCl_3$) δ (ppm): 30.37, 119.18, 122.24, 127.80

9,10-dihydroanthracene was extracted with diethyl ether. The combined organic layers were washed with water, saturated aqueous sodium thiosulfate, and brine. The resulting solution was dried over magnesium sulfate then concentrated under reduced pressure and characterized by ^{1}H (400 MHz, $CDCl_3$) δ (ppm): 3.87 (s, 4H), 7.11-7.14 (m, 4H), 7.21-7.25 (m, 4H);^{13}C NMR (100 MHz, $CDCl_3$) δ (ppm): 36.20, 126.12, 127.42, 136.71

1,2-diphenylethane was extracted with diethyl ether. The combined organic layers were washed with water, saturated aqueous sodium thiosulfate, and brine. The resulting solution was dried over magnesium sulfate then concentrated under reduced pressure and characterized by ^{1}H (400 MHz, $CDCl_3$) δ (ppm): 2.85 (s, 4H), 7.10-7.22 (m, 10H);^{13}C NMR (100 MHz, $CDCl_3$) δ (ppm): 30.38, 126.56, 127.67, 128.71, 137.37

5.2.3.2 Procedure for Stopped Flow Kinetics Studies

Kinetic experiments were performed with a computer-controlled SX.18 MV stopped- flow spectrophotometer (Applied Photophysics Ltd. Surrey, UK). Solutions

were injected separately into the stopped-flow system using airtight, capped BD syringes prepared in a glove box under argon atmosphere. Between each experiment, the cell block was washed with dilute HNO_3 (1x), Deionized H_2O (1x), and THF (3x) before additional anhydrous deoxygenated THF washes (3x). The reaction rates were determined from the decay of SmI_2 at 560 nm. Kinetic measurements were carried out at 25°C unless otherwise specified.

5.3 Results and Discussion

5.3.1 Synthetic Studies with the SmI_2-Ammonia System and Comparison to SmI_2-Water

To gauge the reactivity of the SmI_2-ammonia reagent, the reduction of a series of arenes by SmI_2-ammonia was observed. Arenes were selected that form sequentially weaker C-H bonds upon initial PCET reduction, as determined via density functional theory (DFT) modeling.[12,13] These arene reductions by SmI_2-ammonia were compared to the same reductions mediated by SmI_2-water, as shown in Scheme 5.3. Both systems were found to quantitatively reduce both acenaphthalene and anthracene as well as affect the approximately 50% reduction of *trans*-stilbene to 1,2-diphenylethane. Moreover, phenanthrene was found to be unreactive in the presence of both SmI_2-ammonia and SmI_2-water.[5] The similarity between the reactivities of SmI_2-ammonia and SmI_2-water with arenes was considered remarkable.

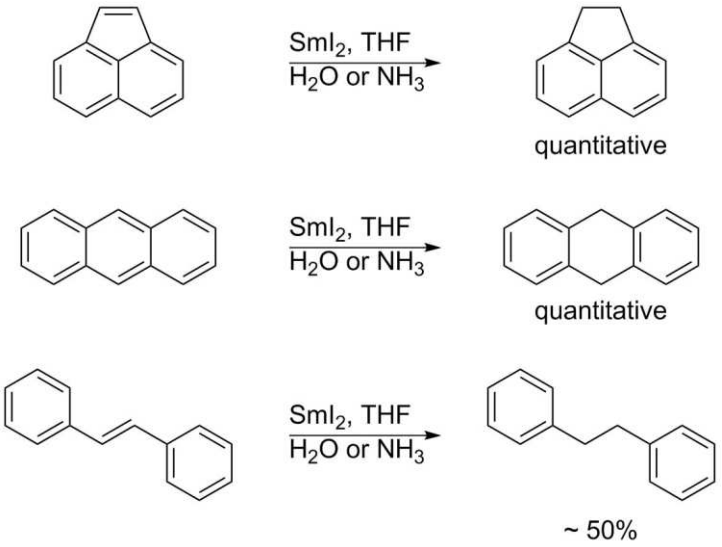

Scheme 5.3. Reaction scheme for the reductions of arenes by SmI_2-ammonia and SmI_2-water[5]

5.3.2 Born-Oppenheimer Molecular Dynamics-Density Functional Theory Computational Studies

Further investigation of the SmI_2-ammonia system and comparison with SmI_2-water was performed computationally by Ramírez-Solís and coworkers at Universidad Autónoma del Estado de Morelos, Facultad de Química, and Instituto de Ciencias Físicas. These studies were performed using Born-Oppenheimer molecular dynamics (BOMD) simulations based on M062X DFT calculations.[14] These simulations were performed using Geraldyn-2.1, which was coupled to Gaussian 09 at 300K.[13,15–18] The SmI_2-ammonia system was simulated as a SmI_2-$(NH_3)_{32}$ microsolvate and was thermalized at 300K over 25 ps, the last 15 ps of which were analyzed for structural, dynamic, and energetic data. This data was compared to that collected for the SmI_2-$(H_2O)_{32}$ microsolvate simulated at the same level of theory with analogous starting conditions.[14]

The SmI_2-ammonia and SmI_2-water microsolvates were initially compared by observation of the simulated coordination environments of the respective Sm(II) metal centers. This comparison revealed a greater average Sm-I distance in the SmI_2-ammonia

microsolvate than in the SmI_2-water microsolvate. Analysis of the individual Sm-I distances in both systems, shown in Figure 5.2, revealed that the difference is due to the ejection of both iodides beyond the second coordination sphere of the Sm(II)-ammonia microsolvate while in the Sm(II)-water microsolvate, one iodide is ejected and one oscillates between the first and second coordination spheres.

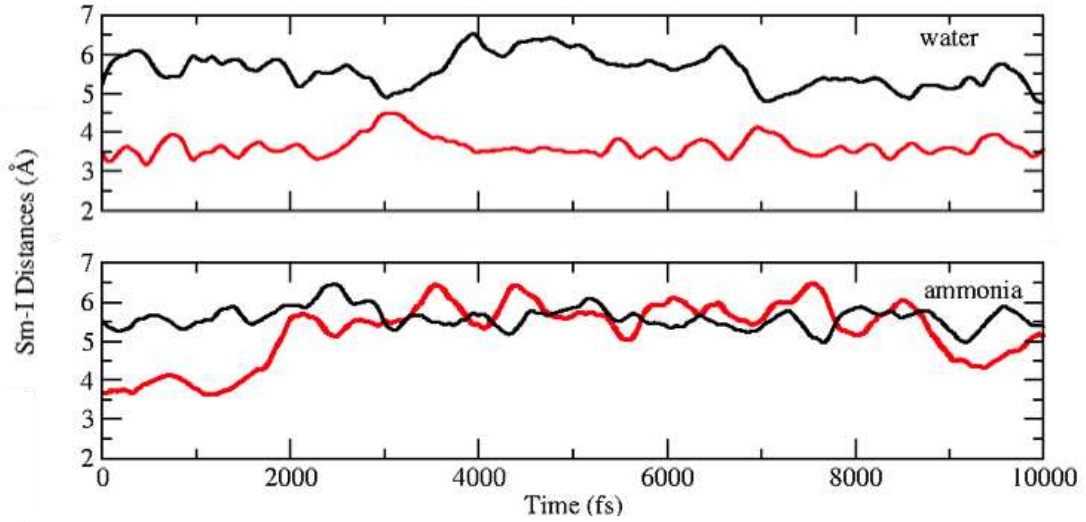

Figure 5.2. Evolution of the Sm-I distances over time for the SmI_2-$(H_2O)_{32}$ and SmI_2-$(NH_3)_{32}$ microsolvates at 300K after thermalization[5]

The effects of the greater Sm-I distance in the Sm(II)-ammonia microsolvate can be seen in the simulated EXAFS spectra for both systems (Figures 5.3 and 5.4). With a scattering atom cutoff distance of 5 Å from Sm(II), the simulated EXAFS spectrum for SmI_2-ammonia shows much greater signal intensity at low wavenumbers than the simulated EXAFS spectrum for SmI_2-water. Both simulated EXAFS spectra with a 5 Å scattering atom cutoff distance are shown in Figure 5.3. This difference at low k was confirmed to be a consequence of the nearby iodide in the SmI_2-water microsolvate via analysis of the simulated EXAFS spectra for both microsolvates with scattering atom cutoffs of 3 Å from Sm(II), shown in Figure 5.4. This shorter cutoff distance excludes

the low-lying iodide in the SmI_2-water microsolvate and yields remarkably similar spectra for both systems at low wavenumbers.

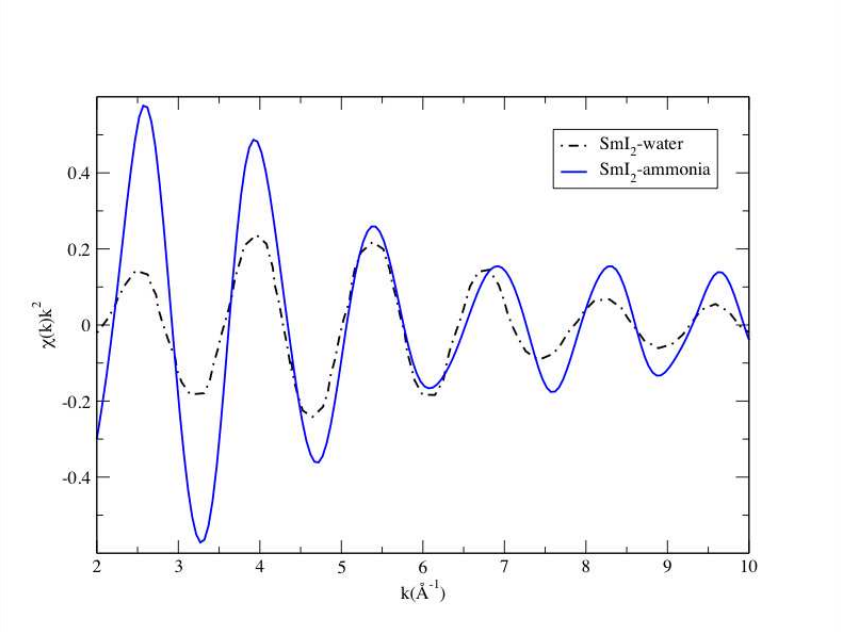

Figure 5.3. Simulated EXAFS spectra for the SmI_2-$(NH_3)_{32}$ (blue) and SmI_2-$(H_2O)_{32}$ (black) microsolvates with scattering atom cutoffs of 5 Å[5]

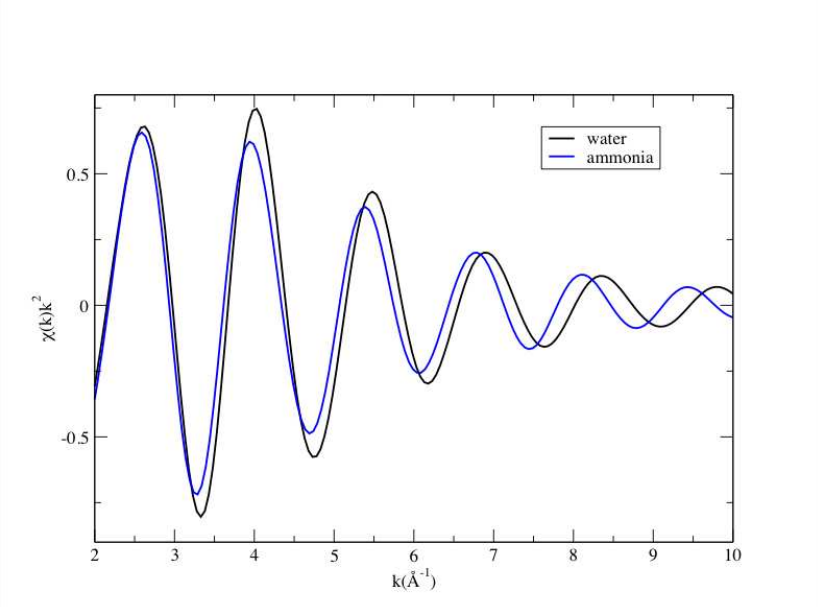

Figure 5.4. Simulated EXAFS spectra for the SmI_2-$(NH_3)_{32}$ (blue) and SmI_2-$(H_2O)_{32}$ (black) microsolvates with scattering atom cutoffs of 3 Å[5]

The differences in iodide solvation are consistent with analysis of the first coordination sphere of the SmI_2-ammonia and SmI_2-water microsolvates, which revealed remarkably similar ammonia and water coordination numbers of 8.4 and 8.5, respectively. The greater steric bulk of ammonia is therefore likely responsible for the observed exclusion of both iodide ligands from the first and second coordination spheres of the Sm(II)-ammonia system.

While the greater steric bulk of ammonia provides rationalization for the greater average Sm-I distance in SmI_2-ammonia, it appears to contrast with the similarity of the Sm(II)-ammonia and Sm(II)-water coordination numbers. It is likely that this discrepancy is due to the greater affinity of Sm(II) for nitrogen compared to oxygen. The difference in affinity also induces a more highly ordered first solvation sphere in the SmI_2-ammonia microsolvate compared to the SmI_2-water microsolvate. This can be observed in the higher wavenumber (> 4 Å) region of the simulated EXAFS spectra in Figure 5.4, which shows significantly slower signal decay for the SmI_2-ammonia microsolvate compared to the SmI_2-water microsolvate.

5.3.3 Kinetic Analysis of the Reduction of Acenaphthalene by SmI_2-Ammonia and SmI_2-Water

5.3.3.1 Kinetic Rate Order Experiments

In order to build upon the insights gained by comparison of the BOMD simulations of the SmI_2-$(NH_3)_{32}$ and SmI_2-$(H_2O)_{32}$ microsolvates, the reductions of acenaphthalene by SmI_2-ammonia and SmI_2-water, shown in Scheme 5.4, were investigated through rate studies using stopped flow kinetic analysis. Observation of the rate of reduction of acenaphthalene by SmI_2-ammonia was complicated by precipitation

of the Sm(II)-ammonia complex at greater than 50 equivalents of ammonia with respect to [SmI_2]. These rate studies were therefore carried out under initial rates conditions, with the reaction components prepared in similar relative concentrations to those used for synthetic studies and with [ammonia] never exceeding 25 equivalents with respect to [SmI_2]. The decay of the characteristic absorbance of SmI_2 at 560nm using stopped flow spectrophotometry was used to track reaction progress. The initial linear portion of the decay curve was fit to a linear function to acquire the k_{obs} for each measurement. Rate measurements were repeated in triplicate with independently prepared samples.

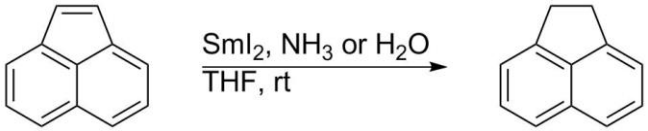

Scheme 5.4. Reaction scheme for the reduction of acenaphthalene by SmI_2-ammonia or SmI_2-water[5]

The rate orders for all components in the SmI_2-ammonia-mediated reduction of acenaphthalene are shown in Table 5.1 and the rate orders for all components in the SmI_2-water-mediated reduction of acenaphthalene are shown in Table 5.2. Due to difficulties collecting initial rates substrate rate order data for the reduction of acenaphthalene by SmI_2-water, the acenaphthalene rate order for that system was determined using pseudo-first order kinetics, with [water] and [acenaphthalene] maintained in excess of 10 equivalents with respect to [SmI_2]. The rate orders for both systems were found to be similar, with first order rate contributions from SmI_2 and acenaphthalene for both SmI_2-ammonia and SmI_2-water. Moreover, the rate orders of ammonia and water were found to be approximately 2 in their respective systems.

Table 5.1. Rate orders for the reduction of acenaphthalene by SmI_2-ammonia[5]

entry	reaction component	order[a]
1	SmI_2	1.00 ± 0.04[b]
2	NH_3	1.96 ± 0.08[c]
3	Acenaphthalene	0.91 ± 0.07[d]

[a]Errors reported as ± σ [b]2-5 mM SmI_2, 100 mM ammonia, 2 mM acenaphthalene in THF. [c]4 mM SmI_2, 12.5-100 mM ammonia, 2 mM acenaphthalene in THF. [d]4 mM SmI_2, 100 mM ammonia, 0.25-2 mM acenaphthalene in THF.

Table 5.2. Rate orders for the reduction of acenaphthalene by SmI_2-water[5]

entry	reaction component	order[a]
1	SmI_2	1.01 ± 0.09[b]
2	H_2O	2.0 ± 0.1[c]
3	Acenaphthalene	1.00 ± 0.05[d]

[a]Errors reported as ± σ. [b]4-8 mM SmI_2, 400 mM water, 2 mM acenaphthalene in THF. [c]4 mM SmI_2, 50-400 mM water, 2 mM acenaphthalene in THF. [d]Pseudo-first order method: 4 mM SmI_2, 100 mM water, 40-70 mM acenaphthalene in THF.

5.3.3.2 Kinetic Activation Parameter Experiments

Rate data was also acquired using initial rates methodology over a 20 °C temperature range to determine the activation parameters for the reductions of acenaphthalene by SmI_2-ammonia and SmI_2-water. Activation parameters for the SmI_2-water-mediated reduction of acenaphthalene were measured under conditions of both 25 and 100 equivalents of water with respect to [SmI_2]. All activation parameter data is displayed in Table 5.3. Remarkably, the activation parameters for the SmI_2-ammonia system with 25 equiv. of NH_3 and the activation parameters for the SmI_2-water system with 100 equiv. of H_2O are strikingly similar. Both systems proceed through highly ordered early transition states with free energies of activation of approximately 20 kcal/mol at 25 °C. This contrasts with the SmI_2-water system with 25 equiv. of H_2O, which displays a less ordered transition state with a higher enthalpic barrier to reaction and a concomitantly higher free energy of activation.

Table 5.3. Activation parameters for the reduction of acenaphthalene by SmI_2-water and SmI_2-ammonia[5]

entry	proton donor	NH_3 (25 equiv.)[a]	H_2O (25 equiv.)[a]	H_2O (100 equiv.)[a]
1	$\Delta H^{\ddagger}$ (kcal mol^{-1})[b]	1.1 ± 0.7	2.1 ± 0.4	7.3 ± 0.9
2	$\Delta S^{\ddagger}$ (cal $mol^{-1}K^{-1}$)[b]	-63 ± 2	-59 ± 1	-48 ± 3
3	$\Delta G^{\ddagger}$ (kcal mol^{-1})[c]	20 ± 1	19.9 ± 0.6	22 ± 1

[a]Conditions: 4 mM SmI_2 and 2 mM acenaphthalene in THF. The activation parameters are the averages of three independent experiments from 15 to 35 °C. [b]Obtained from $\ln(k_{obs}h/kT) - \Delta H^{\ddagger}/RT + \Delta S^{\ddagger}/R$ and errors are reported as ±σ. [c]Calculated from $\Delta G = \Delta H^{\ddagger} - T\Delta S^{\ddagger}$ and errors are reported as ±σ.

The similarity between the activation parameters for the SmI_2-ammonia and SmI_2-water systems at 25 and 100 equiv. of ammonia and water, respectively, is in good agreement with the similar coordination numbers for the two systems determined by BOMD simulations. The combination of these results suggests that at synthetically relevant concentrations of ammonia and water, the SmI_2-ammonia and SmI_2-water systems not only adopt similar structures in solution but also behave similarly in the presence of substrates. However, the impact of the greater affinity of Sm(II) for ammonia is evident from the greater concentration of water compared to ammonia in solution required for the SmI_2-water reagent to achieve the same reactivity as the SmI_2-ammonia reagent.

5.3.4 Thermodynamic Comparison of Coordination-Induced Bond Weakening in SmI_2-Ammonia and SmI_2-Water

The degree of bond weakening in ammonia and water upon coordination to Sm(II) was also investigated. Since both the SmI_2-ammonia and SmI_2-water systems were able to achieve approximately 50% reduction of *trans*-stilbene and were unreactive in the presence of more stable arenes, the BDFE of the C-H bond formed upon the initial PCET reduction of *trans*-stilbene was taken as an upper limit on the N-H and O-H BDFEs of ammonia and water bound to Sm(II). This comparison enabled the

determination of at least 61.5 kcal/mol of N-H bond weakening upon coordination of ammonia to Sm(II) as shown in Scheme 5.5. The same comparison for SmI_2-water in Scheme 5.6 shows the similar determination of at least 73.8 kcal/mol of O-H bond weakening upon coordination of water to Sm(II).

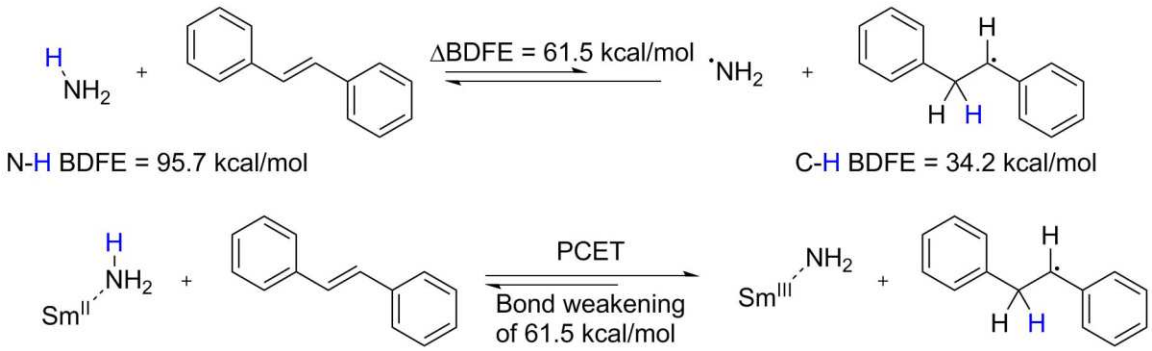

Scheme 5.5. Estimate of the degree of N-H bond-weakening upon coordination of ammonia to SmI_2 in THF[5]

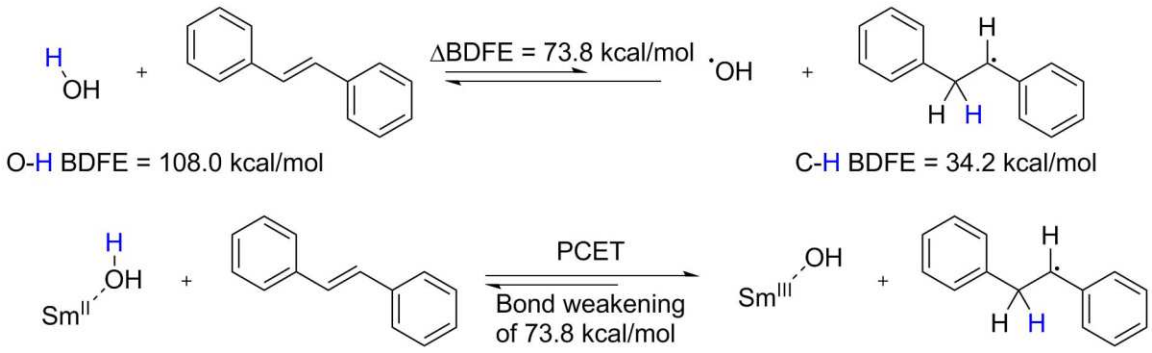

Scheme 5.6. Estimate of the degree of O-H bond-weakening upon coordination of water to SmI_2 in THF[5,19]

The determination of a greater degree of bond weakening in water compared to ammonia upon coordination to Sm(II) is consistent with other reports of bond weakening in ammonia (Figure 5.5) and water (Figure 5.6) upon coordination with low-valent metals.[20–27] This trend is in good agreement with our hypothesis that coordination-induced bond weakening is driven by backdonation from a low-valent metal into the X-H σ*-antibonding LUMO of the ligand. Since the HOMO-LUMO gap of water is greater than that of ammonia, population of the LUMO with electron density from a coordinating

low-valent metal is expected to induce a greater degree of bond destabilization in the O-H bond of water than in the N-H bond of ammonia.[28] A more thorough analysis of the relationship between ligand HOMO-LUMO gap and coordination-induced bond weakening is presented in Chapter 7.

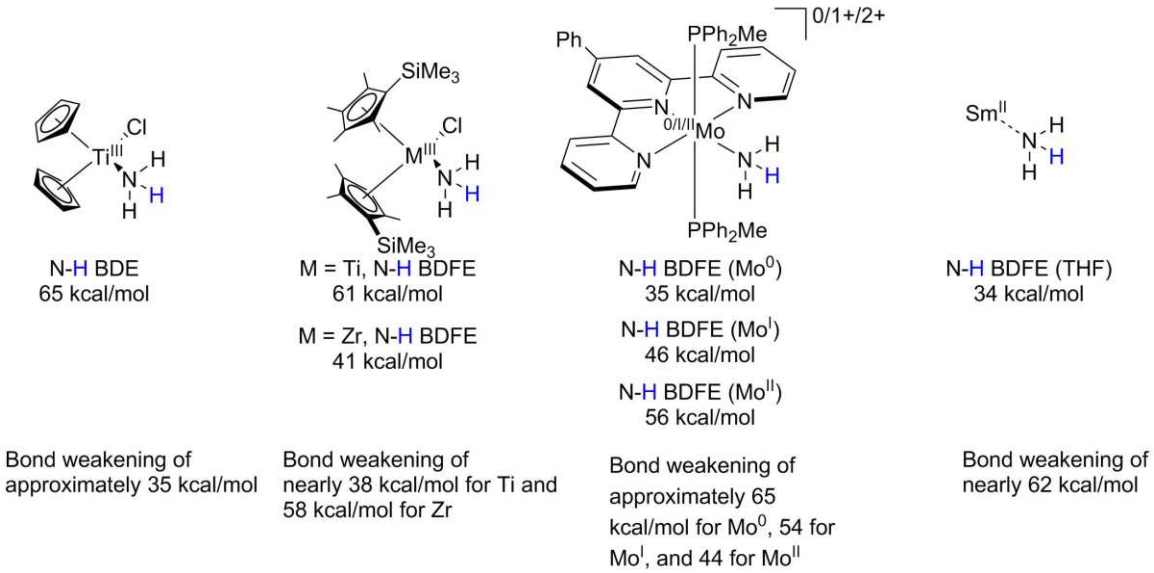

Figure 5.5. Examples of N-H bond weakening upon coordination to a low-valent metal[20–22]

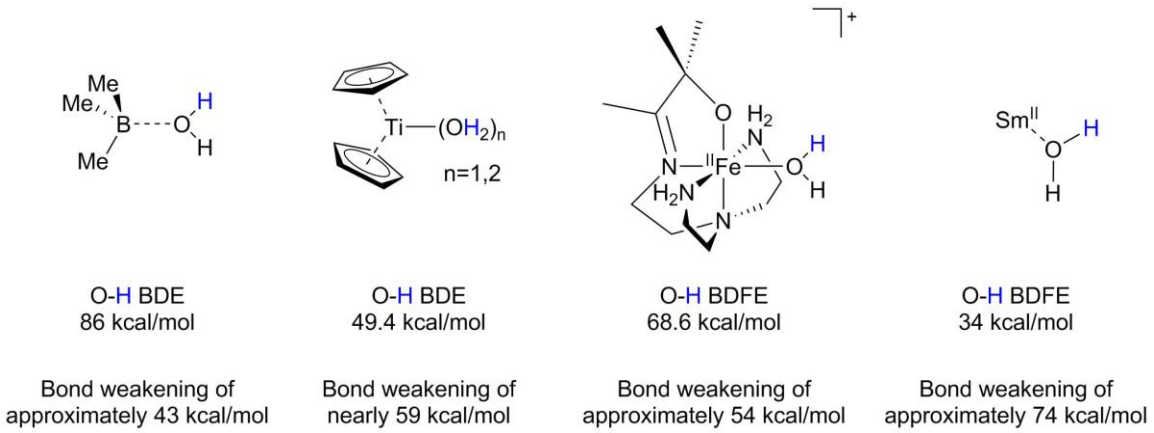

Figure 5.6. Examples of O-H bond weakening upon coordination to a low-valent metal[20,23–27]

Additionally, the nearly 62 kcal/mol of N-H bond weakening upon coordination of ammonia to Sm(II) represents the greatest degree of coordination-induced bond

weakening in any reagent utilizing ammonia as a proton source. Moreover, much like the SmI_2-water reagent, the SmI_2-ammonia reagent is remarkable for its ability to facilitate reductions of substrates despite its remarkably low 34 kcal/mol N-H BDFE, which is well below the 48 kcal/mol thermodynamic threshold for spontaneous H_2 gas evolution.[21,29–33]

5.4 Conclusions

The synthetic studies and thermodynamic calculations presented *vide supra* demonstrate that SmI_2-ammonia is a powerful PCET reductant capable of forming bonds as weak as 34 kcal/mol. This is enabled by an N-H bond weakening of nearly 62 kcal/mol upon coordination of ammonia to Sm(II), which is the greatest degree of bond weakening in ammonia reported to date.

Furthermore, the SmI_2-ammonia and SmI_2-water reagents were found to be remarkably similar at synthetically relevant concentrations. This similarity despite the greater steric bulk of ammonia was attributed to the greater affinity of Sm(II) for nitrogen compared to oxygen. The greater azaphilicity of Sm(II) was supported by greater shifts in the UV-Vis spectrum of SmI_2 with increasing concentrations of ammonia compared to water as well as by the greater average Sm-I distance observed in the simulated $SmI_2(NH_3)_{32}$ microsolvate compared to the $SmI_2(H_2O)_{32}$ microsolvate.

The high affinity of ammonia for Sm(II) and the similar reactivity of SmI_2-ammonia to SmI_2-water combined with the facile preparation of the SmI_2-ammonia reagent make it a potential alternative to SmI_2-water as a potent reductant in organic synthesis.

5.5 References

(1) Chciuk, T. V.; Anderson, W. R.; Flowers, R. A. High-Affinity Proton Donors Promote Proton-Coupled Electron Transfer by Samarium Diiodide. *Angew.*

Chemie Int. Ed. **2016**, *55* (20), 6033–6036.

(2) Ramírez-Solís, A.; Bartulovich, C. O.; León-Pimentel, C. I.; Saint-Martin, H.; Boekell, N. G.; Flowers, R. A. Proton Donor Effects on the Reactivity of SmI2. Experimental and Theoretical Studies on Methanol Solvation vs. Aqueous Solvation. *Dalt. Trans.* **2020**, *49* (23), 7897–7902.

(3) Chciuk, T. V; Li, A. M.; Vazquez-Lopez, A.; Anderson, W. R.; Flowers, R. A. Secondary Amides as Hydrogen Atom Transfer Promoters for Reactions of Samarium Diiodide. *Org. Lett.* **2016**, *19*, 290−293.

(4) Maity, S.; Flowers, R. A.; Hoz, S. Aza versus Oxophilicity of SmI2 : A Break of a Paradigm. *Chem. - A Eur. J.* **2017**, *23* (67), 17070–17077.

(5) Ramírez-Solís, A.; Boekell, N. G.; León-Pimentel, I.; Saint-Martin, H.; Bartulovich, C. O.; Flowers, R. A. Ammonia Solvation vs Aqueous Solvation of Samarium Diiodide. A Theoretical and Experimental Approach to Understanding Bond Activation Upon Coordination to Sm(II). *J. Org. Chem* **2022**, *87* (3), 1689–1697.

(6) *World Fertilizer Trends and Outlook to 2022*; Rome, 2019.

(7) Smith, C.; Hill, A. K.; Torrente-Murciano, L. Current and Future Role of Haber–Bosch Ammonia in a Carbon-Free Energy Landscape. *Energy Environ. Sci.* **2020**, *13* (2), 331–344.

(8) *Storage and Handling of Anhydrous Ammonia.* | *Occupational Safety and Health Administration*; United States of America.

(9) Valera-Medina, A.; Amer-Hatem, F.; Azad, A. K.; Dedoussi, I. C.; De Joannon, M.; Fernandes, R. X.; Glarborg, P.; Hashemi, H.; He, X.; Mashruk, S.; et al. Review on Ammonia as a Potential Fuel: From Synthesis to Economics. *Energy and Fuels* **2021**, *35* (9), 6964–7029.

(10) Dunn, P. L.; Cook, B. J.; Johnson, S. I.; Appel, A. M.; Bullock, R. M. Oxidation of Ammonia with Molecular Complexes. *J. Am. Chem. Soc.* **2020**, *142* (42), 17845–17858.

(11) Yun Zhao; Setzler, B. P.; Wang, J.; Nash, J.; Wang, T.; Xu, B.; Yan, Y. An Efficient Direct Ammonia Fuel Cell for Affordable Carbon-Neutral Transportation. *Joule* **2019**, *3*, 2472–2484.

(12) Bartulovich, C. O.; Flowers, R. A. Coordination-Induced O-H Bond Weakening in Sm(II)-Water Complexes. *Dalt. Trans.* **2019**, *48* (43), 16142–16147.

(13) Gaussian 09, Revision D.01, M. J. Frisch, G. W. Trucks, H. B. Schlegel, G. E. Scuseria, M. A. Robb, J. R. Cheeseman, G. Scalmani, V. Barone, B. Mennucci, G. A. Petersson, H. Nakatsuji, M. Caricato, X. Li, H. P. Hratchian, A. F. Izmaylov, J.

Bloino, G. Zheng, J. L. Sonnenberg, M. Hada, M. Ehara, K. Toyota, R. Fukuda, J. Hasegawa, M. Ishida, T. Nakajima, Y. Honda, O. Kitao, H. Nakai, T. Vreven, J. A. Montgomery, Jr., J. E. Peralta, F. Ogliaro, M. Bearpark, J. J. Heyd, E. Brothers, K. N. Kudin, V. N. Staroverov, T. Keith, R. Kobayashi, J. Normand, K. Raghavachari, A. Rendell, J. C. Burant, S. S. Iyengar, J. Tomasi, M. Cossi, N. Rega, J. M. Millam, M. Klene, J. E. Knox, J. B. Cross, V. Bakken, C. Adamo, J. Jaramillo, R. Gomperts, R. E. Stratmann, O. Yazyev, A. J. Austin, R. Cammi, C. Pomelli, J. W. Ochterski, R. L. Martin, K. Morokuma, V. G. Zakrzewski, G. A. Voth, P. Salvador, J. J. Dannenberg, S. Dapprich, A. D. Daniels, O. Farkas, J. B. Foresman, J. V. Ortiz, J. Cioslowski, and D. J. Fox, Gaussian, Inc., Wallingford CT, 2013

(14) Ramírez-Solís, A.; Amaro-Estrada, J. I.; Hernández-Cobos, J.; Maron, L.; México, M. Aqueous Solvation of SmI2 : A Born-Oppenheimer Molecular Dynamics Density Functional Theory Cluster Approach. *J. Phys. Chem. A* **2017**, *121*, 2293−2297.

(15) Christophe Raynaud, Laurent Maron, J.-P. D. and F. J. Reconsidering Car–Parrinello Molecular Dynamics Using Direct Propagation of Molecular Orbitals Developed upon Gaussian Type Atomic Orbitals. *Phys. Chem. Chem. Phys.* **2004**, 4226–4232.

(16) Bergner, A.; Dolg, M.; Küchle, W.; Stoll, H.; Preuß, H. Ab Initio Energy-Adjusted Pseudopotentials for Elements of Groups 13-17. *Mol. Phys.* **1993**, *80* (6), 1431–1441.

(17) Dolg, M.; Stoll, H.; Preuss, H.; Pitzer, R. M. Relativistic and Correlation Effects for Element 105 (Hahnium, Ha). A Comparative Study of M and MO (M = Nb, Ta, Ha) Using Energy-Adjusted Ab Initio Pseudopotentials. *J. Phys. Chem.* **1993**, *97* (22), 5852–5859.

(18) Ramirez-Solis, A.; Amaro-Estrada, J. I.; Hernández-Cobos, J.; Maron, L. Aqueous Solvation of SmI3: A Born-Oppenheimer Molecular Dynamics Density Functional Theory Cluster Approach. *Inorg. Chem.* **2018**, *57* (5), 2843–2850.

(19) Chciuk, T. V; Anderson, W. R.; Flowers, R. A. Reversibility of Ketone Reduction by SmI2-Water and Formation of Organosamarium Intermediates. *Organometallics* **2017**, *36*, 4579−4583.

(20) Paradas, M.; Campaña, A. G.; Jimé Nez, T.; Robles, R.; Oltra, J. E.; Buñ, E.; Justicia, J.; Cá, D. J.; Cuerva, J. M. Understanding the Exceptional Hydrogen-Atom Donor Characteristics of Water in TiIII-Mediated Free-Radical Chemistry. *J. Am. Chem. Soc.* **2010**, *132*, 12748–12756.

(21) Pappas, I.; Chirik, P. J. Ammonia Synthesis by Hydrogenolysis of Titanium-Nitrogen Bonds Using Proton Coupled Electron Transfer. *J. Am. Chem. Soc.* **2015**, *137* (10), 3498–3501.

(22) Bezdek, M. J.; Guo, S.; Chirik, P. J. Coordination-Induced Weakening of Ammonia, Water, and Hydrazine X–H Bonds in a Molybdenum Complex. *Science* **2016**, *354* (6313), 730–733.

(23) Spiegel, D. A.; Wiberg, K. B.; Schacherer, L. N.; Medeiros, M. R.; Wood, J. L. Deoxygenation of Alcohols Employing Water as the Hydrogen Atom Source. *J. Am. Chem. Soc.* **2005**, *127*, 12513–12515.

(24) Cuerva, J. M.; Campaña, A. G.; Justicia, J.; Rosales, A.; Oller-López, J. L.; Robles, R.; Cárdenas, D. J.; Buñuel, E.; Oltra, J. E. Water: The Ideal Hydrogen-Atom Source in Free-Radical Chemistry Mediated by TiIII and Other Single-Electron-Transfer Metals? *Angew. Chemie Int. Ed.* **2006**, *45* (33), 5522–5526.

(25) Gansäuer, A.; Behlendorf, M.; Cangönül, A.; Kube, C.; Cuerva, J. M.; Friedrich, J.; van Gastel, M. H2O Activation for Hydrogen-Atom Transfer: Correct Structures and Revised Mechanisms. *Angew. Chemie Int. Ed.* **2012**, *51* (13), 3266–3270.

(26) Rosales, A.; Rodríguez-García, I. Cp2TiCl/D2O/Mn, a Formidable Reagent for the Deuteration of Organic Compounds. *Beilstein J. Org. Chem.* **2016**, *12*, 1585–1589.

(27) Brines, L. M.; Coggins, M. K.; Chaau, P.; Poon, Y.; Toledo, S.; Kaminsky, W.; Kirk, M. L.; Kovacs, J. A. Water-Soluble Fe(II)−H2O Complex with a Weak O−H Bond Transfers a Hydrogen Atom via an Observable Monomeric Fe(III)−OH. *J. Am. Chem. Soc.* **2015**, *137*, 2253−2264.

(28) NIST Standard Reference Database Number 101. In *NIST Computational Chemistry Comparison and Benchmark Database*; Johnson III, R. D., Ed.

(29) Bezdek, M. J.; Pappas, I.; Chirik, P. J. *Nitrogen Fixation*; Nishibayashi, Y., Ed.; Topics in Organometallic Chemistry; Springer International Publishing: Cham, 2017.

(30) Pappas, I.; Chirik, P. J. Catalytic Proton Coupled Electron Transfer from Metal Hydrides to Titanocene Amides, Hydrazides and Imides: Determination of Thermodynamic Parameters Relevant to Nitrogen Fixation. *J. Am. Chem. Soc.* **2016**, *138*, 13379−13389.

(31) Karlin, K. D. *Progress in Inorganic Chemistry. Volume 58*; 2014.

(32) Stephan, G. C.; Sivasankar, C.; Studt, F.; Tuczek, F. Energetics and Mechanism of Ammonia Synthesis through the Chatt Cycle: Conditions for a Catalytic Mode and Comparison with the Schrock Cycle. *Chem. – A Eur. J.* **2008**, *14* (2), 644–652.

(33) Warren, J. J.; Tronic, T. A.; Mayer, J. M. The Thermochemistry of Proton-Coupled Electron Transfer Reagents and Its Implications. *Chem. Rev.* **2010**, *110* (12), 6961–7001.

Chapter 6. Studies of Coordination-Induced Bond Weakening in the Reductions of Substrates by $SmBr_2$-NMEA

6.1 Background and Significance

6.1.1 Coordination-Induced Bond Weakening in SmI_2-Proton Donor Reagents

The reduction of substrates by SmI_2-water through PCET has been attributed to significant weakening of the O-H bond of water upon coordination to Sm(II).[1,2] Given the reduction of arenes as challenging as *trans*-stilbene by SmI_2, an upper limit on the O-H bond strength of water coordinated to Sm(II) was placed at 34.1 kcal/mol. This reactivity enabled the determination of an O-H bond weakening of 73.9 kcal/mol upon coordination of water to Sm(II).[2]

The remarkably weak O-H bond of the Sm(II)-water complex has also been utilized in synthesis for the reductions of several challenging substrates. Work by Procter and coworkers demonstrated facile ring size-selective reduction of six-membered lactones by SmI_2-water as shown in Scheme 6.1.[3] Other carbonyl substrates that are typically recalcitrant to single electron reduction, including several derivatives of Meldrum's acid, were also found to be reduced under mild conditions by SmI_2-water.[4]

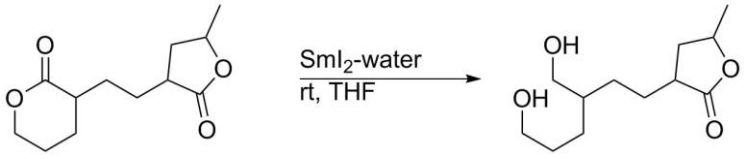

Scheme 6.1. Reaction scheme for the ring size-selective reduction of a six-membered lactone by SmI_2-water[3]

Work by Mayer and coworkers further extended the scope of SmI_2-water reductions to include a series of electron rich enamines under mild conditions.[5] This reactivity is remarkable since enamines are commonly oxidized in synthetic processes. Moreover, the reduction shown in Scheme 6.2 enabled the determination of at least 76

kcal/mol of O-H bond weakening upon coordination of water to Sm(II) based on literature data for the BDFE of the C-H bond formed upon the initial PCET reduction of a conjugated enamine. The resulting 32 kcal/mol O-H bond of the Sm(II)-water complex was noted by Mayer as being the weakest bond in a reagent reported to date that is stable enough to promote productive reductions.[5]

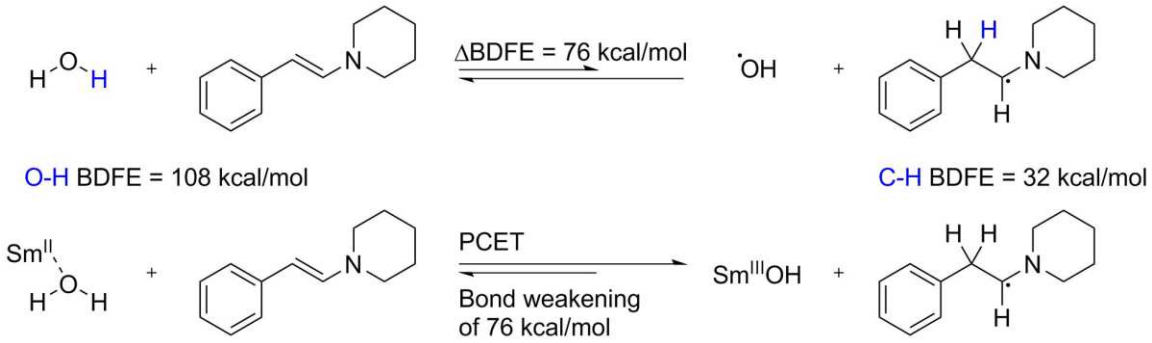

Scheme 6.2. Reaction scheme and bond strength comparison for the reduction of an enamine by SmI_2-water[5]

6.1.2 Chelating Proton Donors as Additives for Sm(II)

Following the discovery of PCET from SmI_2-water, water was thought to be unique as an additive for SmI_2. However, subsequent studies of SmI_2-proton donor systems revealed that Sm(II) reagents in combination with a number of other highly-coordinating proton donor ligands are capable of mediating PCET reductions.[6–8] The scope of PCET-promoting ligands includes high-affinity chelating alcohol ligands like ethylene glycol (EG) and diethylene glycol (DEG). Both the SmI_2-EG and SmI_2-DEG reagents were found to reduce anthracene as shown in Scheme 6.3, allowing for a determination of O-H BDFEs of nearly 36.5 kcal/mol in both complexes, concomitant with approximately 50 kcal/mol of bond weakening for both alcohols upon coordination to Sm(II).[8]

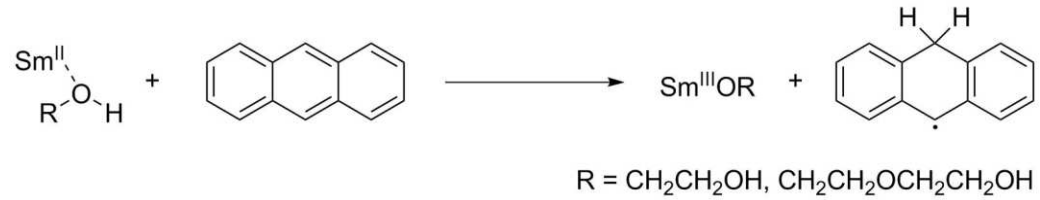

Scheme 6.3. Reaction scheme for the initial PCET reduction of anthracene by SmI_2-EG and SmI_2-DEG[8]

6.1.3 Comparison of Azaphilicity and Oxophilicity in Sm(II)

The affinity of water and alcohols as additives for Sm(II) is a consequence of the oxophilicity of Sm(II) reagents. The affinity of Sm(II) for oxygen is also utilized in synthesis, wherein Sm(II) reagents are commonly employed in the reduction of carbonyl-containing substrates.[9] However, recent advances in the scope of Sm(II)-mediated reductions have included several challenging nitrogen-containing substrates. Examples of this can be found in Mayer's reduction of enamines by SmI_2-water as well as in the reduction of nitrogen gas by SmI_2-water in conjunction with a molybdenum nitrogen-binding catalyst by Nishibayashi and coworkers.[5,10] Moreover, nitrogen-containing ligands like ammonia and 2-pyrrolidinone have recently been utilized as additives for SmI_2 to form potent PCET reductants.[7,11] A study by Hoz and Flowers provides context for these Sm(II)-nitrogen interactions by highlighting the significant affinity of Sm(II) for nitrogen, which was found to be even greater than the affinity of Sm(II) for oxygen.[12]

The comparison between the affinity of Sm(II) for nitrogen and oxygen was made by observing the change in the UV-Vis spectrum of SmI_2 in the presence of increasing concentrations of oxygen- and nitrogen-containing ligands.[12] As shown in Figures 6.1-6.3, the substitution of alcohol functional groups in EG with amines in ethanolamine (EA) or ethylenediamine (EDA) induces a significantly greater shift in the UV-Vis spectrum of SmI_2 at equivalent ligand concentrations for each alcohol replaced. These

results are consistent with a significantly greater affinity of Sm(II) for nitrogen compared to oxygen.[12]

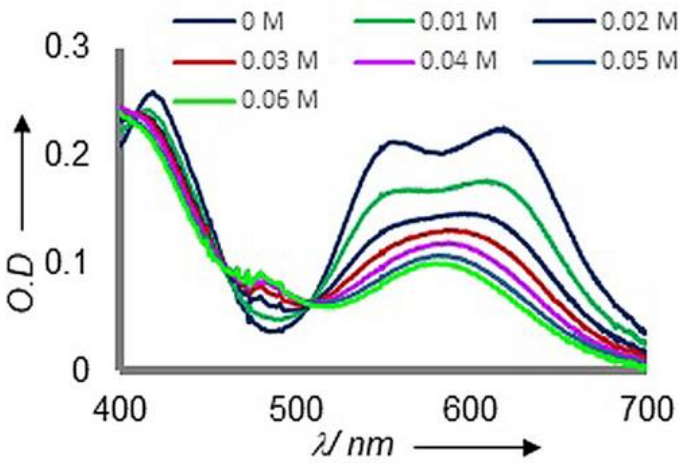

Figure 6.1. UV-Vis spectra of SmI_2 in the presence of 0-0.06 M of EG[12]

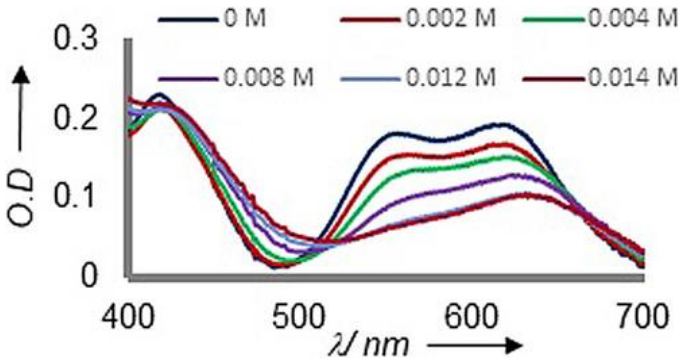

Figure 6.2. UV-Vis spectra of SmI_2 in the presence of 0-0.014 M of EA[12]

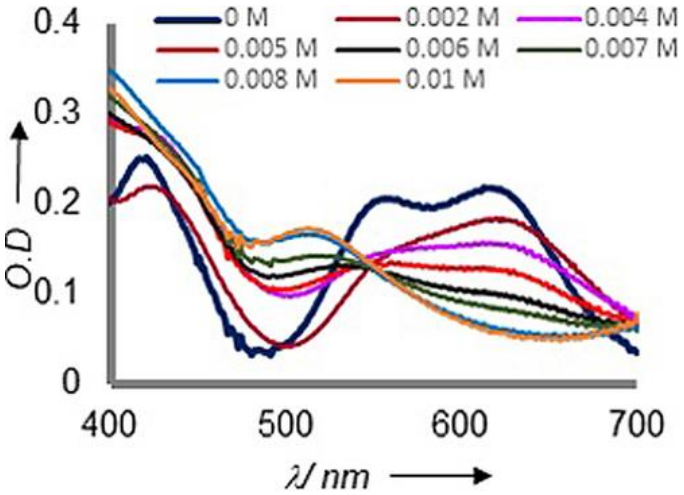

Figure 6.3. UV-Vis spectra of SmI_2 in the presence of 0-0.01 M of EDA[12]

The effect of the greater affinity of Sm(II) for nitrogen on coordination-induced bond weakening can be seen in the thermodynamic cycle in Scheme 6.4, which relates the affinity of a ligand for Sm(II) to the degree of bond weakening induced upon ligand coordination to Sm(II).[8] The relationship between metal-ligand affinity and coordination-induced bond weakening is consistent with the characterization of SmI_2-ammonia as a potent PCET reductant as described in Chapter 5.[11] Moreover, this relationship suggests that other high-affinity nitrogen-containing ligands should also be capable of promoting challenging PCET reductions as additives for Sm(II).

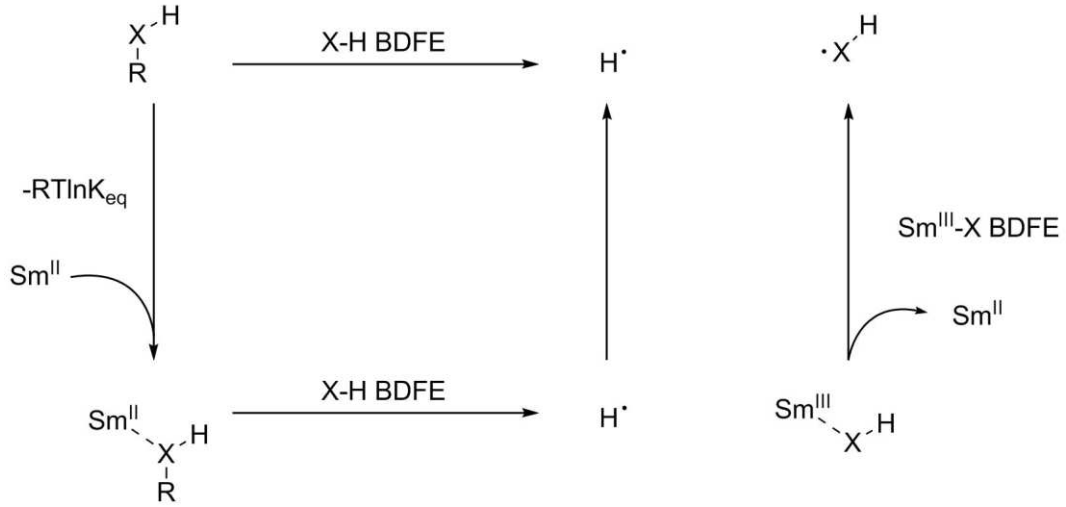

Scheme 6.4. Thermodynamic cycle for hydrogen atom loss from a free and Sm(II)-bound protic ligand[8]

6.1.4 Ethanolamines as Proton Donor Additives for Sm(II)

6.1.4.1 *N*,*N*-Dimethylethanolamine as a Proton Donor Additive for Sm(II)

In addition to the ability of amines and water individually to form powerful PCET reductants with SmI_2, work by Hilmersson has demonstrated that the combination of SmI_2 with both water and an aprotic amine produces powerful reductants. These SmI_2-water-amine reductants have been shown to facilitate the reduction of a wide range of

challenging substrates such as the reduction of an unactivated imine by SmI_2-water-PMDTA (PMDTA = *N*,*N*′,*N*″,*N*″-pentamethyldiethylenetriamine) shown in Scheme 6.5.[13–22]

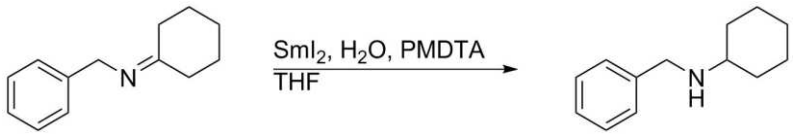

Scheme 6.5. Reaction scheme for the reduction of an unactivated imine by SmI_2-water-PMDTA[13]

As an additive for SmI_2, *N*,*N*-dimethylethanolamine (DMEA) fills the roles of both an alcohol an aprotic amine. Moreover, the ability of DMEA to chelate Sm(II) provides a high degree of kinetic metal-ligand affinity, which promotes the formation of a potent Sm(II)-DMEA reducing system at relatively low DMEA concentrations. Under conditions of as few as two equivalents of DMEA to SmI_2, the Sm(II)-DMEA system has been demonstrated to facilitate the reductive ring opening of a series of N-tosylated aziridines as shown in Scheme 6.6.[23] Further addition of hexamethylphosphoramide (HMPA) to the SmI_2-DMEA reagent has been shown to enable the regioselective reductive ring opening of α,β-epoxy esters as shown in Scheme 6.7.[24]

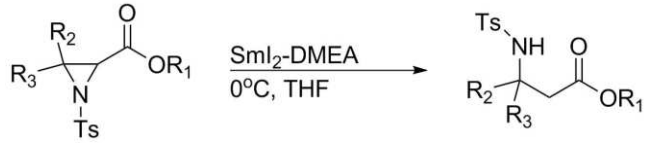

Scheme 6.6. Reaction scheme for the reductive ring opening of an N-tosylated aziridine by SmI_2-DMEA[23]

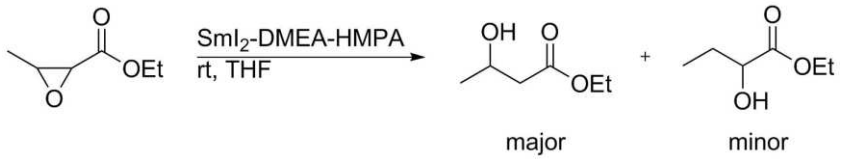

Scheme 6.7. Reaction scheme for the regioselective reductive ring opening of an α,β-epoxy ester[24]

6.1.4.2 *N*-Methylethanolamine as a Proton Donor Additive for Sm(II)

The steric bulk of proton donor additives has been observed to have a significant impact on the reducing power of the resulting Sm(II)-proton donor complex. This paradigm is demonstrated by the difference in concentration of water and methanol required to induce PCET reactivity in the Sm(II)-water and Sm(II)-methanol reductants.[6] A similar enhancement in reactivity is observed upon substitution of DMEA for *N*-methylethanolamine (NMEA) as an additive for SmI_2. While SmI_2-DMEA is able to facilitate the reduction of arenes no more challenging than anthracene, SmI_2-NMEA has been shown to quantitatively reduce *trans*-stilbene.[12] Moreover, SmI_2-NMEA is able to facilitate the approximately 50% reduction of phenanthrene, enabling the determination of an O-H BDFE of at most 25.3 kcal/mol for the Sm(II)-NMEA complex, concomitant with bond weakening of approximately 65.1 kcal/mol upon coordination of NMEA to Sm(II) as shown in Scheme 6.8.

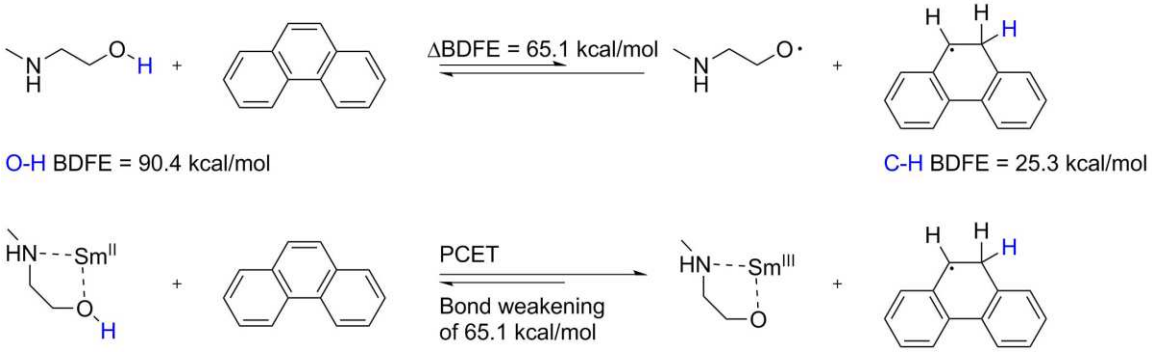

Scheme 6.8. Reaction scheme and bond strength comparison for the reduction of phenanthrene by SmI_2-NMEA[12]

6.2 Experimental Details

6.2.1 Materials

Samarium powder was purchased from Acros Organics. Samarium diiodide was generated by the standard method of samarium metal combined with iodine in THF and

allowed to stir for at least 4 hours. Iodometric titrations were then performed to verify concentration of SmI_2 for use. Tetrahydrofuran was purified by a solvent purification system (Innovative Technology Inc.; MA). Substrates and additives were purchased from Alfa Aesar and Tokyo Chemical International and used without further purification. Liquid substrates were deoxygenated by bubbling with argon gas prior to use.

6.2.2 Instrumentation

^1H NMR and ^{13}C $\{^1H\}$ NMR spectra were recorded in $CDCl_3$ on a Bruker 400 MHz spectrometer at 400 and 125 MHz respectively. The ^1H NMR chemical shifts are given as δ values in ppm relative to TMS (0 ppm) as the internal reference. The $^{13}C\{1H\}$ NMR shifts are expressed with respect to the $CDCl_3$ (77.0 ppm). GCMS analyses were performed with a Shimadzu GCMS-QP2010 Ultra. GC analyses were performed using a Shimadzu Gas Chromatograph GC-2010 Plus with biphenyl as an internal standard. UV-Visible spectra experiments were performed with a computer-controlled SX.18 MV stopped-flow spectrophotometer (Applied Photophysics Ltd. Surrey, UK). Solutions were prepared under a dry argon atmosphere in flame dried glassware.

6.2.3 Methods

6.2.3.1 Procedure for Preparation of $SmBr_2$

SmI_2 was generated by the standard method of samarium metal combined with iodine in THF and allowed to stir for at least 4 hours. The solution of SmI_2 was then allowed to settle and the supernatant was withdrawn and added to a flame dried vial equipped with a magnetic stir bar. This solution was further charged with four equivalents of either tetrabutylammonium bromide (TBABr) or LiBr and allowed to stir

for 15 minutes until the solution was observed to change color from the characteristic blue of SmI_2 to the deep purple of samarium dibromide ($SmBr_2$).

6.2.3.2 General Procedure for Reductions of Substrates by $SmBr_2$-NMEA

Substrate (0.33 mmol arenes, 0.2 mmol esters, 0.33 mmol alkynes, 0.33 mmol N-containing substrates) was added to a 10 mL solution of 0.1 M $SmBr_2$ in a flame dried vial equipped with a magnetic stir bar under an argon atmosphere. Under stirring, NMEA (15 mmol, 1.2 mL) was added to the solution, which was allowed to react until discoloration of the characteristic purple of $SmBr_2$ was observed.

6.2.3.2.1 Procedure for Reductions of Arenes by $SmBr_2$-NMEA

Substrate (0.33 mmol, 0.059 g *trans*-stilbene, 0.042 g naphthalene, 0.052 g 1-methoxynaphthalene, 0.048 g 1-fluoronaphthalene, 0.051 g biphenyl) was added to a 10 mL solution of 0.1 M $SmBr_2$ in a flame dried vial equipped with a magnetic stir bar under an argon atmosphere. Under stirring, NMEA (15 mmol, 1.2 mL) was added to the solution, which was allowed to react until discoloration of the characteristic purple of $SmBr_2$ was observed. The solution was then quenched in air followed by 0.1 M HCl. The aqueous layer was extracted three times with diethyl ether. The organic layers were then combined and washed with deionized water, sodium thiosulfate, and brine before being dried over magnesium sulfate and concentrated under reduced pressure.

6.2.3.2.2 Procedure for Reductions of Esters by $SmBr_2$-NMEA

Substrate (0.2 mmol, 0.033 g hydrocinnamic methyl ester, 0.037 g methyl 2-allylhex-5-enoate, 0.044 g methyl 2-benzylhex-5-enoate, 0.046 g methyl 2-(3-methylbenzyl)hex-5-enoate, 0.050 g methyl 2-(3-methoxybenzyl)hex-5-enoate) was added to a 10 mL solution of 0.1 M $SmBr_2$ in a flame dried vial equipped with a magnetic

stir bar under an argon atmosphere. Under stirring, NMEA (15 mmol, 1.2 mL) was added to the solution, which was allowed to react until discoloration of the characteristic purple of $SmBr_2$ was observed. The solution was then quenched in air followed by 0.1 M HCl. The aqueous layer was extracted three times with diethyl ether. The organic layers were then combined and washed with deionized water, sodium thiosulfate, and brine before being dried over magnesium sulfate and concentrated under reduced pressure.

6.2.3.2.3 Procedure for Reductions of Alkynes by $SmBr_2$-NMEA

Substrate (0.33 mmol, 60 mL 5-decyne, 58 mL 4-decyne, 48 mL 4-octyne, 69 mL 6-dodecyne) was added to a 10 mL solution of 0.1 M $SmBr_2$ in a flame dried vial equipped with a magnetic stir bar under an argon atmosphere. Under stirring, NMEA (15 mmol, 1.2 mL) was added to the solution, which was allowed to react until discoloration of the characteristic purple of $SmBr_2$ was observed. The solution was then quenched in air followed by 0.1 M HCl. The aqueous layer was extracted three times with diethyl ether. The organic layers were then combined and washed with deionized water, sodium thiosulfate, and brine before being dried over magnesium sulfate and concentrated under reduced pressure.

6.2.3.2.4 Procedure for Reductions of N-Containing Substrates by $SmBr_2$-NMEA

Substrate (0.33 mmol, 0.052 g azobenzene, 0.036 g phenylhydrazine) was added to a 10 mL solution of 0.1 M $SmBr_2$ in a flame dried vial equipped with a magnetic stir bar under an argon atmosphere. Under stirring, NMEA (15 mmol, 1.2 mL) was added to the solution, which was allowed to react until discoloration of the characteristic purple of $SmBr_2$ was observed. The solution was quenched in air followed by 0.2 M aqueous NaOH. The organic layer was extracted three times with diethyl ether. The organic

layers were then combined and dried over magnesium sulfate and concentrated under reduced pressure.

6.2.3.2.5 Procedure for GCMS Yields of Reductions by $SmBr_2$-NMEA

Substrate (0.33 mmol arenes, 0.2 mmol esters, 0.33 mmol alkynes, 0.33 mmol N-containing substrates) was added to a 10 mL solution of 0.1 M $SmBr_2$ in a flame dried vial equipped with a magnetic stir bar under an argon atmosphere. Under stirring, NMEA (15 mmol, 1.2 mL) was added to the solution, which was allowed to react until discoloration of the characteristic purple of $SmBr_2$ was observed. Quenching of the solution was followed by the addition of biphenyl (0.33 mmol, 0.051 g for arenes, alkynes, and N-containing substrates; 0.031 g for esters). The solution was then extracted into diethyl ether and dried over magnesium sulfate. The dry solution was then analyzed by GCMS.

6.2.3.2.6 Procedure for Isolation of Products of Reductions by $SmBr_2$-NMEA

1,4-dihydronaphthalene was extracted with diethyl ether and dried over magnesium sulfate. The combined organic layers were washed with water, saturated aqueous sodium thiosulfate, and brine. The resulting solution was dried over magnesium sulfate then concentrated under reduced pressure and characterized by ^1H (400 MHz, $CDCl_3$) δ (ppm): 3.39 (d, 4H), 5.91 (m, 2H), 7.14 (m, 4H);^{13}C NMR (100 MHz, $CDCl_3$) δ (ppm): 29.76, 124.77, 125.90, 128.46, 134.20

1,4-dihydro-5-methoxynaphthalene was extracted with diethyl ether and dried over magnesium sulfate. The combined organic layers were washed with water, saturated aqueous sodium thiosulfate, and brine. The resulting solution was dried over magnesium sulfate then concentrated under reduced pressure and characterized by ^1H (400 MHz,

$CDCl_3$) δ (ppm): 3.30 (m, 2H), 3.43 (m, 2H), 3.83 (s, 3H), 5.92 (m, 2H), 6.70 (d, 1H), 6.75 (d, 1H), 7.15 (m, 1H);^{13}C NMR (100 MHz, $CDCl_3$) δ (ppm): 24.28, 29.60, 55.32, 107.12, 120.72, 123.91, 125.23, 126.48, 134.55, 157.01

1,4-dihydro-5-fluoronaphthalene was extracted with diethyl ether and dried over magnesium sulfate. The combined organic layers were washed with water, saturated aqueous sodium thiosulfate, and brine. The resulting solution was dried over magnesium sulfate then concentrated under reduced pressure and characterized by ^{1}H (400 MHz, $CDCl_3$) δ (ppm): 3.22 (s, 4H), 5.98 (m, 2H), 7.14 (d, 1H), 7.32 (m, 1H), 7.60 (m, 1H);^{13}C NMR (100 MHz, $CDCl_3$) δ (ppm): 23.80, 30.60, 112.40, 125.40, 125.40, 127.20, 137.90, 161.40

Cis-5-decene was extracted with diethyl ether and dried over magnesium sulfate. The combined organic layers were washed with water, saturated aqueous sodium thiosulfate, and brine. The resulting solution was dried over magnesium sulfate then concentrated under reduced pressure and characterized by ^{1}H (400 MHz, $CDCl_3$) δ (ppm): 0.87-0.93 (m, 6H), 1.25-1.51 (m, 8H), 1.95-2.08 (m, 4H), 5.33-5.37 (m, 2H);^{13}C NMR (100 MHz, $CDCl_3$) δ (ppm): 14.15, 22.50, 27.05, 32.12, 129.99

Cis-4-decene was extracted with diethyl ether and dried over magnesium sulfate. The combined organic layers were washed with water, saturated aqueous sodium thiosulfate, and brine. The resulting solution was dried over magnesium sulfate then concentrated under reduced pressure and characterized by ^{1}H (400 MHz, $CDCl_3$) δ (ppm): 0.85-0.93 (m, 3H), 0.96 (t, 3H), 1.23-1.40 (m, 6H), 1.44-1.53 (m, 2H), 1.96-2.05 (m, 4H), 5.33-5.38 (m, 2H);^{13}C NMR (100 MHz, $CDCl_3$) δ (ppm): 14.15, 14.21, 22.73, 23.04, 27.32, 29.42, 29.60, 31.67, 129.75, 130.24

Cis-6-dodecene was extracted with diethyl ether. The combined organic layers were washed with water, saturated aqueous sodium thiosulfate, and brine. The resulting solution was dried over magnesium sulfate then concentrated under reduced pressure and characterized by ^{1}H (400 MHz, $CDCl_3$) δ (ppm): 0.85-0.94 (m, 6H), 1.22-1.40 (m, 12H), 2.02 (q, 4H), 5.34- 5.37 (m, 2H);^{13}C NMR (100 MHz, $CDCl_3$) δ (ppm): 14.23, 22.75, 27.33, 29.62, 31.69, 130.05

2-allyl-5-methylcyclopentan-1-ol was extracted with diethyl ether. The combined organic layers were washed with water, saturated aqueous sodium thiosulfate, and brine. The resulting solution was dried over magnesium sulfate then concentrated under reduced pressure and characterized by ^{1}H (400 MHz, $CDCl_3$) δ (ppm): 0.98 (d, 3H), 1.05-1.50 (m, 4H), 2.03-2.13 (m, 1H), 2.24-2.33 (m, 1H), 4.96-5.11 (m, 2H), 5.79-5.91 (m, 1H);^{13}C NMR (100 MHz, $CDCl_3$) δ (ppm): 14.00, 29.02, 30.83, 37.84, 39.08, 46.70, 115.69, 137.78

2-benzyl-5-methylcyclopentan-1-ol was extracted with diethyl ether. The combined organic layers were washed with water, saturated aqueous sodium thiosulfate, and brine. The resulting solution was dried over magnesium sulfate then concentrated under reduced pressure and characterized by ^{1}H (400 MHz, $CDCl_3$) δ (ppm): 0.99 (d, 3H), 1.40-1.56 (m, 3H), 1.94-2.27 (m, 3H), 2.63 (dd, 1H), 2.90 (dd, 1H), 3.69 (dd, 1H), 7.18-7.34 (m, 5H);^{13}C NMR (100 MHz, $CDCl_3$) δ (ppm): 19.96, 29.13, 31.07, 35.53, 42.43, 45.21, 81.05, 125.86, 128.45, 128.89, 142.02

2-methyl-5-(3-methylbenzyl)cyclopentan-1-ol was extracted with diethyl ether. The combined organic layers were washed with water, saturated aqueous sodium thiosulfate, and brine. The resulting solution was dried over magnesium sulfate then

concentrated under reduced pressure and characterized by ^{1}H (400 MHz, $CDCl_3$) δ (ppm): 1.02 (d, 3H), 1.39-1.48 (m, 1H), 1.50-1.61 (m, 1H), 1.72-1.82 (m, 2H), 1.89-2.00 (m, 1H), 2.11-2.21 (m, 1H), 2.34 (s, 3H), 2.65 (dd, 1H), 2.83 (dd, 1H), 3.75 (t, 1H), 6.99-7.08 (m, 3H), 7.18 (t, 1H);^{13}C NMR (100 MHz, $CDCl_3$) δ (ppm): 14.50, 21.60, 28.90, 30.00, 36.30, 36.90, 47.90, 125.90, 126.60, 128.40, 129.70, 138.00, 142.10

2-methyl-5-(3-methoxybenzyl)cyclopentan-1-ol was extracted with diethyl ether. The combined organic layers were washed with water, saturated aqueous sodium thiosulfate, and brine. The resulting solution was dried over magnesium sulfate then concentrated under reduced pressure and characterized by ^{1}H (400 MHz, $CDCl_3$) δ (ppm): 1.00 (d, 3H), 1.04-1.26 (m, 1H), 1.31-1.56 (m, 1H), 1.66, 1.94 (m, 3H), 1.94-2.11 m, 2H), 2.11-2.24 (m, 1H), 2.59 (dd, 1H), 2.88 (dd, 1H), 3.69 (dd, 1H), 6.73- 6.86 (m, 3H), 7.21 (td, 1H);^{13}C NMR (100 MHz, $CDCl_3$) δ (ppm): 14.23, 19.98, 29.07, 30.77, 42.39, 45.16, 55.27, 80.11, 110.99, 114.74, 121.35, 129.44, 143.75, 159.73

3-phenylpropan-1-ol was extracted with diethyl ether. The combined organic layers were washed with water, saturated aqueous sodium thiosulfate, and brine. The resulting solution was dried over magnesium sulfate then concentrated under reduced pressure and characterized by ^{1}H (400 MHz, $CDCl_3$) δ (ppm): 1.91 (p, 1H), 2.66 (t, 1H), 2.73 (t, 1H), 2.97 (t, 1H), 3.69 (t, 2H), 7.18-7.34 (m, 5H)

1,2-diphenylhydrazine was extracted with diethyl ether. The combined organic layers were washed with 2 M NaOH. The resulting solution was dried over magnesium sulfate then concentrated under reduced pressure and characterized by ^{1}H (400 MHz, $CDCl_3$) δ (ppm): 6.69-6.80 (m, 6H), 7.34-7.39 (m, 4H)

Aniline was extracted with diethyl ether. The combined organic layers were washed with 2 M NaOH. The resulting solution was dried over magnesium sulfate then concentrated under reduced pressure and characterized by ^{1}H (400 MHz, $CDCl_3$) δ (ppm): 6.66-6.95 (m, 3H), 7.12-7.25 (m, 2H)

Decane-1,5-diol was extracted with diethyl ether. The combined organic layers were washed with water, saturated aqueous sodium thiosulfate, and brine. The resulting solution was dried over magnesium sulfate then concentrated under reduced pressure and characterized by ^{1}H (400 MHz, $CDCl_3$) δ (ppm): 0.90 (t, 3H), 1.23-1.67 (m, 14H), 3.56-3.63 (m, 1H), 3.65 (t, 2H)

Hexane-1,6-diol was extracted with diethyl ether. The resulting solution was dried over magnesium sulfate then concentrated under reduced pressure and characterized by ^{1}H (400 MHz, $CDCl_3$) δ (ppm): 1.22-1.36 (m, 4H), 1.47-1.63 (m, 4H), 3.95 (t, 4H)

Heptane-1,4-diol was extracted with diethyl ether. The combined organic layers were washed with water, saturated aqueous sodium thiosulfate, and brine. The resulting solution was dried over magnesium sulfate then concentrated under reduced pressure and characterized by ^{1}H (400 MHz, $CDCl_3$) δ (ppm): 0.96 (t, 3H), 1.25-1.78 (m, 8H), 6.34-3.78 (m, 3H)

6.2.3.3 Procedure for Stopped Flow Kinetics Studies

Kinetic experiments were performed with a computer-controlled SX.18 MV stopped- flow spectrophotometer (Applied Photophysics Ltd. Surrey, UK). Solutions were injected separately into the stopped-flow system using airtight, capped BD syringes prepared in a glove box under argon atmosphere. Between each experiment, the cell block was washed with dilute HNO_3 (1x), Deionized H_2O (1x), and THF (3x) before

additional anhydrous deoxygenated THF washes (3x). The reaction rates were determined from the decay of $SmBr_2$ at 540 nm. Kinetic measurements were carried out at 25°C unless otherwise specified.

6.3 Results and Discussion

6.3.1 Optimization of an Electron Rich Sm(II)-Chelating Proton Donor System

Given that ligand affinity for Sm(II) can be used to tune the reducing power of Sm(II)-proton donor reductants, a series of Sm(II)-chelating proton donor systems were investigated for their stability and metal-ligand affinity. Several electron rich Sm(II) reagents; $SmBr_2$, samarium dichloride ($SmCl_2$), decamethyl samarocene ($SmCp^*_2$), and samarium *bis*-hexamethyldisilazane ($Sm(HMDS)_2$) were selected for this study. Each of these Sm(II) reagents was combined with 15 equivalents of either EG or EA under an argon atmosphere. The resulting solutions were monitored over 10 minutes with a pressure sensor to track the rate of hydrogen gas evolution. The combination of $SmBr_2$ and EA proved to be the most stable against H_2 evolution, with the remaining combinations evolving hydrogen gas too rapidly to enable their use in synthesis.

To further optimize the stability and reducing power of the $SmBr_2$-chelating proton donor system, $SmBr_2$-EA was compared to $SmBr_2$-NMEA and $SmBr_2$-DMEA. This comparison was made by observing the rate of hydrogen gas evolution from each system as well as by observing the shift in the UV-Vis spectrum of $SmBr_2$ with increasing [ligand]. The resulting UV-Vis spectra are shown in Figures 6.4-6.6. The results of these experiments were consistent with EA having the greatest affinity for $SmBr_2$ and DMEA having both the lowest affinity for $SmBr_2$. Concomitantly, the $SmBr_2$-EA reagent exhibited the greatest rate of H_2 gas evolution while the $SmBr_2$-

DMEA reagent exhibited the slowest. However, while NMEA displayed a much greater affinity for $SmBr_2$ than did DMEA, $SmBr_2$-NMEA was found to be only slightly less stable against H_2 gas evolution than $SmBr_2$-DMEA. The $SmBr_2$-NMEA system was therefore chosen for further synthetic and kinetic studies.

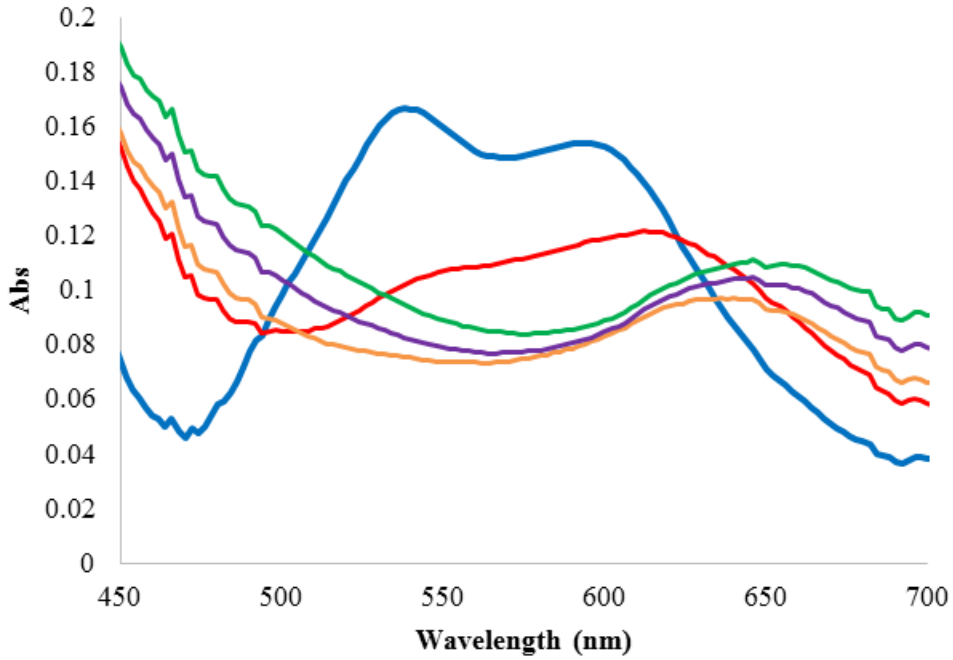

Figure 6.4. UV-Vis spectrum of $SmBr_2$ in the presence of increasing [EA] (0 eq blue, 5 eq red, 10 eq orange, 15 eq purple, 20 eq green)

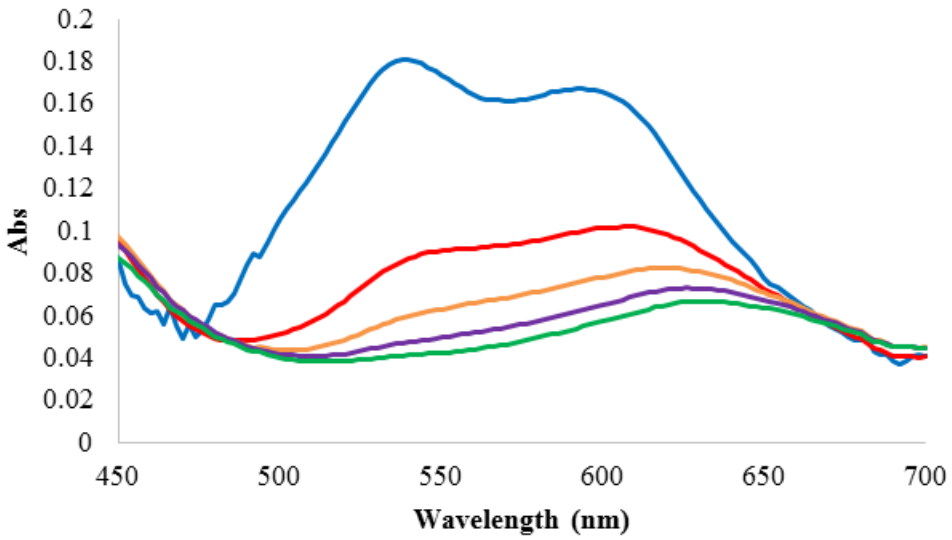

Figure 6.5. UV-Vis spectrum of $SmBr_2$ in the presence of increasing [NMEA] (0 eq blue, 5 eq red, 10 eq orange, 15 eq purple, 20 eq green)

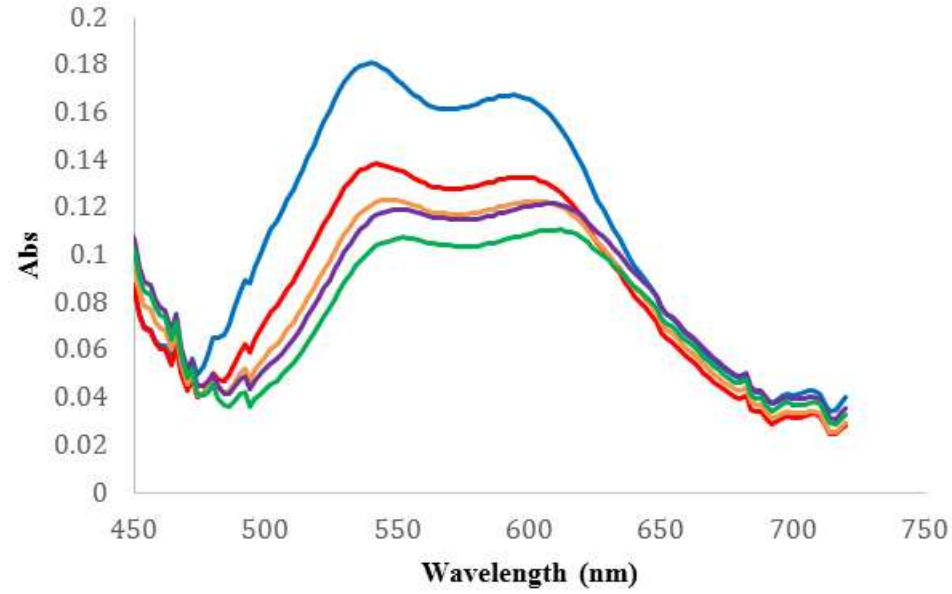

Figure 6.6. UV-Vis spectrum of $SmBr_2$ in the presence of increasing [DMEA] (0 eq blue, 5 eq red, 10 eq orange, 15 eq purple, 20 eq green)

6.3.2 Synthetic Investigations of the Scope of Reductions by $SmBr_2$-NMEA

A series of arenes, shown in Scheme 6.9, that form progressively weaker C-H bonds upon initial PCET reduction were chosen as preliminary substrates for reduction by $SmBr_2$-NMEA. Among these arenes, naphthalene and biphenyl are

exceptionally recalcitrant to single electron reduction. The successful reduction of these substrates by $SmBr_2$-NMEA is remarkable given the mild conditions under which they proceeded since these reductions are commonly achieved under conditions of a Birch reduction using lithium metal in liquid ammonia.[25]

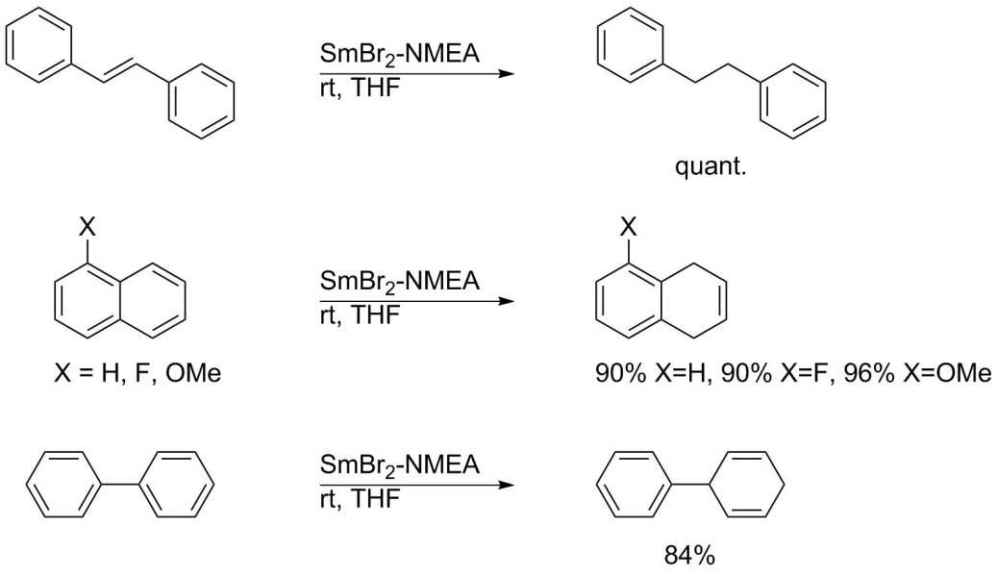

Scheme 6.9. Reaction schemes for the reduction of *trans*-stilbene, naphthalene, 1-fluoronaphthalene, 1-methoxynaphthalene, and biphenyl by $SmBr_2$-NMEA

With the effective Birch reduction of several challenging reductions by $SmBr_2$-NMEA in hand, the reductions of other challenging substrates were investigated. Several alkynes, shown in Scheme 6.10, were found to be readily reduced by $SmBr_2$-NMEA, furnishing primarily the corresponding *cis*-alkenes with small quantities of the corresponding alkanes.

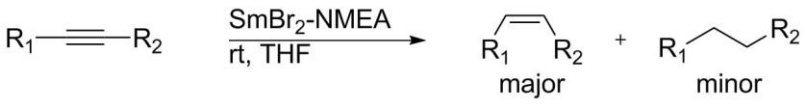

$R_1 = CH_3CH_2CH_2CH_2$ $R_2 = CH_3CH_2CH_2CH_2$	88%
$R_1 = CH_3CH_2CH_2$ $R_2 = CH_3CH_2CH_2CH_2CH_2$	82%
$R_1 = CH_3CH_2CH_2CH_2CH_2$ $R_2 = CH_3CH_2CH_2CH_2CH_2$	92%

Scheme 6.10. Reduction scheme and scope for the reduction of alkynes by $SmBr_2$-NMEA with associated yields of *cis*-alkene products

A series of unactivated esters, including lactones, were next examined as substrates for reduction by $SmBr_2$-NMEA. These substrates, shown in Scheme 6.11, include several that are commonly recalcitrant to reduction even by other powerful Sm(II) reductants.[3] Remarkably, each of these substrates was reduced quantitatively by $SmBr_2$-NMEA.

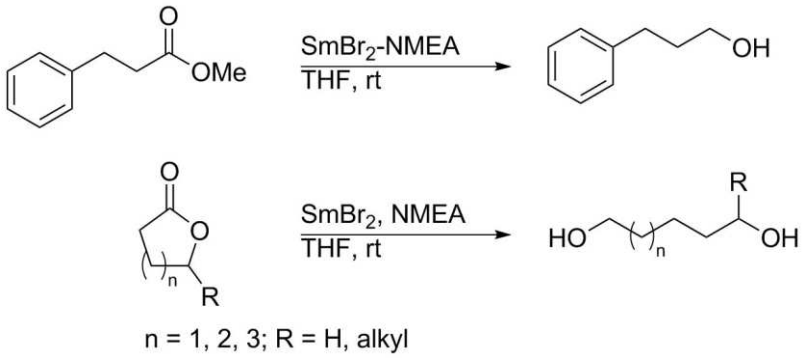

Scheme 6.11. Reaction scheme for the reduction of unactivated esters and lactones by $SmBr_2$-NMEA

Previous investigations of the reduction of esters by Sm(II) reductants revealed the presence of a C-centered ketyl radical intermediate as shown in Scheme 6.12.[26] It was reasoned that if the reduction of esters by $SmBr_2$-NMEA proceeds through the same intermediate, then the addition of a pendant radicalphile to the ester substrate should allow for intramolecular radical addition and cyclization. For this purpose, a series of unactivated methyl esters with pendant olefins were prepared. Gratifyingly, reduction of these substrates by $SmBr_2$-NMEA induced a 5-*exo*-trig cyclization yielding the cyclic alcohols shown in Scheme 6.13. Moreover, reduction of these substrates by a discrete Sm(II)-water-amine system yielded no cyclization, highlighting the unique role of NMEA as a chelating additive for Sm(II).

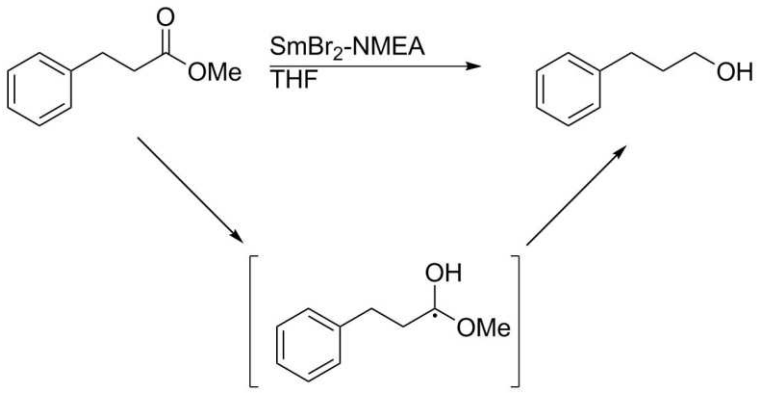

Scheme 6.12. Reaction scheme and proposed intermediate for the reduction of a methyl ester by $SmBr_2$-NMEA

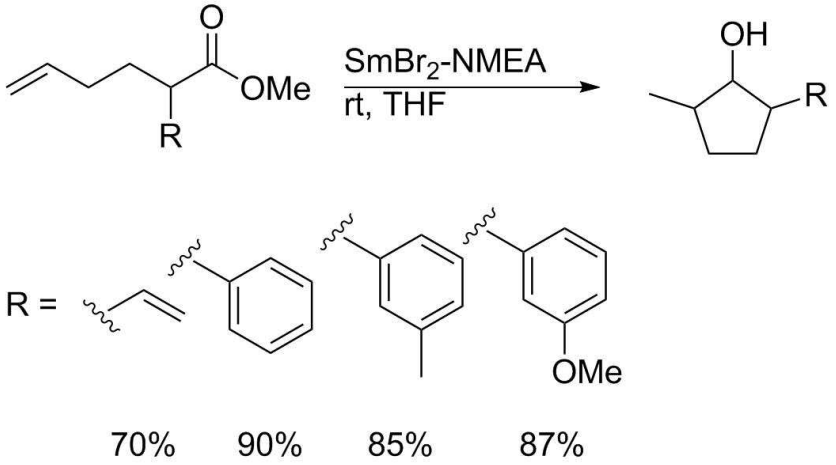

Scheme 6.13. Reaction scheme and scope for the 5-*exo*-trig reductive cyclization of methyl esters with pendant olefins

Given the successful reduction of the wide range of challenging substrates *vide supra*, the reduction of analogs to intermediates in nitrogen gas fixation process were attempted. The first substrate investigated for this purpose was azobenzene, which was chosen as an analog to diazene. As shown in Scheme 6.14, the N=N π-bond of azobenzene was rapidly reduced by SmBr2-NMEA to yield a quantitative amount of 1,2-diphenylhydrazine. However, the N-N σ-bond remained intact even in the presence of excess $SmBr_2$-NMEA. This was proposed to be the result of steric interference by the two phenyl groups present in 1,2-diphenylhydrazine. Accordingly, the reduction of phenylhydrazine was attempted and was found to proceed rapidly, yielding aniline

quantitatively as shown in Scheme 6.15. The balance of the material in this reaction is likely ammonia, which was too volatile for isolation.

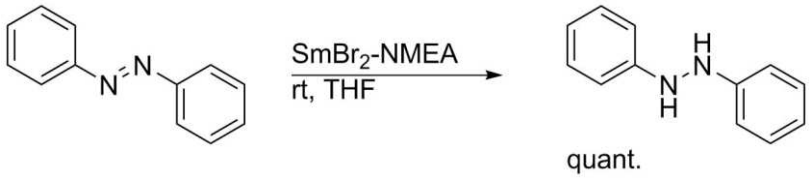

Scheme 6.14. Reaction scheme for the reduction of azobenzene by $SmBr_2$-NMEA

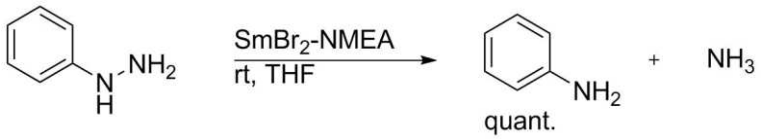

Scheme 6.15 Reaction scheme for the reduction of phenylhydrazine by $SmBr_2$-NMEA

6.3.3 Kinetic Analysis of the Reduction of 1-Methoxynaphthalene by $SmBr_2$-NMEA

6.3.3.1 Kinetic Rate Order Experiments

The mechanism of substrate reduction was investigated via rate studies performed using stopped flow kinetic analysis. These studies were performed using 1-methoxynaphthalene as a model substrate due to its moderate rate of reduction by $SmBr_2$-NMEA. Rate data was gathered under pseudo-first order conditions, with [NMEA] and [1-methoxynaphthalene] maintained in excess of ten equivalents with respect to [$SmBr_2$]. The reaction progress was measured as the decay of the characteristic absorbance of $SmBr_2$ at 540 nm. The value of k_{obs} for each measurement was acquired as the exponent value of a single exponential function fit to the decay curve. All rate measurements were performed three times with independently prepared samples. The rate order for $SmBr_2$ was obtained using the fractional times method. The results of these experiments are shown in Table 6.1. The rate orders of all three components were found to be near unity, indicating that the rate limiting step in this reaction is the initial PCET reduction of 1-methoxynaphthalene by a $SmBr_2$-NMEA complex.

Table 6.1. Rate orders for the reduction of 1-methoxynaphthalene by $SmBr_2$-NMEA

entry	reaction component	rate order[a]
1	$SmBr_2$	1[b]
2	NMEA	1.0 ± 0.1[c]
3	1-methoxynaphthalene	0.8 ± 0.01[d]

[a]Errors reported as ± σ. [b]Fractional times method. [c]10 mM $SmBr_2$, 60-100 mM 1-methoxynaphthalene, 150 mM NMEA in THF. [d]10 mM $SmBr_2$, 100 mM 1-methoxynaphthalene, 50-250 mM NMEA in THF.

6.3.3.2 Kinetic Activation Parameter Experiments

Rate data was also acquired using pseudo-first order methodology over a temperature range of 20°C to acquire activation parameters for the reduction of 1-methoxynaphthalene by $SmBr_2$-NMEA. The results of these experiments are shown in Table 6.2. The observed low $\Delta H^{\ddagger}$ and high $\Delta S^{\ddagger}$ are consistent with a relatively ordered late transition state for the reduction of 1-methoxynaphthalene by $SmBr_2$-NMEA.

Table 6.2. Activation parameters for the reduction of 1-methoxynaphthalene by $SmBr_2$-NMEA

entry	activation parameter	value[a]
1	$\Delta H^{\ddagger}$ (kcal/mol)[b]	9.2 ± 0.2
2	$\Delta S^{\ddagger}$ (cal/molK)[b]	-34 ± 2
3	$\Delta G^{\ddagger}$ (kcal/mol @ 25°C)[c]	19.3 ± 0.3

[a]Conditions: 10 mM $SmBr_2$, 100 mM 1-methoxynaphthalene, 150 mM NMEA in THF. Temperature varied between 15 and 35 °C. Errors reported as ± σ. [b]Obtained from $\ln\left(\frac{k_{obs}h}{kT}\right) = \frac{\Delta H^{\ddagger}}{RT} + \frac{\Delta S^{\ddagger}}{R}$ [c]Obtained from $\Delta G^{\ddagger} = \Delta H^{\ddagger} - T\Delta S^{\ddagger}$

6.3.3.3 Deuterium Kinetic Isotope Effect Experiments

The deuterium kinetic isotope effect for the reduction of 1-methoxynaphthalene by $SmBr_2$-NMEA was determined by substituting NMEA in the reaction with NMEA-d_2, which was prepared by isotope exchange with D_2O. The observed difference in the rate of reduction of 1-methoxynaphthalene by $SmBr_2$-NMEA and $SmBr_2$-NMEA-d_2 revealed a k_H/k_D value of 1.1. This value is consistent with the determination of a late transition state based on the activation parameter data *vide supra*.

Furthermore, similarly low k_H/k_D values have been observed in other PCET reductions.[1,27]

6.3.4 Thermodynamic Analysis of Coordination-Induced Bond Weakening in $SmBr_2$-NMEA

Given the PCET reduction of arenes by $SmBr_2$-NMEA, the degree of bond weakening in NMEA upon coordination to $SmBr_2$ can be determined. However, both the oxygen and nitrogen moieties of NMEA contain an X-H bond and formal hydrogen atom transfer from either functional group is plausible. To address this, it was noted that while Sm(II)-DMEA reductants, which lack an N-H group, are capable of facilitating the reduction of arenes, similar reactivity is not observed in Sm(II)-EDA reductants, which lack an O-H group. Therefore, $SmBr_2$-NMEA likely donates a formal hydrogen atom to substrates from the alcohol functional group of NMEA. Comparison of the strength of the O-H bond of NMEA with the C-H bond formed upon the initial PCET reduction of biphenyl, shown in Scheme 6.16, reveals a minimum of 70.3 kcal/mol of weakening in the O-H bond of NMEA upon coordination to $SmBr_2$.

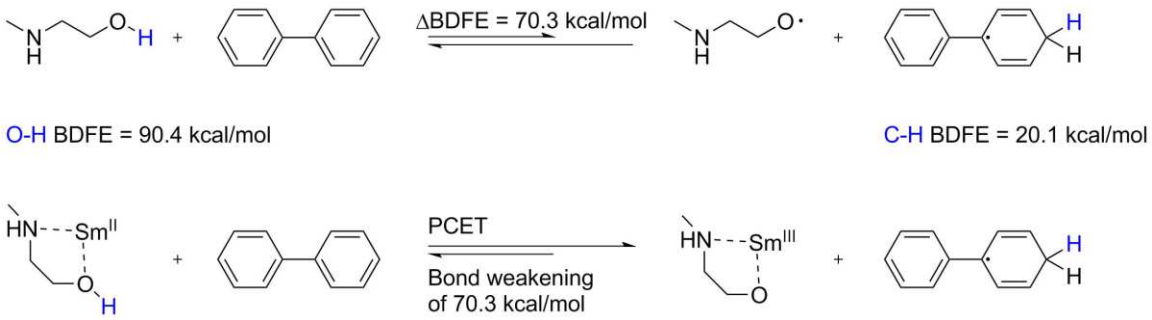

Scheme 6.16. Reaction scheme and bond strength comparison for the reduction of biphenyl by $SmBr_2$-NMEA

6.4 Conclusions

The results discussed above demonstrate that the $SmBr_2$-NMEA reagent is a versatile and powerful reductant, capable of mediating the mild reduction of substrates

that are typically reduced by lithium metal in liquid ammonia. These reductions are enabled by the exceptionally weak O-H bond formed upon the coordination of NMEA to $SmBr_2$. With an O-H bond strength of no more than 20.1 kcal/mol, $SmBr_2$-NMEA has by far the lowest X-H BDFE of any coordination-induced bond weakening reagent reported to date that is sufficiently stable to facilitate the reduction of substrates. Furthermore, the significant O-H bond weakening in NMEA upon coordination to $SmBr_2$ is consistent with the hypothesis that ligand affinity for Sm(II) can be used to tune the reactivity of Sm(II) coordination-induced bond weakening systems.

6.5 References

(1) Chciuk, T. V.; Flowers, R. A. Proton-Coupled Electron Transfer in the Reduction of Arenes by SmI2-Water Complexes. *J. Am. Chem. Soc.* **2015**, *137* (35), 11526–11531.

(2) Chciuk, T. V; Anderson, W. R.; Flowers, R. A. Reversibility of Ketone Reduction by SmI2-Water and Formation of Organosamarium Intermediates. *Organometallics* **2017**, *36*, 4579−4583.

(3) Duffy, L. A.; Matsubara, H.; Procter, D. J. A Ring Size-Selective Reduction of Lactones Using SmI2 and H2O. *J. Am. Chem. Soc.* **2008**, *130* (4), 1136–1137.

(4) Guazzelli, G.; De Grazia, S.; Collins, K. D.; Matsubara, H.; Spain, M.; Procter, D. J. Selective Reductions of Cyclic 1,3-Diesters Using SmI2 and H2O. *J. Am. Chem. Soc.* **2009**, *131* (21), 7214–7215.

(5) Kolmar, S. S.; Mayer, J. M. SmI2(H2O)n Reduction of Electron Rich Enamines by Proton-Coupled Electron Transfer. *J. Am. Chem. Soc.* **2017**, *139* (31), 10687−10692.

(6) Ramírez-Solís, A.; Bartulovich, C. O.; León-Pimentel, C. I.; Saint-Martin, H.; Boekell, N. G.; Flowers, R. A. Proton Donor Effects on the Reactivity of SmI2. Experimental and Theoretical Studies on Methanol Solvation vs. Aqueous Solvation. *Dalt. Trans.* **2020**, *49* (23), 7897–7902.

(7) Chciuk, T. V; Li, A. M.; Vazquez-Lopez, A.; Anderson, W. R.; Flowers, R. A. Secondary Amides as Hydrogen Atom Transfer Promoters for Reactions of Samarium Diiodide. *Org. Lett.* **2016**, *19*, 290−293.

(8) Chciuk, T. V.; Anderson, W. R.; Flowers, R. A. High-Affinity Proton Donors

Promote Proton-Coupled Electron Transfer by Samarium Diiodide. *Angew. Chemie Int. Ed.* **2016**, *55* (20), 6033–6036.

(9) Bartulovich, C. O.; Flowers, R. A. Coordination-Induced O-H Bond Weakening in Sm(II)-Water Complexes. *Dalt. Trans.* **2019**, *48* (43), 16129–16462.

(10) Ashida, Y.; Arashiba, K.; Nakajima, K.; Nishibayashi, Y. Molybdenum-Catalysed Ammonia Production with Samarium Diiodide and Alcohols or Water. *Nature* **2019**, *568* (7753), 536–540.

(11) Ramírez-Solís, A.; Boekell, N. G.; León-Pimentel, I.; Saint-Martin, H.; Bartulovich, C. O.; Flowers, R. A. Ammonia Solvation vs Aqueous Solvation of Samarium Diiodide. A Theoretical and Experimental Approach to Understanding Bond Activation Upon Coordination to Sm(II). *J. Org. Chem* **2022**, *87* (3), 1689–1697.

(12) Maity, S.; Flowers, R. A.; Hoz, S. Aza versus Oxophilicity of SmI2: A Break of a Paradigm. *Chem. - A Eur. J.* **2017**, *23* (67), 17070–17077.

(13) Dahlén, A.; Hilmersson, G. Instantaneous SmI 2 -H 2 O-Mediated Reduction of Dialkyl Ketones Induced by Amines in THF. *Tetrahedron Lett.* **2002**, *43* (40), 7197–7200.

(14) Dahlén, A.; Petersson, A.; Hilmersson, G. Diastereoselective Intramolecular SmI 2 -H 2 O-Amine Mediated Couplings. *Org. Biomol. Chem.* **2003**, *1* (14), 2423–2426.

(15) Dahlén, A.; Sundgren, A.; Lahmann, M.; Oscarson, S.; Hilmersson, G. SmI2/Water/Amine Mediates Cleavage of Allyl Ether Protected Alcohols: Application in Carbohydrate Synthesis and Mechanistic Considerations. *Org. Lett.* **2003**, *5* (22), 4085–4088.

(16) Davis, T. A.; Chopade, P. R.; Hilmersson, G.; Flowers, R. A. Reduction of β-Hydroxyketones by Sml2/H2O/ Et3N. *Org. Lett.* **2005**, *7* (1), 119–122.

(17) Dahlén, A.; Hilmersson, G. Mechanistic Study of the SmI2/H2O/Amine-Mediated Reduction of Alkyl Halides: Amine Base Strength (PKBH+) Dependent Rate. *J. Am. Chem. Soc.* **2005**, *127* (23), 8340–8347.

(18) Ankner, T.; Hilmersson, G. Instantaneous SmI2/H2O/Amine Mediated Reduction of Nitroalkanes and α,β-Unsaturated Nitroalkenes. *Tetrahedron Lett.* **2007**, *48* (32), 5707–5710.

(19) Ankner, T.; Hilmersson, G. Instantaneous Deprotection of Tosylamides and Esters with Sml 2/Amine/Water. *Org. Lett.* **2009**, *11* (3), 503–506.

(20) Ankner, T.; Hilmersson, G. SmI2/H2O/Amine Promoted Reductive Cleavage of Benzyl-Heteroatom Bonds: Optimization and Mechanism. *Tetrahedron* **2009**, *65* (52), 10856–10862.

(21) Janjetovic, M.; Träff, A. M.; Ankner, T.; Wettergren, J.; Hilmersson, G. Solvent Dependent Reductive Defluorination of Aliphatic C-F Bonds Employing Sm(HMDS)2. *Chem. Commun.* **2013**, *49* (18), 1826–1828.

(22) Szostak, M.; Spain, M.; Parmar, D.; Procter, D. J. Selective Reductive Transformations Using Samarium Diiodide-Water. *Chem. Commun.* **2012**, *48* (3), 330–346.

(23) Molander, G. A.; Stengel, P. J. Reduction of 2-Acylaziridines by Samarium(II) Iodide. An Efficient and Regioselective Route to β-Amino Carbonyl Compounds. *Tetrahedron* **1997**, *53* (26), 8887–8912.

(24) Otsubo, K.; Inanaga, J.; Yamaguchi, M. SmI2-Induced Highly Regioselective Reduction of α,β-Epoxy Esters and γ,δ-Epoxy-α,β-Unsaturated Esters. An Efficient Route to Optically Active β-Hydroxy and δ-Hydroxy Esters. *Tetrahedron Lett.* **1987**, *28* (38), 4437–4440.

(25) Rabideau, P. W.; Marcinow, Z. The Birch Reduction of Aromatic Compounds. *Org. React.* **1992**, 1–334.

(26) Chciuk, T. V; Anderson, W. R.; Flowers, R. A. Proton-Coupled Electron Transfer in the Reduction of Carbonyls by Samarium Diiodide-Water Complexes. *J. Am. Chem. Soc.* **2016**, *138*, 8738−8741.

(27) Ramírez-Solís, A.; Bartulovich, C. O.; Chciuk, T. V; Hernández-Cobos, J.; Saint-Martin, H.; Maron, L.; Anderson, W. R.; Li, A. M.; Flowers II, R. A. Experimental and Theoretical Studies on the Implications of Halide-Dependent Aqueous Solvation of Sm(II). *J. Am. Chem. Soc.* **2018**, *140*, 16731−16739.

Chapter 7: Studies on Backdonation as the Basis for Coordination-Induced Bond Weakening

7.1 Background and Significance

7.1.1 Coordination-Induced Bond Weakening in Synthesis

The first identification of coordination-induced bond weakening in a synthetic system appears in a study by Wood and coworkers investigating the reduction of xanthate esters by trialkylboranes and water.[1] Their findings revealed that upon the coordination of water to trimethylborane, the O-H bond of water is weakened by approximately 43 kcal/mol. This bond weakening was found to enable the hydrogenation of a series of xanthate esters through the proposed mechanism shown in Scheme 7.1.[1]

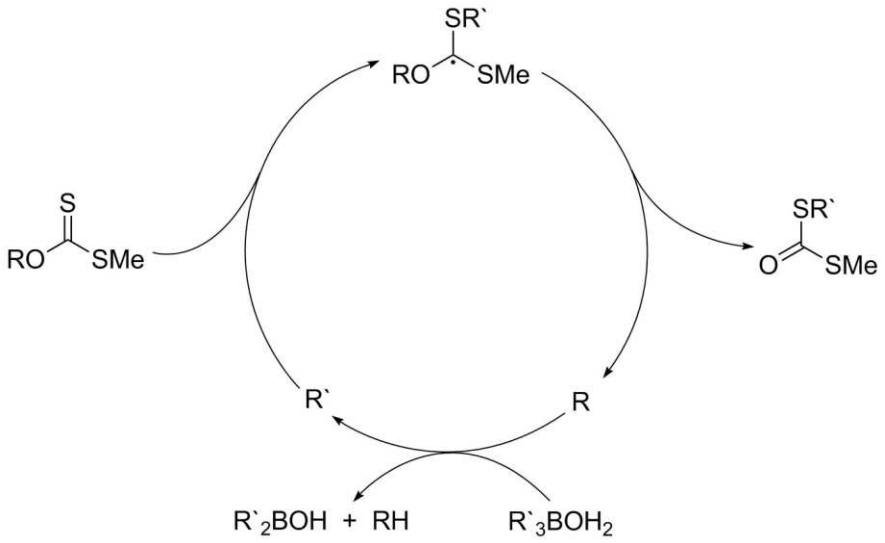

Scheme 7.1. Proposed catalytic cycle for the reduction of xanthates by trialkylborane-water[1]

Coordination-induced bond weakening has also been employed in synthesis by Gansäuer and coworkers for the catalytic reductive ring opening of epoxides by a low-valent titanocene modified with a pendant amide.[2] These reductions are enabled by the approximately 40 kcal/mol reduction in the N-H BDFE of the amide group upon coordination of the amide carbonyl to Ti(III). Further functionalization of the

titanocene(III)-amide catalyst to the chiral form shown in Scheme 7.2 facilitated the enantioselective reduction of epoxides to chiral alcohols with an enantiomeric ratio as high as 86:14.[2]

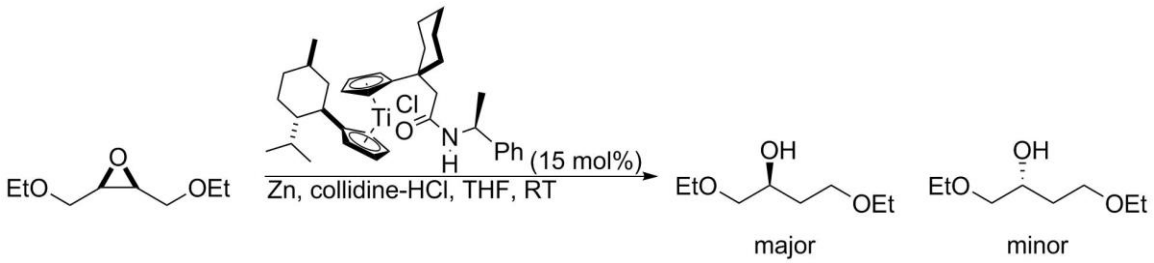

Scheme 7.2. Reaction scheme for the enantioselective ring opening of an epoxide by a chiral titanocene catalyst[2]

Nishibayashi and coworkers further demonstrate the utility of coordination-induced bond weakening strategies in synthesis in their seminal report on the reduction of nitrogen gas by a SmI_2-water coordination-induced bond weakening system with a molybdenum N_2-binding catalyst.[3] Remarkably, under optimized conditions, the SmI_2-water-Mo(PCP) (PCP = 1,3-bis((di-*tert*-butylphosphino)methyl)benzimidazol-2-ylidine) (Scheme 7.3) system achieved an approximately 92% yield of ammonia from nitrogen gas.

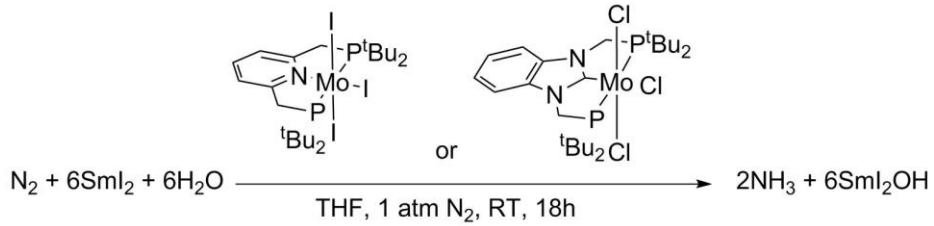

Scheme 7.3. Reaction scheme for the molybdenum PNP/PCP catalyzed reduction of N_2 to NH_3 by SmI_2-H_2O[3]

Stahl and coworkers further extended the scope of coordination-induced bond weakening reactions to the catalytic oxidation of a range of alcohols to aldehydes by a (bpy)Cu^{I}(NMI) TEMPO system (bpy = 2,2`-bipyridine, NMI = N-methylimidazole).[4] As

shown in Scheme 7.4, alcohol oxidation by TEMPO in this system is enabled by O-H bond weakening in the alcohol upon coordination to Cu(I).

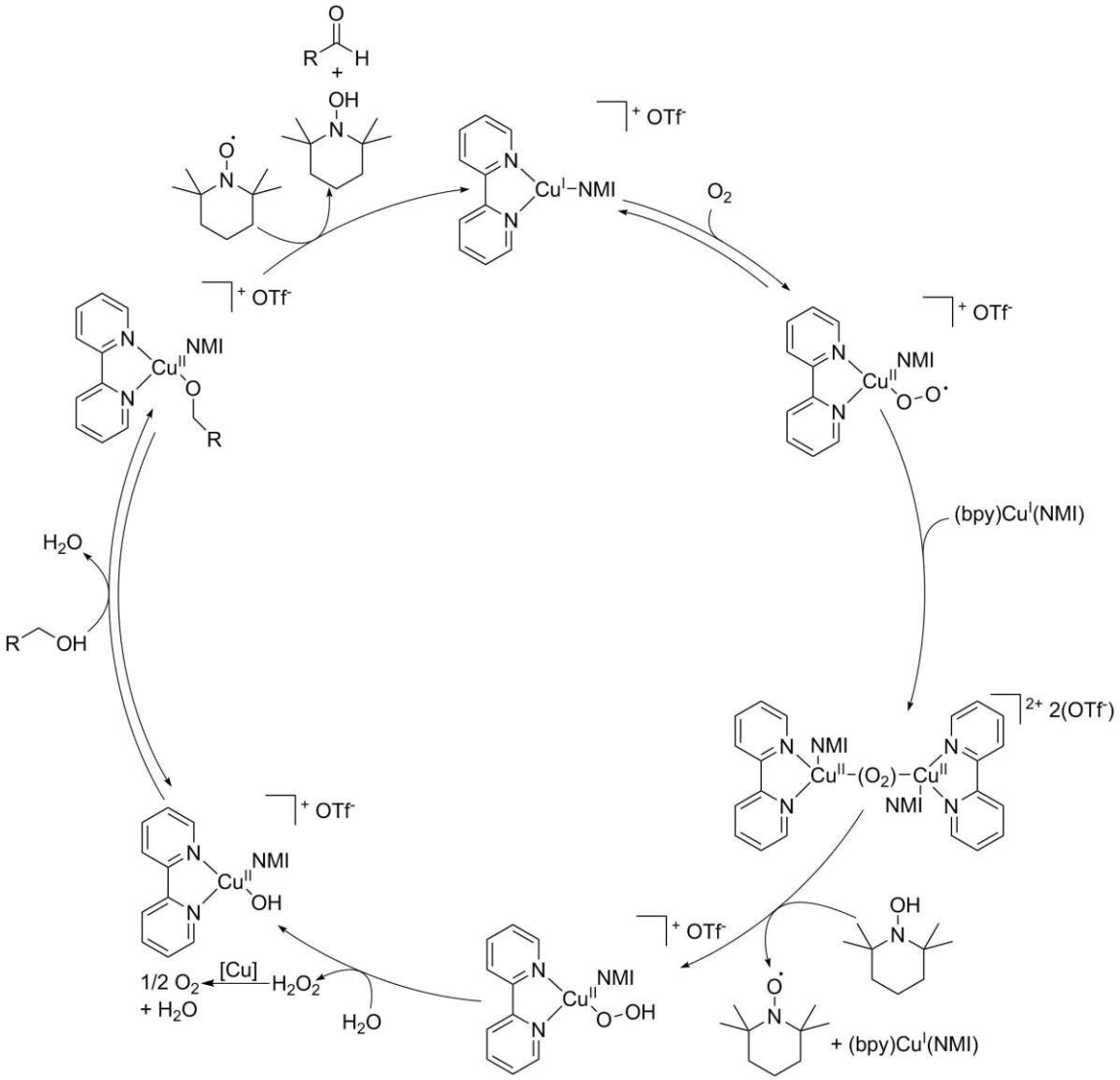

Scheme 7.4. Catalytic cycle for the Cu^{I}-TEMPO-mediated aerobic oxidation of primary alcohols[4]

7.1.2 Coordination-Induced Bond Weakening in Nature

In addition to the implementations in synthesis *vide supra*, coordination-induced bond weakening has also been identified in biological systems. Photosystem II, which is integral to oxygenic biophotosynthesis, is a notable example of coordination-induced bond weakening in nature.[5] Within photosystem II, a low-valent manganese cluster

known as the oxygen-evolving complex coordinates two molecules of water. Computational modeling has revealed that upon coordination of water to manganese, the first and second O-H bonds of water are weakened by approximately 32.5 and 15.5 kcal/mol, respectively.[5] This weakening enables the total dehydrogenation of water by proximal tyrosine residues as shown in Scheme 7.5 yielding four hydrogen atom equivalents and a molecule of oxygen gas.

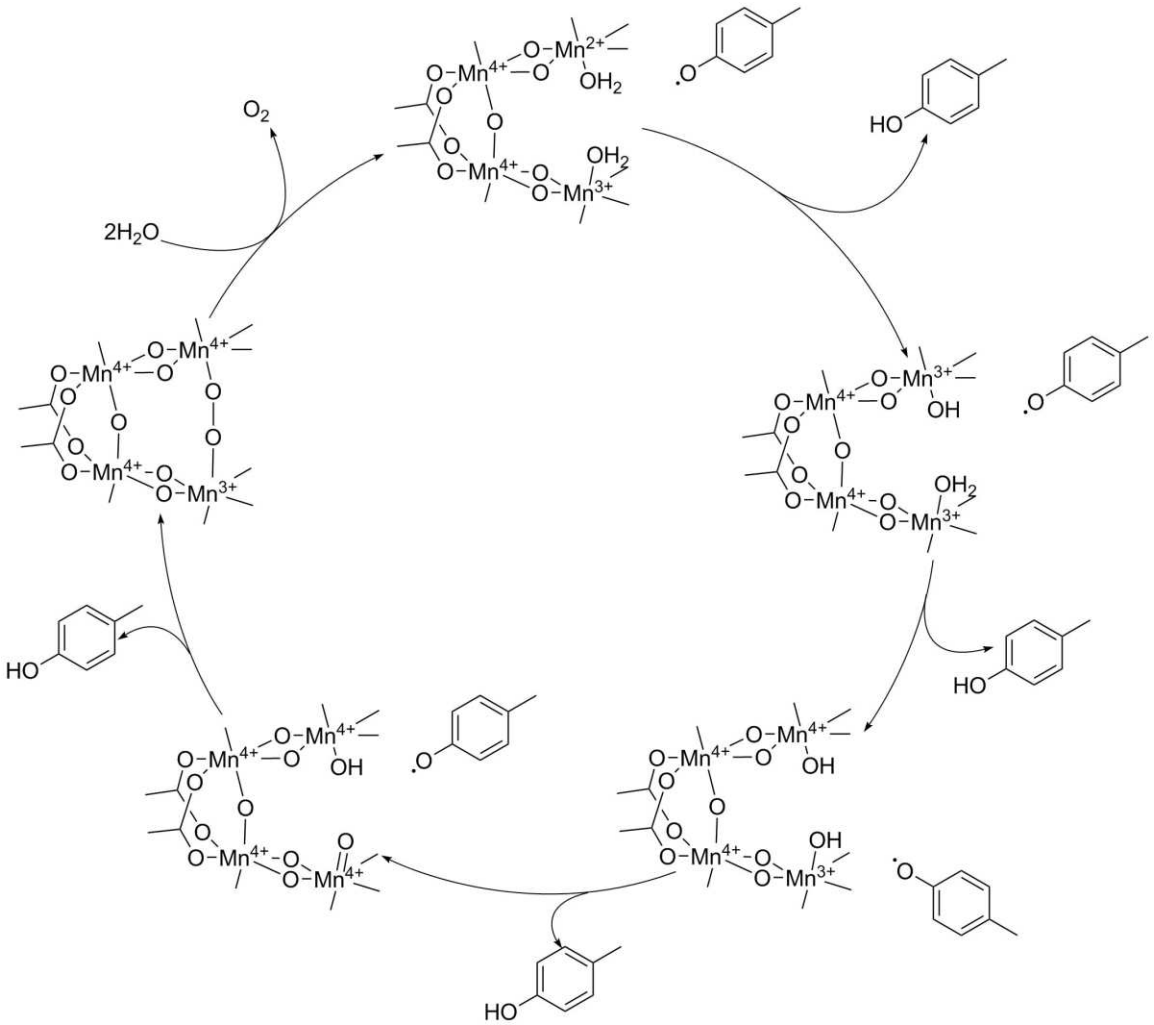

Scheme 7.5. S-state catalytic cycle for water oxidation and oxygen gas evolution by the oxygen-evolving complex[5]

7.1.3 Hypotheses for the Basis of Coordination-Induced Bond Weakening

Despite the importance of coordination-induced bond weakening in the synthetic and natural processes as outlined above, the underlying physical basis for coordination-induced bond weakening remains largely uninvestigated and poorly understood. In a report on C-H bond weakening in a copper(II) complex, Stack and coworkers proposed the formation of a Cu(II)-σ-complex as shown in Scheme 7.6.[6] This determination was informed by computational and spectroscopic analysis that was consistent with Cu-H interaction and backdonation from Cu(II) into the ligand C-H σ*-antibonding orbital.

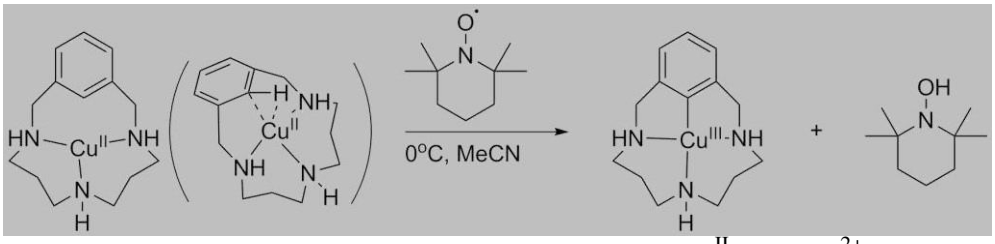

Scheme 7.6. Reaction scheme for the dehydrogenation of $[Cu^{II}(H33m)]^{2+}$ by TEMPO[6]

Additionally, in our investigation of the SmI_2-ammonia system, we proposed that coordination-induced bond weakening in Sm(II) systems may also be driven by backdonation from low-valent samarium into the σ*-antibonding orbitals of coordinating protic ligands.[7] This hypothesis was proposed to rationalize the greater degree of bond weakening observed in water compared to ammonia upon coordination to Sm(II) despite the greater affinity of Sm(II) for ammonia.

7.2 Experimental Details

7.2.1 Materials

Samarium and ytterbium powder were purchased from Acros Organics. Samarium diiodide was generated by the standard method of samarium metal combined with iodine in THF and allowed to stir for at least 4 hours. Ytterbium diiodide was

generated by combination of ytterbium metal with 1,2-diiodoethane and allowed to stir for at least 4 hours. Titanocene chloride was generated by the reduction of Cp_2TiCl_2 with zinc metal. Iodometric titrations were then performed to verify concentration of SmI_2 for use. Tetrahydrofuran was purified by a solvent purification system (Innovative Technology Inc.; MA). Methyl crotonate was purchased from Alfa Aesar and used without further purification.

7.2.2 Instrumentation

^{1}H NMR spectra were recorded in MeCN-d_3 on a Bruker 500 MHz spectrometer at 500 MHz in a J. Young NMR tube. The ^{1}H NMR chemical shifts are given as δ values in ppm relative to TMS (0 ppm) as the internal reference. Solutions were prepared under a dry argon atmosphere in flame dried glassware.

7.2.3 Methods

7.2.3.1 Procedure for ^{1}H NMR Shift Experiments

A 1 mL solution of low-valent metal in MeCN-d_3 (0.04 M SmI_2, 0.025 M YbI_2, 0.01 M Cp_2TiCl) was prepared in a J. Young NMR tube. Methyl crotonate (0.008 mmol, 0.84 μL for SmI_2; 0.005 mmol, 0.52 μL for YbI_2; 0.002 mmol, 0.21 μL for Cp_2TiCl) was added to the J. Young NMR tube. Solutions were observed immediately by ^{1}H NMR.

7.3 Results and Discussion

7.3.1 Methyl Crotonate ^{1}H NMR Shift Experiments

A series of ^{1}H NMR shift experiments were undertaken in order to test the hypothesis of backdonation from a low-valent metal into a ligand antibonding orbital. This method was adapted from a method developed by Childs and coworkers for the quantification of the interaction between unsaturated carbonyls and coordinating Lewis

acids.[8] It was reasoned that backdonation from a low-valent metal into a ligand antibonding orbital should be observed as an upfield shift in ^{1}H NMR peaks corresponding to protons in functional groups that are conjugated to the metal center. The low-valent metals utilized in these experiments were samarium diiodide (SmI_2), ytterbium diiodide (YbI_2) and titanocene chloride (Cp_2TiCl). Methyl crotonate was used as a coordinating ligand due to its stability against reduction by the chosen low-valent metal complexes. The overlaid ^{1}H NMR spectra for methyl crotonate uncomplexed and in the presence of five equivalents of SmI_2, YbI_2, and Cp_2TiCl, respectively, are shown in Figure 7.1.

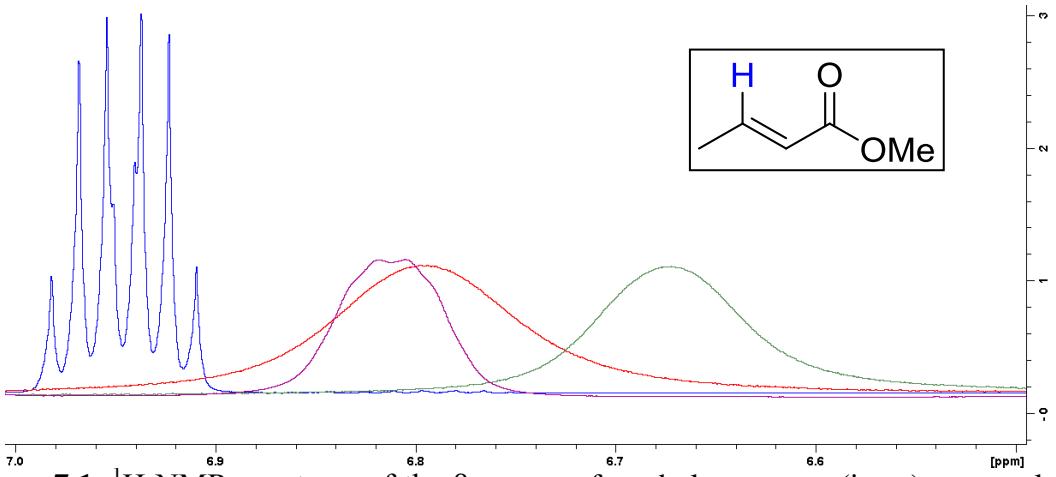

Figure 7.1. ^{1}H NMR spectrum of the β-proton of methyl crotonate (inset) uncomplexed (blue, 6.95 ppm) and in the presence of SmI_2 (green, 6.67 ppm), YbI_2 (red, 6.80 ppm), and Cp_2TiCl (purple, 6.81 ppm)

In the presence of each low-valent metal, the β-proton of methyl crotonate was observed to undergo an upfield shift, with the magnitude of the shift following the trend of SmI_2 > YbI_2 > Cp_2TiCl. Notably, this trend mirrors the trend of increasing redox potentials for these low-valent complexes.[9–11] The correlation of these two trends is consistent with the Bordwell equation (Equation 7.1), which relates the redox potential of a coordination-induced bond weakening complex with its X-H BDFE. The observed

upfield ^{1}H NMR shift in the β-proton of methyl crotonate was therefore interpreted as consistent with C-H bond weakening in methyl crotonate upon coordination to the low-valent metal complexes through backdonation into a ligand antibonding orbital.

$$BDFE = 23.06E^0 + 1.37pK_a + C_G \qquad (7.1)$$

7.3.2 Correlation of Energy Differences Between Ligand σ-Bonding and σ*-Antibonding Orbitals with Degree of Coordination-Induced Bond Weakening

Given spectroscopic evidence of backdonation from low-valent metals into a ligand antibonding orbital, the relationship between the difference in energy of the ligand X-H σ-bonding and σ*-antibonding orbitals ($\Delta E_{\sigma-\sigma^*}$) and the degree of X-H bond weakening (ΔBDFE) upon ligand coordination to a low-valent was examined. Bond weakening data was drawn from literature reports of low-valent metal complexes for which coordination-induced bond weakening in at least three ligands had been observed. Where available, bond weakening values were used as reported. For reports that contain only the X-H BDFE of the complexed ligands, the X-H BDFEs of the uncomplexed ligands were calculated using density functional theory (DFT) at the same level of theory as in the relevant report.[12–15] Values for $\Delta E_{\sigma-\sigma^*}$ were calculated as the difference in energy between the lowest energy occupied and highest energy unoccupied eigenvalues furnished via natural population analysis and validated by comparison with differences in the relevant σ-bonding and σ*-antibonding orbital energies calculated via natural bond orbital analysis using the APFD functional and a 6-311+G(2d,p) basis set.[16–19] The plots of ΔBDFE vs. $\Delta E_{\sigma-\sigma^*}$ for (^{Ph}Tpy)(PPh_2Me)$_2$Mo$^+$, (η^5-$C_5Me_4SiMe_3$)$_2$Ti, Cp_2TiCl, and SmI_2 are shown in Figures 7.2-7.5, respectively.

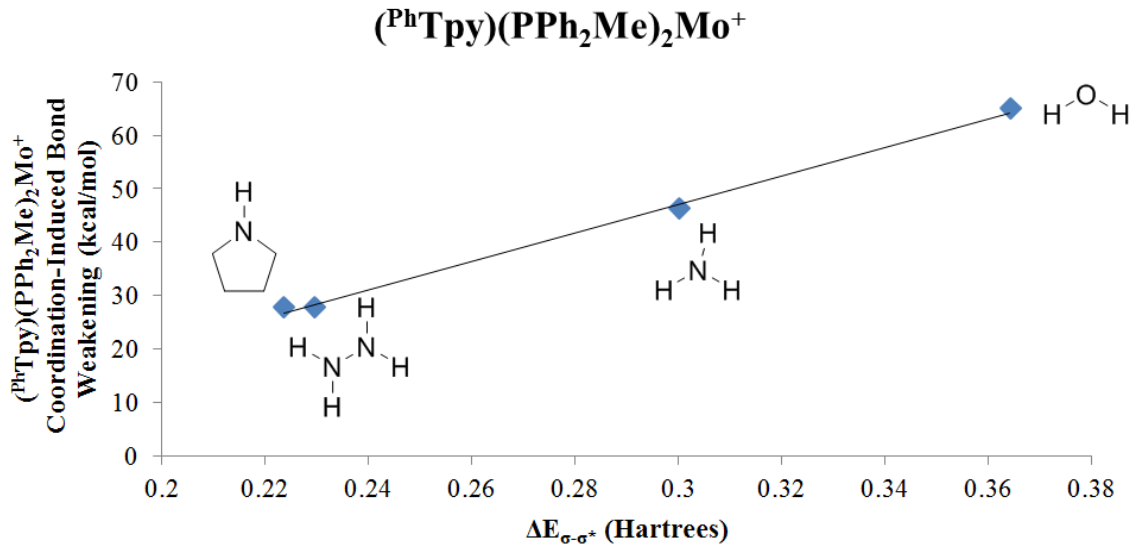

Figure 7.2. Coordination-induced bond weakening vs. ligand $\Delta E_{\sigma-\sigma^*}$ in $(^{Ph}Tpy)(PPh_2Me)_2Mo^+$ complexes ($R^2 > 0.99$)[20,21]

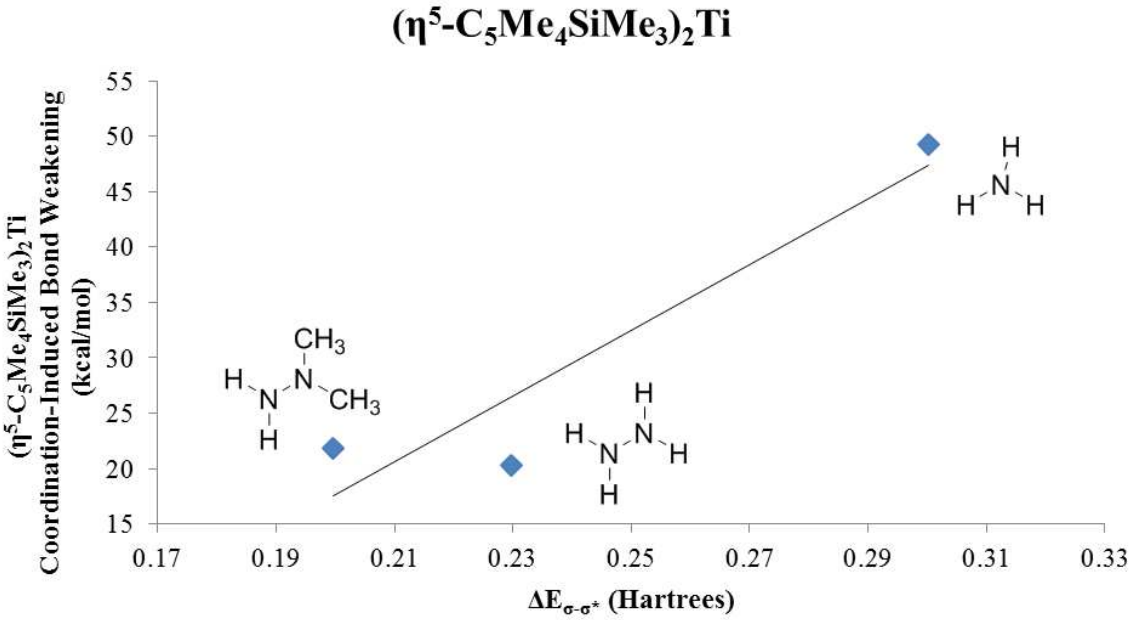

Figure 7.3. Coordination-induced bond weakening vs. ligand $\Delta E_{\sigma-\sigma^*}$ in $(\eta^5\text{-}C_5Me_4SiMe_3)_2Ti$ complexes ($R^2 = 0.89$)[22]

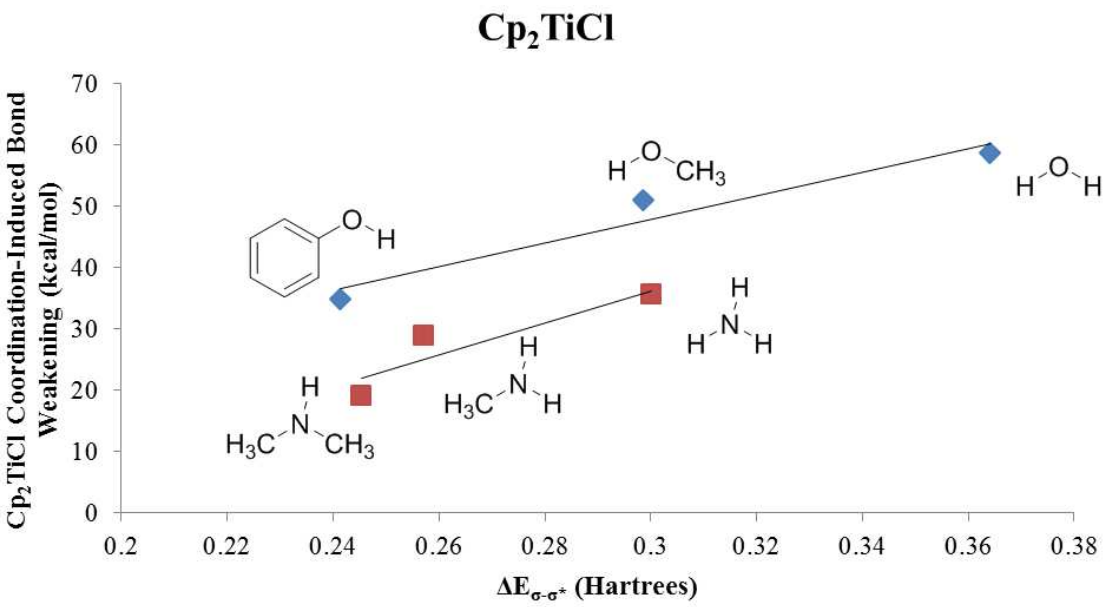

Figure 7.4. Coordination-induced bond weakening vs. ligand $\Delta E_{\sigma-\sigma^*}$ in Cp_2TiCl complexes (blue diamonds $R^2 = 0.94$, red squares $R^2 = 0.84$)[23]

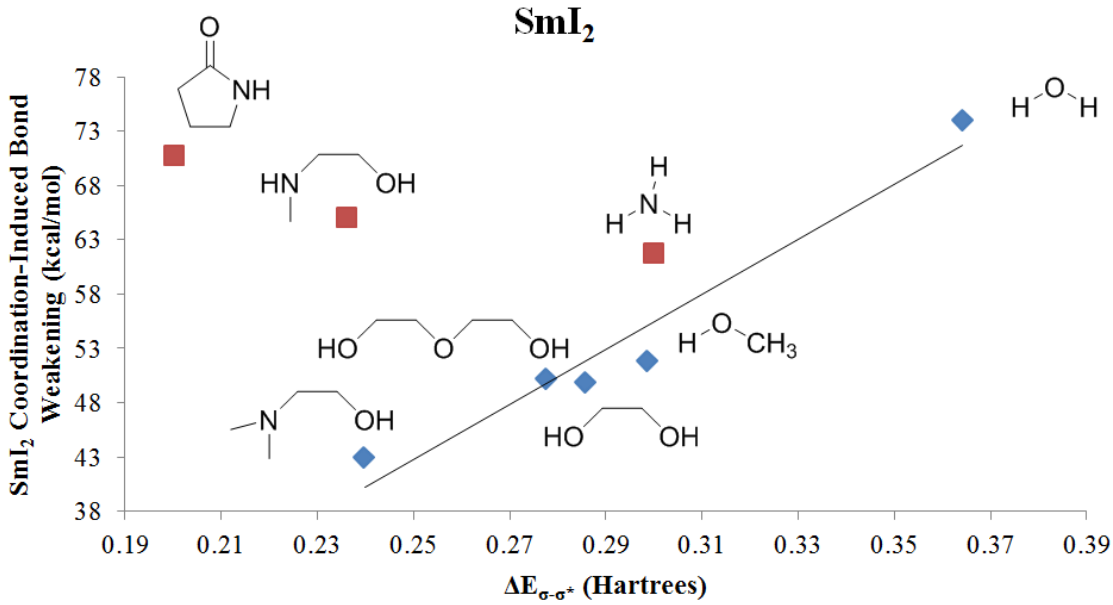

Figure 7.5. Coordination-induced bond weakening vs. ligand $\Delta E_{\sigma-\sigma^*}$ in SmI_2 complexes ($R^2 = 0.95$)[7,24–28]

The correlation between ΔBDFE and $\Delta E_{\sigma-\sigma^*}$ in these plots provides evidence of backdonation into a ligand X-H σ*-antibonding orbital as a significant driving force for coordination-induced bond weakening. Previous chapters in this dissertation contain

discussions of the effects of metal-ligand affinity in the magnitude of coordination-induced bond weakening. Those effects can also be seen in Figure 7.4 in the separate trends for oxygen- and nitrogen-containing ligands coordinated to Cp_2TiCl. The greater ΔBDFEs observed for O-H compared to N-H ligands with similar $\Delta E_{\sigma-\sigma^*}$ values was attributed to the significant oxophilicity of titanium.[29] Likewise, the positions of the data points for ammonia, N-methylethanolamine (NMEA), and 2-pyrrolidinone above the trend line for alcohols and water in Figure 7.5 reflect the greater affinity of Sm(II) for nitrogen compared to oxygen.[25] Additionally, the significant deviations of NMEA and 2-pyrrolidinone from the trend line in Figure 7.5 are likely a consequence of the increased redox potential of the Sm(II) complex formed upon coordination of these strongly-coordinating ligands.[25,26]

7.4 Conclusions

The upshift in the ^1H NMR peak for the β-proton of methyl crotonate in the presence of a series of low-valent metals provides novel evidence for backdonation from a low-valent metal into a ligand antibonding orbital. The magnitude of the upfield shift was found to correlate with the trend for X-H BDFE predicted by the Bordwell equation. This is consistent with backdonation into a ligand X-H σ*-antibonding orbital as a driving force for coordination-induced bond weakening.

The relationship between σ*-backdonation and bond weakening was further investigated by comparing the ΔBDFE values for a range of ligands upon coordination to a series of low-valent metals to the computed $\Delta E_{\sigma-\sigma^*}$ values for those ligands. These plots revealed a significant degree of correlation (R^2 = 0.84-0.99) between the ΔBDFE and $\Delta E_{\sigma-\sigma^*}$ values for ligands across four different low-valent metal complexes.[7,20–28] These

results are further compelling evidence that coordination-induced bond weakening is driven predominantly by backdonation from a low-valent metal into the X-H σ*-antibonding orbital of a coordinated protic ligand.

Additionally, separate trends were observed in the correlation of ΔBDFE and $\Delta E_{\sigma-\sigma^*}$ values for ligands with different X-H functional groups. This change in behavior upon change in ligand functional group is consistent with the hypothesis that greater metal-ligand affinity induces a greater X-H ΔBDFE.[28] Specifically, the greater ΔBDFEs observed for alcohols and water compared to amines coordinated to Cp_2TiCl reflects the high affinity of Ti(III) for oxygen.[29] Likewise, the greater affinity of Sm(II) for nitrogen compared to oxygen predicts the greater ΔBDFEs for ammonia, N-methylethanolamine, and 2-pyrrolidinone compared to the trend line for alcohols and water coordinated to SmI_2.[25]

As a corollary to the correlation of ΔBDFE and $\Delta E_{\sigma-\sigma^*}$ values presented herein, the calculated $\Delta E_{\sigma-\sigma^*}$ value for a ligand can likely be used to predict the ΔBDFE of that ligand upon coordination to a low-valent metal complex. This strategy enables the screening of potential coordination-induced bond weakening systems without the need to synthesize and characterize them individually.

7.5 References

(1) Spiegel, D. A.; Wiberg, K. B.; Schacherer, L. N.; Medeiros, M. R.; Wood, J. L. Deoxygenation of Alcohols Employing Water as the Hydrogen Atom Source. *J. Am. Chem. Soc.* **2005**, *127*, 12513–12515.

(2) Zhang, Y.-Q.; Jakoby, V.; Stainer, K.; Schmer, A.; Klare, S.; Bauer, M.; Grimme, S.; Cuerva, J. M.; Gansäuer, A. Amide-Substituted Titanocenes in Hydrogen-Atom Transfer Catalysis. *Angew. Chemie Int. Ed.* **2016**, *55* (4), 1523–1526.

(3) Ashida, Y.; Arashiba, K.; Nakajima, K.; Nishibayashi, Y. Molybdenum-Catalysed Ammonia Production with Samarium Diiodide and Alcohols or Water. *Nature* **2019**, *568* (7753), 536–540.

(4) Hoover, J. M.; Ryland, B. L.; Stahl, S. S. Mechanism of Copper(I)/TEMPO-Catalyzed Aerobic Alcohol Oxidation. *J. Am. Chem. Soc.* **2013**, *135*, 2357–2367.

(5) Hoganson, C. W.; Babcock, G. T. A Metalloradical Mechanism for the Generation of Oxygen from Water in Photosynthesis. *Science* **1997**, *277* (5334), 1953–1956.

(6) Ribas, X.; Calle, C.; Poater, A.; Casitas, A.; Gó mez, L.; Xifra, R.; Parella, T.; Benet-Buchholz, J.; Schweiger, A.; Mitrikas, G.; et al. Facile C-H Bond Cleavage via a Proton-Coupled Electron Transfer Involving a C-H···Cu II Interaction. *J. Am. Chem. Soc.* **2010**, *132*, 12299–12306.

(7) Ramírez-Solís, A.; Boekell, N. G.; León-Pimentel, I.; Saint-Martin, H.; Bartulovich, C. O.; Flowers, R. A. Ammonia Solvation vs Aqueous Solvation of Samarium Diiodide. A Theoretical and Experimental Approach to Understanding Bond Activation Upon Coordination to Sm(II). *J. Org. Chem* **2022**, *87* (3), 1689–1697.

(8) Childs, R. F.; Lindsay Mulholland, D.; D Alan Nixon, A. N.; Nixon, A. The Lewis Acid Complexes of α,β-Unsaturated Carbonyl and Nitrile Compounds. A Nuclear Magnetic Resonance Study. *Can. J. Chem.* **2011**, *60* (6), 801–808.

(9) Morss, L. R. Thermochemical Properties of Yttrium, Lanthanum, and the Lanthanide Elements and Ions. *Chem. Rev.* **1976**, *76* (6), 827–841.

(10) Mugnier, Y.; Moise, C.; Laviron, E. Electrochemical Studies of Organometallic Compounds : I. On the Reversibility of the First Reduction Stage of Titanocene Dichloride. *J. Organomet. Chem.* **1981**, *204* (1), 61–66.

(11) Samuel, E.; Vedel, J. Electrochemical and Chemical Reduction of Titanocene Dihalides-An EPR Study. *Organometallics* **1989**, *8*, 237–241.

(12) Gaussian 09, Revision D.01, M. J. Frisch, G. W. Trucks, H. B. Schlegel, G. E. Scuseria, M. A. Robb, J. R. Cheeseman, G. Scalmani, V. Barone, B. Mennucci, G. A. Petersson, H. Nakatsuji, M. Caricato, X. Li, H. P. Hratchian, A. F. Izmaylov, J. Bloino, G. Zheng, J. L. Sonnenberg, M. Hada, M. Ehara, K. Toyota, R. Fukuda, J. Hasegawa, M. Ishida, T. Nakajima, Y. Honda, O. Kitao, H. Nakai, T. Vreven, J. A. Montgomery, Jr., J. E. Peralta, F. Ogliaro, M. Bearpark, J. J. Heyd, E. Brothers, K. N. Kudin, V. N. Staroverov, T. Keith, R. Kobayashi, J. Normand, K. Raghavachari, A. Rendell, J. C. Burant, S. S. Iyengar, J. Tomasi, M. Cossi, N. Rega, J. M. Millam, M. Klene, J. E. Knox, J. B. Cross, V. Bakken, C. Adamo, J. Jaramillo, R. Gomperts, R. E. Stratmann, O. Yazyev, A. J. Austin, R. Cammi, C. Pomelli, J. W. Ochterski, R. L. Martin, K. Morokuma, V. G. Zakrzewski, G. A. Voth, P. Salvador, J. J. Dannenberg, S. Dapprich, A. D. Daniels, O. Farkas, J. B. Foresman, J. V. Ortiz, J. Cioslowski, and D. J. Fox, Gaussian, Inc., Wallingford CT, 2013

(13) Becke, A. D. Density Functional Calculations of Molecular Bond Energies. *J.*

Chem. Phys. **1998**, *84* (8), 4524.

(14) Becke, A. D. Density-Functional Thermochemistry. III. The Role of Exact Exchange. *J. Chem. Phys.* **1998**, *98* (7), 5648.

(15) Lee, C.; Yang, W.; Parr, R. G. Development of the Colle-Salvetti Correlation-Energy Formula into a Functional of the Electron Density. *Phys. Rev. B* **1988**, *37* (2), 785.

(16) Austin, A.; Petersson, G. A.; Frisch, M. J.; Dobek, F. J.; Scalmani, G.; Throssell, K. A Density Functional with Spherical Atom Dispersion Terms. *J. Chem. Theory Comput.* **2012**, *8* (12), 4989–5007.

(17) McLean, A. D.; Chandler, G. S. Contracted Gaussian Basis Sets for Molecular Calculations. I. Second Row Atoms, Z=11–18. *J. Chem. Phys.* **2008**, *72* (10), 5639.

(18) Krishnan, R.; Binkley, J. S.; Seeger, R.; Pople, J. A. Self-Consistent Molecular Orbital Methods. XX. A Basis Set for Correlated Wave Functions. *J. Chem. Phys.* **2008**, *72* (1), 650.

(19) Reed, A. E.; Weinstock, R. B.; Weinhold, F. Natural Population Analysis. *J. Chem. Phys.* **1998**, *83* (2), 735.

(20) Bezdek, M. J.; Guo, S.; Chirik, P. J. Coordination-Induced Weakening of Ammonia, Water, and Hydrazine X–H Bonds in a Molybdenum Complex. *Science* **2016**, *354* (6313), 730–733.

(21) Bezdek, M. J.; Pelczer, I.; Chirik, P. J. Coordination-Induced N–H Bond Weakening in a Molybdenum Pyrrolidine Complex: Isotopic Labeling Provides Insight into the Pathway for H2 Evolution. *Organometallics* **2020**, *39* (16), 3050–3059.

(22) Pappas, I.; Chirik, P. J. Catalytic Proton Coupled Electron Transfer from Metal Hydrides to Titanocene Amides, Hydrazides and Imides: Determination of Thermodynamic Parameters Relevant to Nitrogen Fixation. *J. Am. Chem. Soc.* **2016**, *138*, 13379−13389.

(23) Paradas, M.; Campaña, A. G.; Jimé Nez, T.; Robles, R.; Oltra, J. E.; Buñ, E.; Justicia, J.; Cá, D. J.; Cuerva, J. M. Understanding the Exceptional Hydrogen-Atom Donor Characteristics of Water in TiIII-Mediated Free-Radical Chemistry. *J. Am. Chem. Soc.* **2010**, *132*, 12748–12756.

(24) Chciuk, T. V; Flowers, R. A. Proton-Coupled Electron Transfer in the Reduction of Arenes by SmI2-Water Complexes. *J. Am. Chem. Soc.* **2015**, *137*, 11526−11531.

(25) Maity, S.; Flowers, R. A.; Hoz, S. Aza versus Oxophilicity of SmI2 : A Break of a

Paradigm. *Chem. - A Eur. J.* **2017**, *23* (67), 17070–17077.

(26) Chciuk, T. V; Li, A. M.; Vazquez-Lopez, A.; Anderson, W. R.; Flowers, R. A. Secondary Amides as Hydrogen Atom Transfer Promoters for Reactions of Samarium Diiodide. *Org. Lett.* **2016**, *19*, 290−293.

(27) Ramírez-Solís, A.; Bartulovich, C. O.; León-Pimentel, C. I.; Saint-Martin, H.; Boekell, N. G.; Flowers, R. A. Proton Donor Effects on the Reactivity of SmI2. Experimental and Theoretical Studies on Methanol Solvation vs. Aqueous Solvation. *Dalt. Trans.* **2020**, *49* (23), 7897–7902.

(28) Chciuk, T. V.; Anderson, W. R.; Flowers, R. A. High-Affinity Proton Donors Promote Proton-Coupled Electron Transfer by Samarium Diiodide. *Angew. Chemie Int. Ed.* **2016**, *55* (20), 6033–6036.

(29) Kepp, K. P. A Quantitative Scale of Oxophilicity and Thiophilicity. *Inorg. Chem.* **2016**, *55* (18), 9461–9470.

Chapter 8: Conclusion

The work discussed in this dissertation focuses on the investigation of coordination-induced bond weakening in divalent samarium reagents. The research presented herein was performed to elucidate the reactivity and mechanisms of reduction of Sm(II) reagents. Given the broad scope of ligands that undergo bond weakening upon coordination to Sm(II), divalent samarium provided a useful platform for the investigation of the physical basis of coordination-induced bond weakening.

Chapter 2 in this dissertation describes investigations into the scope and mechanism of the selective reductions of pyridines and quinolines by SmI_2-water. The facile reduction of these substrates under mild conditions is remarkable given their typical recalcitrance to single electron reduction. Substitution of the SmI_2-water reagent with SmI_2-deuterium oxide was found to afford convenient access to a range of selectively deuterated piperidine and 1,2,3,4-tetrahydroquinoline products. Moreover, selectively reduced polycyclic dimers of the pyridine and quinoline substrates were isolated and characterized. Steric occlusion of the 2- and 3-positions of the pyridine ring in these substrates was found to mitigate dimer formation, allowing for a degree of steric control over the product distribution in the reductions of pyridines and quinolines by SmI_2-water.

The mechanisms of oxime and oxime ether reductions by SmI_2 and SmI_2-water were investigated in Chapter 3. Kinetic studies revealed a rate limiting initial PCET in the reduction of substrates by SmI_2-water and a rate limiting initial ET in the reduction of substrates by dry SmI_2. Additionally, unactivated oximes and oxime ethers were found to be more stable than activated oximes and oxime ethers against reduction by both SmI_2

and SmI_2-water. These results were combined with computational modeling of the stability of the products of substrate C=N and N-O bond reduction to propose initial C=N bond reduction by both SmI_2 and SmI_2-water. These mechanisms are consistent with the body of literature reports of oxime reductions by Sm(II) reagents.

In Chapter 4, the basis of the remarkable stability of the SmI_2-water reagent against H_2 gas evolution was examined. Kinetic studies ruled out rate limiting self-association between Sm(II)-water complexes due to coulombic repulsion as a barrier to H_2 gas evolution. Moreover, deuterium labeling studies ruled out H-atom abstraction from the bulk THF solvent as a pathway for H_2 gas evolution from SmI_2-water. Density functional theory modeling of H-atom loss from a family of seven-coordinate $Sm^{II}(THF)_n(H_2O)_m$ complexes (n + m = 7) complexes was also performed by Vlaisavljevich and coworkers at the University of South Dakota. The results revealed nearly isoenergetic free energies of H-atom loss between the complexes modeled. Notably, these free energies of H-atom loss were similar to the free energy of activation measured for the evolution of H_2 gas from SmI_2-water. The barrier to H_2 gas evolution from SmI_2-water was therefore proposed to be the enthalpic O-H bond activation necessary for the Sm(II)-water complex to reduce the strong O-H bond of a second molecule of water.

In the fifth chapter of this dissertation, investigations of the SmI_2-ammonia reductant and comparison to the SmI_2-water reductant are discussed. Synthetic studies revealed a remarkable degree of similarity between the reactivity of the SmI_2-ammonia and SmI_2-water reagents with arenes. Further similarities in the coordination numbers and structures of the Sm(II)-ammonia and Sm(II)-water complexes were revealed by

BOMD-DFT simulations performed by Ramírez-Solís and coworkers at Universidad Autónoma del Estado de Morelos, Facultad de Química, and Instituto de Ciencias Físicas. Kinetic studies on the reduction of acenaphthalene by both systems revealed further similarities between the SmI_2-ammonia and SmI_2-water systems under synthetic conditions. However, it was also observed that the greater affinity of Sm(II) for nitrogen than for oxygen enables the formation of a potent Sm(II) reductant at lower concentrations of ammonia than water in solution. Finally, comparison with other coordination-induced ammonia N-H bond weakening systems revealed that coordination of ammonia to Sm(II) induces the greatest degree of N-H bond weakening in ammonia reported to date.

Chapter 6 focuses on the development of the $SmBr_2$-NMEA reducing system, which was informed by the thermodynamic relationship between Sm(II)-ligand affinity and degree of coordination-induced bond weakening experienced by the ligand. The $SmBr_2$-NMEA system was found to reduce a number of challenging arenes, including some that are commonly reduced using lithium metal in liquid ammonia. Diverse functionalized substrates including alkynes and unactivated methyl esters were also found to be amenable to reduction by $SmBr_2$-NMEA under mild conditions. Moreover, reduction of unactivated esters with pendant olefin groups was found to induce 5-*exo*-trig cyclization yielding primary alcohols. Analogs to intermediates of the nitrogen fixation process were also investigated as substrates for reduction by $SmBr_2$-NMEA. Gratifyingly, both the N=N double bond of azobenzene and the N-N single bond of phenylhydrazine were readily reduced by $SmBr_2$-NMEA.

Finally, Chapter 7 discusses the investigation of the hypothesis that backdonation

from a low-valent metal into a ligand C-H σ*-antibonding orbital provides the driving force for observed coordination-induced bond weakening phenomena. Analysis of ^{1}H NMR spectra of methyl crotonate in the presence of low-valent Sm, Yb, and Ti complexes revealed shielding of the ligand β-proton consistent with backdonation from each low-valent metal complex. Computationally determined ligand $\Delta E_{\sigma-\sigma^*}$ values were the plotted against ΔBDFE values for the same ligands upon coordination to four different low-valent metal complexes. The significant correlations in these plots was interpreted as evidence of backdonation from a low-valent metal into a ligand X-H σ*-antibonding orbital as a significant driving force for coordination-induced bond weakening.

In summary, the work presented in this dissertation has demonstrated the reduction of substrates that are commonly reduced via catalytic hydrogenation or Birch reduction under mild conditions using Sm(II)-proton donor reagents. Moreover, the mechanistic elucidation of both substrate reduction and H_2 gas evolution by Sm(II)-proton donor reagents herein has the potential to inform the future use of Sm(II) coordination-induced bond weakening systems in synthesis. Finally, evidence of backdonation from several low-valent metals into ligand X-H σ*-antibonding orbitals provides insight into the physical basis of coordination-induced bond weakening and enables rational design of novel coordination-induced bond weakening systems.

Chapter 9. Appendix

9.1 Studies of the Reductions of Pyridines and Quinolines by SmI_2-Water

9.1.1 ^{1}H NMR Data

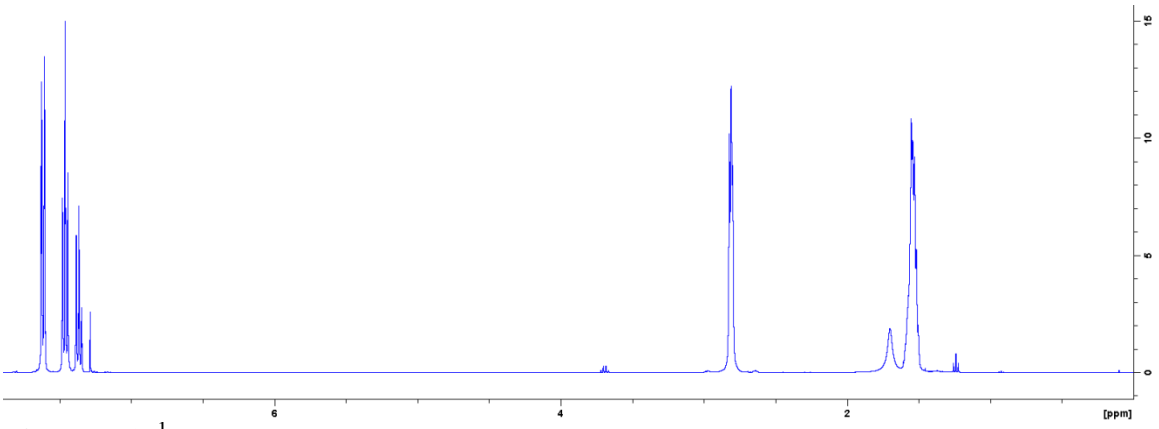

Figure 9.1. ^{1}H NMR spectrum of piperidine

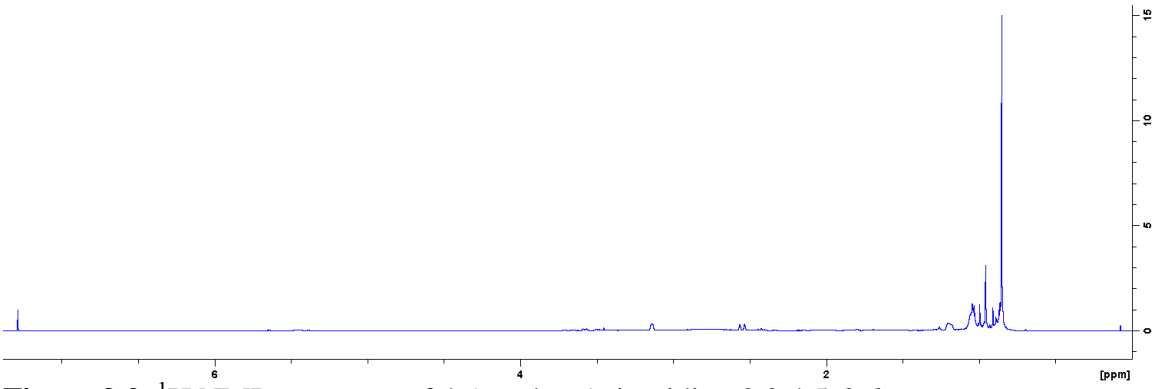

Figure 9.2. ^{1}H NMR spectrum of 4-(*tert*-buty)piperidine-2,3,4,5,6-d_5

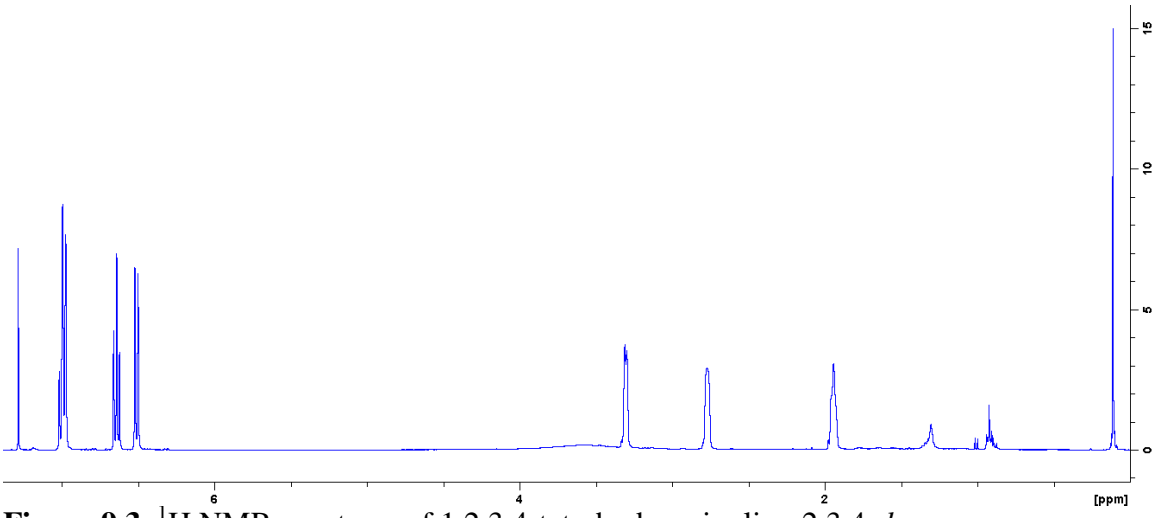

Figure 9.3. ^{1}H NMR spectrum of 1,2,3,4-tetrahydroquinoline-2,3,4-d_3

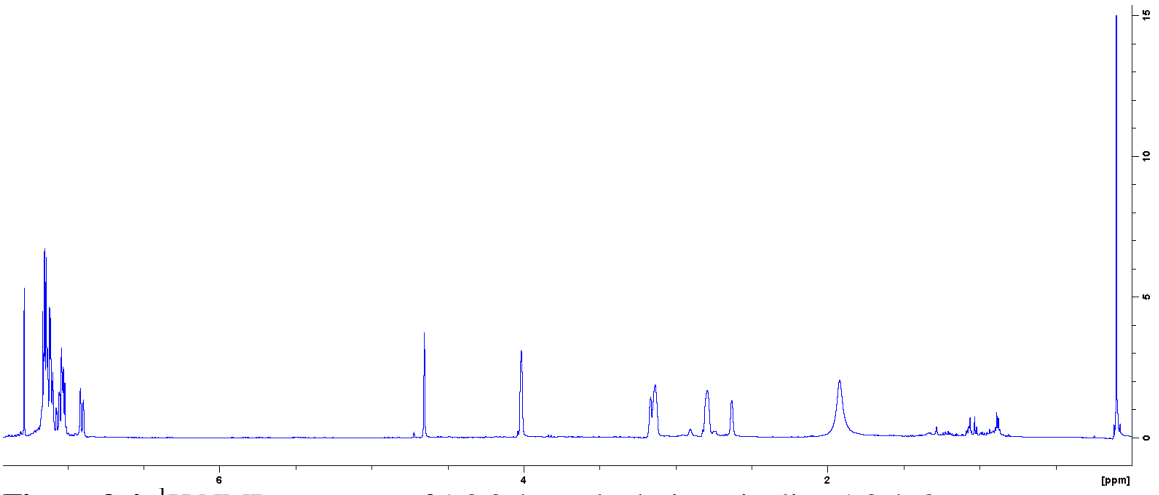

Figure 9.4. ^{1}H NMR spectrum of 1,2,3,4-tetrahydroisoquinoline-1,3,4-d_3

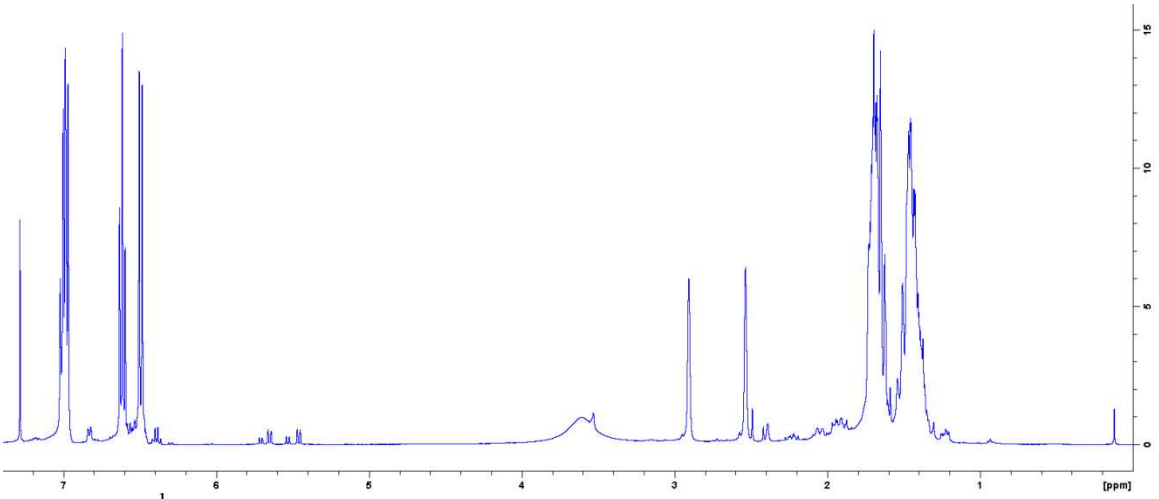

Figure 9.5. ^{1}H NMR spectrum of 1,2,3,4,4a,9,9a,10-octahydroacridine-4a,9,9a-d_3

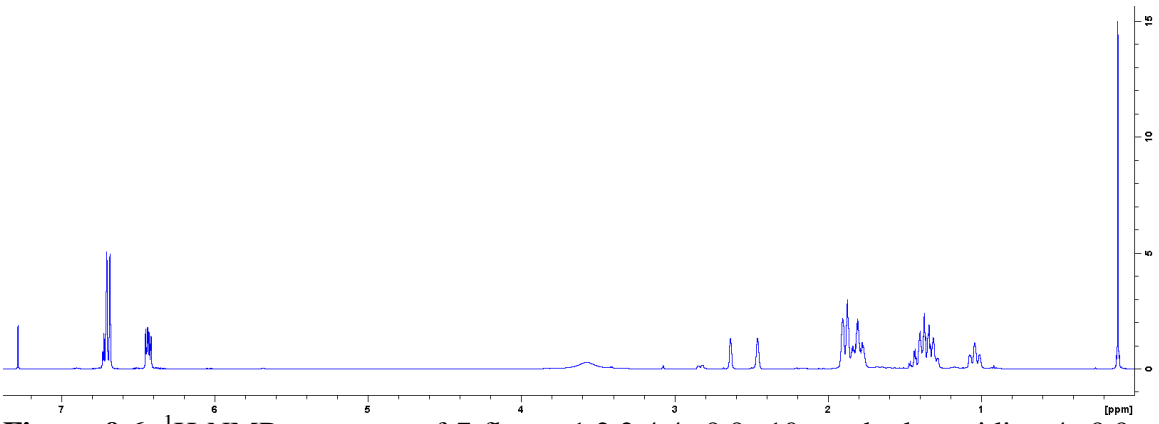

Figure 9.6. ^{1}H NMR spectrum of 7-fluoro-1,2,3,4,4a,9,9a,10-octahydroacridine-4a,9,9a-d_3

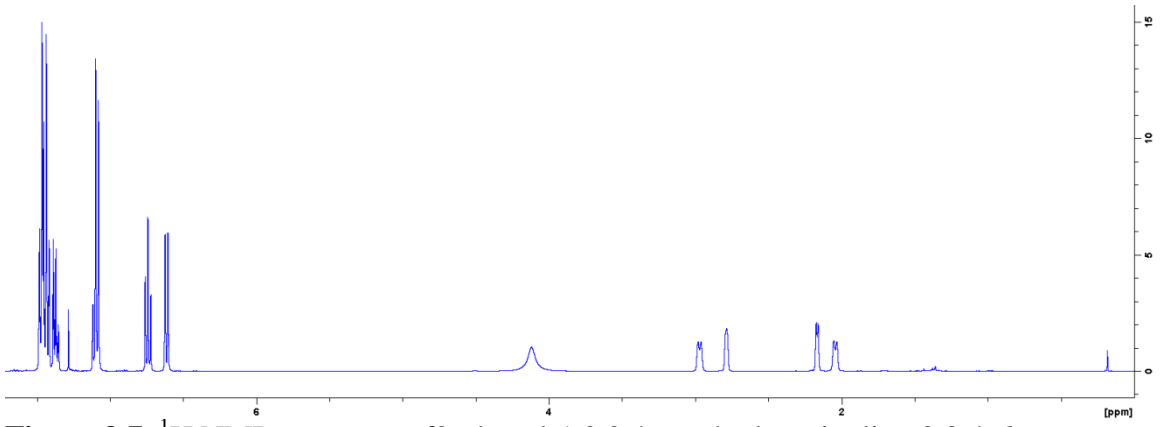

Figure 9.7. ^{1}H NMR spectrum of2-phenyl-1,2,3,4-tetrahydroquinoline-2,3,4-d_3

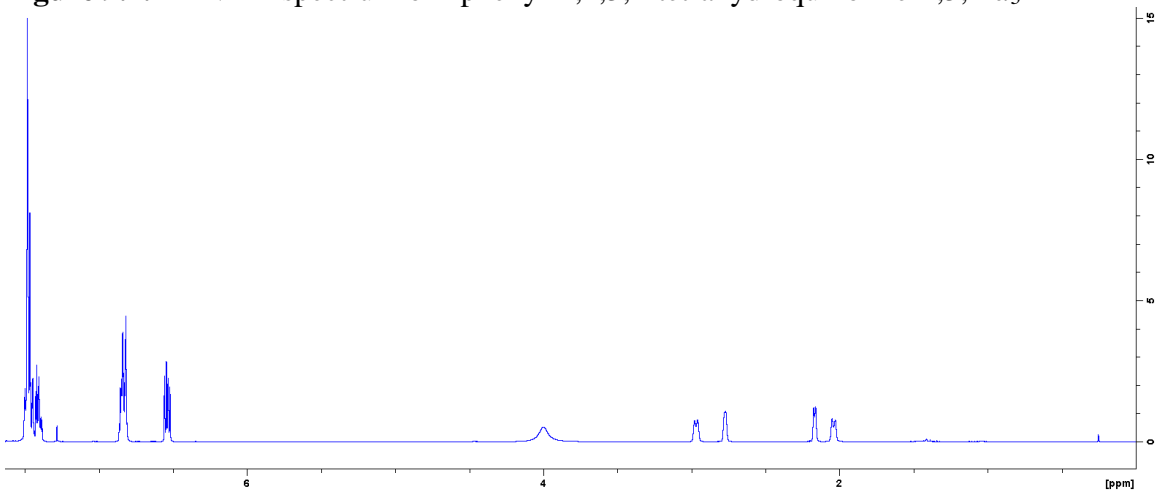

Figure 9.8. ^{1}H NMR spectrum of 6-fluoro-2-phenyl-1,2,3,4-tetrahydroquinoline-2,3,4-d_3

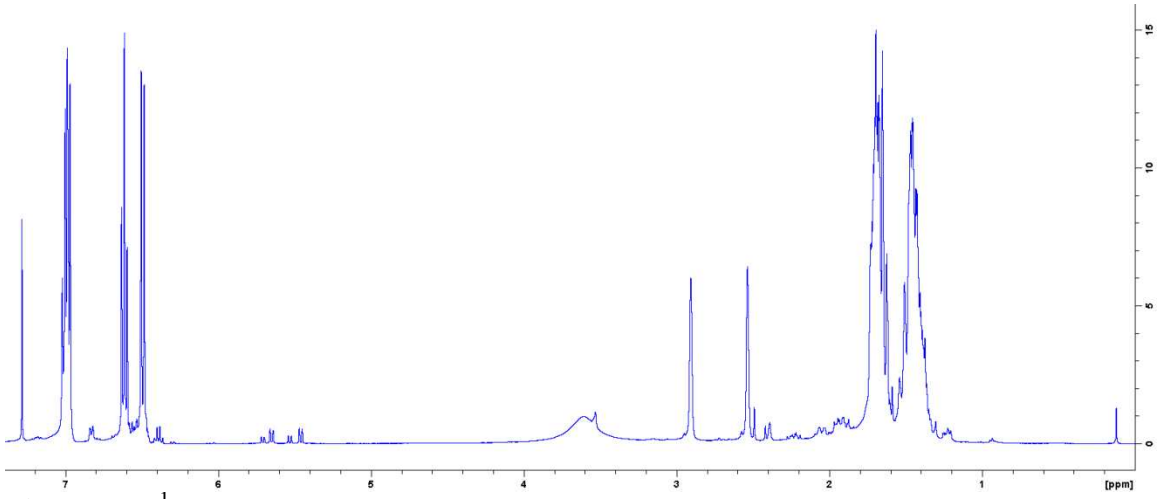

Figure 9.9. ^{1}H NMR spectrum of 5,6,6a,7,12,12a-hexahydrobenzo[c]acridine-6a,7,12a-d_3

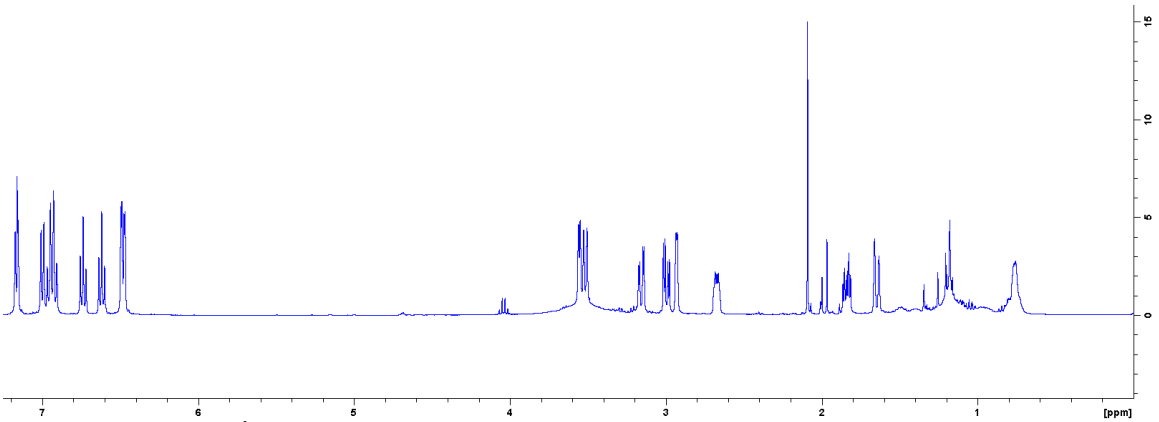

Figure 9.10. ^{1}H NMR spectrum of 5a,6,11,12,12a,13-hexahydro-5H-6,12-methanobenzo[6,7]azepino[4,3-b]quinoline

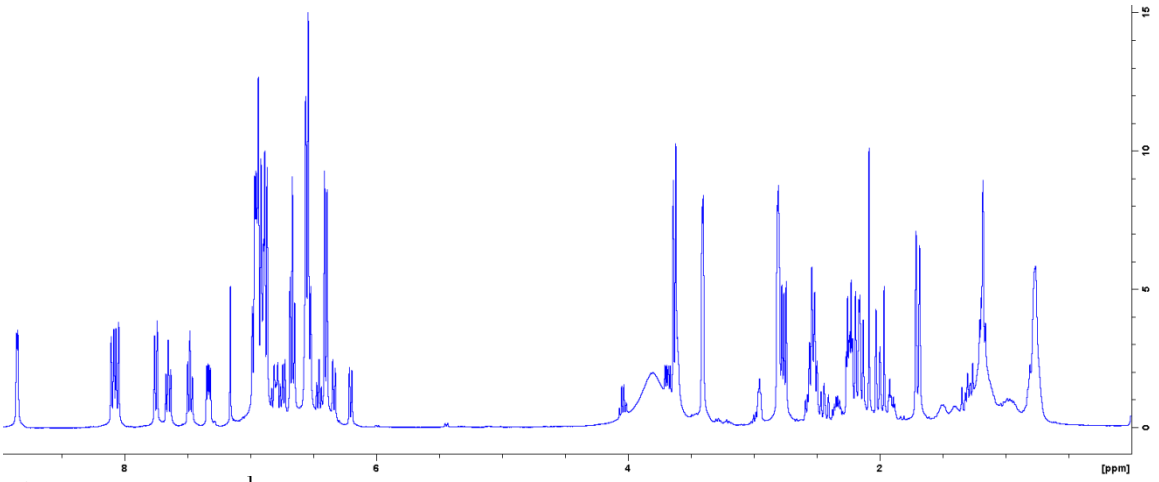

Figure 9.11. ^{1}H NMR spectrum of 5a,6,7,12,12a,13-hexahydro-5H-6,12-methanobenzo[6,7]azepino[3,4-b]quinoline

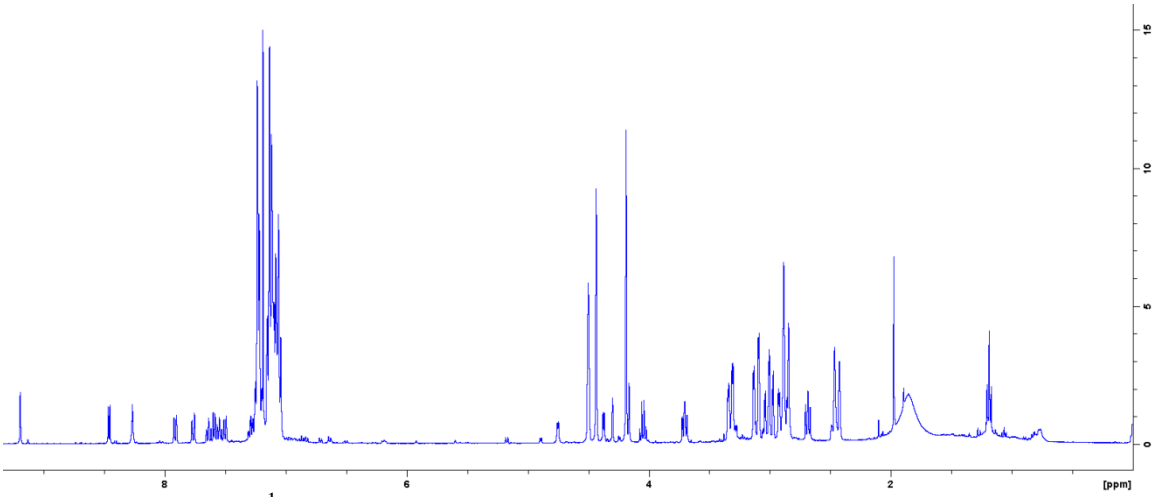

Figure 9.12. ^{1}H NMR spectrum of 5,6,8,13,13a,14-hexahydro-6,14-methanobenzo[4,5][1,3]diazepino[1,7-b]isoquinoline

9.1.2 ^{13}C NMR Data

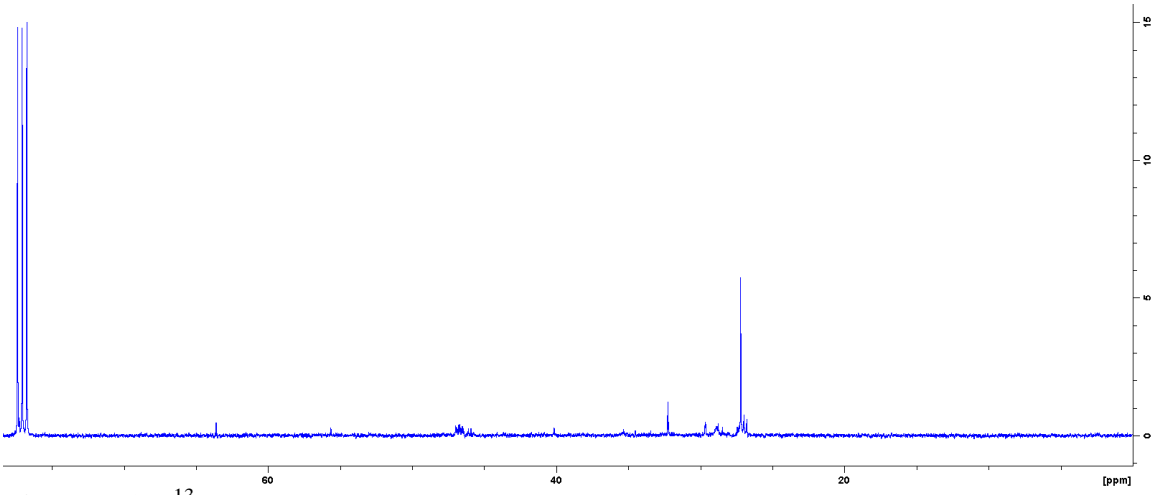

Figure 9.13. ^{13}C NMR spectrum of 4-(*tert*-buty)piperidine-2,3,4,5,6-d_5

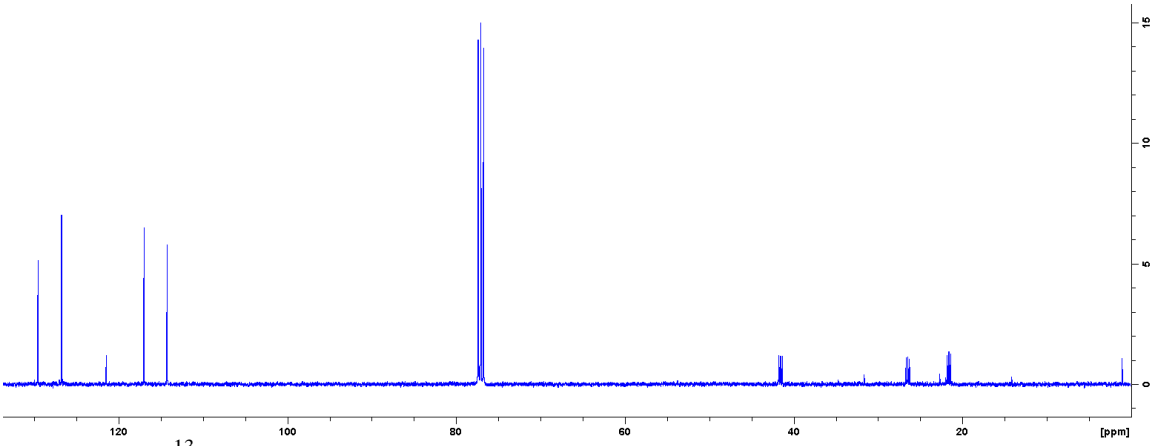

Figure 9.14. ^{13}C NMR spectrum of 1,2,3,4-tetrahydroquinoline-2,3,4-d_3

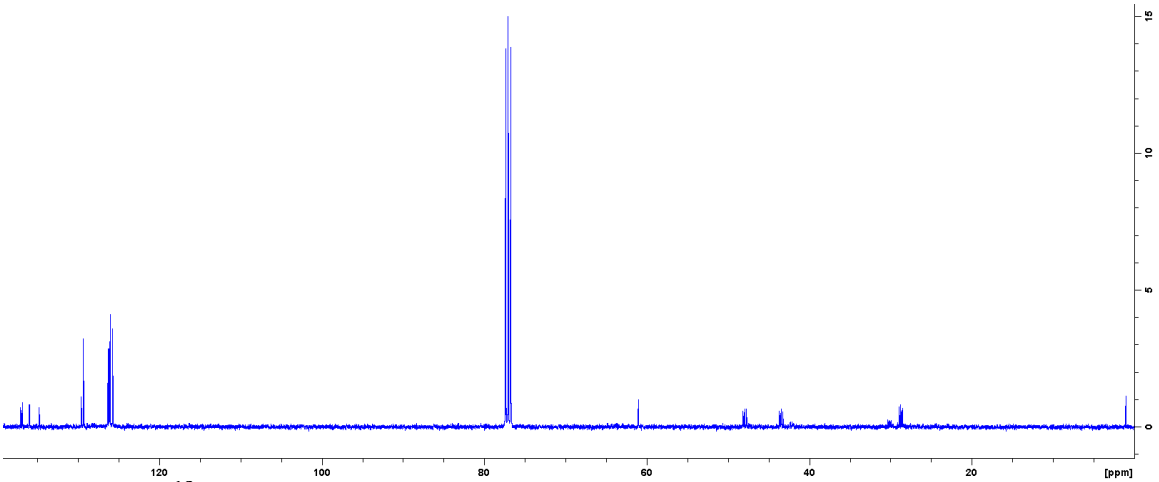

Figure 9.15. ^{13}C NMR spectrum of 1,2,3,4-tetrahydroisoquinoline-1,3,4-d_3

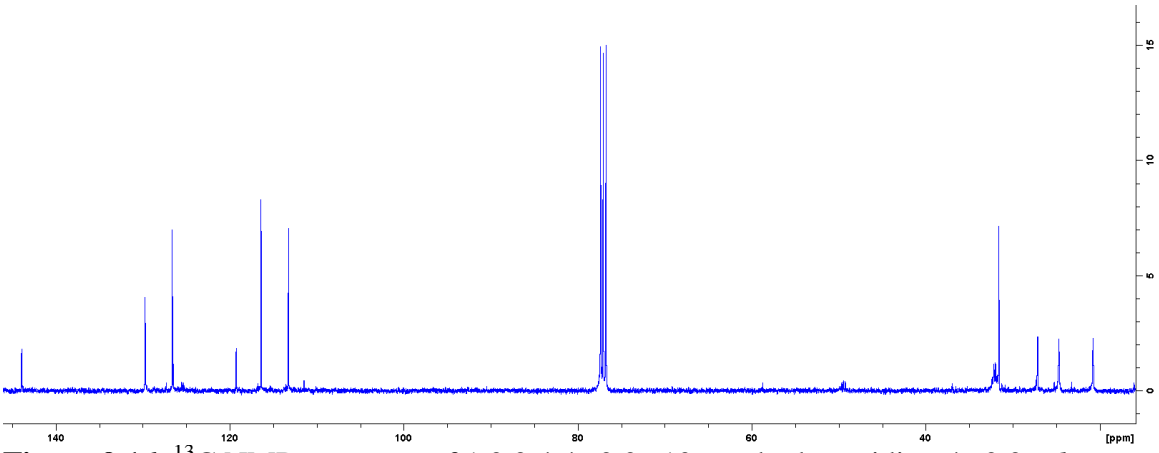

Figure 9.16. ^{13}C NMR spectrum of 1,2,3,4,4a,9,9a,10-octahydroacridine-4a,9,9a-d_3

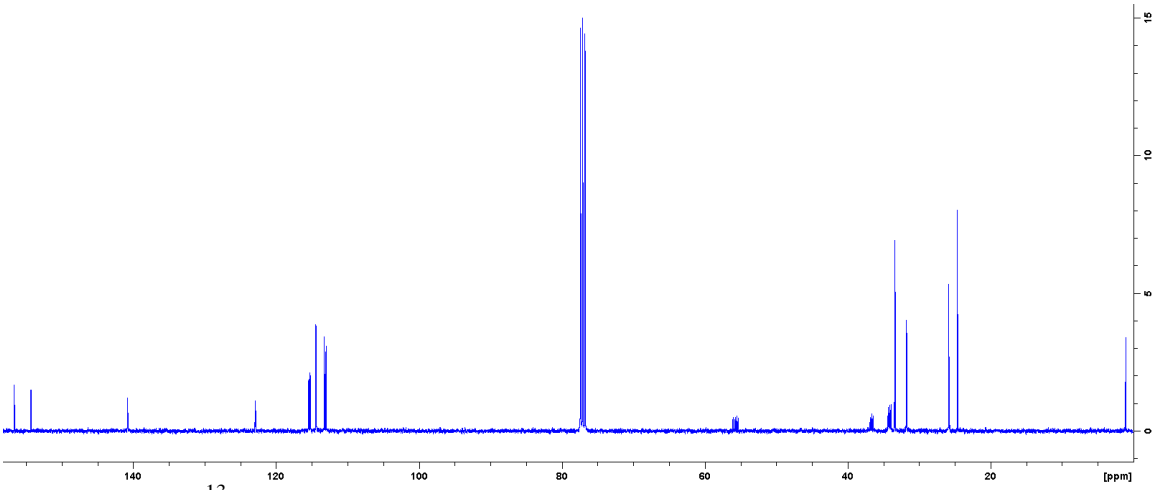

Figure 9.17. ^{13}C NMR spectrum of 7-fluoro-1,2,3,4,4a,9,9a,10-octahydroacridine-4a,9,9a-d_3

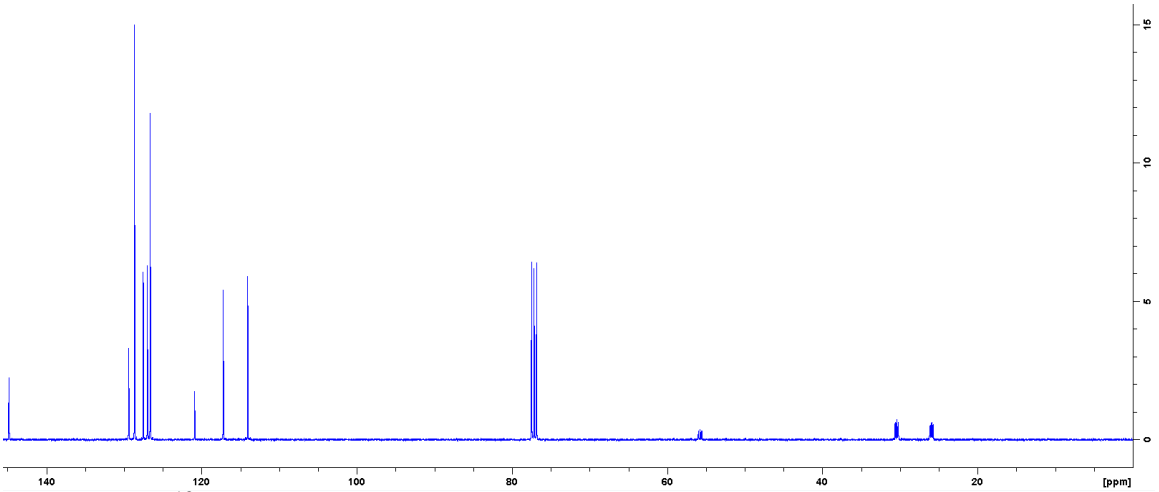

Figure 9.18. ^{13}C NMR spectrum of 2-phenyl-1,2,3,4-tetrahydroquinoline-2,3,4-d_3

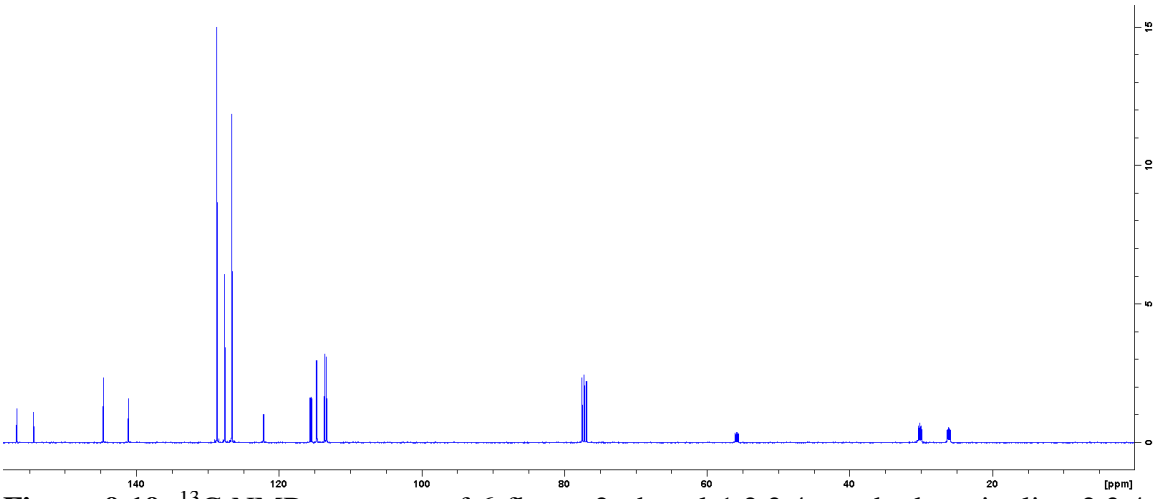

Figure 9.19. ^{13}C NMR spectrum of 6-fluoro-2-phenyl-1,2,3,4-tetrahydroquinoline-2,3,4-d_3

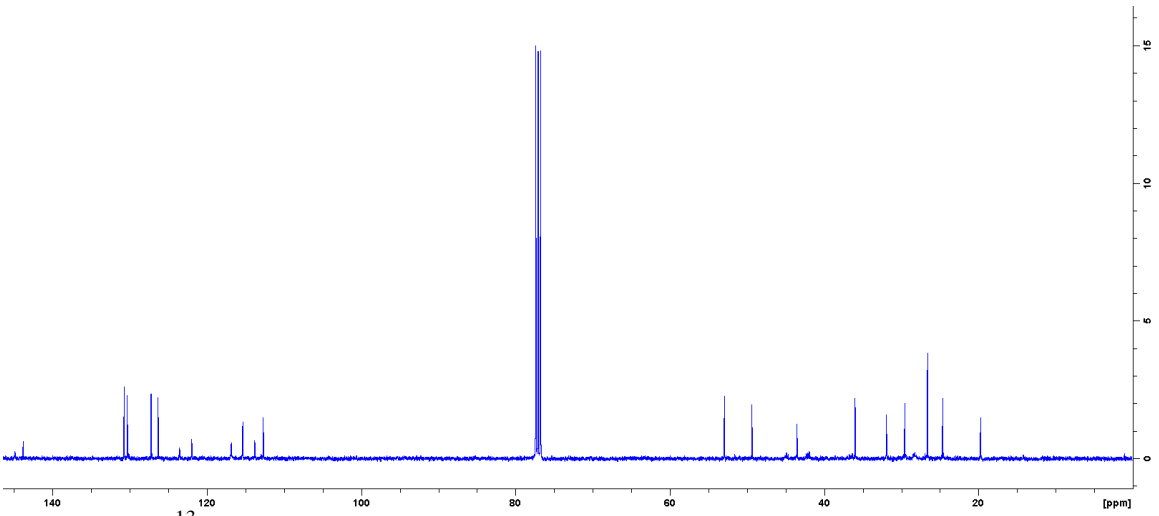

Figure 9.20. ^{13}C NMR spectrum of 5,6,6a,7,12,12a-hexahydrobenzo[c]acridine-6a,7,12a-d_3

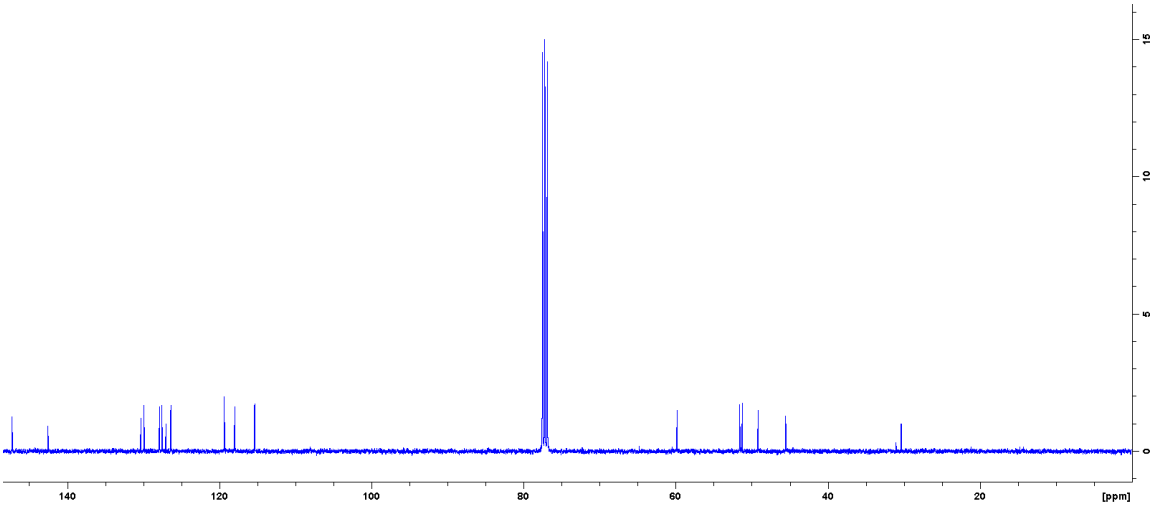

Figure 9.21. ^{13}C NMR spectrum of 5a,6,11,12,12a,13-hexahydro-5H-6,12-methanobenzo[6,7]azepino[4,3-b]quinoline

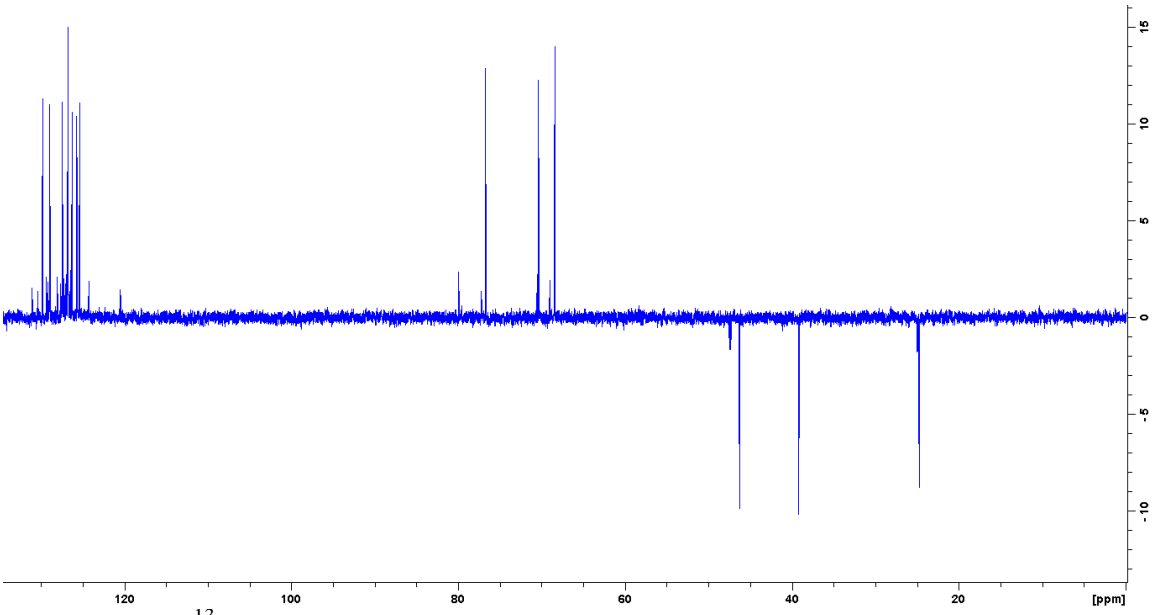

Figure 9.22. ^{13}C DEPT145 NMR spectrum of 5a,6,7,12,12a,13-hexahydro-5H-6,12-methanobenzo[6,7]azepino[3,4-b]quinoline

9.1.3 Kinetics Data

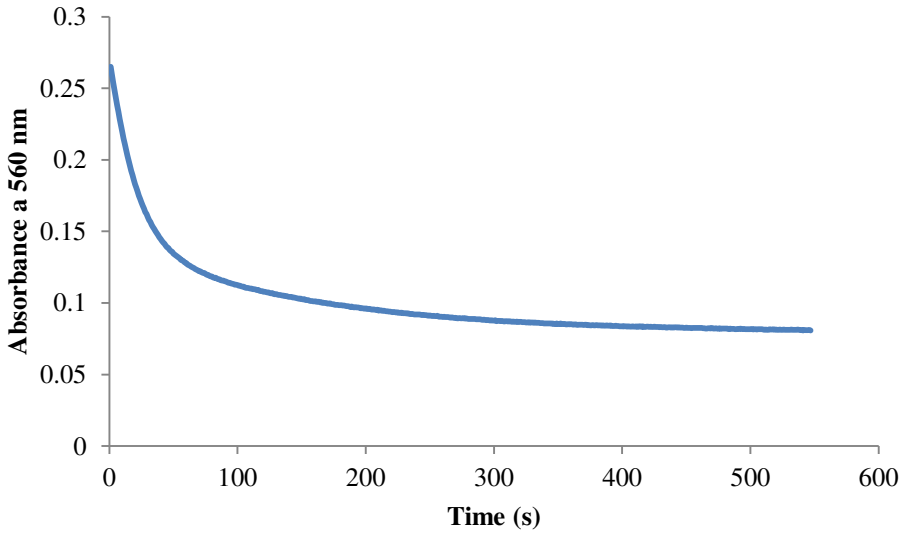

Figure 9.23. Representative plot of the decay curve for SmI_2 at 560 nm in the presence of mM pyridine and water

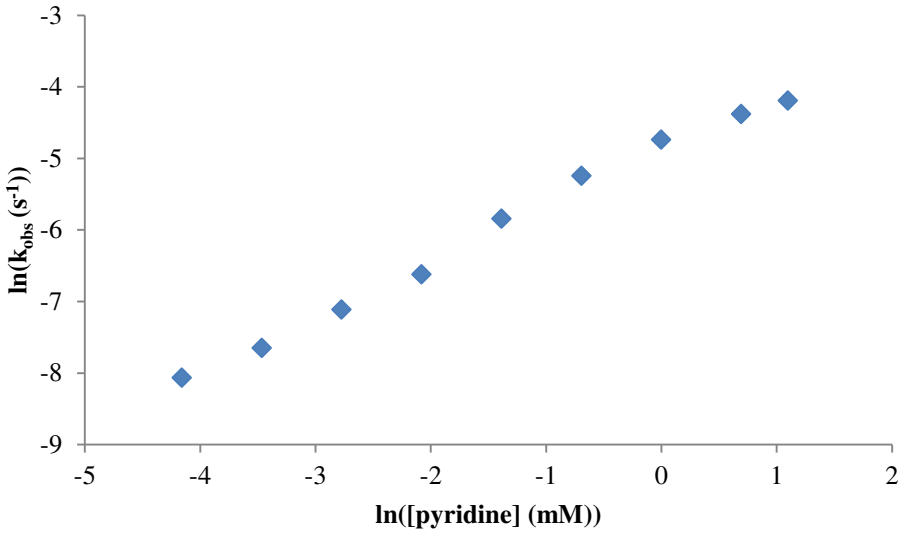

Figure 9.24. Plot of ln(k_{obs}) vs ln([pyridine]) for the reduction of pyridine by SmI_2-water

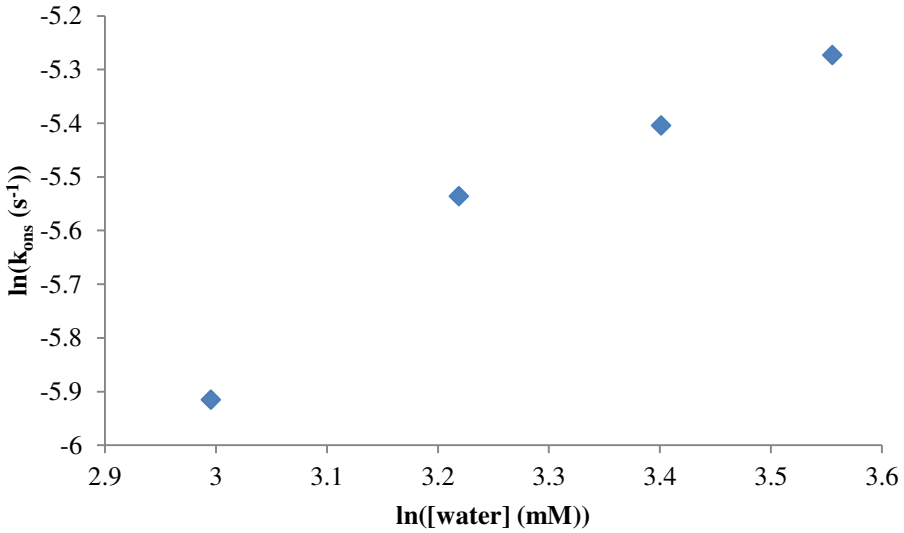

Figure 9.25. Plot of ln(k_{obs}) vs ln([water]) for the reduction of pyridine by SmI_2-water

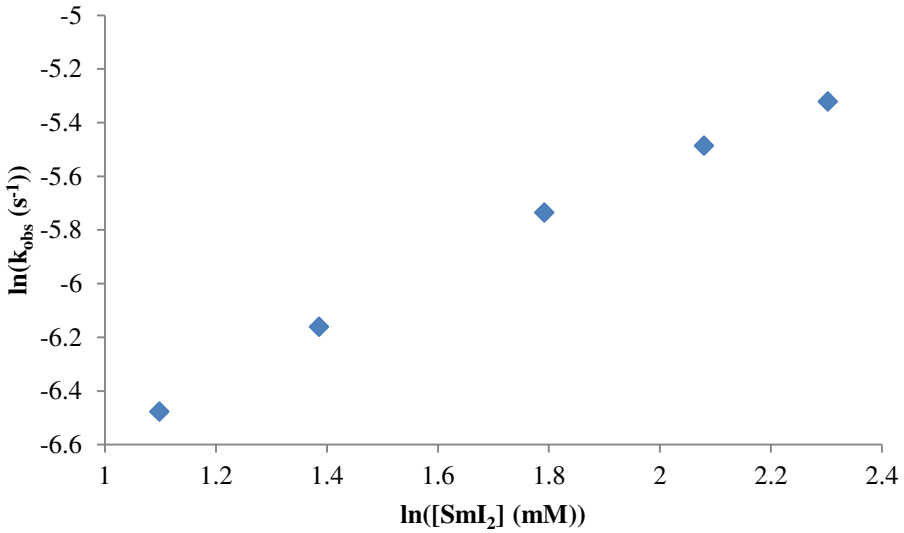

Figure 9.26. Plot of $\ln(k_{obs})$ vs $\ln([SmI_2])$ for the reduction of pyridine by SmI_2-water

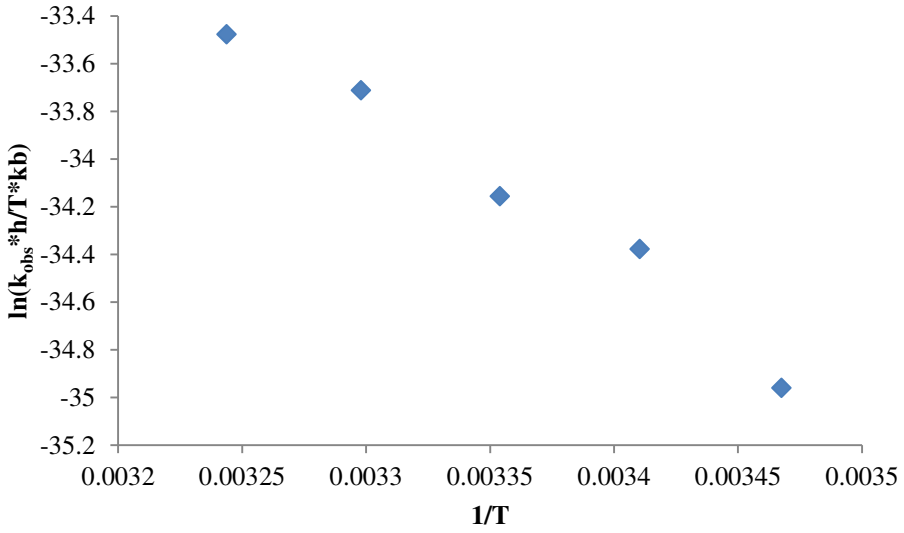

Figure 9.27. Plot of $\ln(k_{obs}*h/T*kb)$ vs 1/T for the reduction of pyridine by SmI_2-water

9.1.4 Computational Details

Gaussian09 programs were used for the calculations with the APF-D hybrid DFT method and the 6-311+G(2d,p) basis set.[1–4] Natural-population analysis was obtained by including pop=npa.[5] Solvation values were calculated using the polarizable continuum model with integral equation formalism IEFPCM with tetrahydrofuran as the solvent.[6,7]

The geometries and frequencies were calculated with the keywords uapfd/6-311+g(2d,p) opt=(calcfc,tight) int=(ultrafine,acc2e=12) pop=npa scrf=(iefpcm,solvent=thf)

9.2 Investigation of the Mechanism of Reduction of Oximes and Oxime Ethers by Divalent Samarium

9.2.1 ^{1}H NMR Data

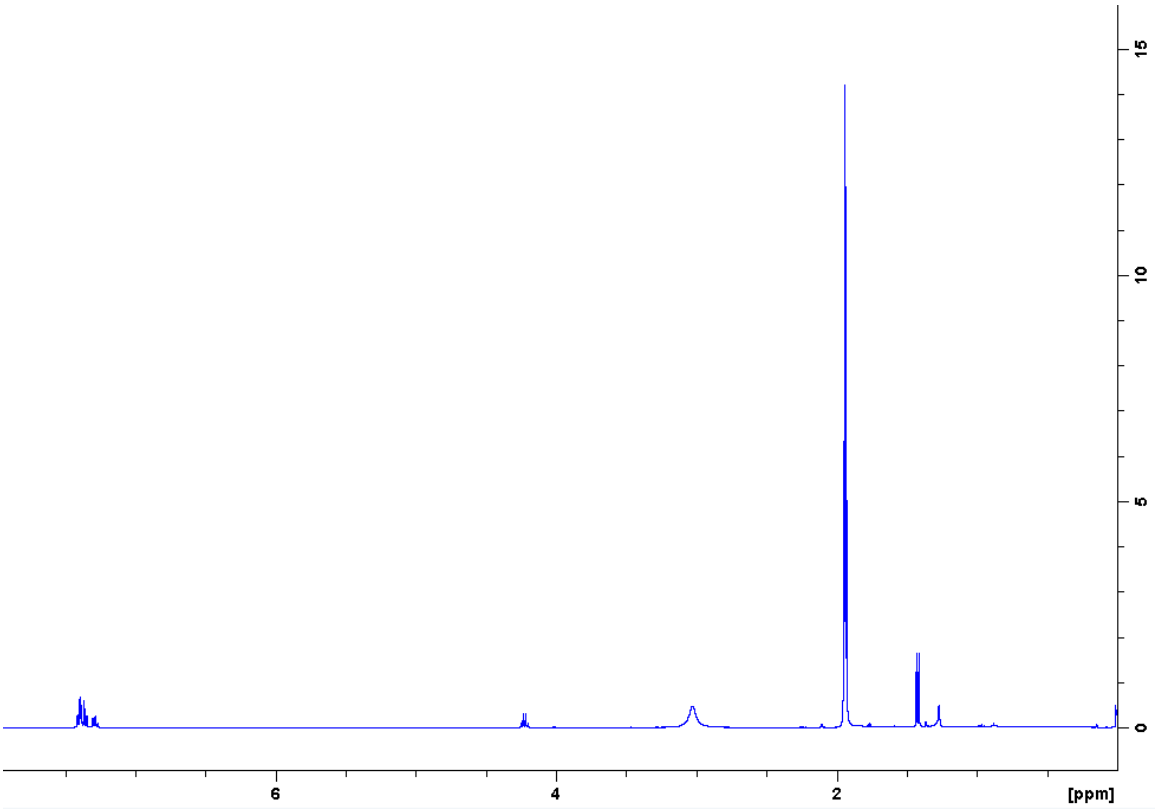

Figure 9.28. ^{1}H NMR spectrum of 1-phenylethan-1-amine

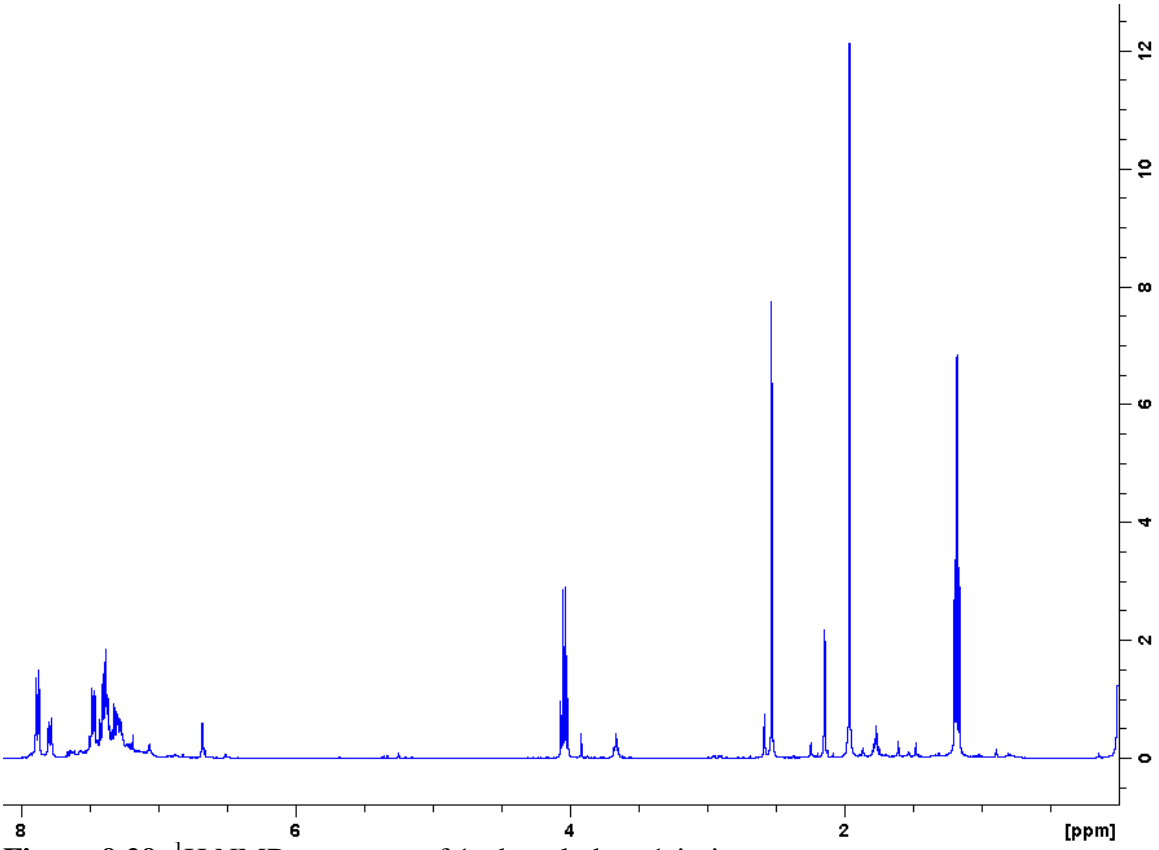

Figure 9.29. ^{1}H NMR spectrum of 1-phenylethan-1-imine

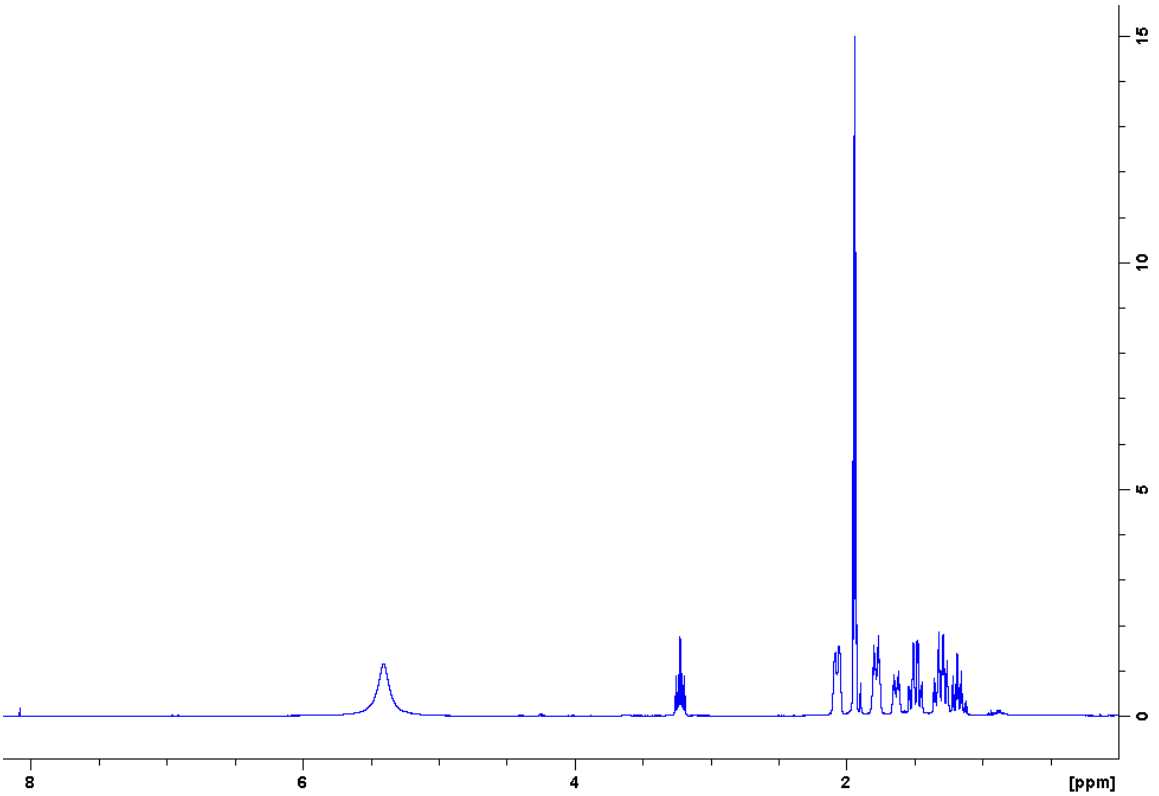

Figure 9.30. ^{1}H NMR spectrum of cyclohexanamine

9.2.2 Kinetics Data

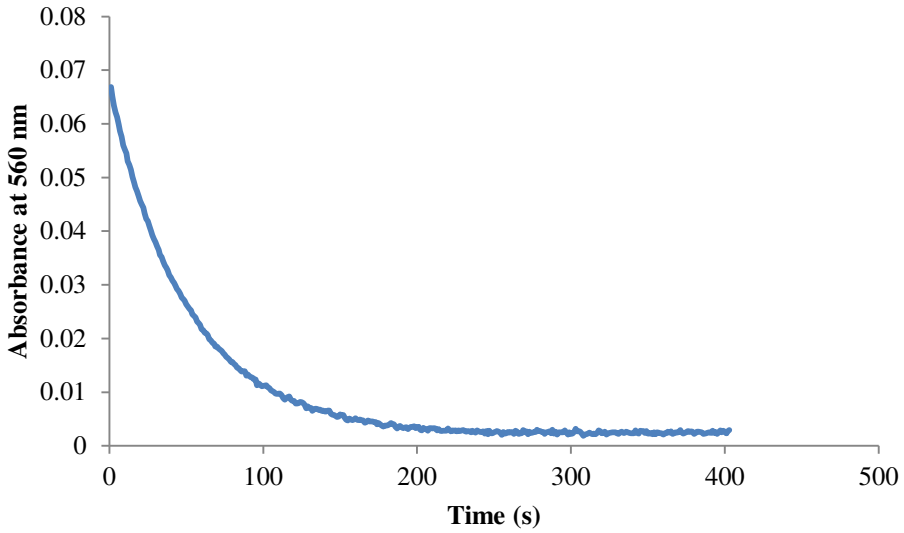

Figure 9.31. Representative plot of the decay curve for SmI_2 at 560 nm in the presence of cyclohexanone oxime and water

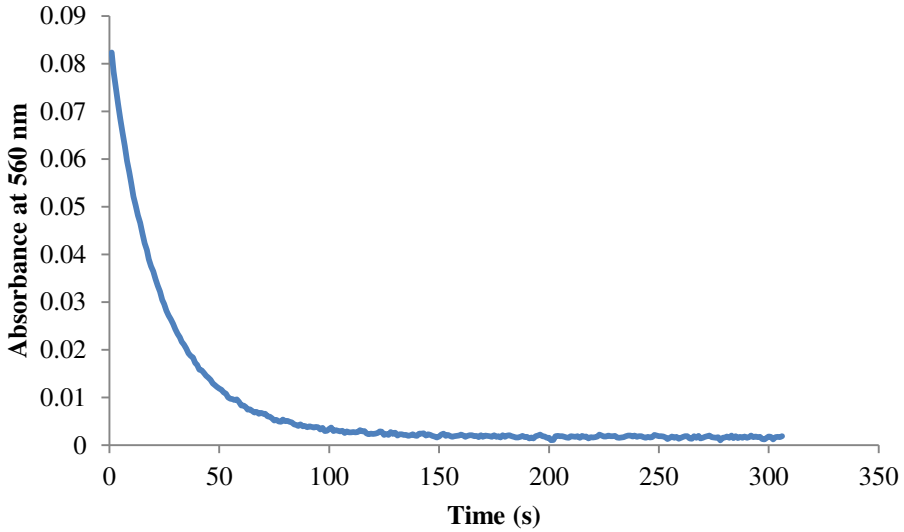

Figure 9.32. Representative plot of the decay curve for SmI_2 at 560 nm in the presence of acetophenone O-methyl oxime

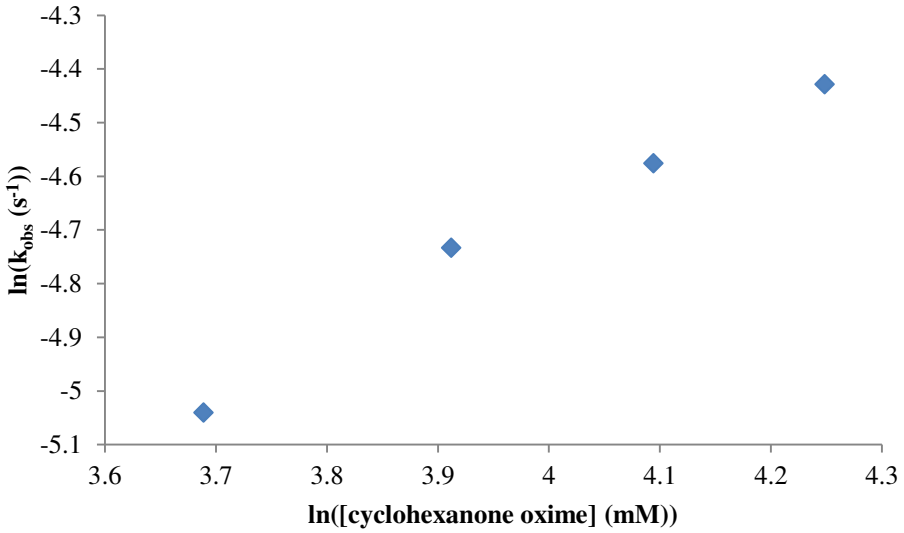

Figure 9.33. Plot of $\ln(k_{obs})$ vs ln([cyclohexanone oxime]) for the reduction of cyclohexanone oxime by SmI_2-water

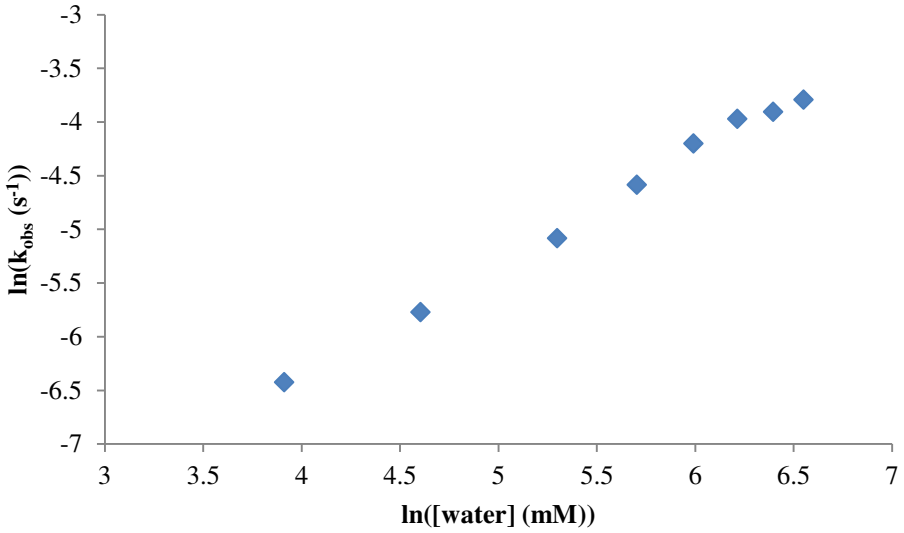

Figure 9.34. Plot of $\ln(k_{obs})$ vs ln([water]) for the reduction of cyclohexanone oxime by SmI_2-water

$A_{0\text{-}1}$	0.199255	0.164414	0.163283	0.176798	0.193219
$A_{0\text{-}2}$	0.211128	0.195451	0.196674	0.206369	0.221406
$A_{0\text{-}3}$	0.149204	0.219146	0.207487	0.222549	0.242937
$A_{1/2\text{-}1}$	0.100051	0.082878	0.082457	0.088409	0.09737
$A_{1/2\text{-}2}$	0.105689	0.098517	0.098446	0.103522	0.111274
$A_{1/2\text{-}3}$	0.075274	0.11001	0.104175	0.11164	0.122895
$A_{3/4\text{-}1}$	0.05009	0.041156	0.041195	0.044645	0.048387
$A_{3/4\text{-}2}$	0.052819	0.049081	0.049551	0.051685	0.055395

$A_{3/4-3}$	0.037912	0.054947	0.052475	0.055819	0.060916
$t_{1/2-1}$	103	74	60	58	55
$t_{1/2-2}$	112	78	64	58	56
$t_{1/2-3}$	101	73	67	60	69
$t_{3/4-1}$	208	134	105	100	96
$t_{3/4-2}$	233	161	133	118	115
$t_{3/4-3}$	221	160	139	127	156
$(t_{3/4}-t_{1/2})/t_{1/2-1}$	1.019417	0.810811	0.75	0.724138	0.745455
$(t_{3/4}-t_{1/2})/t_{1/2-2}$	1.080357	1.064103	1.078125	1.034483	1.053571
$(t_{3/4}-t_{1/2})/t_{1/2-3}$	1.188119	1.191781	1.074627	1.116667	1.26087
$(t_{3/4}-t_{1/2})/t_{1/2-avg}$	1.095964	1.022231	0.967584	0.958429	1.019965

Table 9.1. Fractional times table to calculate the rate order of SmI_2 in the reduction of cyclohexanone oxime by SmI_2-water

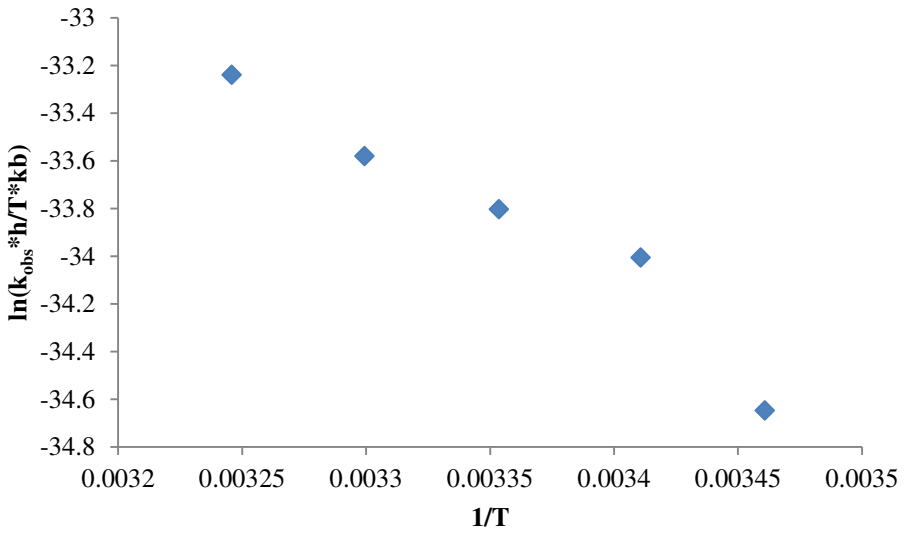

Figure 9.35. Plot of $\ln(k_{obs}*h/T*kb)$ vs 1/T for the reduction of cyclohexanone oxime by SmI_2-water

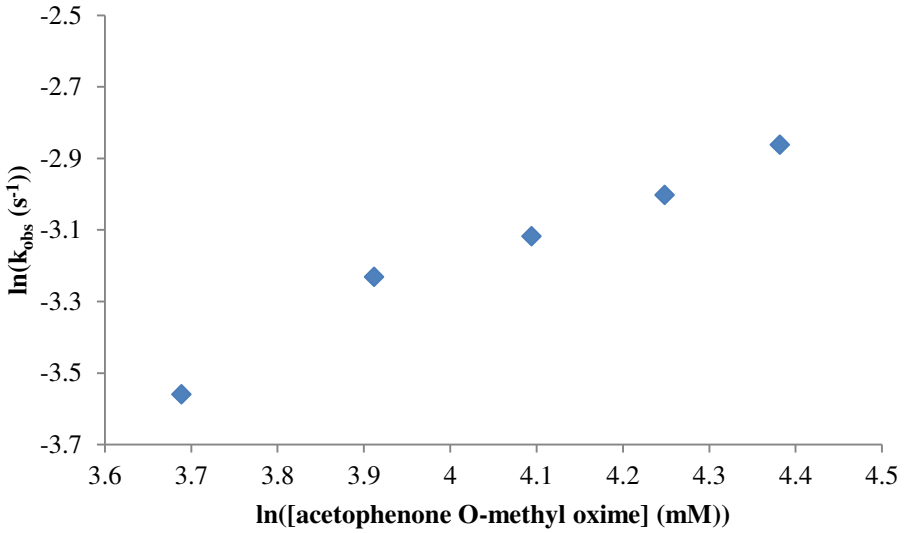

Figure 9.36. Plot of ln(k_{obs}) vs ln([acetophenone O-methyl oxime]) for the reduction of acetophenone O-methyl oxime by SmI_2

	40mM	50mM	60mM	70mM	80mM
$A_{0\text{-}1}$	0.08038	0.082323	0.094182	0.07403	0.082197
$A_{0\text{-}2}$	0.151603	0.159855	0.162849	0.164889	0.167021
$A_{0\text{-}3}$	0.149204	0.196791	0.193429	0.199007	0.18041
$A_{1/2\text{-}1}$	0.0402	0.04236	0.04786	0.038147	0.041843
$A_{1/2\text{-}2}$	0.076174	0.080855	0.083773	0.08552	0.085773
$A_{1/2\text{-}3}$	0.075274	0.100809	0.097438	0.102558	0.092129
$A_{3/4\text{-}1}$	0.020216	0.021095	0.024289	0.019101	0.021873
$A_{3/4\text{-}2}$	0.038364	0.040551	0.041812	0.042294	0.042803
$A_{3/4\text{-}3}$	0.037912	0.049466	0.048878	0.050919	0.046725
$t_{1/2\text{-}1}$	24	22	21	20	18
$t_{1/2\text{-}2}$	26	19	17	15	14
$t_{1/2\text{-}3}$	103	20	18	15	14
$t_{3/4\text{-}1}$	51	34	31	28	23
$t_{3/4\text{-}2}$	54	40	36	32	31
$t_{3/4\text{-}3}$	221	45	39	33	30
$(t_{3/4}\text{-}t_{1/2})/t_{1/2\text{-}1}$	1.125	0.545455	0.47619	0.4	0.277778
$(t_{3/4}\text{-}t_{1/2})/t_{1/2\text{-}2}$	1.076923	1.105263	1.117647	1.133333	1.214286
$(t_{3/4}\text{-}t_{1/2})/t_{1/2\text{-}3}$	1.145631	1.25	1.166667	1.2	1.142857
$(t_{3/4}\text{-}t_{1/2})/t_{1/2\text{-}avg}$	1.115851	0.966906	0.920168	0.911111	0.878307

Table 9.2. Fractional times table to calculate the rate order of SmI_2 in the reduction of acetophenone O-methyl oxime by SmI_2

9.2.3 Computational Details

Gaussian09 programs were used for the calculations with the APF-D hybrid DFT method and the 6-311+G(2d,p) basis set.[1–4] Natural-population analysis was obtained by including pop=npa.[5] Solvation values were calculated using the polarizable continuum model with integral equation formalism IEFPCM with tetrahydrofuran as the solvent.[6,7] The geometries and frequencies were calculated with the keywords uapfd/6-311+g(2d,p) opt=(calcfc,tight) int=(ultrafine,acc2e=12) pop=npa scrf=(iefpcm,solvent=thf)

9.3 Investigation of the Unusual Stability of SmI_2-Water

9.3.1 ^{1}H NMR Data

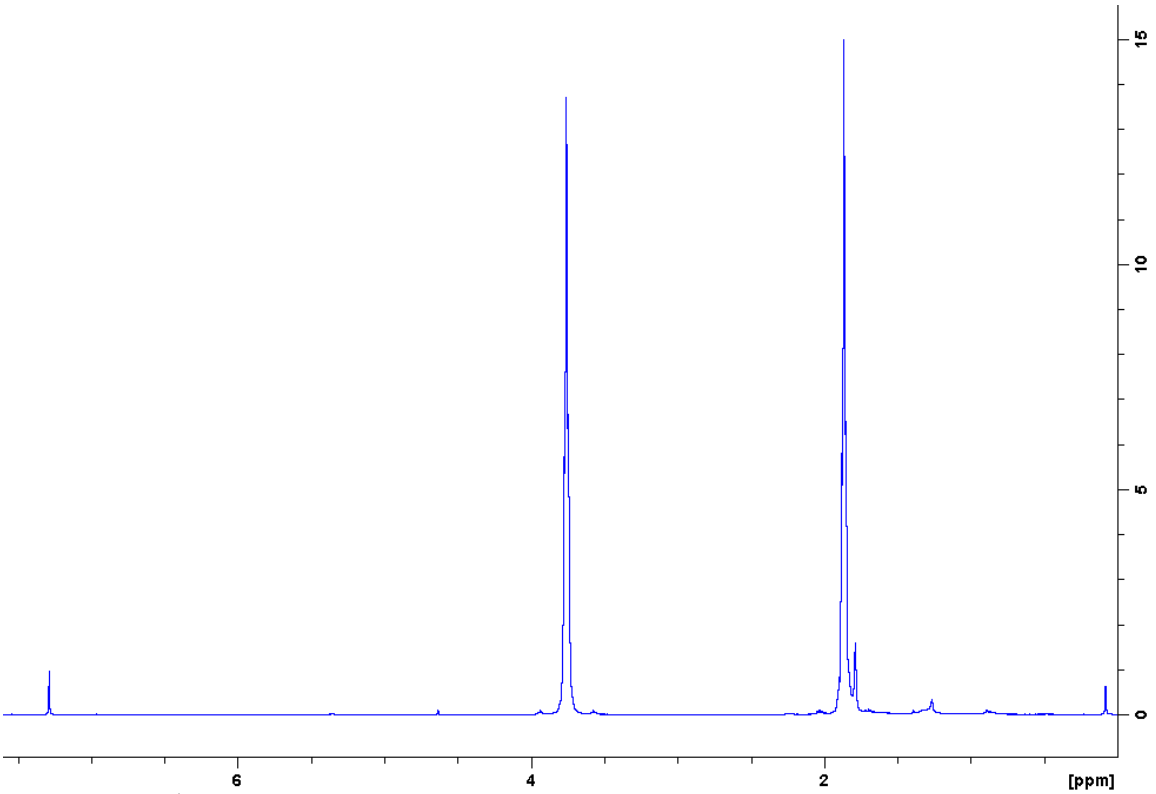

Figure 9.37. ^{1}H NMR spectrum of H_2 gas

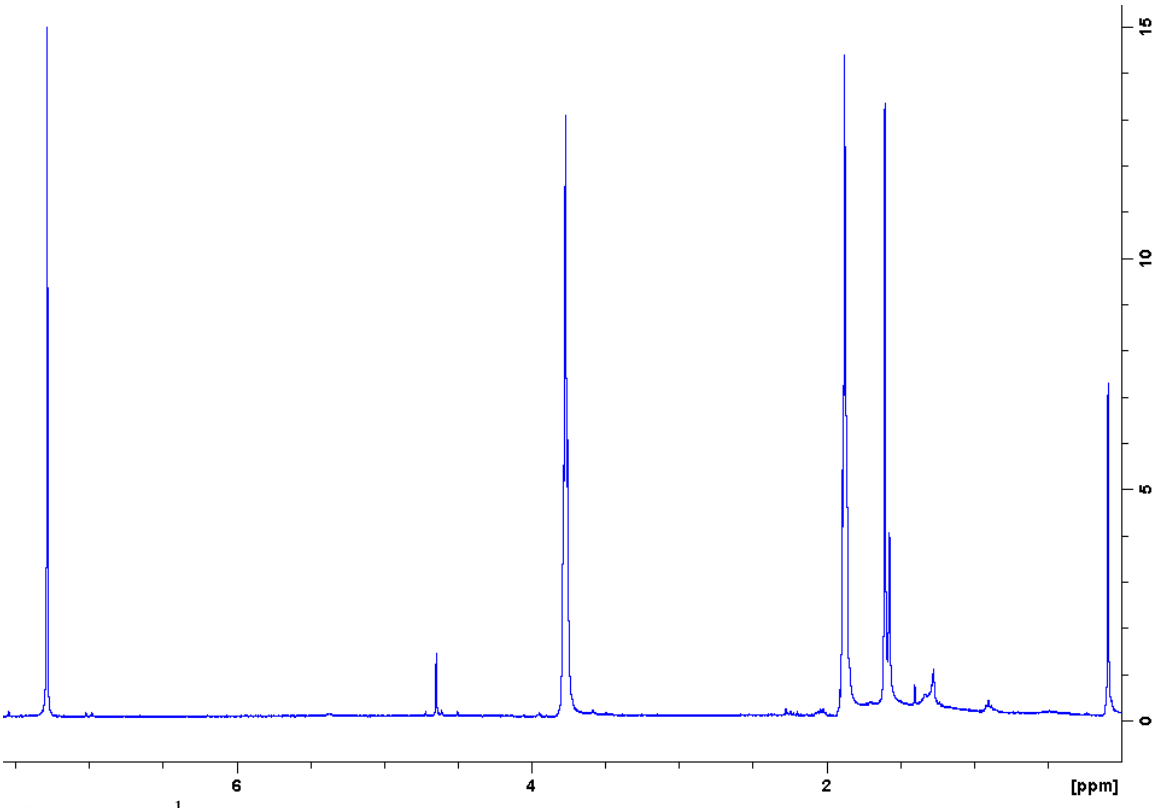

Figure 9.38. ^{1}H NMR spectrum of H_2 and HD gas

9.3.2 Kinetics Data

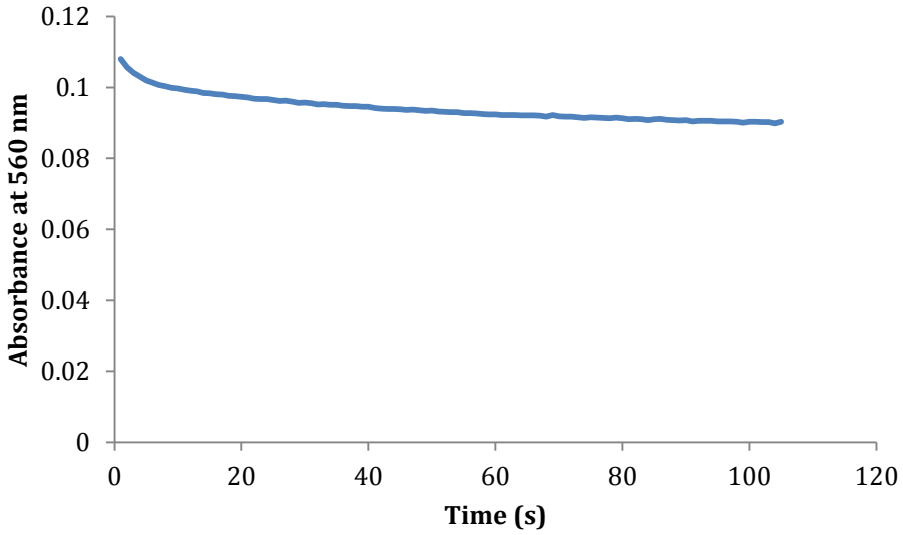

Figure 9.39. Representative plot of the decay curve for SmI_2 at 560 nm in the presence of water

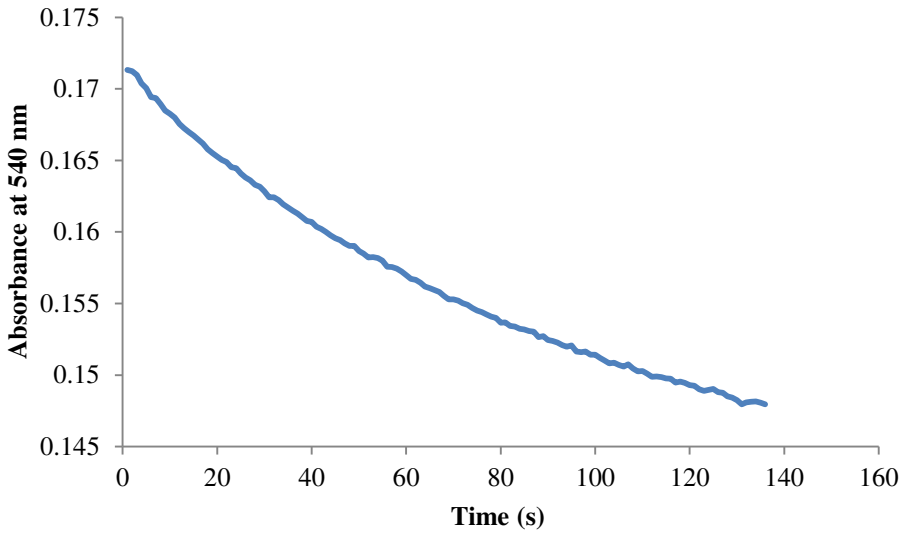

Figure 9.40. Representative plot of the decay curve for $SmBr_2$ at 540 nm in the presence of water

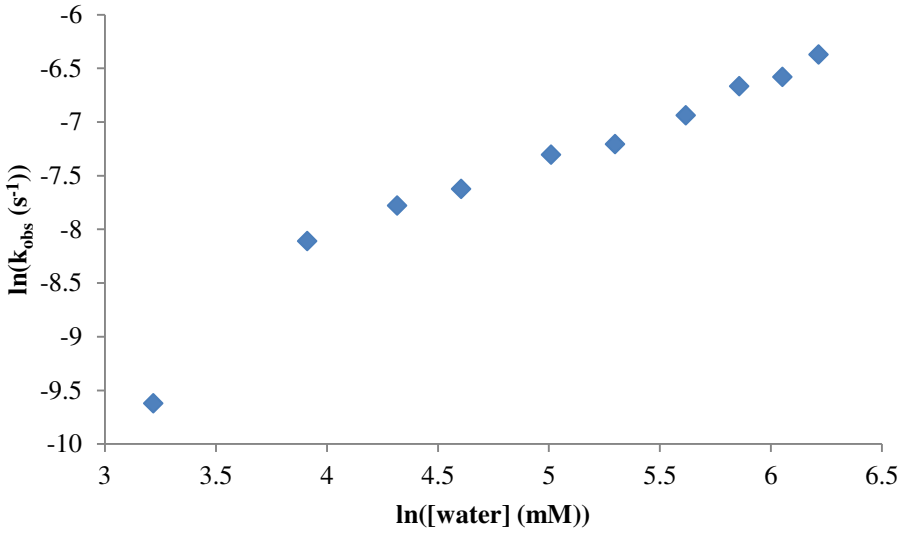

Figure 9.41. Plot of $\ln(k_{obs})$ vs ln([water]) for the evolution of H_2 gas from SmI_2-water

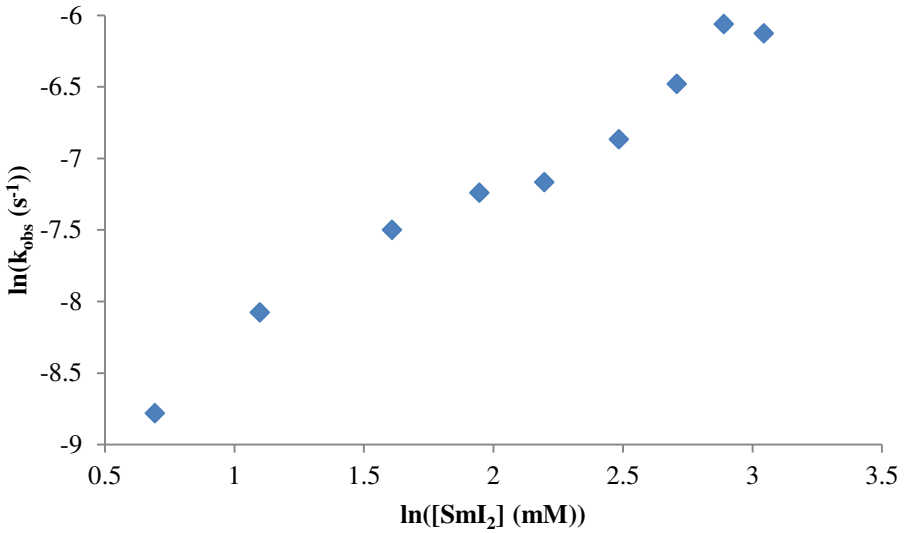

Figure 9.42. Plot of $\ln(k_{obs})$ vs $\ln([SmI_2])$ for the evolution of H_2 gas from SmI_2-water

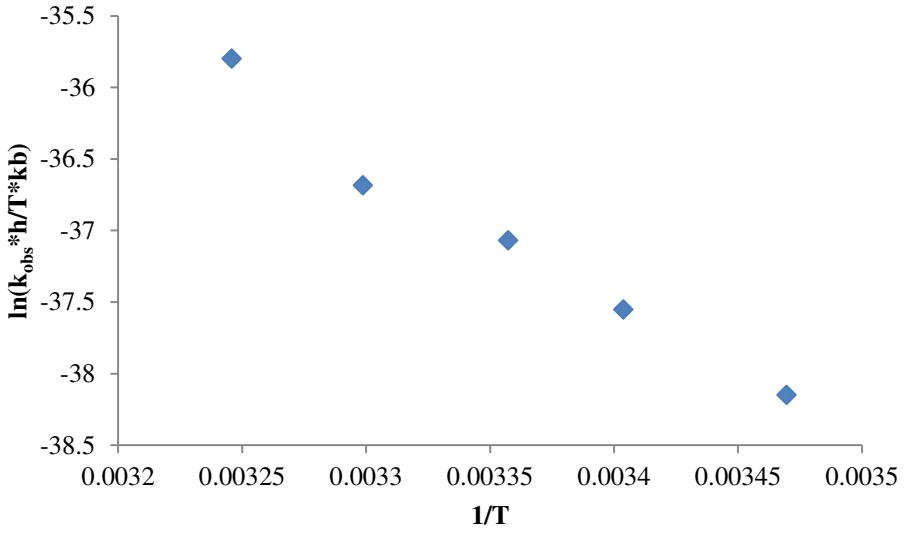

Figure 9.43. Plot of $\ln(k_{obs}*h/T*kb)$ vs 1/T for the evolution of H_2 gas from SmI_2-water

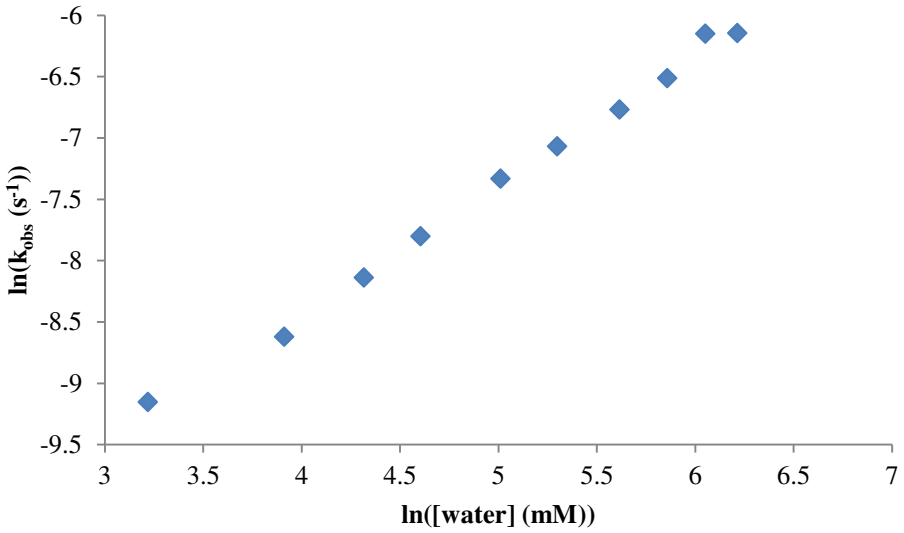

Figure 9.44. Plot of $\ln(k_{obs})$ vs $\ln([water])$ for the evolution of H_2 gas from $SmBr_2$-water

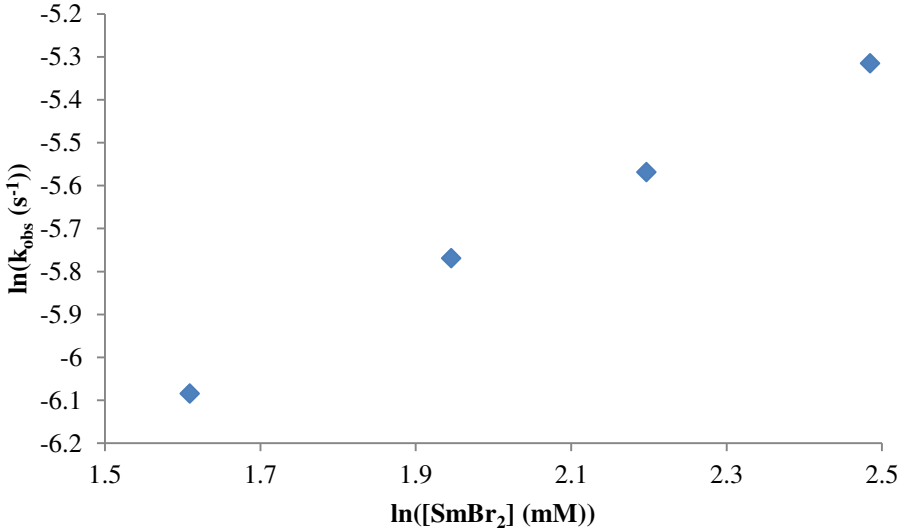

Figure 9.45. Plot of $\ln(k_{obs})$ vs $\ln([SmBr_2])$ for the evolution of H_2 gas from $SmBr_2$-water

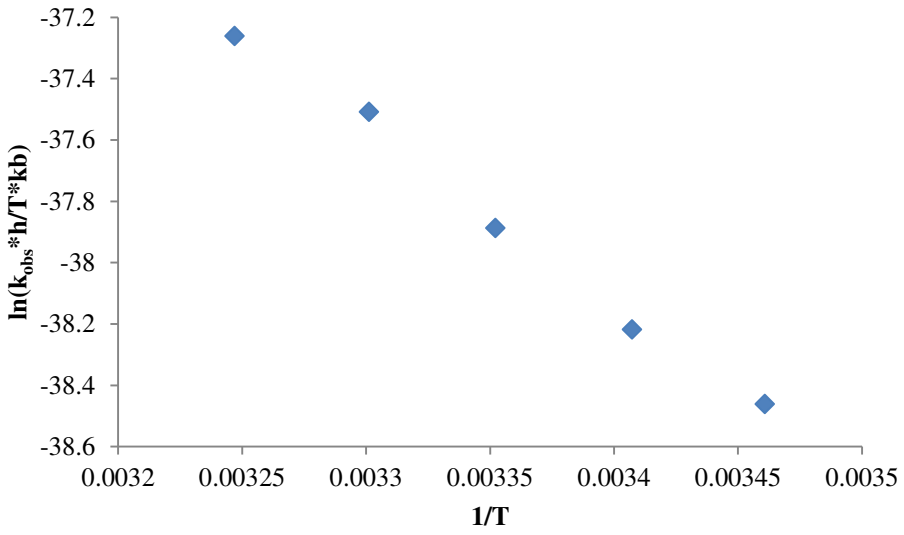

Figure 9.46. Plot of $\ln(k_{obs}*h/T*kb)$ vs 1/T for the evolution of H_2 gas from $SmBr_2$-water

9.4 Theoretical and Mechanistic Studies of the SmI_2-Ammonia Bond Weakening System

9.4.1 ^{1}H NMR Data

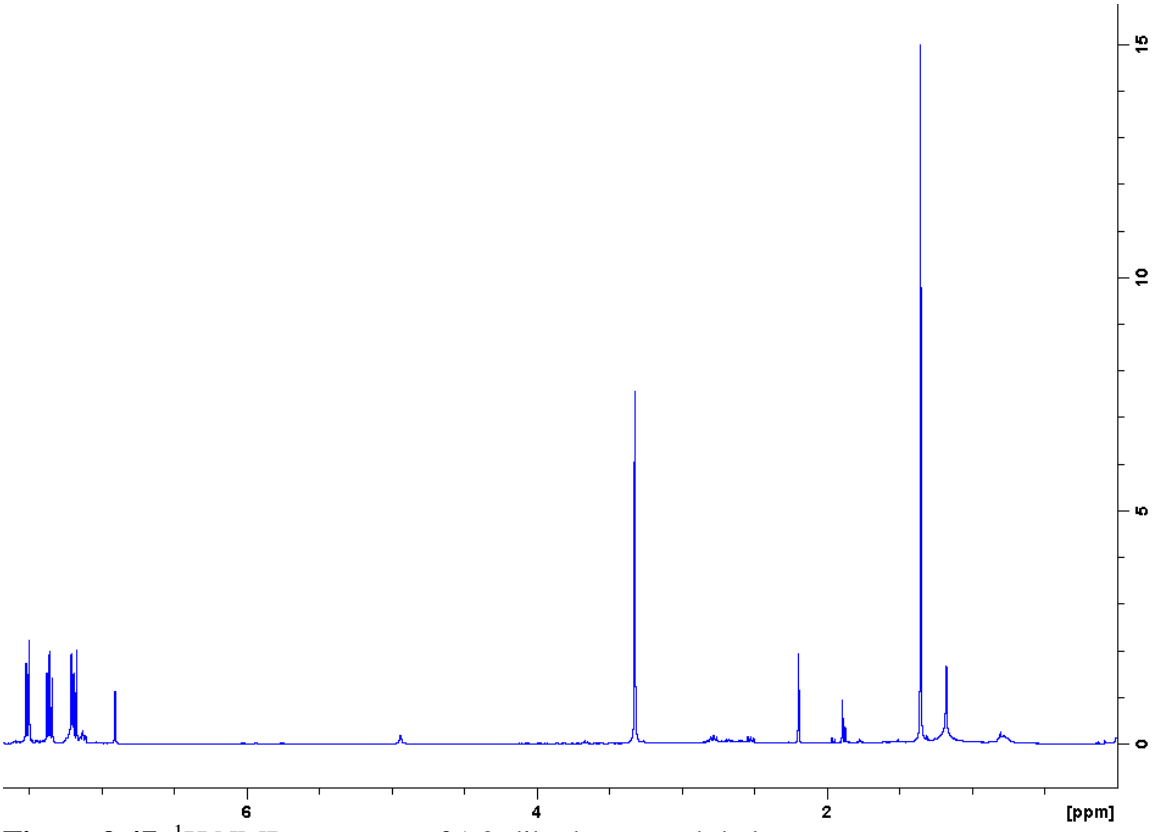

Figure 9.47. ^{1}H NMR spectrum of 1,2-dihydroacenaphthalene

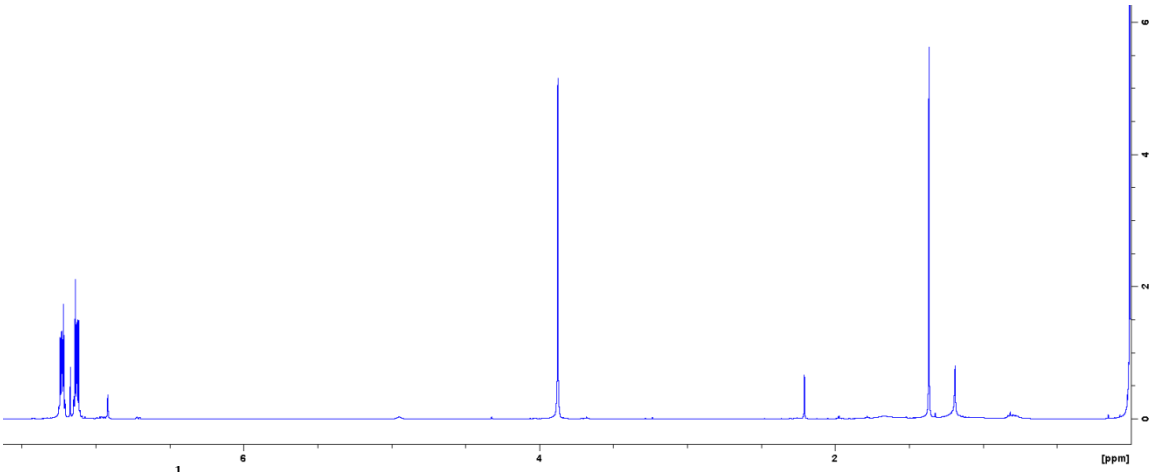

Figure 9.48. ^{1}H NMR spectrum of 9,10-dihydroanthracene

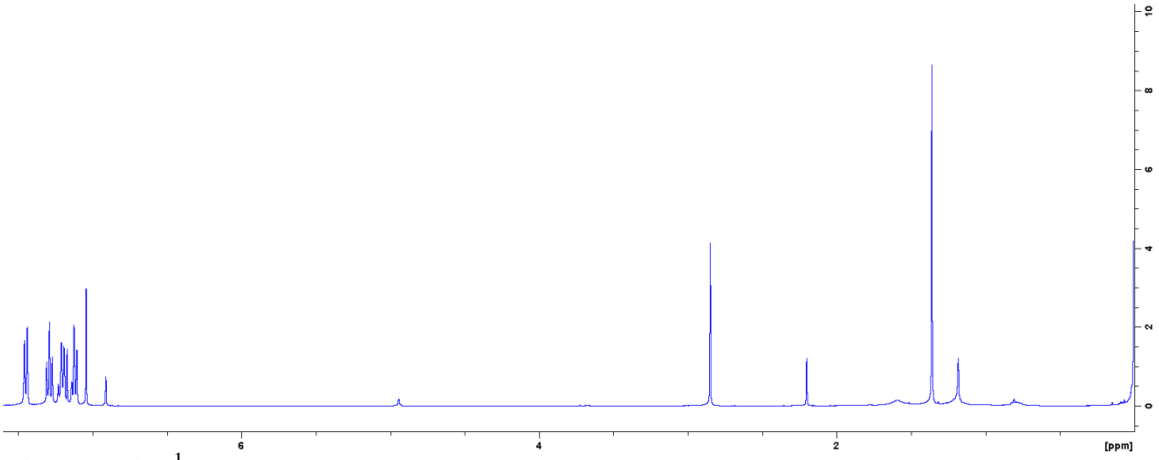

Figure 9.49. ^{1}H NMR spectrum of 1,2-diphenylethane

9.4.2 ^{13}C NMR Data

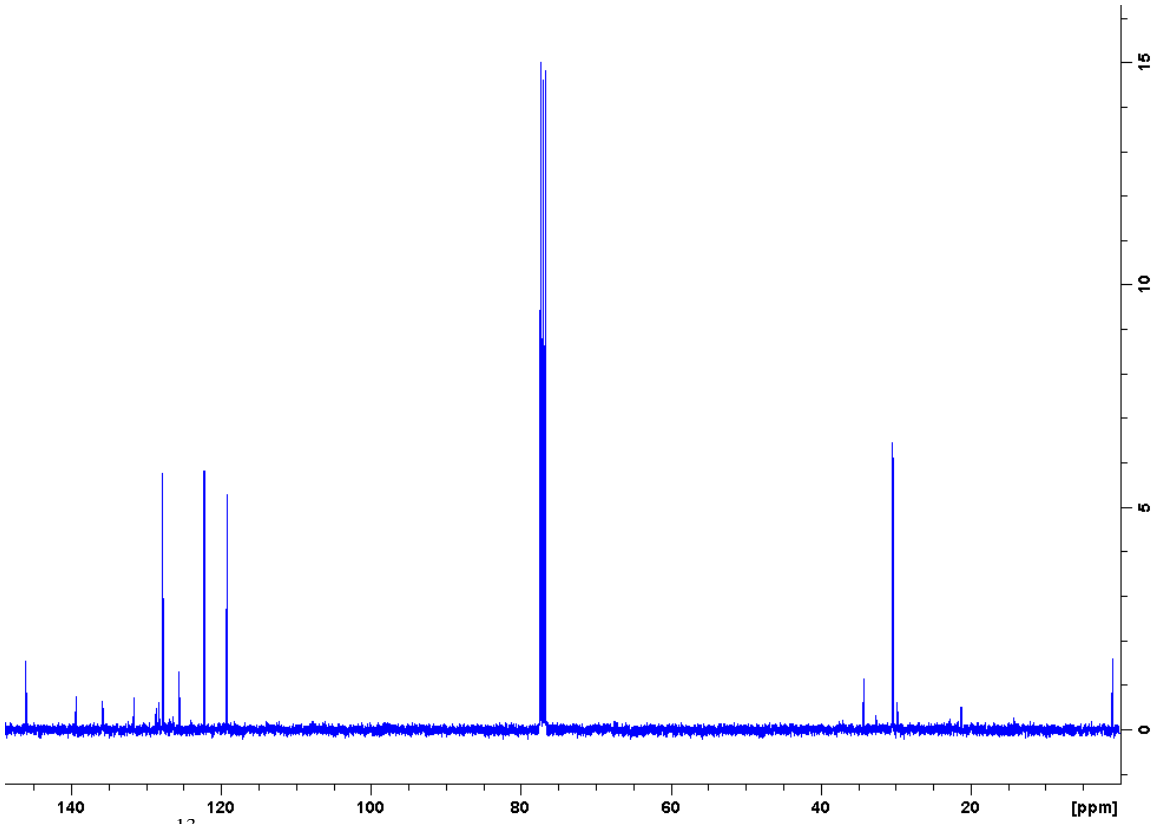

Figure 9.50. ^{13}C NMR spectrum of 1,2-dihydroacenaphthalene

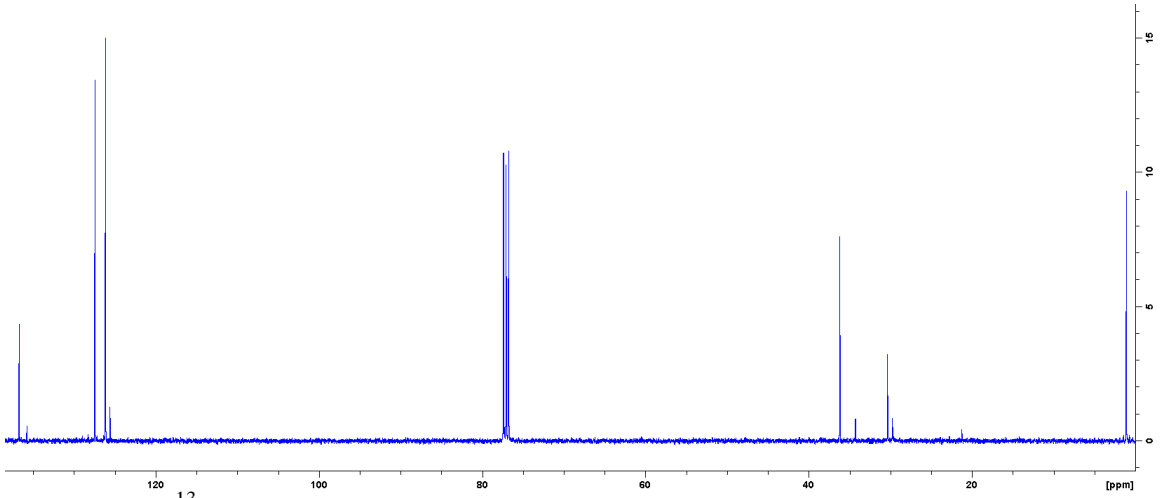

Figure 9.51. ^{13}C NMR spectrum of 9,10-dihydroanthracene

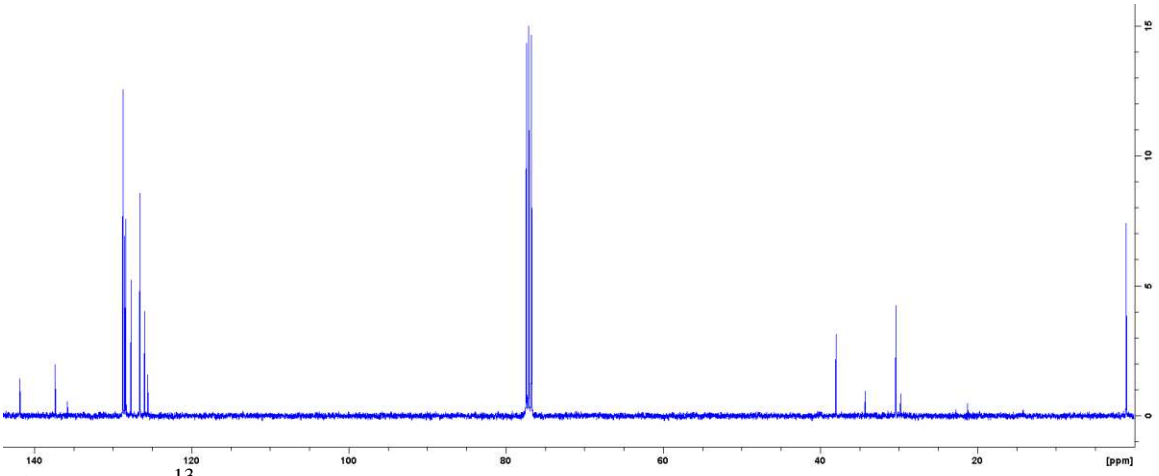

Figure 9.52. ^{13}C NMR spectrum of 1,2-diphenylethane

9.4.3 Kinetics Data

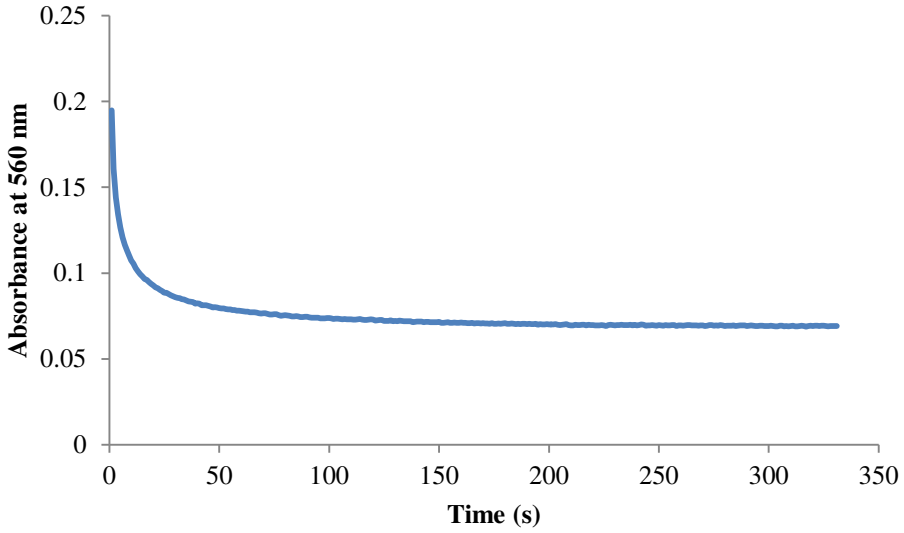

Figure 9.53. Representative plot of the decay curve for SmI_2 at 560 nm in the presence of acenaphthalene and ammonia

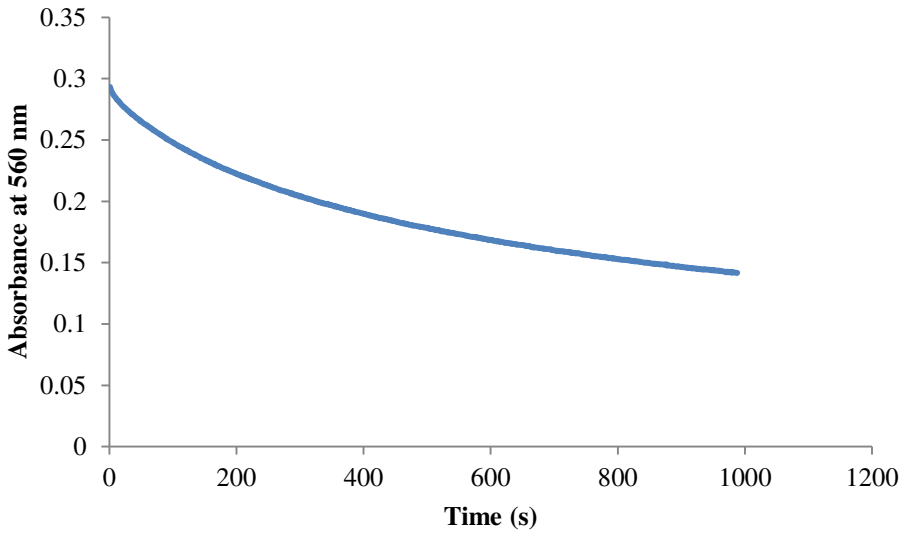

Figure 9.54. Representative plot of the decay curve for SmI_2 at 560 nm in the presence of acenaphthalene and 100 mM water

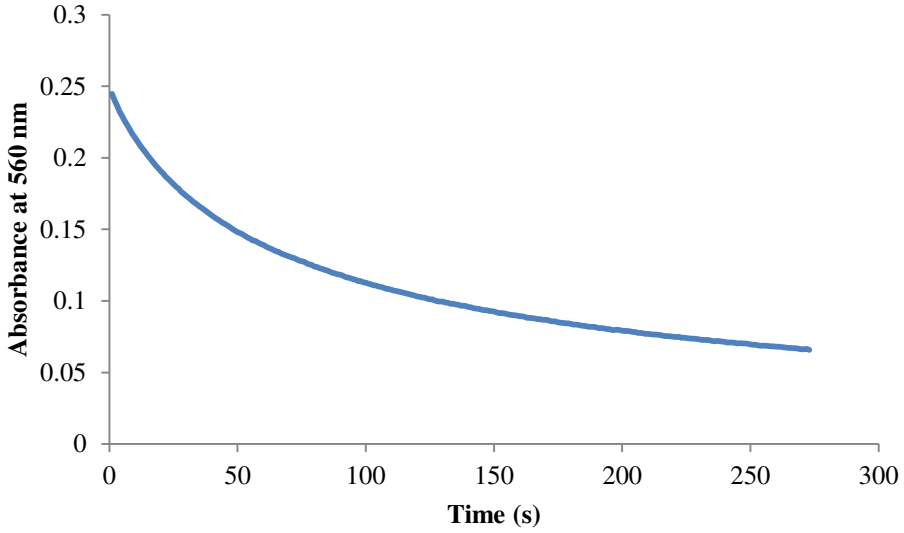

Figure 9.55. Representative plot of the decay curve for SmI_2 at 560 nm in the presence of acenaphthalene and 400 mM water

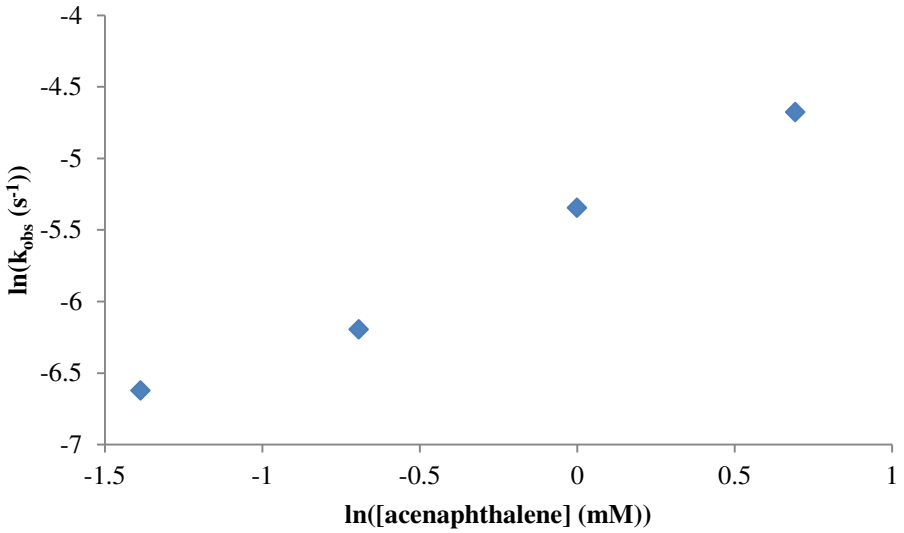

Figure 9.56. Plot of ln(k_{obs}) vs ln([acenaphthalene]) for the reduction of acenaphthalene by SmI_2-ammonia

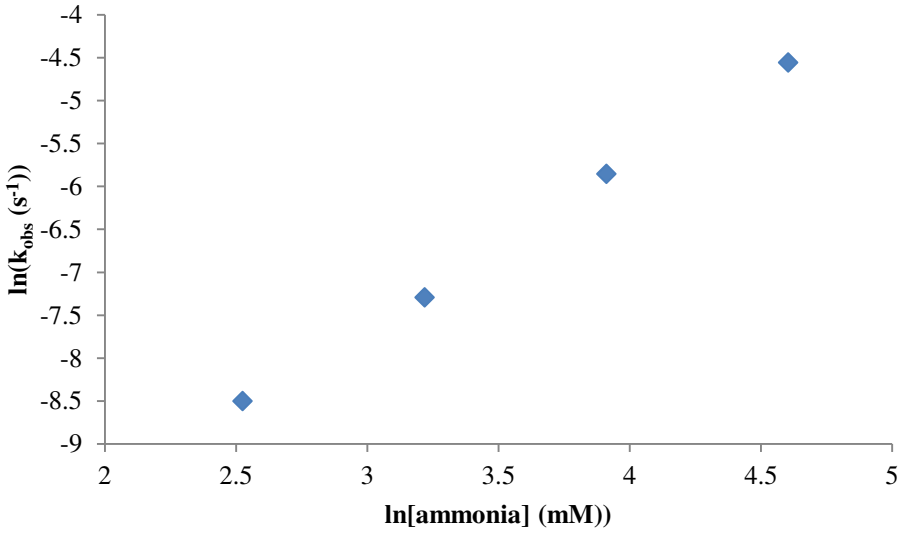

Figure 9.57. Plot of ln(k_{obs}) vs ln([ammonia]) for the reduction of acenaphthalene by SmI_2-ammonia

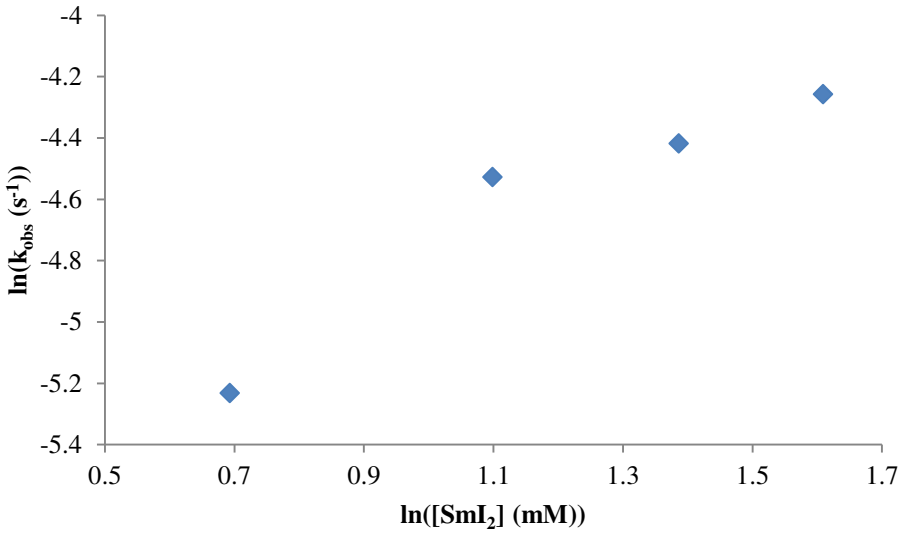

Figure 9.58. Plot of $\ln(k_{obs})$ vs $\ln([SmI_2])$ for the reduction of acenaphthalene by SmI_2-ammonia

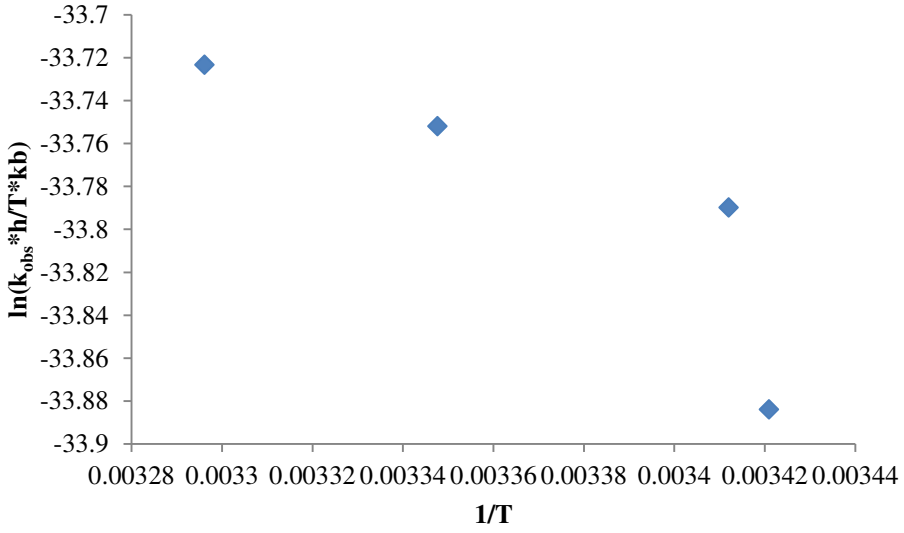

Figure 9.59. Plot of $\ln(k_{obs}*h/T*kb)$ vs 1/T for the reduction of acenaphthalene by SmI_2-ammonia

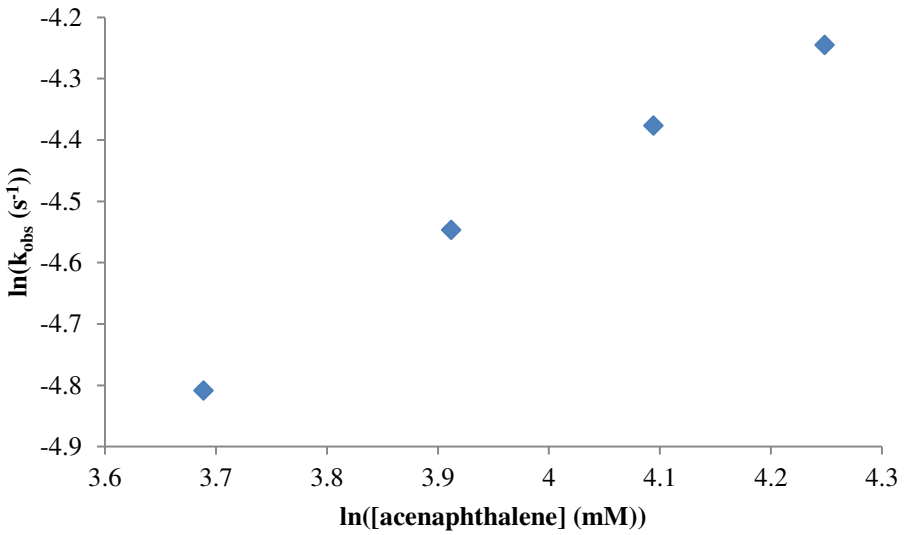

Figure 9.60. Plot of $\ln(k_{obs})$ vs ln([acenaphthalene]) for the reduction of acenaphthalene by SmI_2-water at 100 mM water

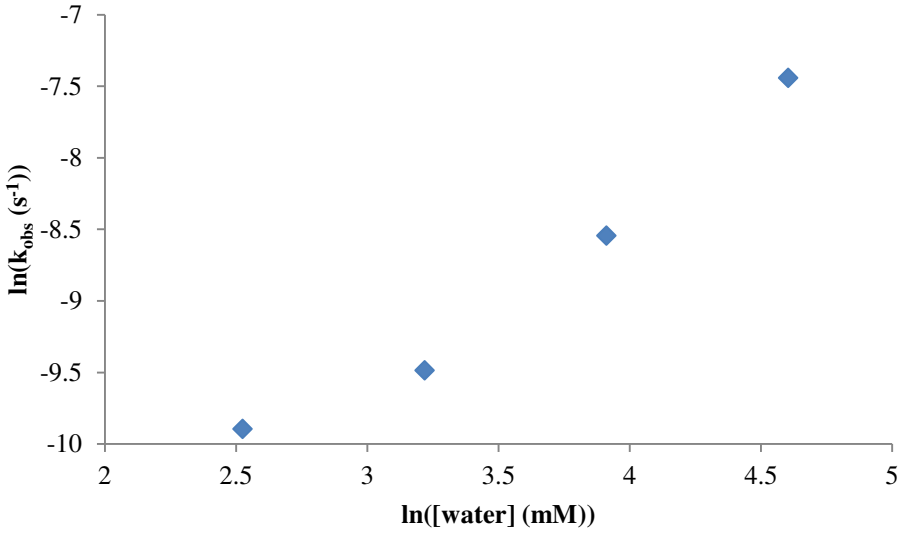

Figure 9.61. Plot of $\ln(k_{obs})$ vs ln([water]) for the reduction of acenaphthalene by SmI_2-water at 100 mM water

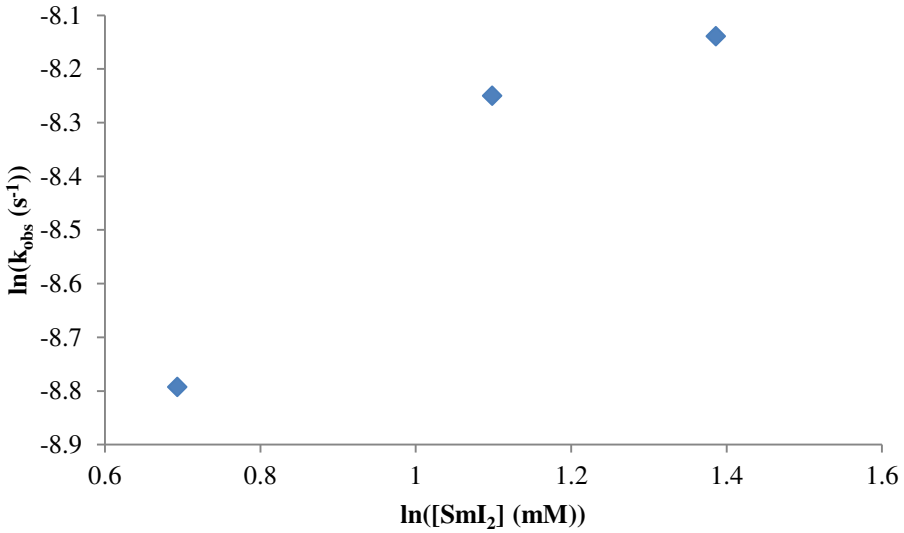

Figure 9.62. Plot of ln(k_{obs}) vs ln([SmI_2]) for the reduction of acenaphthalene by SmI_2-water at 100 mM water

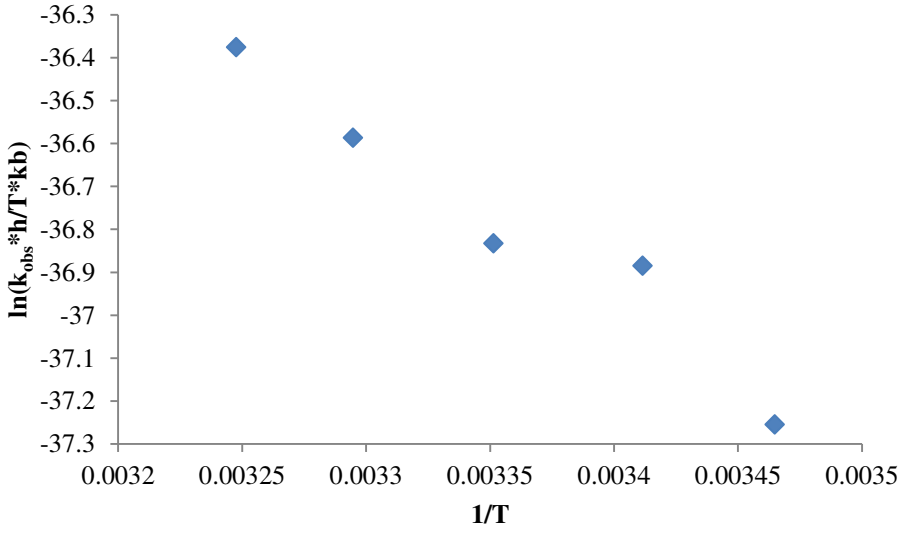

Figure 9.63. Plot of ln(k_{obs}*h/T*kb) vs 1/T for the reduction of acenaphthalene by SmI_2-water at 100mM water

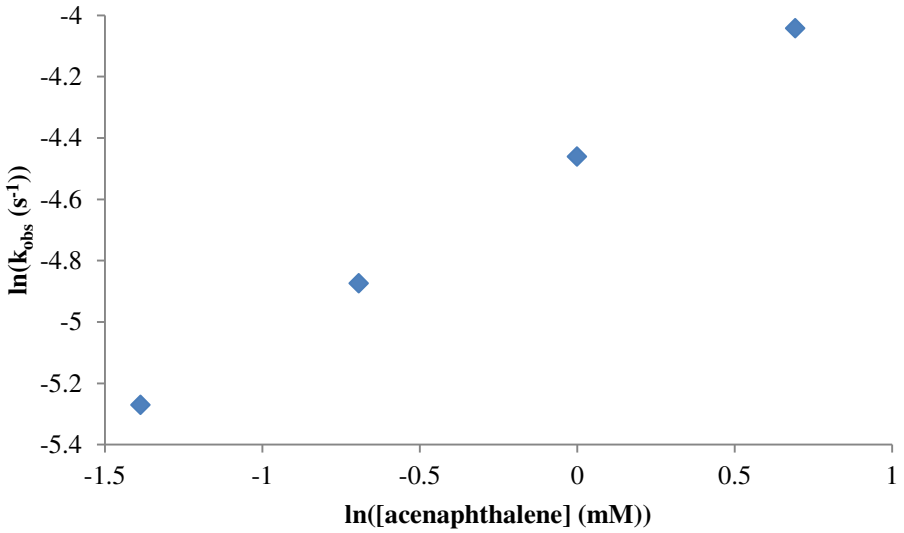

Figure 9.64. Plot of ln(k_{obs}) vs ln([acenaphthalene]) for the reduction of acenaphthalene by SmI_2-water at 400 mM water

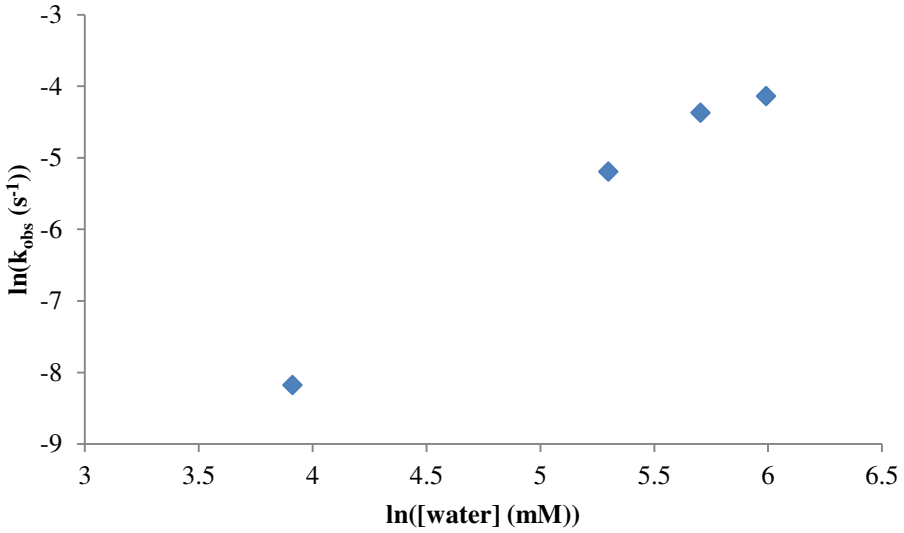

Figure 9.65. Plot of ln(k_{obs}) vs ln([water]) for the reduction of acenaphthalene by SmI_2-water at 400 mM water

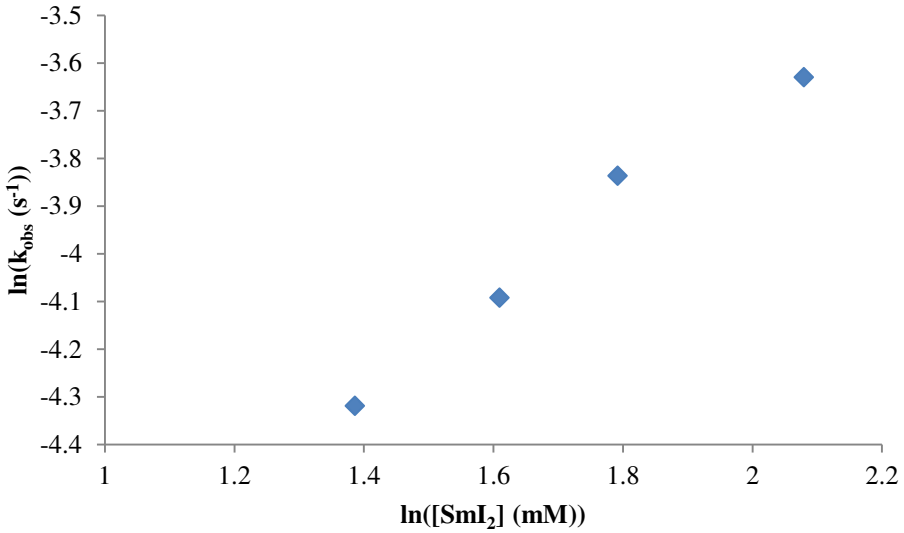

Figure 9.66. Plot of $\ln(k_{obs})$ vs $\ln([SmI_2])$ for the reduction of acenaphthalene by SmI_2-water at 400 mM water

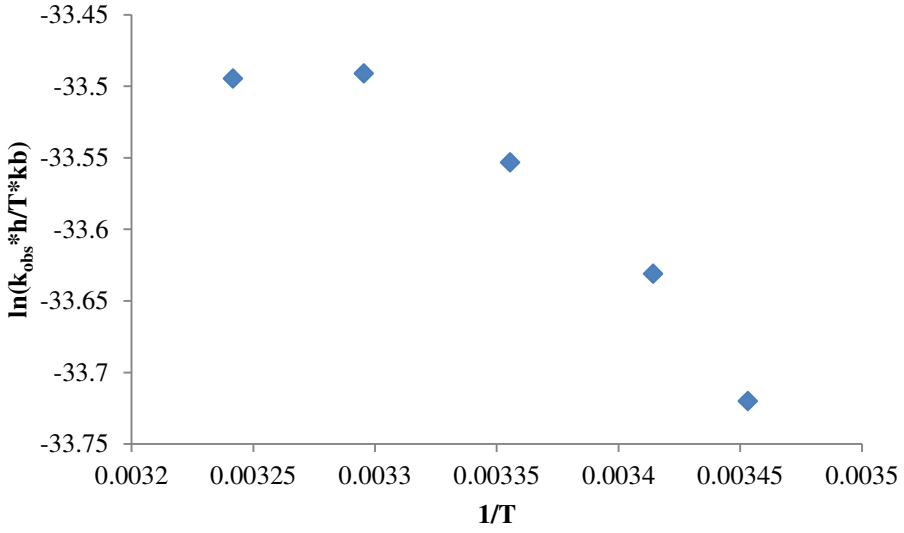

Figure 9.67. Plot of $\ln(k_{obs}*h/T*kb)$ vs 1/T for the reduction of acenaphthalene by SmI_2-water at 400mM water

9.4.4 Computational Details

Gaussian09 programs were used for the calculations with the APF-D hybrid DFT method and the 6-311+G(2d,p) basis set.[1–4] Natural-population analysis was obtained by including pop=npa.[5] Solvation values were calculated using the polarizable continuum model with integral equation formalism IEFPCM with tetrahydrofuran as the solvent.[6,7]

The geometries and frequencies were calculated with the keywords uapfd/6-311+g(2d,p) opt=(calcfc,tight) int=(ultrafine,acc2e=12) pop=npa scrf=(iefpcm,solvent=thf)

9.5 Studies of Coordination-Induced Bond Weakening in the Reductions of Substrates by $SmBr_2$-NMEA

9.5.1 ^{1}H NMR Data

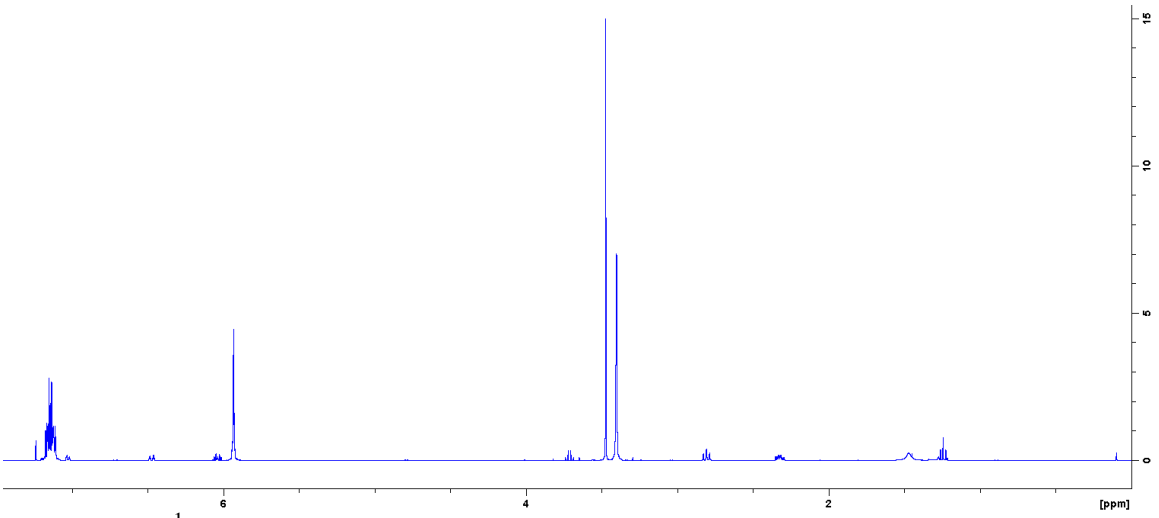

Figure 9.68. ^{1}H NMR spectrum of 1,4-dihydronaphthalene

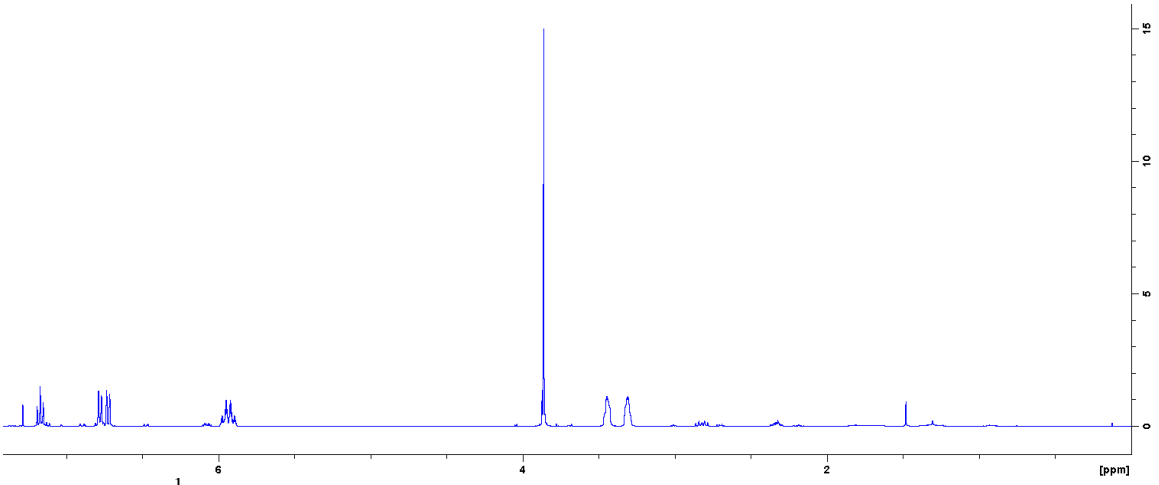

Figure 9.69. ^{1}H NMR spectrum of 1,4-dihydro-5-methoxynaphthalene

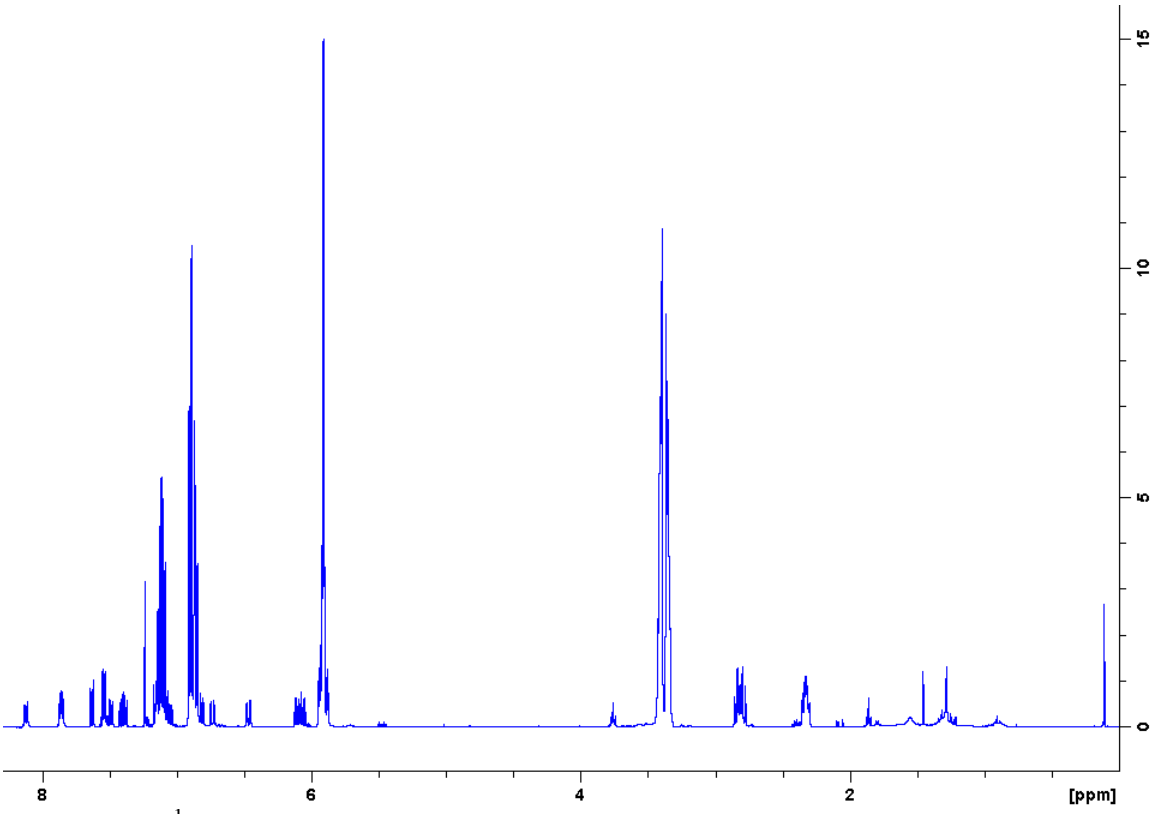

Figure 9.70. ^{1}H NMR spectrum of 1,4-dihydro-5-fluoronaphthalene

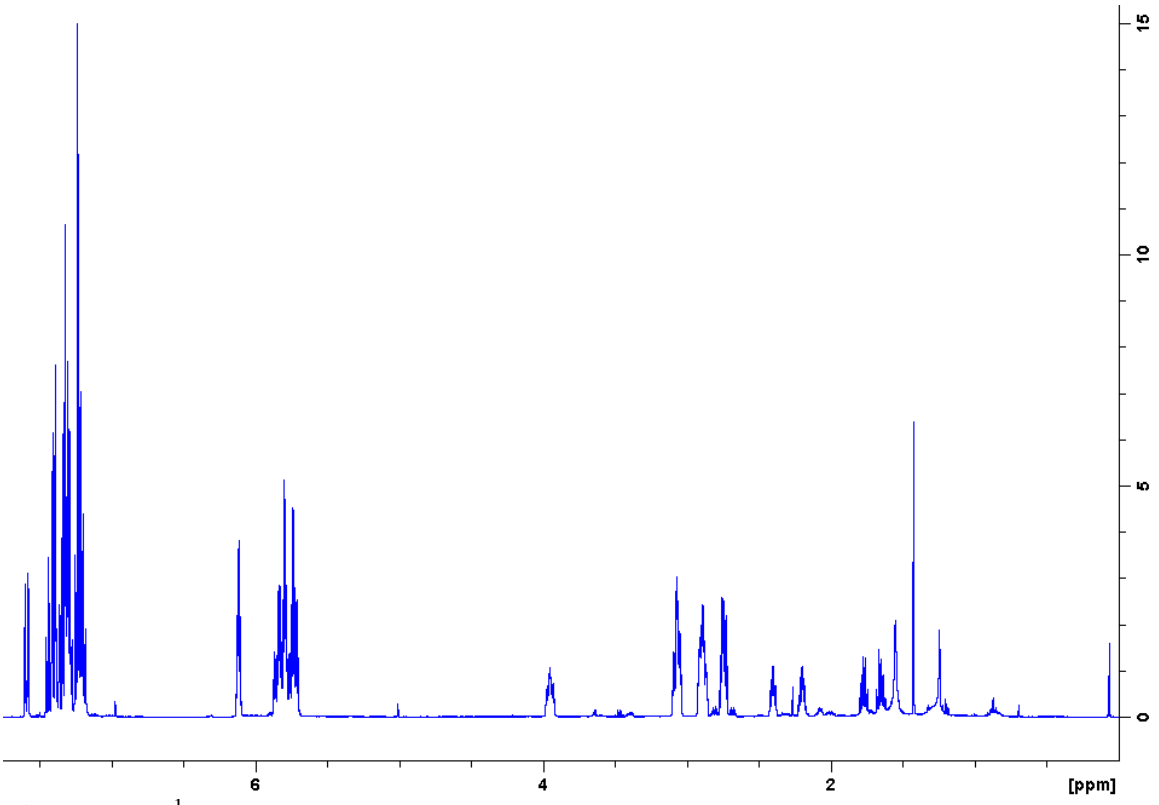

Figure 9.71. ^{1}H NMR spectrum of 1,4-dihydro-1,1`-biphenyl

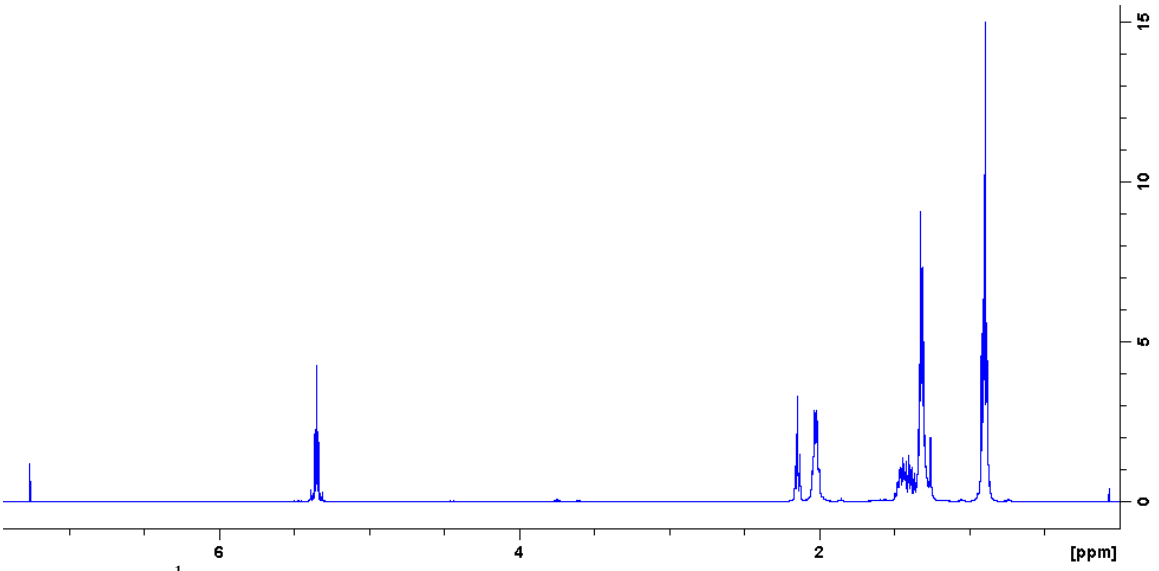

Figure 9.72. ^{1}H NMR spectrum of *cis*-5-decene

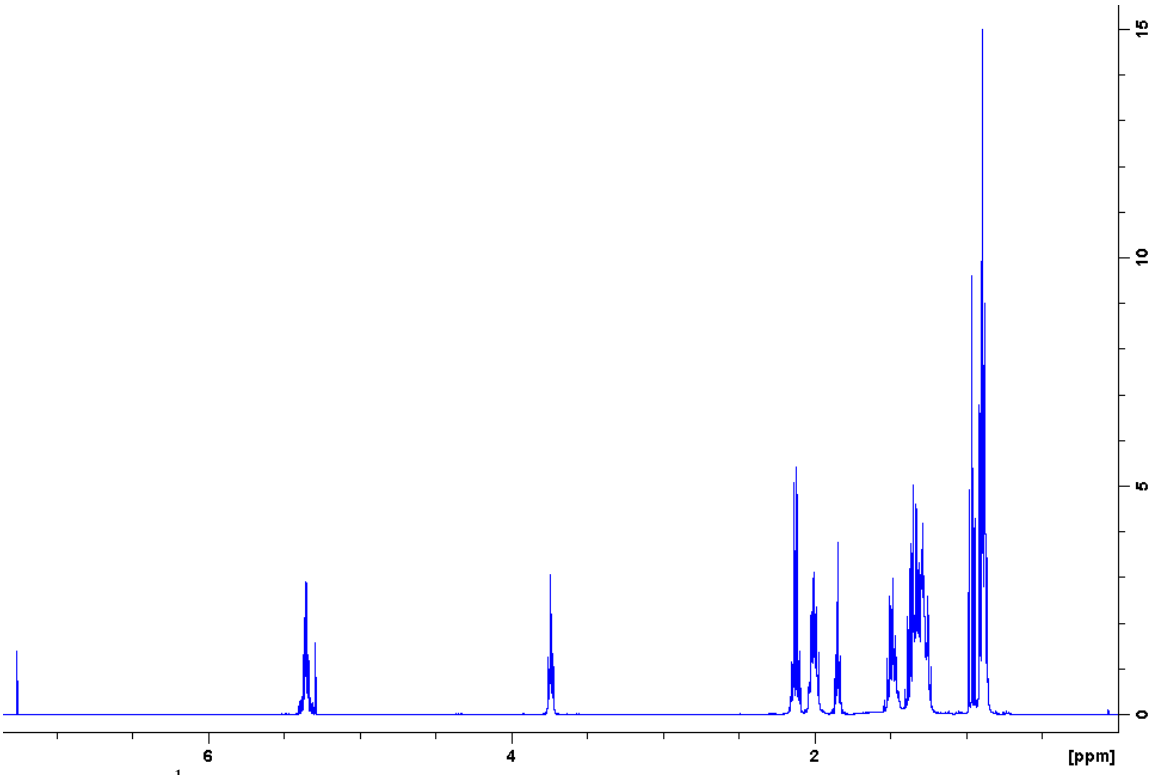

Figure 9.73. ^{1}H NMR spectrum of *cis*-4-decene

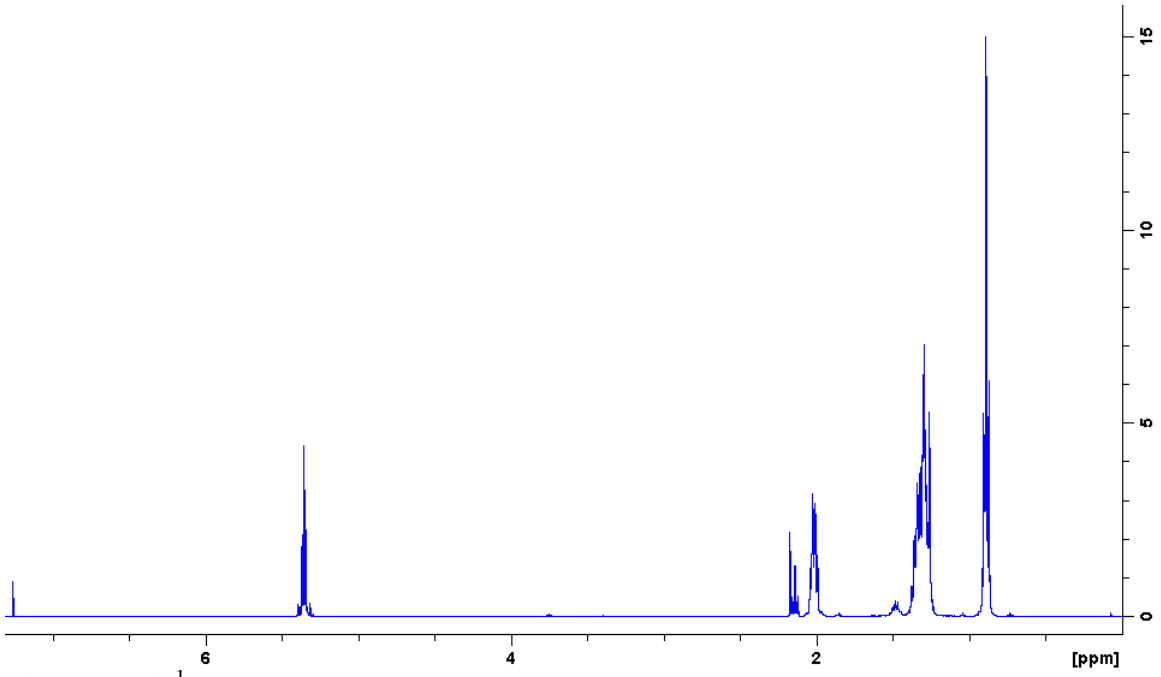

Figure 9.74. ^{1}H NMR spectrum of *cis*-6-dodecene

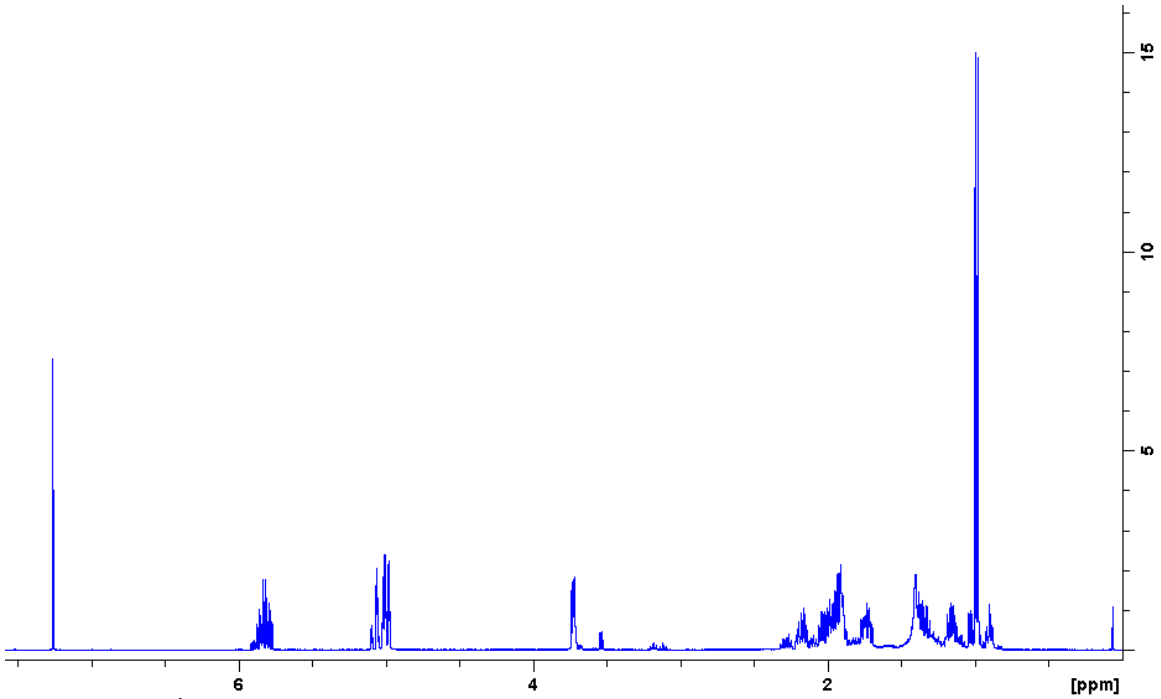

Figure 9.75. ^{1}H NMR spectrum of 2-allyl-5-methylcyclopentan-1-ol

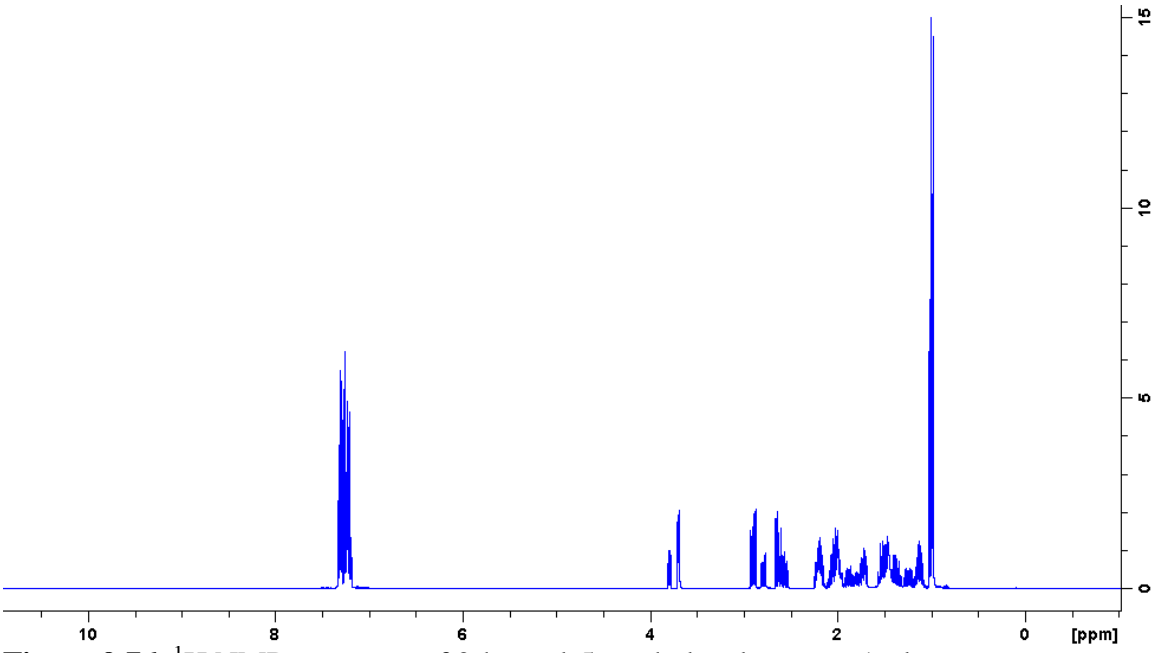

Figure 9.76. ^{1}H NMR spectrum of 2-benzyl-5-methylcyclopentan-1-ol

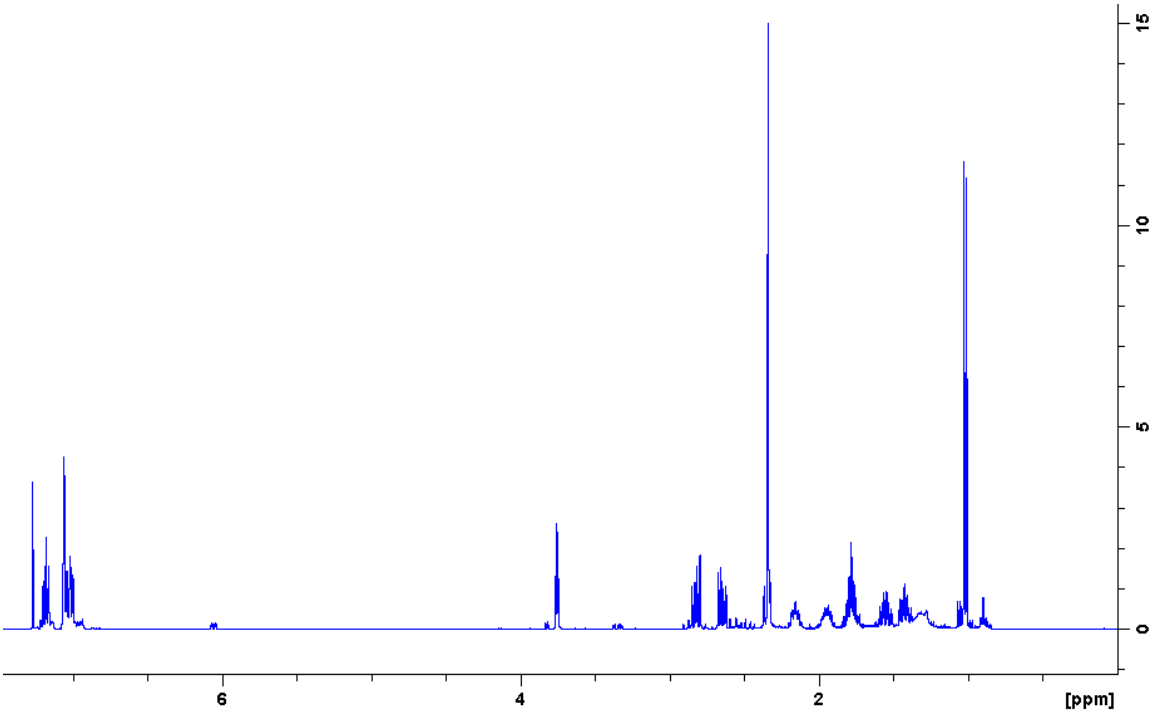

Figure 9.77. ^{1}H NMR spectrum of 2-methyl-5-(3-methylbenzyl)cyclopentan-1-ol

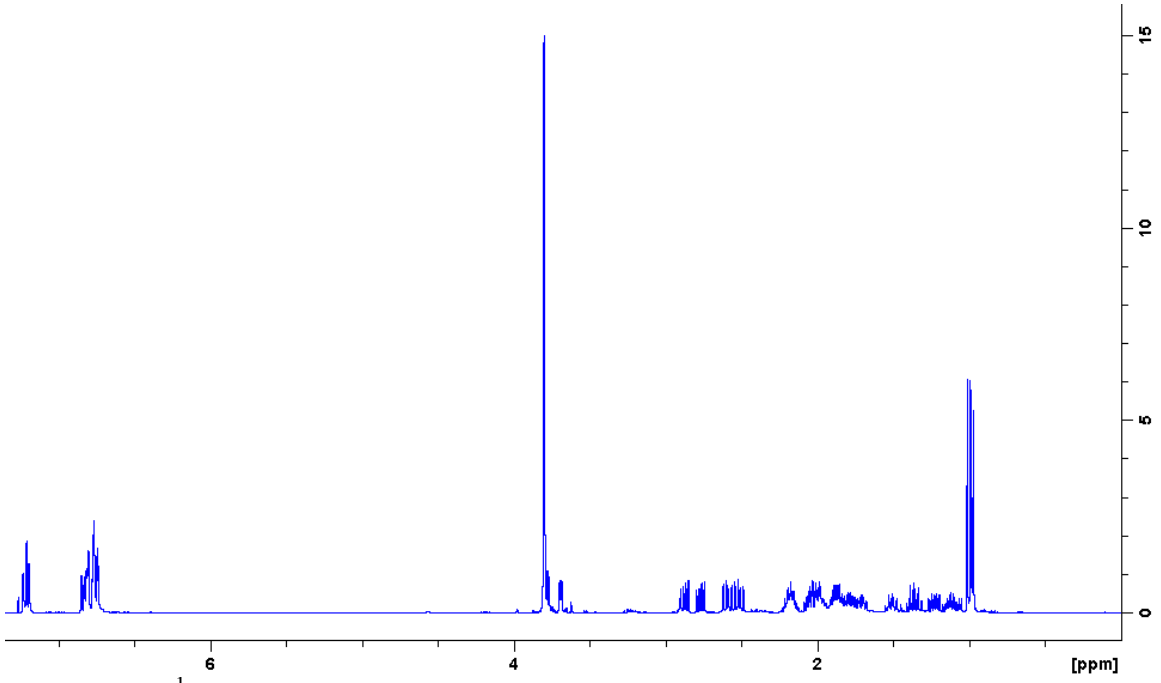

Figure 9.78. ^{1}H NMR spectrum of 2-methyl-5-(3-methoxybenzyl)cyclopentan-1-ol

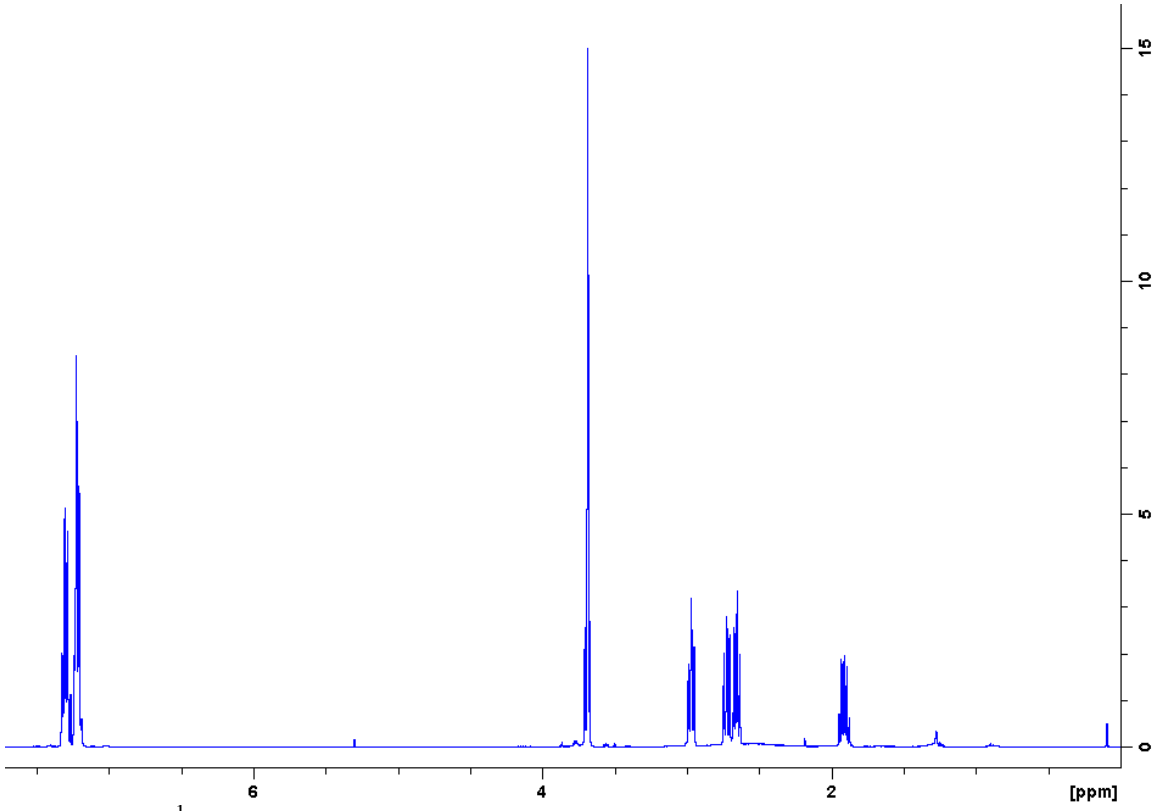

Figure 9.79. ^{1}H NMR spectrum of 3-phenylpropan-1-ol

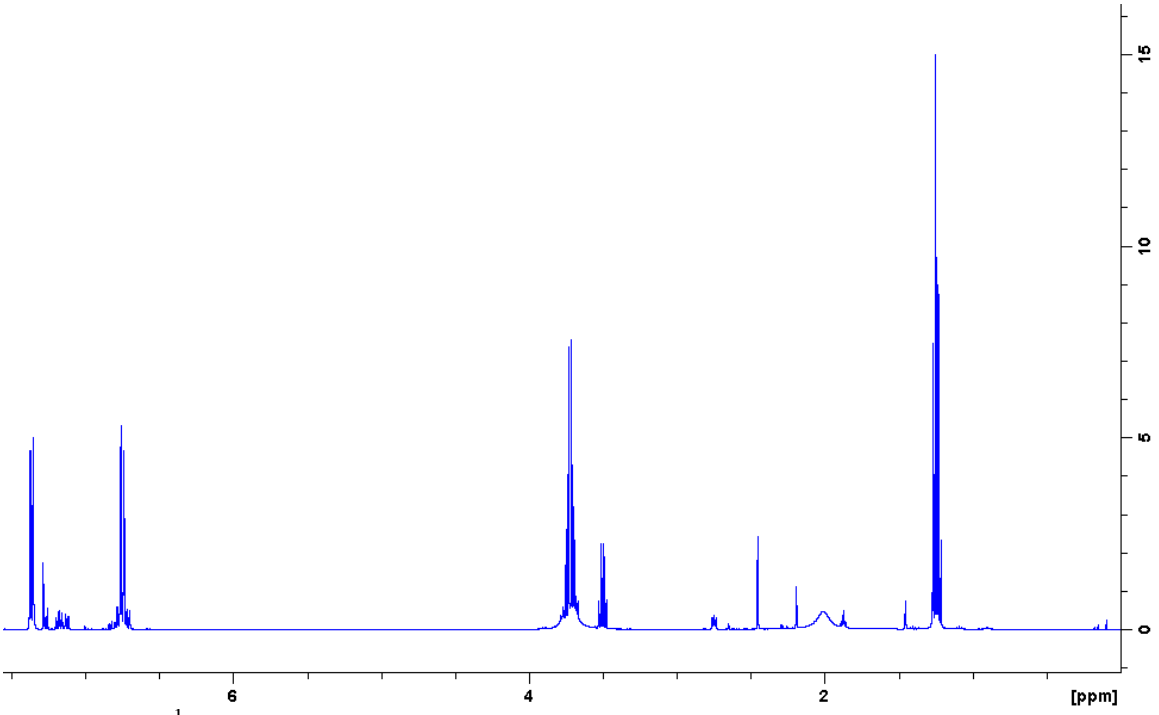

Figure 9.80. ^{1}H NMR spectrum of 1,2-diphenylhydrazine

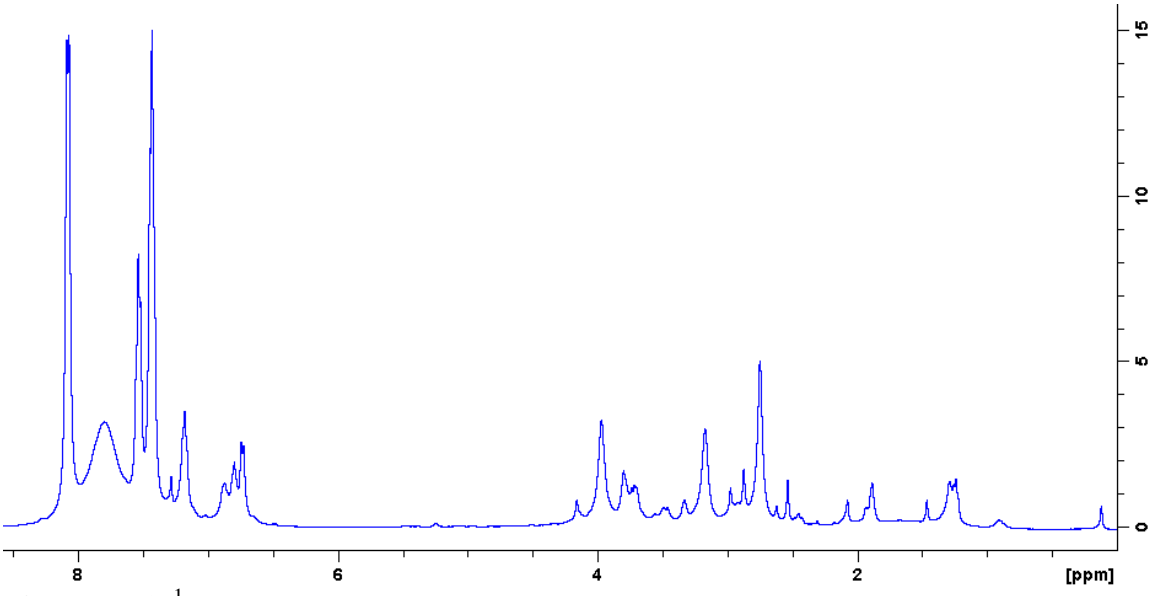

Figure 9.81. ^{1}H NMR spectrum of aniline

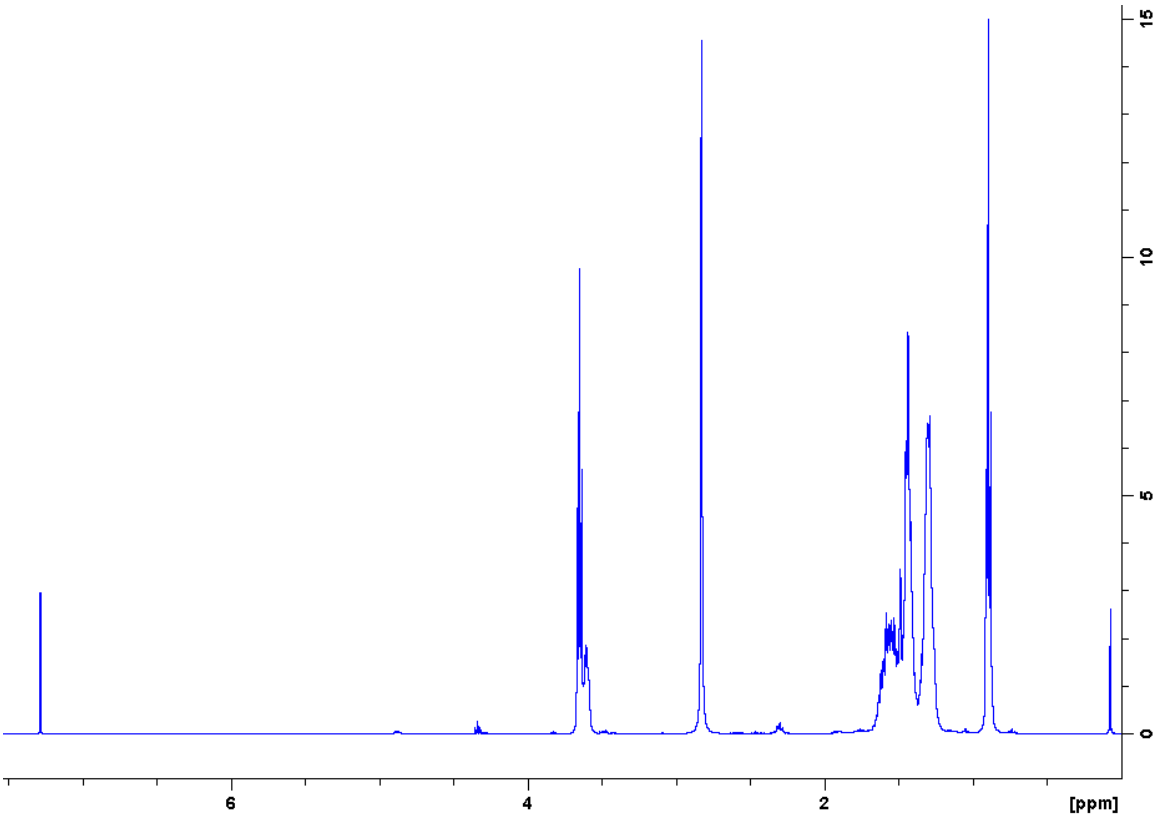

Figure 9.82. ^{1}H NMR spectrum of decane-1,5-diol

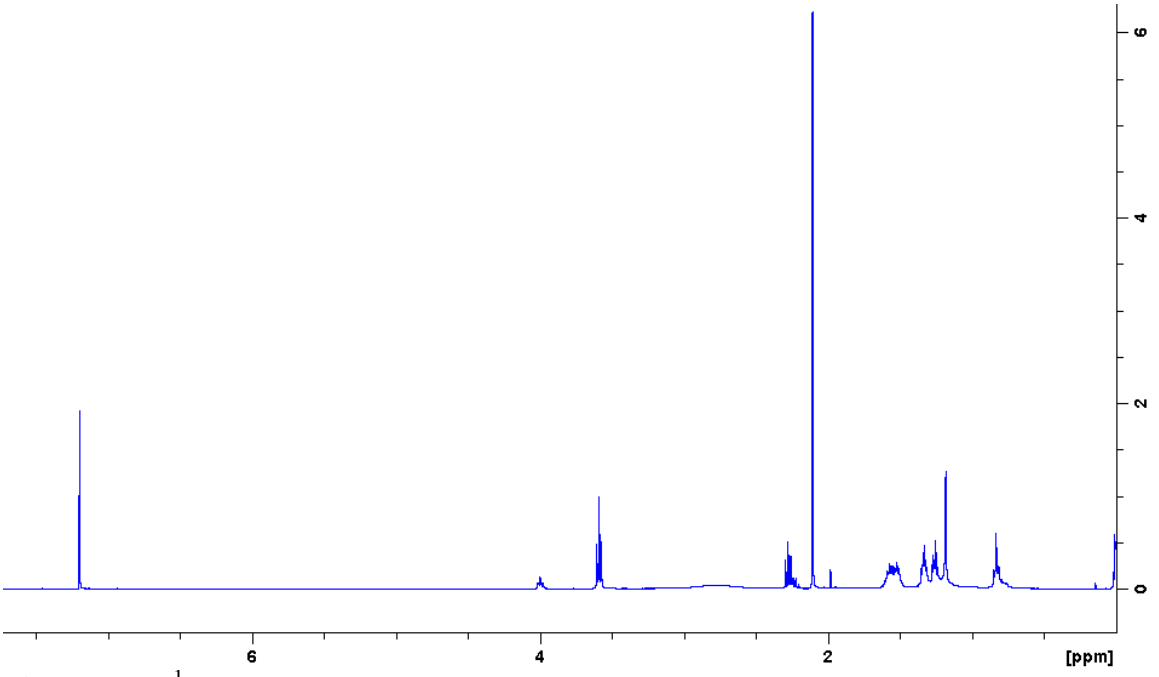

Figure 9.83. ^{1}H NMR spectrum of hexane-1,6-diol

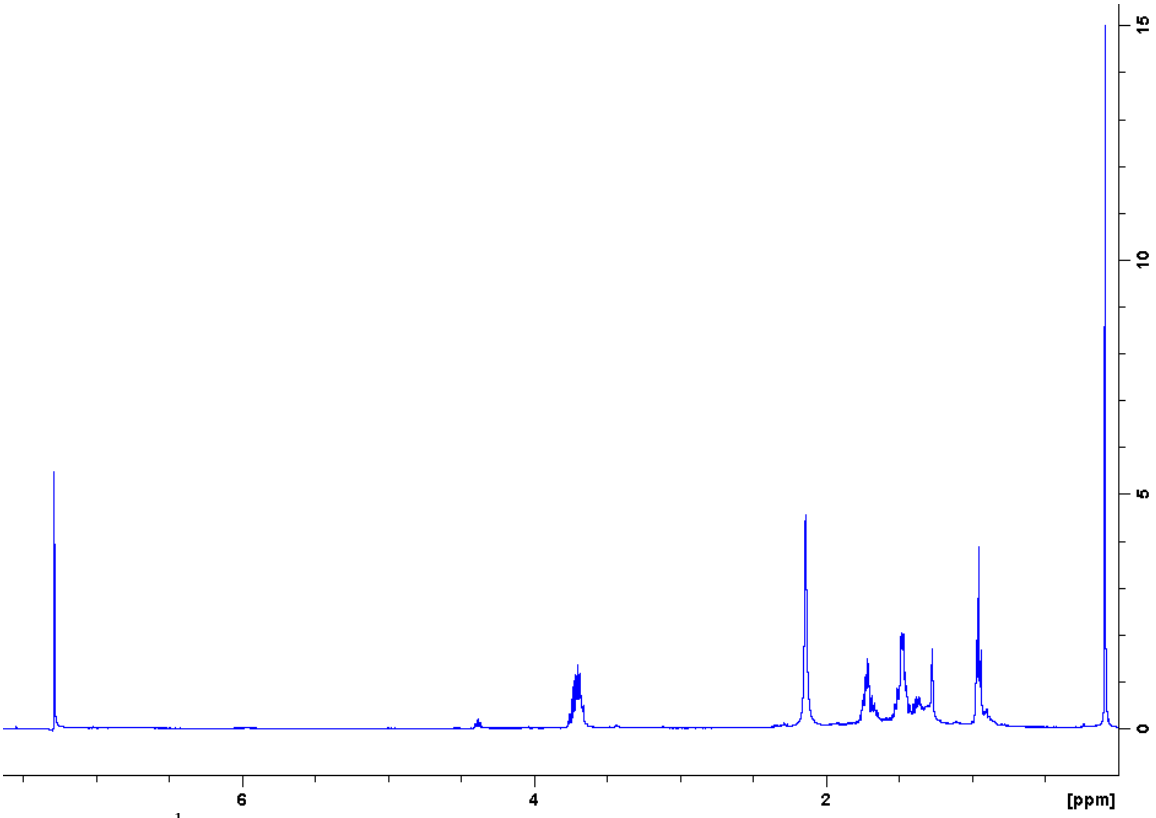

Figure 9.84. ^{1}H NMR spectrum of heptane-1,4-diol

9.5.2 ^{13}C NMR Data

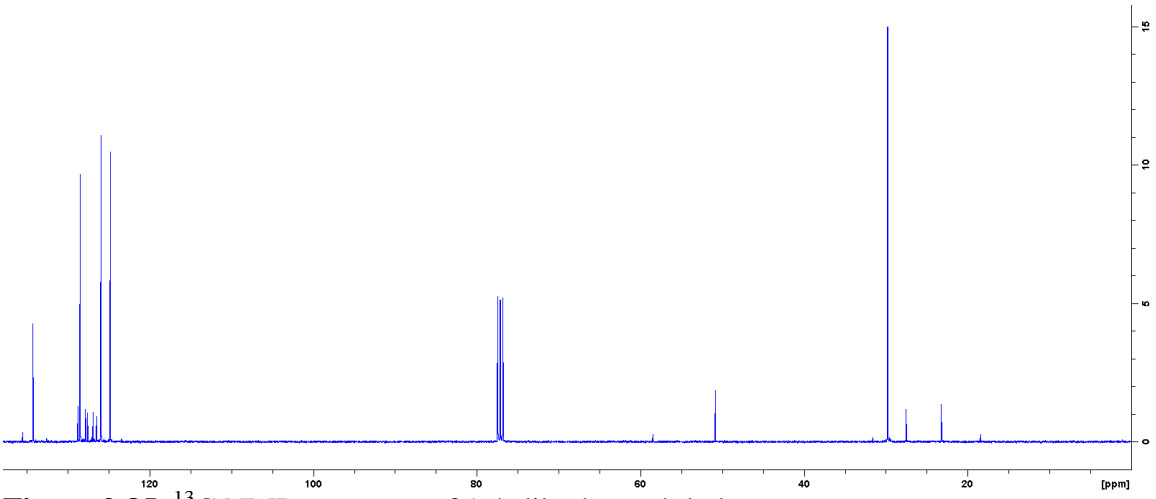

Figure 9.85. ^{13}C NMR spectrum of 1,4-dihydronaphthalene

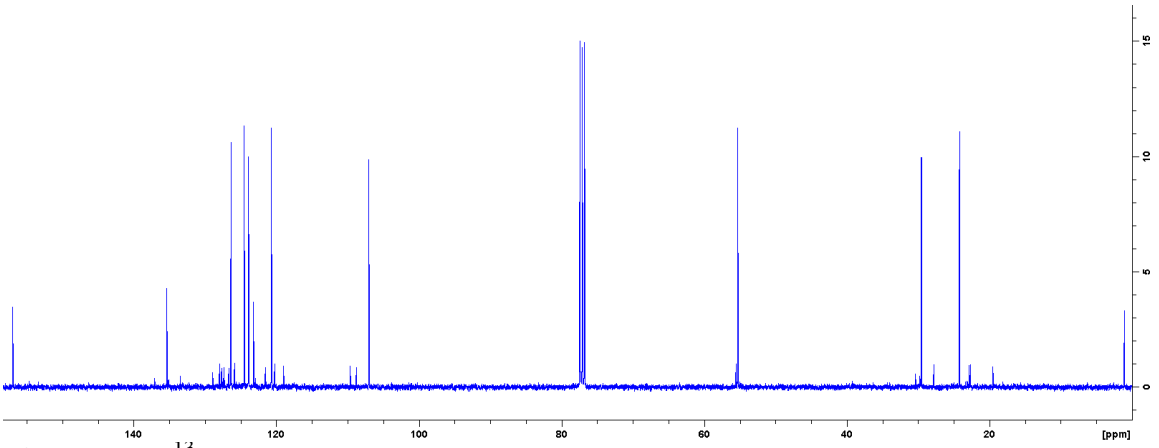

Figure 9.86. ^{13}C NMR spectrum of 1,4-dihydro-5-methoxynaphthalene

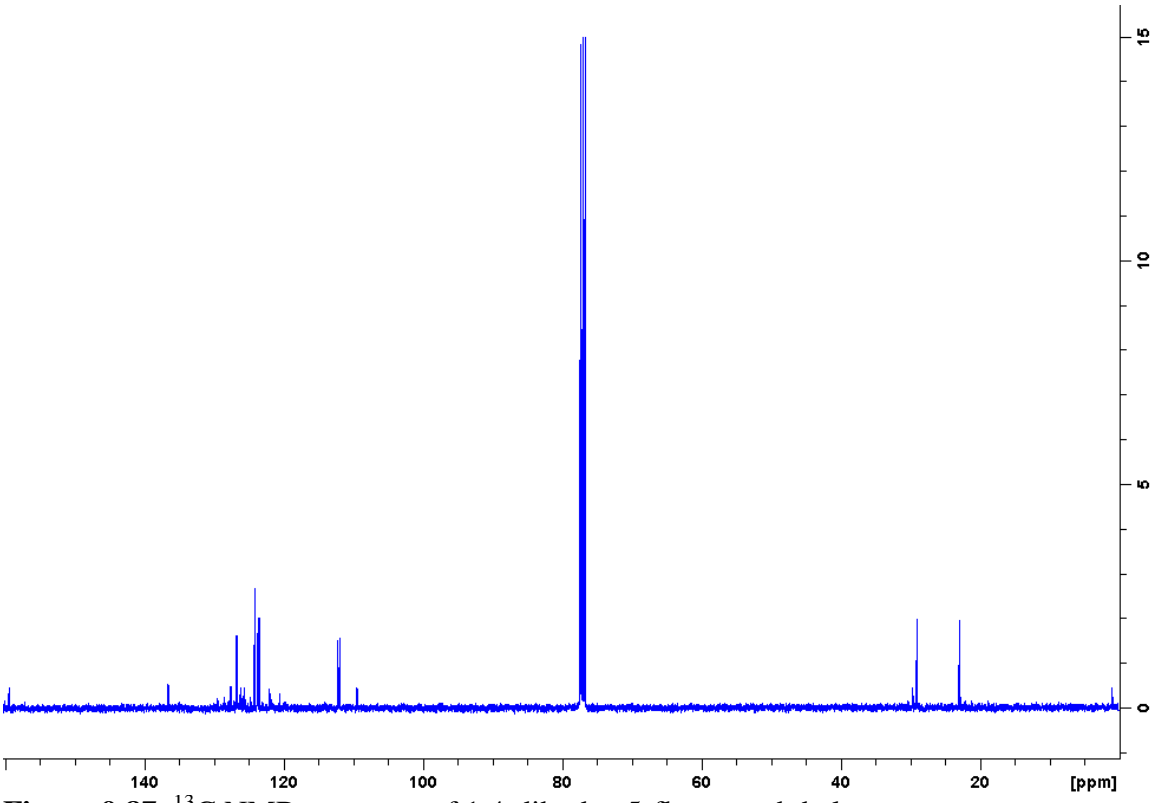

Figure 9.87. ^{13}C NMR spectrum of 1,4-dihydro-5-fluoronaphthalene

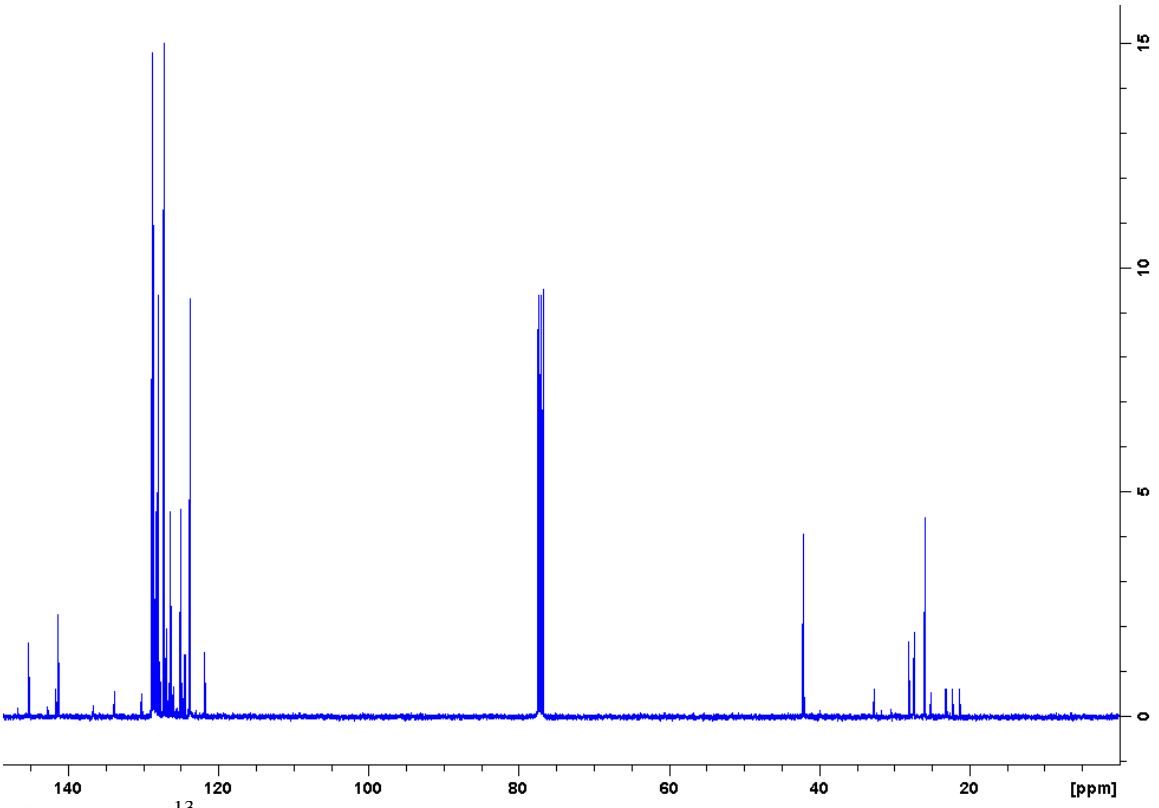

Figure 9.88. ^{13}C NMR spectrum of 1,4-dihydro-1,1`-biphenyl

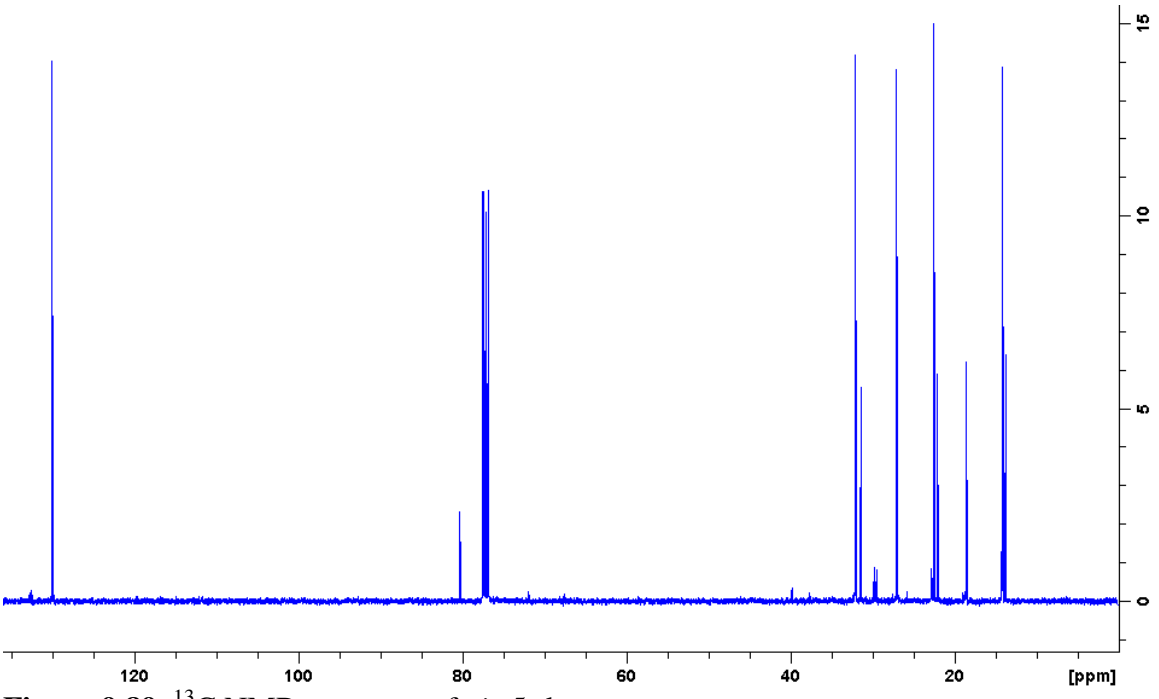

Figure 9.89. ^{13}C NMR spectrum of *cis*-5-decene

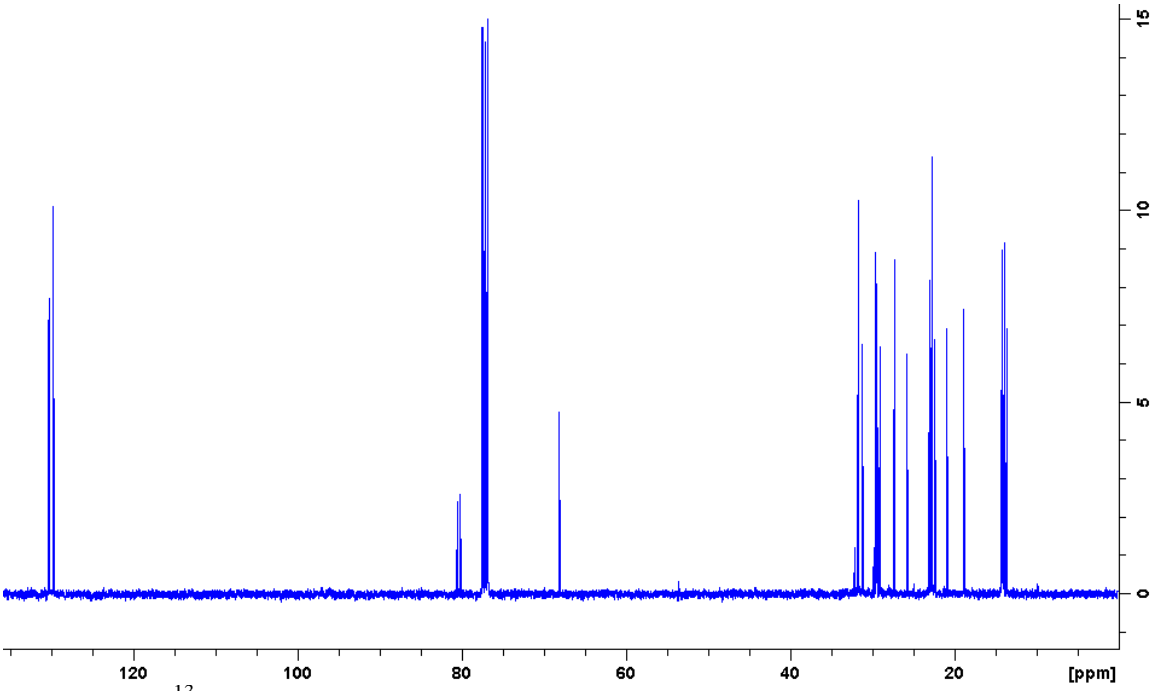

Figure 9.90. ^{13}C NMR spectrum of c*is*-4-decene

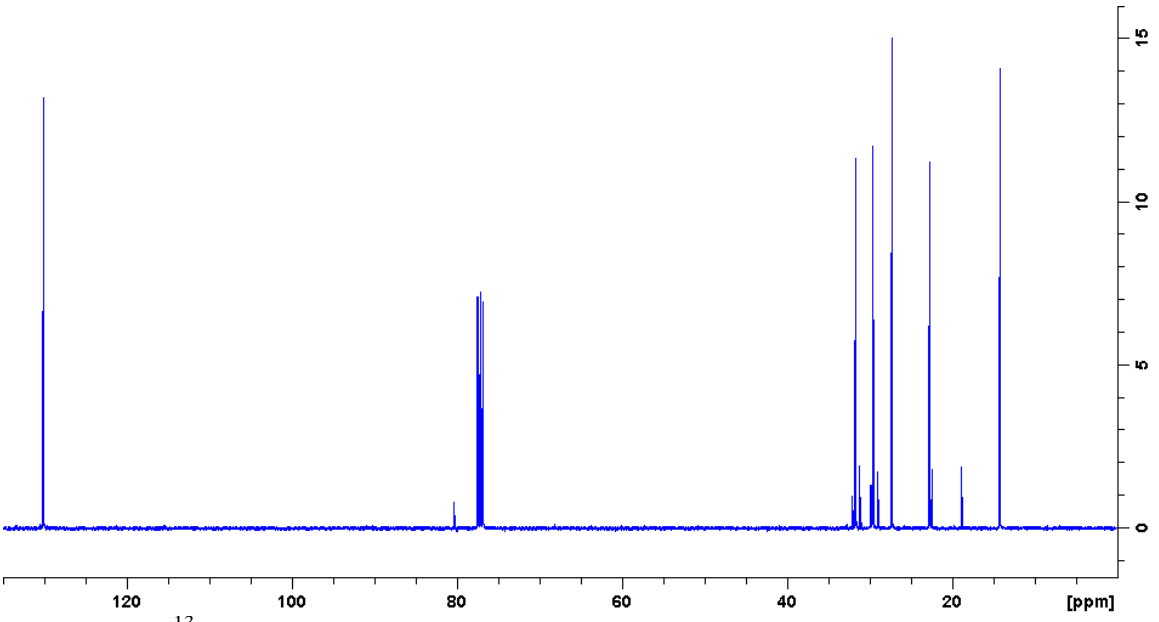

Figure 9.91. ^{13}C NMR spectrum of *cis*-6-dodecene

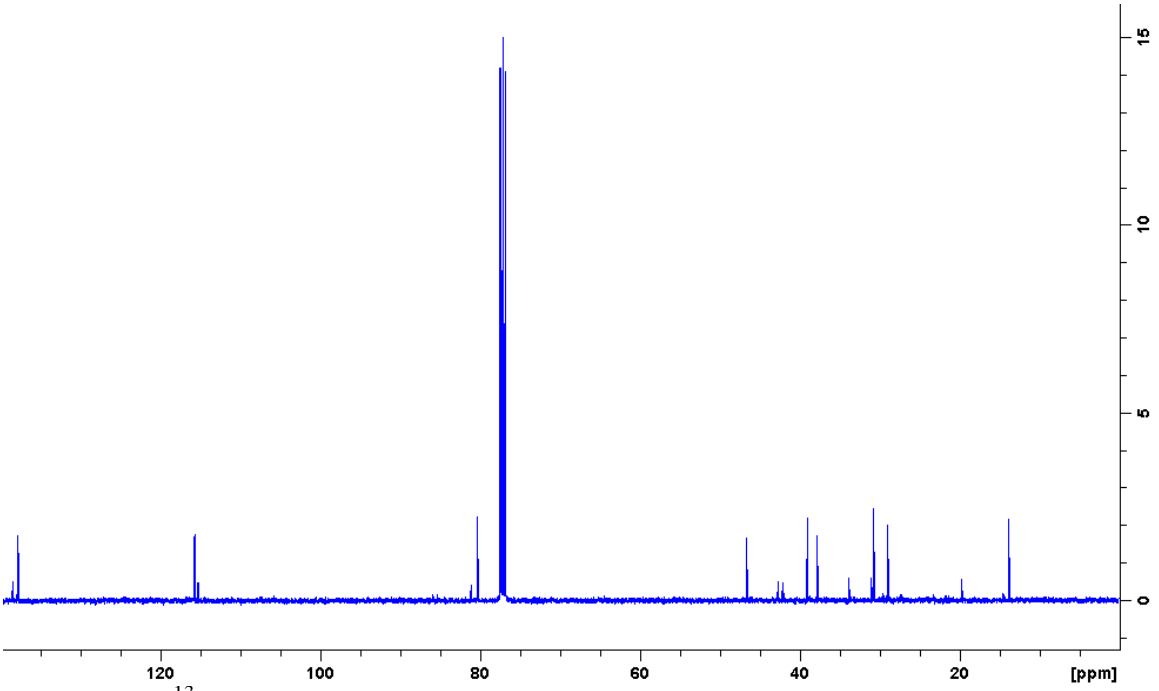

Figure 9.92. ^{13}C NMR spectrum of 2-allyl-5-methylcyclopentan-1-ol

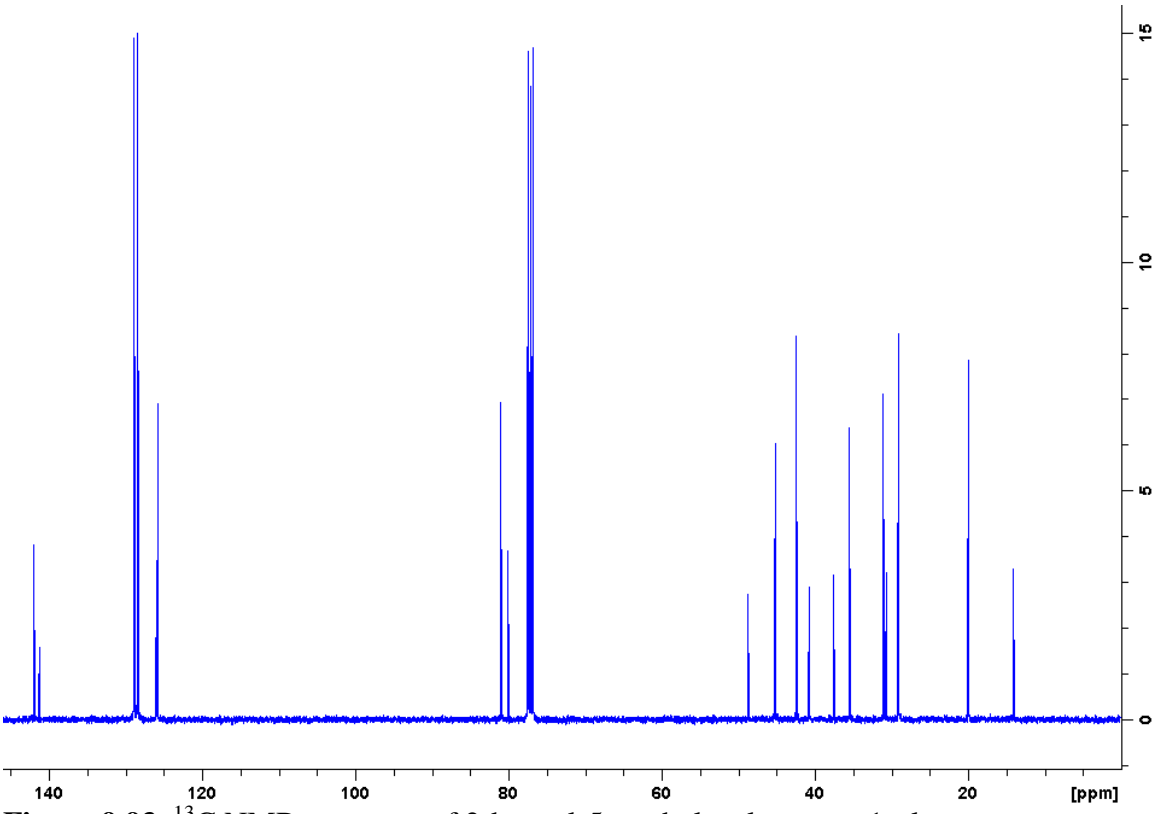

Figure 9.93. ^{13}C NMR spectrum of 2-benzyl-5-methylcyclopentan-1-ol

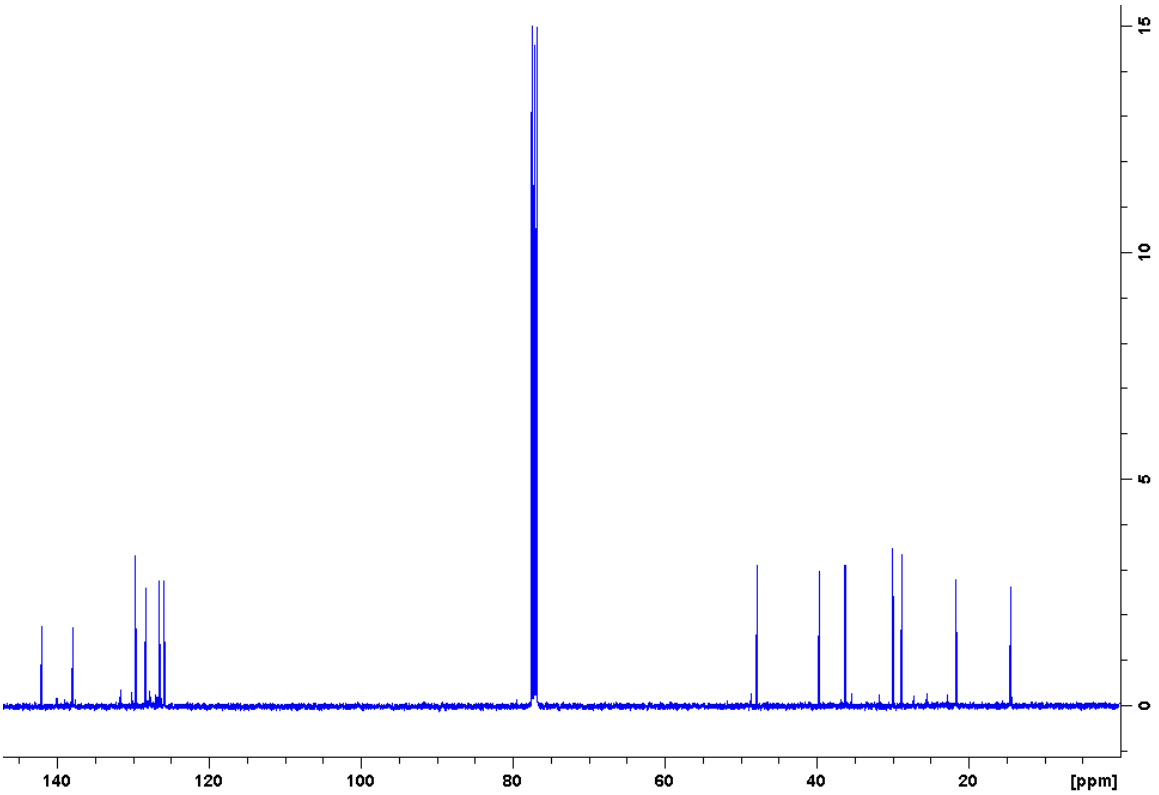

Figure 9.94. ^{13}C NMR spectrum of 2-methyl-5-(3-methylbenzyl)cyclopentan-1-ol

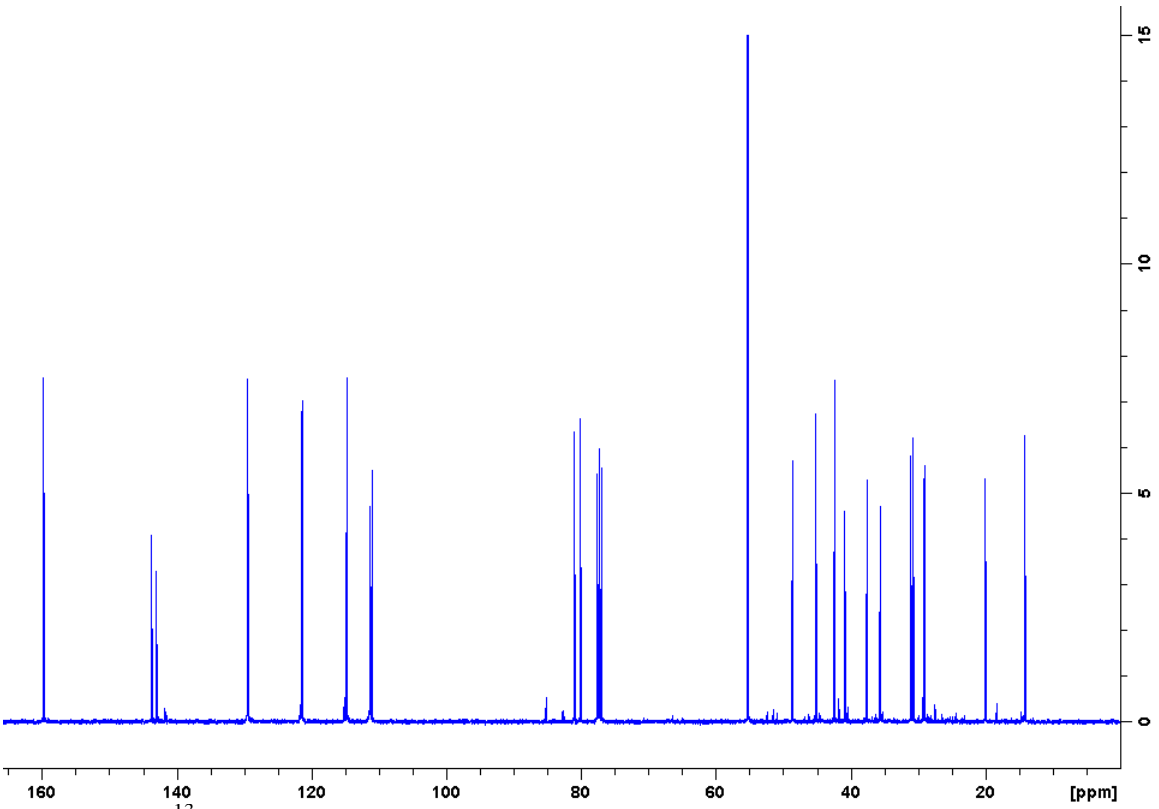

Figure 9.95. ^{13}C NMR spectrum of 2-methyl-5-(3-methoxybenzyl)cyclopentan-1-ol

9.5.3 Kinetics Data

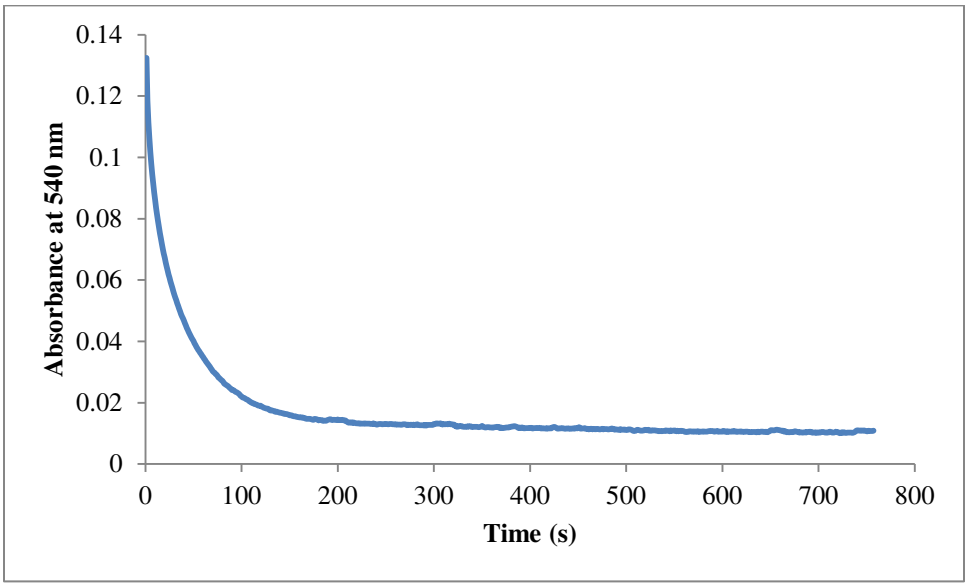

Figure 9.96. Representative plot of the decay curve for SmI_2 at 560 nm in the presence of acenaphthalene and 400 mM water

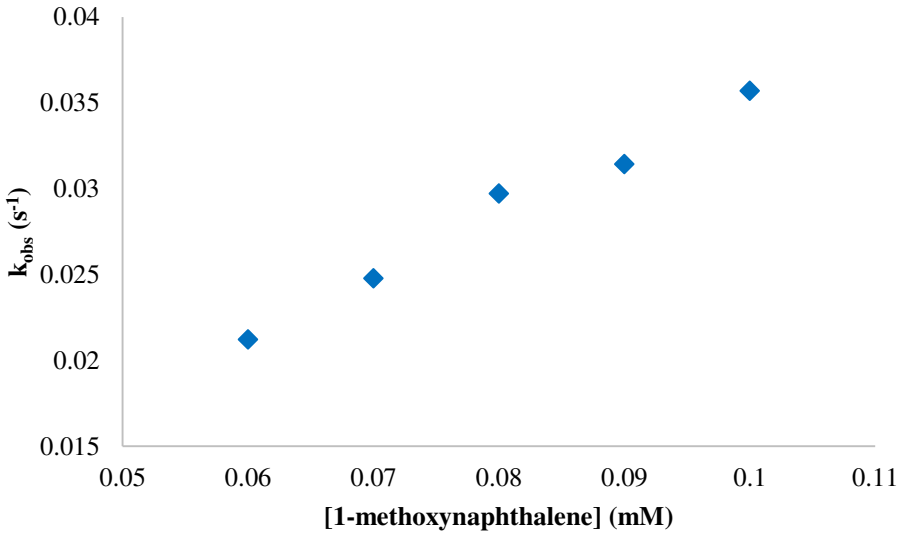

Figure 9.97. Plot of $\ln(k_{obs})$ vs $\ln([1\text{-methoxynaphthalene}])$ for the reduction of 1-methoxynaphthalene by $SmBr_2$-NMEA

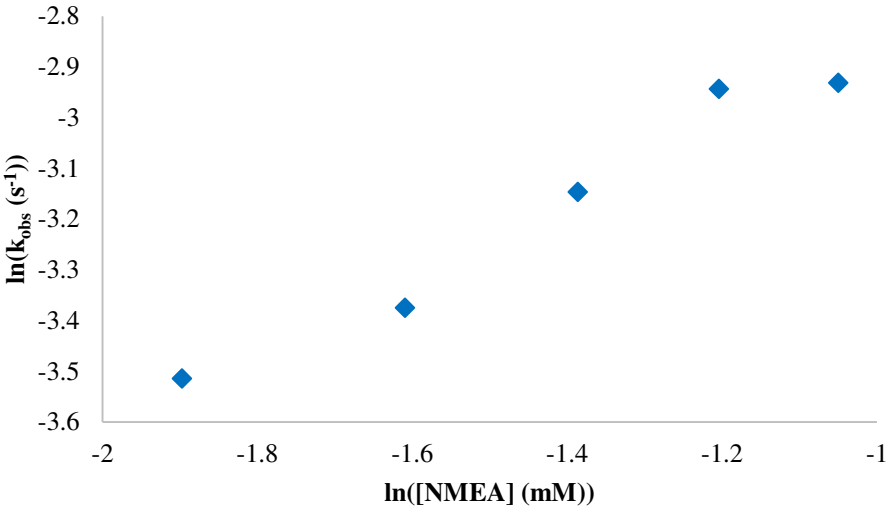

Figure 9.98. Plot of ln(k_{obs}) vs ln([NMEA]) for the reduction of 1-methoxynaphthalene by $SmBr_2$-NMEA

[1-methoxynaphthaene] (mM)	Trial	A_0	$A_{1/2}$	$A_{3/4}$	$t_{1/2}$	$t_{3/4}$	$(t_{3/4}-t_{1/2})/t_{1/2}$
60	A	0.134	0.067	0.033	16	35	1.2
60	B	0.122	0.061	0.030	17	39	1.3
70	A	0.128	0.064	0.032	12	30	1.5
70	B	0.140	0.070	0.035	14	33	1.4
80	A	0.141	0.070	0.035	12	30	1.5
90	A	0.138	0.069	0.034	12	24	1.0
100	A	0.131	0.065	0.032	11	25	1.3
						Average:	1.3
						Order:	1

Table 9.3. Fractional times table to calculate the rate order of $SmBr_2$ in the reduction of 1-methoxynaphthalene by $SmBr_2$-NMEA

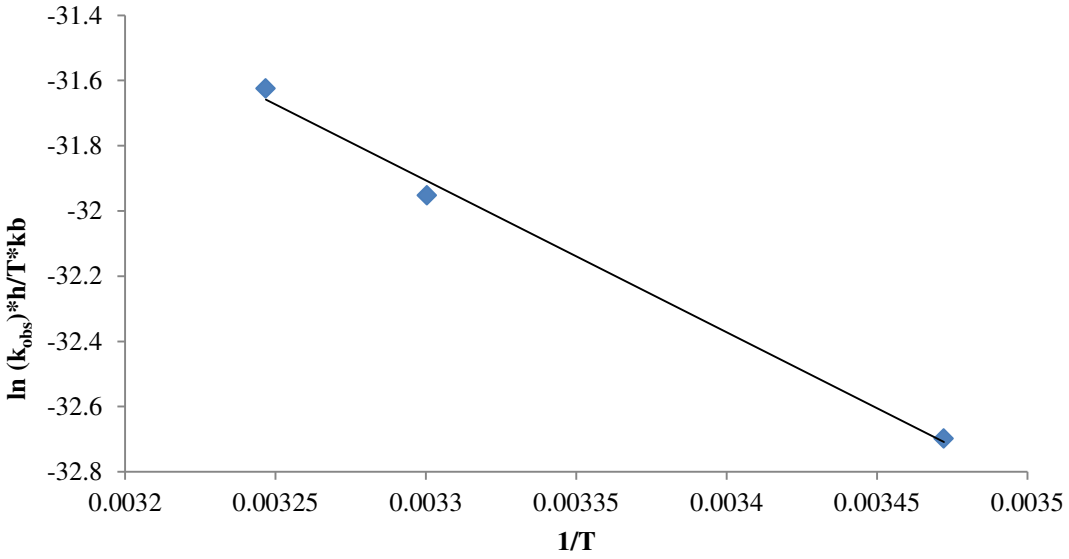

Figure 9.99. Plot of ln(k_{obs}*h/T*kb) vs 1/T for the reduction of acenaphthalene by 1-methoxynaphthalene by $SmBr_2$-NMEA

9.5.4 Computational Details

Gaussian09 programs were used for the calculations with the APF-D hybrid DFT method and the 6-311+G(2d,p) basis set.[1–4] Natural-population analysis was obtained by including pop=npa.[5] Solvation values were calculated using the polarizable continuum model with integral equation formalism IEFPCM with tetrahydrofuran as the solvent.[6,7] The geometries and frequencies were calculated with the keywords uapfd/6-311+g(2d,p) opt=(calcfc,tight) int=(ultrafine,acc2e=12) pop=npa scrf=(iefpcm,solvent=thf)

9.6 Studies on Backdonation as the Basis for Coordination-Induced Bond Weakening

9.6.1 ^{1}H NMR Data

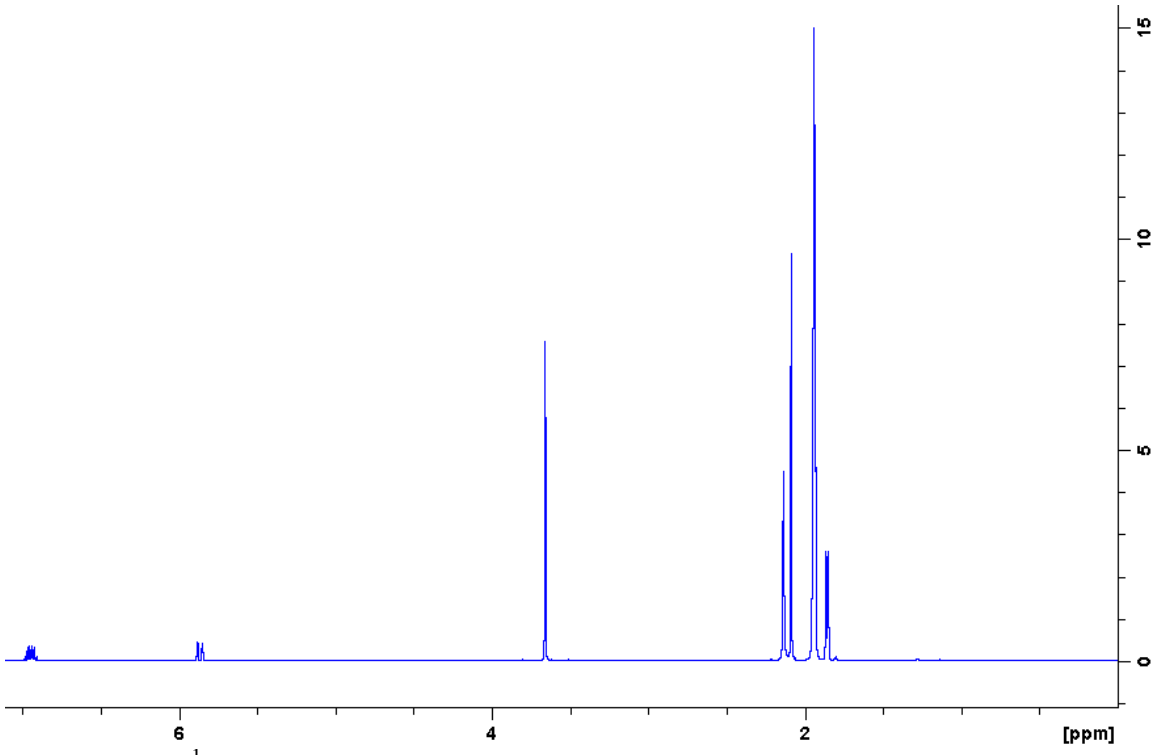

Figure 9.100. ^{1}H NMR spectrum of methyl crotonate

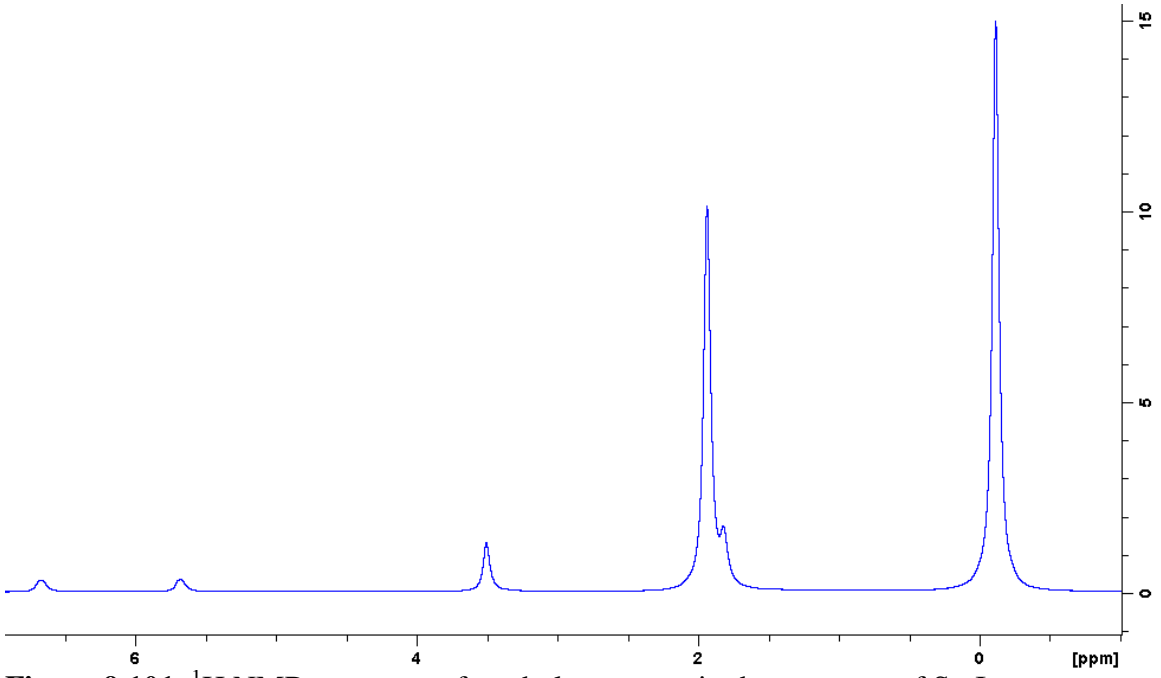

Figure 9.101. ^{1}H NMR spectrum of methyl crotonate in the presence of SmI_2

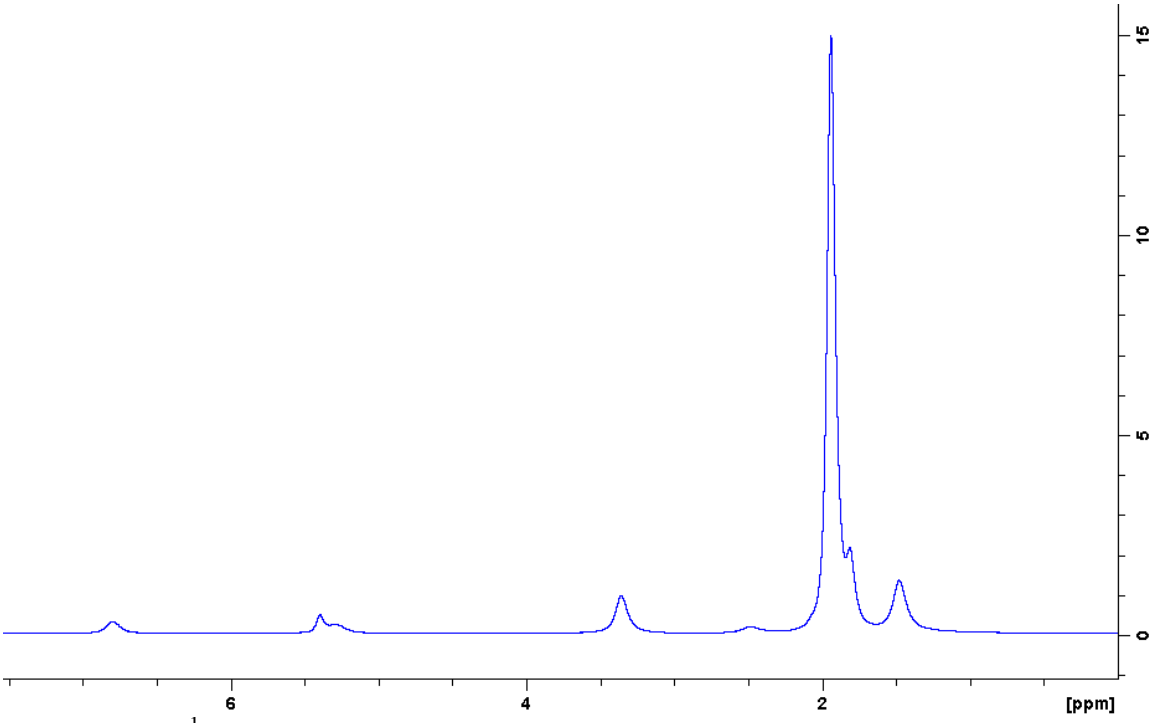

Figure 9.102. ^{1}H NMR spectrum of methyl crotonate in the presence of YbI_2

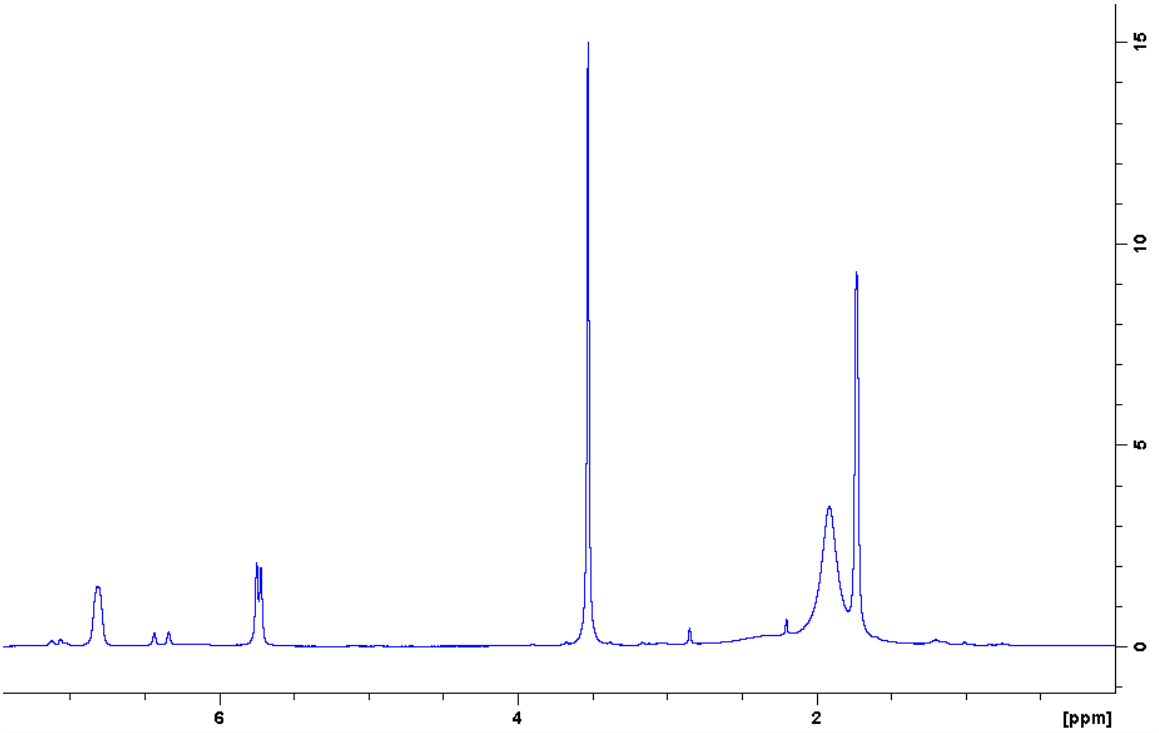

Figure 9.103. ^{1}H NMR spectrum of methyl crotonate in the presence of Cp_2TiCl

9.6.2 Computational Details

Gaussian09 programs were used for the calculations of the $\Delta E_{\sigma-\sigma^*}$ values with the APF-D hybrid DFT method and the 6-311+G(2d,p) basis set.[1–4] Natural-population analysis was obtained by including pop=npa.[5] The geometries and frequencies were calculated with the keywords uapfd/6-311+g(2d,p) opt=(calcfc,tight) int=(ultrafine,acc2e=12) pop=npa. The $\Delta E_{\sigma-\sigma^*}$ values were calculated at the same level of theory using natural bond order analysis with the keywords uapfd/6-311+g(2d,p) opt=(calcfc,tight) int=(ultrafine,acc2e=12) pop=nbo.[8] This analysis was found to produce the same trends observed in the data gathered through natural population analysis.

Gaussian09 programs were used for the calculations of the ΔBDFE values with the B3LYP hybrid DFT method and the def2-TZVP basis set.[1,9–11] The geometries and frequencies were calculated with the keywords opt=(calcfc,tight) int=(ultrafine,acc2e=12) freq ub3lyp/def2svpp.

9.7 References

(1) Gaussian 09, Revision D.01, M. J. Frisch, G. W. Trucks, H. B. Schlegel, G. E. Scuseria, M. A. Robb, J. R. Cheeseman, G. Scalmani, V. Barone, B. Mennucci, G. A. Petersson, H. Nakatsuji, M. Caricato, X. Li, H. P. Hratchian, A. F. Izmaylov, J. Bloino, G. Zheng, J. L. Sonnenberg, M. Hada, M. Ehara, K. Toyota, R. Fukuda, J. Hasegawa, M. Ishida, T. Nakajima, Y. Honda, O. Kitao, H. Nakai, T. Vreven, J. A. Montgomery, Jr., J. E. Peralta, F. Ogliaro, M. Bearpark, J. J. Heyd, E. Brothers, K. N. Kudin, V. N. Staroverov, T. Keith, R. Kobayashi, J. Normand, K. Raghavachari, A. Rendell, J. C. Burant, S. S. Iyengar, J. Tomasi, M. Cossi, N. Rega, J. M. Millam, M. Klene, J. E. Knox, J. B. Cross, V. Bakken, C. Adamo, J. Jaramillo, R. Gomperts, R. E. Stratmann, O. Yazyev, A. J. Austin, R. Cammi, C. Pomelli, J. W. Ochterski, R. L. Martin, K. Morokuma, V. G. Zakrzewski, G. A. Voth, P. Salvador, J. J. Dannenberg, S. Dapprich, A. D. Daniels, O. Farkas, J. B. Foresman, J. V. Ortiz, J. Cioslowski, and D. J. Fox, Gaussian, Inc., Wallingford CT, 2013

(2) Austin, A.; Petersson, G. A.; Frisch, M. J.; Dobek, F. J.; Scalmani, G.; Throssell, K. A Density Functional with Spherical Atom Dispersion Terms. *J. Chem. Theory Comput.* **2012**, *8* (12), 4989–5007.

(3) McLean, A. D.; Chandler, G. S. Contracted Gaussian Basis Sets for Molecular Calculations. I. Second Row Atoms, Z=11–18. *J. Chem. Phys.* **2008**, *72* (10),

5639.

(4) Krishnan, R.; Binkley, J. S.; Seeger, R.; Pople, J. A. Self-Consistent Molecular Orbital Methods. XX. A Basis Set for Correlated Wave Functions. *J. Chem. Phys.* **2008**, *72* (1), 650.

(5) Reed, A. E.; Weinstock, R. B.; Weinhold, F. Natural Population Analysis. *J. Chem. Phys.* **1998**, *83* (2), 735.

(6) Cancès, E.; Mennucci, B.; Tomasi, J. A New Integral Equation Formalism for the Polarizable Continuum Model: Theoretical Background and Applications to Isotropic and Anisotropic Dielectrics. *J. Chem. Phys.* **1998**, *107* (8), 3032.

(7) Tomasi, J.; Mennucci, B.; Cammi, R. Quantum Mechanical Continuum Solvation Models. *Chem. Rev.* **2005**, *105* (8), 2999–3093.

(8) NBO Version 3.1, E. D. Glendening, A. E. Reed, J. E. Carpenter, and F. Weinhold.

(9) Becke, A. D. Density Functional Calculations of Molecular Bond Energies. *J. Chem. Phys.* **1998**, *84* (8), 4524.

(10) Becke, A. D. Density-Functional Thermochemistry. III. The Role of Exact Exchange. *J. Chem. Phys.* **1998**, *98* (7), 5648.

(11) Lee, C.; Yang, W.; Parr, R. G. Development of the Colle-Salvetti Correlation-Energy Formula into a Functional of the Electron Density. *Phys. Rev. B* **1988**, *37* (2), 785.

Nick Boekell
nick.boekell@gmail.com

Education

Lehigh University
Bethlehem, PA
Ph.D., Organic Chemistry 2017-present

Trinity College
Hartford, CT
B.S., Chemistry and Mathematics 2013-2017

Publications

Ramírez-Solís, A.; Boekell, N. G.; León-Pimentel, I.; Saint-Martin, H.; Bartulovich, C. O.; Flowers, R. A. Ammonia Solvation vs Aqueous Solvation of Samarium Diiodide. A Theoretical and Experimental Approach to Understanding Bond Activation Upon Coordination to Sm(II). *J. Org. Chem* **2022**, *87* (3), 1689–1697.

Ramírez-Solís, A.; Bartulovich, C. O.; León-Pimentel, C. I.; Saint-Martin, H.; Boekell, N. G.; Flowers, R. A. Proton Donor Effects on the Reactivity of SmI2. Experimental and Theoretical Studies on Methanol Solvation vs. Aqueous Solvation. *Dalt. Trans.* **2020**, *49* (23), 7897–7902.

Boekell, N. G.; Cerone, D. J.;Boucher, M. M.; Quach, P. K.; Tentchou, W. B. N.; Reavis, C. G.; Okoh, I. I.; Reid, J. O. A.; Berg, H. E.; Chang, B. A.; Brindle, C. S. Triarylmethyl Cation Catalysis: A Tunable Lewis Acid Organocatalyst for the Synthesis of Bisindolylmethanes. *SynOpen* **2017**, *1*, 97-102.

Boekell, N. G. and Flowers, R. A. Coordination-Induced Bond Weakening. *Manuscript in preparation*

Boekell, N. G.; Bartulovich, C. O.; Maity, S.; Flowers, R. A. Accessing Unusual Reactivity through Chelation-Promoted Bond Weakening. *Manuscript in progress*

Boekell, N. G.; Oloyede, U. N.; Chciuk, T. V.; Flowers, R. A. Coordination-Induced Bond Weakening as a Consequence of Low-Valent Metal Backdonation into Ligand X-H σ*-Antibonding Orbitals. *Manuscript in preparation*

Boekell, N.G.; Fasihianifard, P.; Bartulovich, C. O.; Vlaisavljeich, B.; Flowers, R. A. Investigating the Unusual Stability of SmI_2-Water in THF Solution. *Manuscript in preparation*

Conference Presentations

ACS-CVS Mount Holyoke College Undergraduate Research Symposium
Trityl Catalysts and the Double Addition Reaction of Benzaldehyde and Indole
Oral Presentation
April 23, 2016

Research Experience

Lehigh University
Bethlehem, PA 2017-present
Research Advisor: Professor Robert A. Flowers II
Coordination-Induced Bond Weakening in Divalent Samarium Reductants

- Kinetic analyses were performed on the reductions of substrates Sm(II) PCET reagents using UV-Visible stopped flow spectrophotometry.
- Kinetic analysis was performed on the evolution of hydrogen gas from Sm(II) PCET reagents using UV-Visible stopped flow spectrophotometry.
- Synthetic investigations were undertaken on the reactivity of Sm(II) with diverse substrate classes and the associated substrate scopes were assessed using GCMS, ESI-MS, HPLC, 1-D NMR (^{1}H and ^{13}C), 2-D NMR (COSY, HMQC, HSQC), UV-Visible spectrophotometry, and IR spectrophotometry.
- Computational investigations were undertaken to support the above kinetic and synthetic studies using Gaussian 09. Computational analysis included natural bond orbital and natural population analysis as well as bond energy calculations.
- Experienced in experimental design, multistep synthesis, dry box technique, and Schlenk line technique.
- Experienced with relevant software including Gaussian 09, ChemDraw, Microsoft Office, Topspin, Scifinder, Mendeley.

Trinity College
Hartford, CT 2016-2017
Research Advisor: Professor Cheyenne S. Brindle
Triarylmethyl Carbocation Organocatalysts for the Synthesis of Bisindolylmethanes

- The substrate scope of triarylmethyl carbocation-mediated cross couplings of indoles to aldehydes was investigated using GCMS and NMR (^{1}H and ^{13}C).

Teaching Experience

Lehigh University
Bethlehem, PA 2017-2019
Teaching Assistant, Organic I Laboratory and Organic II Laboratory

Trinity College
Hartford, CT 2016
Teaching Assistant, Physical Chemistry I Laboratory